

**Quantitative understanding of complex light-dependent
and phytohormone triggered plant signaling pathways in
the orthogonal system of mammalian cells**

Inaugural-Dissertation

zur Erlangung des Doktorgrades
der Mathematisch-Naturwissenschaftlichen Fakultät
der Heinrich-Heine-Universität Düsseldorf

vorgelegt von

Tim Blomeier
aus Bielefeld

Düsseldorf, Mai 2021

aus dem Institut für Synthetische Biologie
der Heinrich-Heine-Universität Düsseldorf

Gedruckt mit der Genehmigung der
Mathematisch-Naturwissenschaftlichen Fakultät der
Heinrich-Heine-Universität Düsseldorf

Berichterstatter:

1. Prof. Dr. Matias D. Zurbriggen

2. Prof. Dr. George Coupland

Tag der mündlichen Prüfung: 05.11.2021

EIDESSTATTLICHE ERKLÄRUNG

Ich versichere an Eides Statt, dass die Dissertation von mir selbständig und ohne unzulässige fremde Hilfe unter Beachtung der „Grundsätze zur Sicherung guter wissenschaftlicher Praxis an der Heinrich-Heine-Universität Düsseldorf“ erstellt worden ist.

Datum

Unterschrift

Table of contents

EIDESSTATTLICHE ERKLÄRUNG	I
DANKSAGUNG	IV
FIGURES	VI
TABLES	VII
ABBREVIATIONS	VIII
SUMMARY	X
1 Introduction	1
1.1 Plant Signaling.....	1
1.1.1 Phytohormones	2
1.1.1.1 Gibberellins.....	3
1.1.2 Light signaling	6
1.1.2.1 Plant phytochromes	8
1.1.2.2 Phytochrome A	9
1.1.2.3 Phytochrome B	10
1.1.2.4 Phytochrome C-E	10
1.1.2.5 Role of phytochrome-PIF interaction	11
1.2 Synthetic biology	13
1.2.1 Application of CRISPR/Cas systems for genetic modification	14
1.2.2 Optogenetics	15
1.2.2.1 Optogenetic switches in mammalian cells.....	16
1.2.2.2 Optogenetics in plants	17
1.2.3 Study of plant signaling in the orthogonal system of mammalian cells.....	18
1.2.3.1 Förster resonance energy transfer (FRET) approaches for analysis of protein interactions.....	21
2 Aims	23
3 Results and Discussion	24
3.1 Quantitative reconstruction of plant signaling networks in the orthogonal system of mammalian cells	24
3.1.1 Quantitative reconstruction of the gibberellin perception mechanism.....	24
3.1.1.1 Mammalian-x-hybrid (MxH) approaches.....	25
3.1.1.2 Microscopy based approaches	29
3.1.2 Synthetic reconstruction of the phytochrome-PIF interaction network in the orthogonal system of mammalian cells	35
3.1.2.1 Mammalian-3-hybrid assays for investigation on interaction of phytochromes and PIFs	36
3.1.2.2 Confocal fluorescence microscopy studies for analysis of PIF-dependent nuclear transport mechanisms of phytochromes.....	40
3.2 Tools for controlling signaling in plant and mammalian cells.....	51
3.2.1 Blue Light-Operated CRISPR/Cas13b-mediated mRNA Knockdown (Lockdown)	51
3.2.2 UV-B light-inducible system (UV-B _{ON}) for the control of gene expression in <i>A. thaliana</i> mesophyll protoplasts	56
4 Conclusion	61

5 Materials and Methods	62
5.1 Mammalian cell experiments	62
5.1.1 Plasmid generation/construction	62
5.1.2 Mammalian cell cultivation and transfection	62
5.1.3 Phytohormone experiments	62
5.1.4 Light experiments in mammalian cells	62
5.1.5 SEAP reporter assay	63
5.1.6 Fixation and imaging of mammalian cells	63
5.1.7 Microscopy	63
5.1.8 FRET-APB experiments	63
5.1.9 FRET-FLIM experiments	64
5.1.10 Luminescence analysis of mammalian cell experiments	64
5.1.11 Quantitative real time PCR	64
5.1.12 Western Blot	64
5.1.13 Cell proliferation assays	64
5.1.14 Statistics	65
5.2 Protoplast experiments	65
5.2.1 Protoplast isolation and transformation	65
5.2.2 UV-Light experiments in protoplasts	65
5.2.3 Luminescence analysis of protoplast experiments	65
5.2.4 Light source and illumination conditions	65
5.3 Plasmids	66
5.4 Oligonucleotides	81
6 References	86
7 Appendix	98
7.1 Original publications and manuscripts	98
7.1.1 Mammalian cell-based platform for quantitative reconstruction of plant signaling pathways	99
7.1.2 Blue Light-Operated CRISPR/Cas13b-Mediated mRNA Knockdown (Lockdown)	139
7.1.3 UV-B light-inducible system for the transcriptional control of gene expression in <i>A. thaliana</i> mesophyll protoplasts	158
7.2 Review articles	176
7.2.1 Synthetic switches and regulatory circuits in plants	177
7.3 Additional publications	200

DANKSAGUNG

Zuallererst möchte ich mich bei Prof. Dr. Matias Zurbriggen dafür bedanken, dass ich meine Doktorarbeit innerhalb der letzten vier Jahre in seinem Institut anfertigen durfte. Ich bin sehr dankbar dafür, dass ich außerordentlich viele neue und spannende Techniken lernen und sogar die eigenverantwortliche Betreuung unseres Mikroskops übernehmen durfte. Das hohe Maß an wissenschaftlicher Freiheit, gepaart mit der Vielzahl an Pflichten haben sowohl meine wissenschaftliche, als auch meine persönliche Selbständigkeit stark gefördert.

Des Weiteren danke ich Prof. Dr. George Coupland für seine Unterstützung während der Zeit meiner Promotion als Mentor bei den jährlichen TAC-Meetings, als auch bei den IMPRS-Retreats.

Ferner gilt mein Dank Prof. Dr. Ute Höcker für die Übernahme eines Platzes in meinem TAC-Komitee. Auch bei ihr möchte ich für die äußerst konstruktiven und spannenden TAC-Meetings bedanken, welche mir auf meinem Weg zur Anfertigung dieser Arbeit enorm weitergeholfen haben.

Ich bedanke mich bei Stephan Wagner für seine tolle Betreuung und die Koordination der TAC-Meetings und IMPRS-Retreats. Vielen Dank für deine unterstützenden Worte und Hilfe im Laufe der letzten Jahre.

Außerdem möchte ich Stefanie Weidtkamp-Peters und Sebastian Hänsch vom CAi für ihre Unterstützung und zahlreichen Ratschläge zur Durchführung und Analyse aller Mikroskopie-basierten Techniken danken.

Ich danke unseren Kooperationspartner, vor allem Prof. Dr. Miguel Blázquez, für die nette und produktive Zusammenarbeit.

Jennifer Andres, wir sind das einzig wahre Team Reconstruction. Mit der Betonung auf Team. Das Zusammenarbeiten mit dir, egal wie stressig oder lang die Tage auch waren, hat in erster Linie immer sehr viel Spaß gemacht. Ob 26 Stunden am Stück Review schreiben, die Konferenz in Finnland oder der ganz normal Laborwahnsinn. Danke, dass du mich immer wieder motiviert hast. Es ist alles andere als selbstverständlich über einen solch langen Zeitraum so gut zusammen zu arbeiten.

Leonie-Alexa Koch, danke für die Kaffeepausen, das Korrekturlesen von jeglichen Texten, deine Geduld und Unterstützung in allen Lebenslagen. Egal ob beim Basteln und Zusammenbauen von Doktorhüten und -wagen nach stressigen Arbeitstagen oder in der Schreibphase während der Corona-Pandemie. Danke, dass ich mich immer auf dich verlassen kann.

Ich möchte mich bei Patrick Fischbach für die immer produktive, aber auch sehr lustige und freundschaftliche Zusammenarbeit bedanken. Ich bin sehr stolz darauf, dass wir deine Projektidee letzten Endes wirklich umsetzen und erfolgreich publizieren konnten.

Mein besonderer Dank gilt Reinhild Wurm, Michaela Gerads und Stefanie Kuschel. Ohne eure Hilfe wäre die Arbeit in dieser Form niemals möglich gewesen. Vielen Dank für eure Unterstützung während der letzten vier Jahre. Ich wünsche euch nur das Beste!

Danke an Dr. Uriel Urquiza für seine Unterstützung bei allen Fragen zu pflanzlichen Signalwegen und der Hilfe bei der Etablierung des UV-Systems in Protoplasten.

Ich danke meinen Studenten Rene, Florian, Giovanni, Gianni und Julia. Vielen Dank für euren Anteil an dieser Arbeit, den ihr während eurer Zeit als Bachelor- oder Masterstudenten geleistet habt.

Ich danke meiner Familie und meinen Freunden, die während meiner Promotion immer ein offenes Ohr für mich hatten und mir mit Rat und Tat zur Seite standen.

Abschließend möchte ich meiner Freundin Lydia danken. Danke dafür, dass du mich während der ganzen Zeit stets ertragen und mich bei meinen Entscheidungen immer unterstützt hast. Ich weiß, dass es gerade in der Schreibphase und dann auch noch mitten in der Corona-Pandemie, nicht immer leicht mit mir war. Danke für alles!

FIGURES

Figure 1.1	Stages of signaling in eukaryotic cells.	1
Figure 1.2	Scheme of phytohormone perception machinery and regulator-protein degradation mechanisms in <i>Arabidopsis thaliana</i> .	3
Figure 1.3	Illustration of the gibberellin perception machinery and DELLA-degradation mechanisms in <i>Arabidopsis</i>	5
Figure 1.4	Overview of <i>Arabidopsis thaliana</i> photoreceptors with detailed information about phytochrome signaling and involved components.	7
Figure 1.5	Scheme of the configuration and function of chimeric transcriptional regulators	14
Figure 1.6	Illustration of the general principle of an optogenetic “light-switch” for transcriptional activation and switches used in the frame of this thesis.	16
Figure 1.7	Illustration of the principle of studying plant signaling pathway components in the orthogonal system of mammalian cells and possible applications.	20
Figure 1.8	Illustration of the FRET measurement of a mCherry- and an EGFP-fused protein and factors essential for such a measurement.	22
Figure 2.1	Synthetic reconstruction of DELLA-mediated regulation of transcriptional activation and comparison of mammalian-x-hybrid experiments analyzing the order of complex-formation during GA-perception in human embryonic kidney cells (HEK-293T).	27
Figure 2.2	Overview of the principles of FRET measurements by acceptor photo-bleaching (FRET-APB) on the example of EGFP fused GID1b and mCherry tagged GAI constructs in mammalian HEK-293T cells.	30
Figure 2.3	Comparison of apparent FRET efficiencies between fluorescently-tagged GAI and GID1b protein constructs in mammalian HEK-293T cells.	32
Figure 2.4	Visualization of apparent FRET efficiencies of FRET-APB measurements and visualization of fluorescence lifetime of fluorescently tagged GID1 fusion proteins in different experimental conditions in mammalian HEK-293T cells.	33
Figure 2.5	Overview of used approaches for the analysis of possible phytochrome-PIF interactions in mammalian cells.	36
Figure 2.6	Mammalian-3-hybrid experiments analyzing interactions of phytochrome A or B and PIF proteins of <i>A. thaliana</i> in Chinese hamster ovary cells (CHO-K1).	38
Figure 2.7	Mammalian-3-hybrid experiments analyzing interactions of phytochrome C or D and PIF proteins of <i>A. thaliana</i> in Chinese hamster ovary cells (CHO-K1).	39
Figure 2.8	Confocal fluorescence microscopy imaging of intracellular localizations of phyA-D fused to mCherry in mammalian HeLa cells under different light conditions.	40
Figure 2.9	Confocal fluorescence microscopy imaging of intracellular localizations of phyA-mCherry and PIF1-8 fused to EGFP in mammalian HeLa cells under different light conditions.	42
Figure 2.10	Confocal fluorescence microscopy imaging of intracellular localizations of phyB-mCherry and PIF1-8 fused to EGFP in mammalian HeLa cells under different light conditions.	44

Figure 2.11	Confocal fluorescence microscopy imaging of intracellular localizations of phyC-mCherry and PIF1-8 fused to EGFP in mammalian HeLa cells under different light conditions.	46
Figure 2.12	Confocal fluorescence microscopy imaging of intracellular localizations of phyD-mCherry and PIF1-8 fused to EGFP in mammalian HeLa cells under different light conditions.	48
Figure 2.13	Design and characterization of the Lockdown system.	52
Figure 2.14	Mode of function and characterization of the UV-B light-induced gene expression system (UV-B _{ON}) for application in <i>A. thaliana</i> protoplasts.	58

TABLES

Table 2.1	Summary of phytochrome interaction and localization studies	50
-----------	---	----

ABBREVIATIONS

ABA	abscisic acid
AD	activation domain
APA	active phytochrome A binding site
APB	active phytochrome B binding site
ARF	auxin response factor
ARR1	ARABIDOPSIS RESPONSE REGULATOR1
<i>A. thaliana</i>	<i>Arabidopsis thaliana</i>
bHLH	basic helix loop helix
BLINK1	blue light-induced K ⁺ channel 1
BR	brassinosteroids
CAAX	prenylation sequence
ChIP	chromatin immunoprecipitation
ChR2	channel rhodopsin 2
CK	cytokinins
Co-R	co-receptor
COP1	CONSTITUTIVE PHOTOMORPHOGENIC1
CRISPR/Cas	clustered regulatory interspaced short palindromic repeats/CRISPR-associated
DBD	DNA binding domain
E	macrolide repressor
<i>E. coli</i>	<i>Escherichia coli</i>
EGFP	enhanced green fluorescent protein
EL222	222 amino acid protein isolated from the marine bacterium <i>Erythrobacter litoralis</i>
ET	ethylene
FHL	FHY1-LIKE
FHY1	FAR-RED ELONGATED HYPOCOTYL1
FLUC	firefly luciferase
FR	far red light
FRET	Förster resonance energy transfer
FRET-APB	Förster resonance energy transfer – acceptor photobleaching
FRET-FLIM	Förster resonance energy transfer – fluorescence lifetime imaging microscopy
GA	gibberellin
GA ₃ -AM	acetoxymethyl ester of gibberellic acid 3
GAI	GA-INSENSITIVE
GAox	GA-oxidase
GGDP	<i>trans</i> -geranylgeranyldiphosphate
GID1	GIBBERELLIN INSENSITIVE DWARF1
GRAS	GAI, RGA and SCARECROW
gRNA	guide RNA
HEK	human embryonic kidney
HIR	high irradiance response
IAA	indole-3-acetic acid, auxin
IRES	internal ribosome entry site
JA	jasmonate
JAZ	JASMONATE-ZIM DOMAIN
KRAB	Krüppel associated box
LOV	light oxygen voltage domain
MXH	mammalian-x-hybrid
NES	nuclear export signal
NLS	nuclear localization sequence

NO	nitric oxide
PAM	protospacer adjacent Motif
PCB	phycocyanobilin
Pfr	far red light-absorbing active conformation of phytochromes
phy	phytochrome
PIF	PHYTOCHROME INTERACTING FACTOR
Pip	pristinamycin
PPI	protein-protein-interaction
Pr	red light-absorbing inactive conformation of phytochromes
PULSE	plant usable light-switch elements
R	red light
RD	repression domain
RGA	REPRESSOR OF GA1-3
RGL	RGA-Like
Rht	REDUCED HIGHT
RLUC	renilla luciferase
RUP1/RUP2	REPRESSOR OF UV-B PHOTOMORPHOGENESIS1 and 2
SA	salicylic acid
SCF	Skp1-Cullin1-F-box (SCF)
SEAP	secreted alkaline phosphatase
SL	strigolactones
SLY1	SLEEPY1
SNE	SNEEZY
TALEN	transcription activator-like effector nucleases
tetR	tetracycline repressor
tetO	tetracycline operator
TF	transcription factor
Tyr31	tyrosine residue 31
UAS	upstream activating sequence
UVR8	UV RESISTANCE LOCUS8
VP16	transcriptional activation domain from the herpes simplex virus type 1 virion protein16
WT	wild type
Y2H	yeast-2-hybrid
ZFN	zincfinger

SUMMARY

Synthetic biology is a highly interdisciplinary field of research, combining modern cell biology with engineering and computer sciences. The synergistic view on biological systems allowed scientists to identify, characterize and reconstruct single components and linear signaling pathways, as well as their conjunction to complex signaling networks. Further the substitution and rearrangement of known building-blocks generated highly novel and quantitatively described approaches and tools. Plant signaling in particular holds a high degree of interconnectivity with many shared or redundant components, impeding the extensive implementation of synthetic switches or circuits *in planta*. With the overall aim of generating approaches for monitoring, quantifying and controlling signaling processes, this work describes the development and characterization of diverse synthetic biology tools for application in (orthogonal) mammalian or plant systems.

The collaborative implementation of mammalian-hybrid and (quantitative) microscopy approaches allowed the generation of a toolbox for synthetic reconstitution of plant signaling in the orthogonal system of mammalian cells. We demonstrated the applicability of our designed approaches, ranging from the perception of the phytohormone gibberellin to deciphering the order of interaction events during formation of the perception complex. Further, selected processes downstream of the GA-perception were quantitatively analyzed for the reconstitution of promoter binding affinities of transcription factors, while the influence of secondary components on their transactivation capability was successfully demonstrated. Besides GA perception, the developed tools were applied for the quantitative description of phytochrome-PIF interactions and their dependence on red light. Moreover, microscopic studies revealed possible novel PIF-mediated nuclear transport mechanisms of phytochromes. For manipulation or control of signaling processes in mammalian and plant cells, we constructed and characterized novel optogenetic tools. While we engineered a blue light-dependent switch for downregulation of exo- and endogenous mRNA levels by expression of the RNA-cleaving CRISPR/Cas13b in different mammalian cells lines, a UV-B activated switch for gene expression in *A. thaliana* mesophyll protoplasts was developed for expanding the, to date, short list of optogenetic tools in plant systems.

This work not only underlines the potential of synthetic biological approaches for deciphering signaling networks and their components, but also indicates their power of opening up a plurality of new perspectives on the design and implementation of novel tools for supporting or upgrading traditional methods.

1 Introduction

Living cells are highly dynamic systems (Lim, 2010). Their fundamental characteristic is the ability to perceive, process and respond to their environment (illustrated in Figure 1.1), in order to fulfill essential physiological functions or to simply survive (Kiel et al., 2010; Lim, 2010; Andres et al., 2019). For the integration of external stimuli, internal molecular signaling networks have evolved, generating changes in gene expression and phenotypic alterations. They underlie a highly spatiotemporal coordination between tissues, cells or even within subcellular compartments (Lim, 2010; Andres et al., 2019). Since signaling is the basis of cellular proliferation, differentiation, migration and stimulation, while defects in these communication cascades can lead to diseases of the organism, the deciphering of signaling pathways is indispensable for many biological fields (Lai, 2004; Vu et al., 2017).

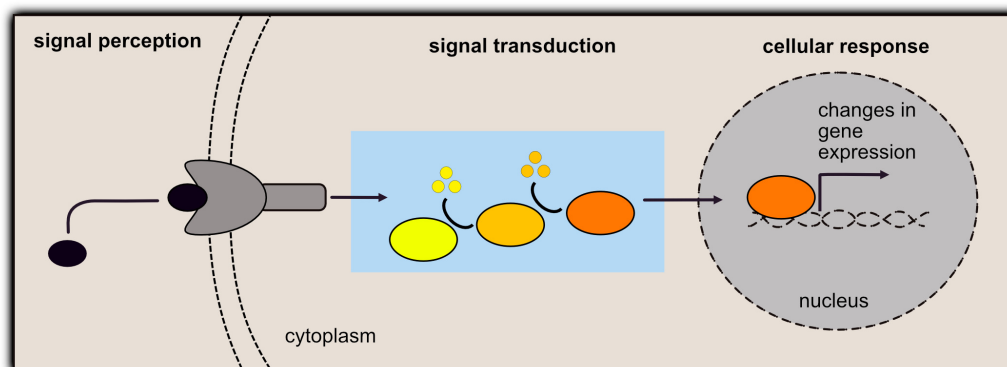


Figure 1.1: Stages of signaling in eukaryotic cells. Living cells are part of highly complex signaling networks. In this connection, cells send and receive a multiplicity of diverse signals. At first signaling molecules from a signaling cell are transported to a target cell and perceived by specific receptors located at the cell surface. Perceived signals are processed and converted to be able to alter the gene expression for enabling a cellular response to the respective signal.

1.1 Plant Signaling

Complexity and synergy of plant signaling networks distribute the needed robustness for responding and adapting to the multiplicity of biotic and abiotic parameters in their sessile life cycle (Casal et al., 2004). Since they are in steady need for integrating these environmental cues in their growth behavior and developmental processes, they have developed a network of highly intertwined signaling pathways. The enormous degree of interaction and feedback between them, as well as a vast level of redundancy of components, fine-tunes their responses with the higher outcome of increased robustness to their surroundings (Koornneef and Pieterse, 2008; Depuydt and Hardtke, 2011; Vanstraelen and Benková, 2012). From the scientific perspective, this interconnection and complexity led to focus on single signals or linear pathways (Sheen, 2010) and impedes our recent understanding of signal perception,

Introduction

processing and transduction (Samodelov and Zurbriggen, 2017) as well as their analysis in plants (unknown interactions, number of components, lack of tools and techniques for quantitative *in vivo* monitoring).

1.1.1 Phytohormones

Plant hormones are typically small, structurally unrelated molecules, conjointly regulating every facet of the plant lifecycle, such as seed germination (Gazzarrini et al., 2015), vegetative growth, flowering (Bernier and Périlleux, 2005), development (Santner et al., 2009; Depuydt and Hardtke, 2011), and responses to their biotic and abiotic environment (Verma et al., 2016). Their activity is strictly regulated at the level of biosynthesis, metabolism and distribution, as well as by the efficiency of its perception and signal transduction, resulting in usually very low concentrations all over the plant with variation between different tissues or developmental stages (Santner et al., 2009; Vanstraelen and Benková, 2012). Adaptation to changes in the plant's environment are often highly connected to changes in plant hormone levels and localization, promoting major adjustments of their transcriptional activity (Santner et al., 2009; Locascio et al., 2013). Modulation in their abundance not only influences its specific pathway, but phytohormone dependent or independent signaling chains, creating a highly connected signaling network (Vanstraelen and Benková, 2012). Research over the last decades helped identifying numerous classes of phytohormones, known as abscisic acid (ABA), auxins (e.g. IAA), brassinosteroids (BRs), cytokinins (CKs), ethylene (ET), gibberellins (GAs), jasmonates (JAs), nitric oxide (NO), salicylic acid (SA) and strigolactones (SLs). Furthermore, knowledge about the processes of phytohormone biosynthesis, the hormone perceiving receptors, as well as their interaction with positive and negative regulator proteins was imparted (Santner et al., 2009). These new findings revealed a similar mechanism of hormone perception and signal transduction between auxins, jasmonates, gibberellins and strigolactones. Recognition of the hormone subsequently triggers binding to transcriptional regulator proteins, inducing its proteasomal degradation and finally the de-repression of the hormone response (Santner et al., 2009). If present, the phytohormone binds either directly to an F-box protein/receptor or an additional co-receptor, which subsequently leads to a complex-formation with the respective downstream response regulator. Auxins and jasmonates are perceived over a two-component perception complex (F-box and regulator protein), with the F-box protein functioning as the receptor, while in case of gibberellins and strigolactones, the hormone is perceived over a co-receptor, creating a three-component perception complex (F-box, co-receptor and regulator protein). Interaction with the F-box protein initiates binding to the highly conserved Skp (Arabidopsis SKP1-related (ASK1))-1-Cullin-F-box (SCF) E3 ubiquitin ligase complex, which mediates ubiquitination of the regulator proteins and finally leads to degradation by the 26S proteasome (Vierstra, 2009; Figure 1.2).

The degraded regulator proteins no longer influence other regulators or transcription factors, initiating the de-repression of downstream signaling events, highly depending on the hormone concentration (Daviere and Achard, 2013).

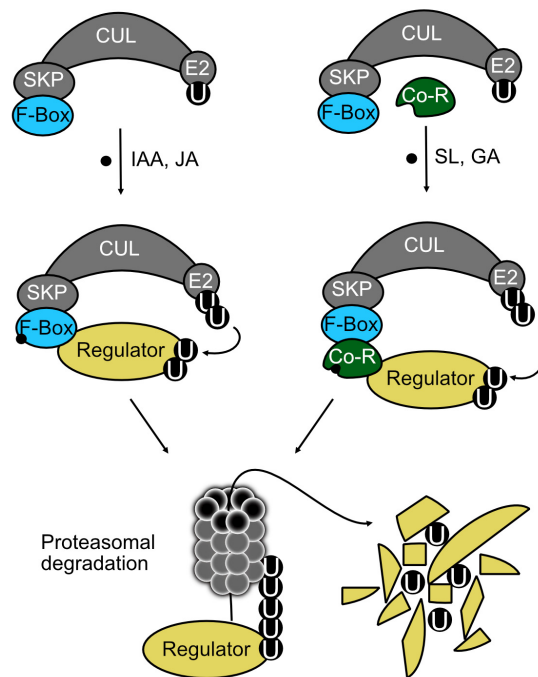


Figure 1.2: Scheme of phytohormone perception machinery and regulator-protein degradation mechanisms in *Arabidopsis thaliana*. The direct phytohormone binding to an F-Box protein of the proteasomal degradation machinery (auxins, jasmonates) or the hormone-triggered association of Co-receptors and F-Box-proteins (strigolactones, gibberellins) generates a higher binding affinity of the SCF E3 ubiquitin ligase complex to a negative regulator protein, inducing polyubiquitination of the regulator, and its subsequent proteasomal degradation (adapted from Samodelov et al., 2016).

1.1.1.1 Gibberellins

Bioactive Gibberellins (GAs) are a class of diterpene phytohormones, responsible for the regulation of a multiplicity of developmental processes like seed germination and plant growth, including leaf expansion and stem elongation (Yamaguchi, 2008; Daviere and Achard, 2013). They are not only present in plants, but are also found in fungi and bacteria, originally described in 1938 in the fungal rice pathogen *Gibberella fujikuroi* (Yabuta and Sumiki, 1938). An increase in wheat and rice yield during the so-called “green revolution” in the 1960s, can be retraced to the introduction of dwarfing traits into plants (Hedden, 2003). The newly cultured plants increased biomass production and possessed an increased resistance to changing weather conditions (Gale and Youssefian, 1985; Evans, 1996). Later identified to impair the effectiveness of GAs, the dwarfing traits were generated by a mutation in the wheat *REDUCED HEIGHT (Rht)* gene. *Rht* encodes for a growth repressor, usually suppressed by GAs, which is an ortholog to one of the *Arabidopsis thaliana* regulators of GA response (Peng et al., 1999). Until now, more than 130 GAs, with only a small number of bioactive forms, have been identified. The large number of non-bioactive GAs is ascribable to most of them being

Introduction

precursors of the bioactive variants, as well as deactivated metabolites. In *A. thaliana*, the major bioactive GAs are GA₁, GA₃, GA₄ and GA₇. Even though GA₁ and GA₄ have been found in a multiplicity of species, assuming them to be comprehensively spread, GA₄ is supposed to be the major bioactive GA variant (Yamaguchi, 2008; Hedden and Thomas, 2012).

GA₁₂ is the common precursor of all bioactive GAs in plants. Originated from the common C₂₀ precursor *trans*-geranylgernyldiphosphate (GGDP), synthesis of bioactive GAs involves three different classes of enzymes, with the final step of 3- β -hydroxylation of the GA-precursors. Through further processing by different oxidases, GA₁₂ is converted into GA₉ or GA₂₀. 3- β -hydroxylation of both by oxidation of their C-3 via the GA3-oxidase (GA3ox) converts GA₉ and GA₂₀ into bioactive GA₄ and GA₁, respectively. Like the mentioned bioactive GAs, GA₃ and GA₇ are likewise biosynthesized from GA₂₀ and GA₉, but with an intermediate step. For generation of GA₃, GA₂₀ is turned into GA₅, before 3- β -hydroxylation converts it into GA₃ (Appleford et al., 2006; Yamaguchi, 2008; Hedden and Thomas, 2012). GA₇ is biosynthesized via GA₉ through its conversion to 2,3-Dihydro-GA₉ and subsequent 3- β -hydroxylation (Farrow and Facchini, 2014). Deactivation of active GAs via 2- β -hydroxylation by GA2-oxidases (GA2ox) is the major catabolic pathway of GAs. This process is highly regulated, enabling the plant to rapidly react to changes in the environment, with adjusting its GA content (Thomas et al., 1999; Appleford et al., 2006).

The already described mechanism of phytohormone signal transduction via targeting transcriptional regulators for proteasome-dependent degradation can also be observed for gibberellins, which are perceived via a three-component perception-complex: Upon GA-perception through the specific receptors GID1a, b and c (GIBBERELLIN INSENSITIVE DWARF1), these receptors undergo a conformational change, enabling the interaction with DELLA regulator-proteins (Sun and Gubler, 2004; Griffiths et al., 2006; Murase et al., 2008). This interaction is followed by a higher affinity of the DELLA-specific F-Box protein SLY1 (SLEEPY1) of the SCF E3 ubiquitin ligase complex to GA-GID-DELLA, targeting them for degradation by the 26S proteasome (McGinnis et al., 2003; Ariizumi et al., 2008; Murase et al., 2008; Ariizumi et al., 2011). Analysis of the crystal structure of the GA-induced GA-GID-DELLA complex deepened the understanding of the mechanism behind the complex formation. GA binds to a specific pocket on GID1. The C3-hydroxyl group of the GA becomes hydrogen bonds to Tyr31 of the GID1, inducing a conformational change of the flexible N-terminal extension of GID1, covering the bound GA (Murase et al., 2008; Shimada et al., 2008). The conformational change subsequently enables binding of the DELLA to the upper surface of the GA-GID1-complex (Griffiths et al., 2006; Ueguchi-Tanaka et al., 2007; Willige et al., 2007) (Figure 1.3 B).

Multiplication of DELLA as well as GID1s in *A. thaliana* has created an immense level of complexity. Today there are three different GA-receptors (GID1a, b and c) known (Nakajima

et al., 2006), as well as five diverse DELLA proteins (GA-INSENSITIVE, GAI; REPRESSOR OF GA1-3, RGA; RGA-LIKE1, RGL1; RGL2 and RGL3) (Dill and Sun, 2001), creating 15 possible interactions, only between these two groups of proteins. Additional to the mentioned F-box protein SLY1, a second F-box protein, called SNEEZY (SNZ) is, even if not as prominent as SLY1, involved in GA-dependent regulation of DELLAs (Ariizumi et al., 2011).

The significant level of redundancy not only facilitates stability to the GA-responses, but also enables distinct functions and affinities of the different components (Suzuki et al., 2009). For example, the three GID1-receptors are largely redundant and show the highest affinity for the biological most relevant gibberellin in *Arabidopsis*, GA₄. Contrary to these observations, they possess exceedingly different expression patterns, spread over different plant organs (Ueguchi-Tanaka et al., 2005; Griffiths et al., 2006; Nakajima et al., 2006; Willige et al., 2007). In addition, they show varying affinities for GA₄ (Nakajima et al., 2006; Suzuki et al., 2009).

DELLA-proteins are part of the plant specific GRAS family of transcriptional regulators (named after the first identified family members GAI, RGA and SCARECROW). Members of this family possess a specific N-terminal GRAS-domain, which distributes the function of transcriptional regulation. DELLAs have two additional N-terminal domains. Both, the DELLA- and the TVHYND-domain are functioning in the transcriptional regulation of the GA-response by mediating the interaction with the N-terminal of the GA-GID1 complex (Silverstone et al., 1998; Peng et al., 1999; Daviere and Achard, 2013) (Figure 1.3 A). The sequential order of complex formation was the objective of former studies in yeast. They indicate the GA-dependent interaction between GID1s and DELLAs as initiation of increased affinity of SCF^{SLY1} the DELLAs, determining the order of complex formation upon GA-perception. Here, a yeast three-hybrid-assay revealed the interaction between RGA and SLY1 only in the presence of GA₃ and the co-expression of GID1a (Griffiths et al., 2006).

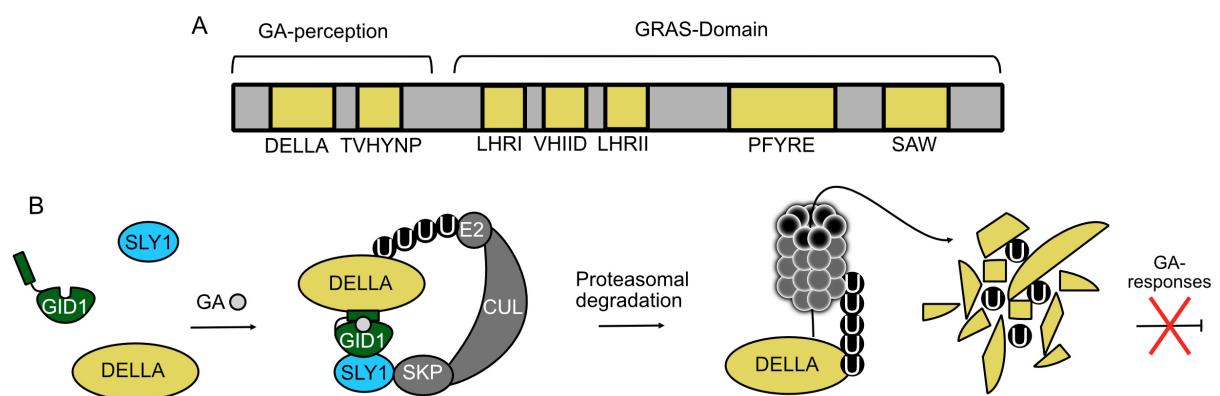


Figure 1.3: Illustration of the gibberellin perception machinery and DELLA-degradation mechanisms in *Arabidopsis*: (A) Schematic overview of the structure of DELLA proteins including the most important domains. (B) Binding of gibberellic acid (GA) to one of the GA-receptors GIBBERELLIN-INSENSITIVE DWARF1 (GID1) a, b or c, enhances the interaction with negative regulator proteins of the DELLA-Family, recruiting the respective DELLA to the F-Box protein SLEEPY (SLY1) of the SCF E3 ubiquitin ligase complex, inducing polyubiquitination of the regulator, and its subsequent proteasomal degradation. Absence of DELLAs prevents them from inhibiting GA-response signaling (Adapted from Daviere and Achard, 2013).

GA takes a major role in the regulation of distinct pathways, through mediation of DELLA degradation (Davière et al., 2008; Locascio et al., 2013; Wang and Deng, 2014). Despite being transcriptional regulators and hubs for integration of different signaling pathways of plant development and stress-responses (Locascio et al., 2013; Marín-de la Rosa et al., 2014), DELLAs lack the typical DNA binding domains. Their influence on transcriptional regulation therefore is mainly mediated through binding to other transcription factors. Their contribution to other signaling networks can be both, stimulating or repressive (Davière and Achard, 2013). On one hand, DELLAs are involved in the cross-talk to other phytohormone response chains by interacting with ARABIDOPSIS RESPONSE REGULATORS (ARRs), which recruit DELLAs to promoters of cytokinin regulated genes (Marín-de la Rosa et al., 2015) or contribute to plant defense by interacting with JASMONATE ZIM-DOMAIN (JAZ) proteins. On the other hand, they integrate hormone and light-signaling by interacting with PHYTOCHROME INTERACTING FACTORS (PIFs) and preventing them from binding to their target promoters (Feng et al., 2008; de Lucas et al., 2008). In total, more than 60 interactors from different regulatory processes have already been identified (Marín-de la Rosa et al., 2014; Marín-de la Rosa et al., 2015).

1.1.2 Light signaling

Because of their sessile way of living, plants are in constant need for adaption to the highly variable light conditions of their environment. Light is not only indispensable for their phototropic energy production, but also the primary abiotic factor for developmental processes and optimal vegetative growth (Klose et al., 2015; Xu et al., 2015). Due to the extraordinary significance of harvesting the energy of light from all wavelengths, plants have developed a complex network of light perception and signal transduction pathways, regulating about 2,500 genes, depending on the diurnal and seasonal duration and color of daylight (Gyula et al., 2003). Through evolution, plants have generated a multiplicity of light perceiving receptors, induced by light from the majority of wavelengths. UVR8 (UV-B RESISTANCE8) perceives UV-B-, cryptochromes, phototropins, zeitlupes cover blue and UV-A-wavelengths, while phytochromes recognize red and far-red light (Galvão and Fankhauser, 2015; Christie and Zurbriggen, 2020; Figure 1.4 A).

Introduction

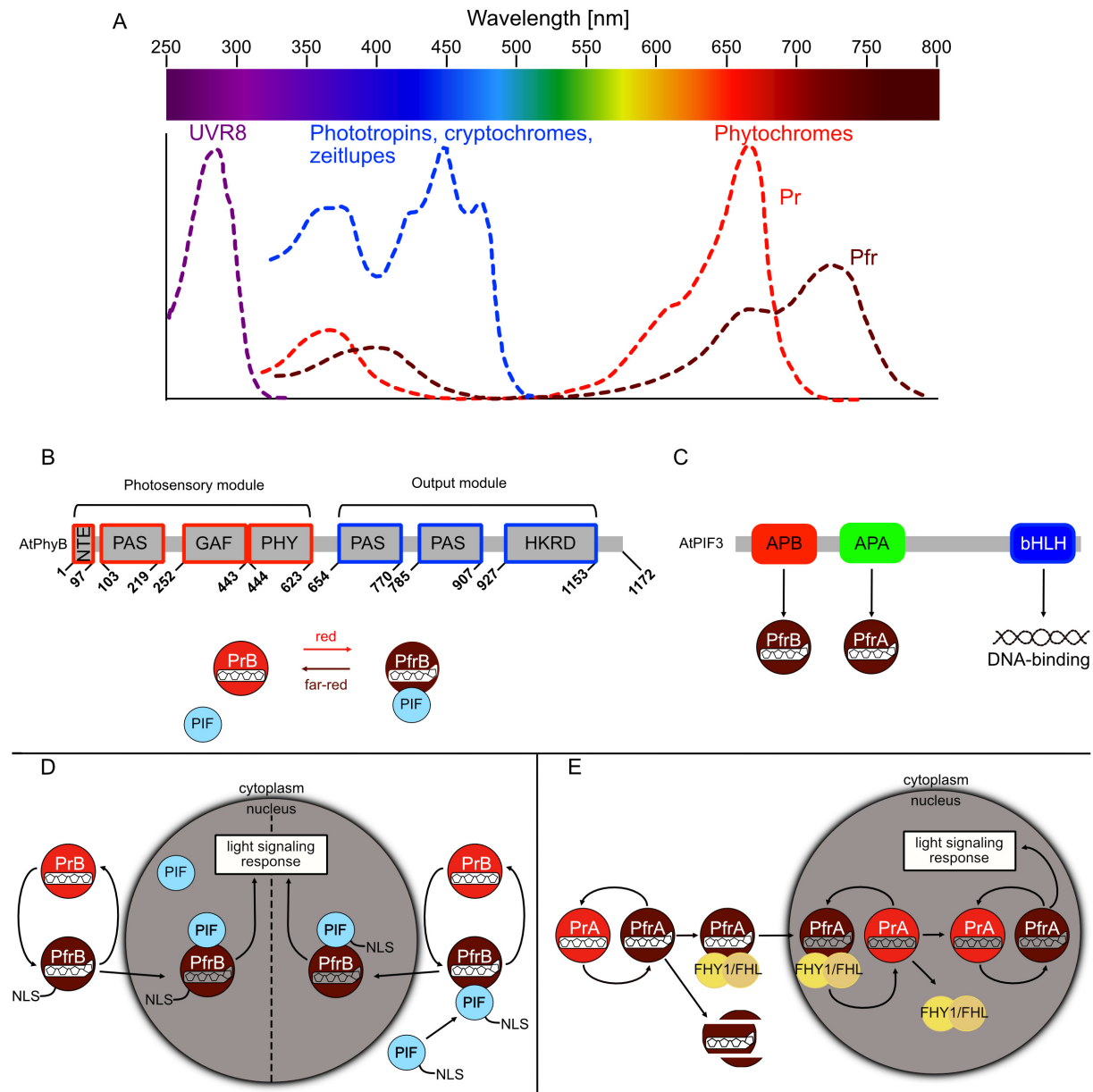


Figure 1.4: Overview of *Arabidopsis thaliana* photoreceptors with detailed information about phytochrome signaling and involved components. (A) Light perception by photosensory receptors. *A. thaliana* possesses specialized receptors for perception of light wavelengths from UV (UVR8) to blue light (phototropins, zeatolopes, cryptochromes) to red and far-red (phytochromes) (adapted from Christie and Zurbriggen, 2020). **(B)** Schematic overview of the phytochrome B domain architecture and its light-dependent interaction with PIFs. phyB consists out of an N-terminal photosensory module with an N-terminal extension (NTE) (red) a C-terminal output module (blue). Function of the respective domains are described in part 1.1.2.1 (adapted from Bae and Choi, 2008). While the non-active PrB-conformer is not able to interact with PIFs, the red light-dependent conformational change to its biological active PfrB form induces this interaction. Irradiation of far red light reverts the conformational change back to PrB and aborts interaction with PIFs. **(C)** Illustration of the bHLH-transcription factor PIF3 and its most important domains. PIF3 possesses an N-terminal active phytochrome B binding domain (APB) and an active phytochrome binding domain (APA) which mediate interaction with the active Pfr-conformer of phyB and phyA, respectively. The family specific bHLH-domain is essential for binding to G- and PBE-box elements of target genes (adapted from Leivar and Quail, 2011). **(D)** Possible nuclear transport mechanisms of phyB. The first mechanism postulates phyB itself has a caged NLS, which is exposed after red light-induced photoconversion to the biological active PfrB conformer. Interaction with transcription factors like PIFs takes place after its migration to the nucleus, inducing light signaling responses (left). The second mechanism acts on the assumption of cytosolic interaction of PIFs and the biological active Pfr conformer. Mediated by the NLS of PIFs, the heterodimer out of phyB and PIF migrates to the nucleus and activates light signaling responses (right). **(E)** Nuclear migration mechanism of phyA. Red light induces the photoconversion of the inactive PrA conformer to the biologically active PfrA form. Cytosolic interaction with the NLS-bearing functional homologues FHY1/FHL mediates the nuclear migration of the complex. After nuclear translocation, the induction of phyA-dependent light signaling responses depends on far red light-induced reconversion to PrA initiating dissociation of PrA from FHY1/FHL and a second red light-induced conversion to PfrA for initiation of phyA-dependent downstream signaling events (adapted from Rausenberger et al., 2011).

1.1.2.1 Plant phytochromes

Plant phytochromes are red- and far-red light perceiving photoreceptors from the phytochrome family, not only found in plants, but also in fungi, cyanobacteria and purple and non-photosynthetic bacteria (Montgomery and Lagarias, 2002; Blumenstein et al., 2005; Froehlich et al., 2005). Consisting of 5 members, *Arabidopsis thaliana* phytochrome (phy) A-E promote photomorphogenic development of the plant (Jiao et al., 2007). Next to the typical three homologous domains (P2/PAS, P3/GAF, P4/PHY) they possess an amino-terminal extension (P1/NTE) in the photosensory module (PSM) as well as two additional PAS-domains, upstream of the carboxy-terminal, non-functional, histidine kinase-related domain (HKRD) (Bae and Choi, 2008; Burgie and Vierstra, 2014) (Figure 1.4 B). Among these domains, the PAS and the GAF domains occur in other protein families. As an example, the photosensory LOV-domain of the UV-A and blue light perceiving phototropin photoreceptors is a GAF domain (Fedorov et al., 2003).

Plant phytochromes are synthesized as dimers of their inactive Pr form in the cytoplasm, with each subunit covalently bound to a linear tetrapyrrole phytochromobilin P Φ B (Gyula et al., 2003). Here, the lyase activity of the PAS domain mediates binding of the chromophore to a specific cysteine of the GAF-domain. Exposure to red light, induces a Z-E photoisomerization of P Φ B (Sineshchekov, 1995; Gartner and Braslavsky, 2003), initiating an allosteric conformational change from the biologically inactive red light absorbing Pr- and the bioactive far-red light absorbing Pfr-conformation of the whole protein (Fischer et al., 2005; Rockwell et al., 2006). In contrast, irradiation of far-red wavelengths or thermal relaxation in darkness (dark reversion), reverts the conformation change (Furuya and Schäfer, 1996). Hence, interaction with the chromophore awards distinctive absorption spectra in a reversible manner. Absorption spectra of both conformations, with maxima at 660 nm (Pr) and 740 nm (Pfr), partially overlap, resulting in an interconvertible, dynamic photoequilibrium, dictated by light intensity and wavelength (Rockwell et al., 2006).

Because of varying physiological and spectrophotometric properties, the five phytochromes are categorized into “light liable” (Type I) or “light stable” (Type II) (Sharrock and Quail, 1989; Fernández et al., 2005). Only phyA is assigned to type I and is responsible for responses to very low fluence rates of light (VLFR) or high fluence rates of continuous far-red irradiation (far-red – high irradiance response, FR-HIR). The four other phytochromes share a wavelength dependent low fluence response (LFR), previously described as a “light switch”: Perception of R (red light) induces signaling, whereas FR (far-red light) immediately blocks signal transduction, in a reversible manner (Yanovsky et al., 1997; Casal et al., 2003). phyA as only type I phytochrome and phyB hold a superior role in the entirety of physiological responses to R and FR, turning them into the best characterized family members over the last decades

(Franklin and Quail, 2010). Even though both possess similar photobiological characteristics, phyA mainly controls FR responses, while phyB demonstrates R induced control of gene transcription. Since the light-dependent nuclear translocation of phys is crucial for signal transduction, their divergent role in relaying R and FR responses might be explained by dissimilar downstream regulation of both (Van Buskirk et al., 2012).

Nuclear allocation of phys is restricted to subnuclear clusters, called nuclear speckles/bodies (NBs), with size and number being highly dependent on quality and quantity of light (Kircher et al., 1999; Yamaguchi et al., 1999; Kircher et al., 2002; Chen et al., 2003; Chen and Chory, 2011). Generation of NBs is essential for photomorphogenic development, referred to being site for many processes like degradation and regulation of activity of transcriptional regulators, as well as storage site for active PfrB, minimizing its reversion (Rausenberger et al., 2010; Ádám et al., 2011; Chen and Chory, 2011; Van Buskirk et al., 2012).

1.1.2.2 Phytochrome A

As the only type I phytochrome, phyA plays a significant role for mediating HIRs under FR-enriched light conditions, like the de-etiolation of seedlings in dense plant canopies (Yanovsky et al., 1995). PhyA mutants lack the ability of reacting to HIRs, indicating its significance under these light conditions (Shinomura et al., 2000). The previously described light-switchable activation of type II phytochromes is not easily transferable to phyA: In darkness, phyA is located in the cytoplasm (Bae and Choi, 2008) and phyA-mediated light-responses substantially depend on nucleo-cytoplasmic shuttling. This process is essentially driven by interaction with the two functional homologous FAR-RED ELONGATED HYPOCOTYL1 (FHY1) and FHY1-LIKE (FHL). Both bear an efficient nuclear import sequence (NLS), a nuclear export signal (NES) and a phytochrome A binding domain (Zeidler et al., 2004; Hiltbrunner et al., 2005; Hiltbrunner et al., 2006; Genoud et al., 2008). The fact, that the detected phyA-level in FR-treated seedlings, by far exceeded the quantity of available FHY1/FHL, underlines the importance of cycling of both transport-mediating proteins for the “piggy-back” mechanism of phyA nuclear transport (Genoud et al., 2008). Overall, phyA activity involves nuclear transport, mediated by FHY1/FHL under R, followed by a FR-dependent cleavage of interaction with FHY/FHL, preventing inhibitory function of both, and a subsequent second R induced conformational change to PfrA for activating its nuclear activity (Figure 1.4 E). This activation mechanism, together with strong degradation of PfrA in the nucleus, is sufficient for shifting the peak of phyA activity from R to FR (Rausenberger et al., 2011). Unlike type II phytochromes phyA appears only in homodimers and does not stably dimerize with other phytochromes (Liu and Sharrock, 2017).

1.1.2.3 Phytochrome B

PhyB is the physiologically predominant type II phytochrome, involved in germination, development of seedlings and mediates shade avoidance responses (Casal, 2013).

Under dark conditions it is, similar to phyA, localized in the cytosol. phyB-mediated signaling involves R induced photoconversion, essential for subsequent nuclear transport and accumulation of the bioactive PfrB. FR irradiation of thermal relaxation reverts PfrB back to the non-active PrB conformer (Kircher et al., 1999). Compared to phyA, the nuclear transport of phyB is independent of FHY1/FHL and less precisely understood (Hiltbrunner et al., 2006). To make things even more complicated, heterodimerization of members of type II phys, impedes observation of the single variants (Clack et al., 2009). One possible mechanism of nuclear transport of phyB postulates an N-terminal intrinsic NLS, exposed by R-induced photoconversion (Sakamoto and Nagatani, 1996; Matsushita et al., 2003; Chen et al., 2005). Although the transport sequence has never been confirmed, it took until 2012, when Pfeiffer et al. demonstrated a PIF3-mediated mechanism *in vitro*, later confirmed *in vivo* in orthogonal mammalian cell systems (Beyer et al., 2015a). This model describes a R-dependent cytosolic interaction of PIF3 with PfrB and subsequent nuclear transport of the complex, enlarging the role of PIFs from important component of phyB-dependent signaling to facilitating its nuclear translocation (Figure 1.4 D). Alongside with the R-dependent interaction of PIF3 (Figure 1.4 B), interaction of one or both conformers with different NLS-containing proteins have been monitored, explaining why phyB is never fully extinct from the nucleus, even in darkness (Yeom et al., 2014; Huang et al., 2016). Thermal reversion of phyB highly depends on temperature, expanding the role of phyB as a R/FR-light sensor to a temperature sensing protein (Jung et al., 2016; Legris et al., 2016; Viczián et al., 2020).

1.1.2.4 Phytochrome C-E

Roles and functions of phyC-E in R/FR light responses and photomorphogenic signaling are minor to phyA and phyB (Kircher et al., 2002). To date, there are only a few experimental observations, describing their behavior and function, with partially controversial results. In 2001, Nagy et al. postulated their nuclear import might be, as opposed to phyA and B, light-independent, while nuclear body formation was strictly observed in R. Contrary, another analysis described the nuclear import of all phytochromes to be regulated by “light-quality and quantity” (Kircher et al., 2002). Until now, evidence for the mechanism of their nuclear transport has not been found. In case of phyE, it was reported that homodimers are transported at very low fluences of light, which are usually perceived by phyA. Despite the similarity, this transport

was independent of FHY1/FHL (Ádám et al., 2013). The independent observation that phyE does not bind PIFs, suggests an unknown transport mechanism (Klose et al., 2015). Nevertheless it is necessary for phyA-mediated induction of seed germination under continuous irradiation of FR (Hennig et al., 2002). The three less described type II phytochromes tend to heterodimerize with phyB (Clack et al., 2009), impeding observation of their individual protein dynamics. While phyC and phyD were also found in homodimers, overexpression of phyE indicated its homodimerization in absence of phyB and D. Heterodimerization with phyB seems to be essential for the functionality of phyC, whereas the nuclear accumulation of phyD occurs independent of light in a phyB lacking background (Ádám et al., 2013). In a phyB mutant background, the remaining type II phys appear to have relevant roles in mediating seed germination and might fine-tune responses primary regulated by phyB (Arana et al., 2014). The members generated diverse functions in seed germination in relation to diverse light (Casal and Sánchez, 1998) and temperature (Heschel et al., 2007; Donohue et al., 2008; Heschel et al., 2008) conditions. Generally, the diversification of phys distributes precise responses to the environmental conditions (Martel et al., 2018).

1.1.2.5 Role of phytochrome-PIF interaction

Phytochrome interacting factors (PIFs) are part of the bHLH superfamily of transcription factors (Toledo-Ortiz et al., 2003), defined by a characteristic bHLH domain (Murre et al., 1989; Murre et al., 1994) (Figure 1.4 C). In general, proteins of this superfamily are hubs for regulation of a multiplicity of developmental processes (Massari and Murre, 2000; Leivar and Monte, 2014). In *A. thaliana*, the family of PIFs consists out of 8 members (PIF1-8) with partially variable but mostly redundant functions. They bind specific G- and PBE-box motifs of DNA through their bHLH-domain, modify gene expression and promote skotomorphogenesis (Martínez-García et al., 2000; Toledo-Ortiz et al., 2003; Al-Sady et al., 2008; Li et al., 2012; Zhang et al., 2013; Huang et al., 2018; Zhang et al., 2020). Therefore, interaction of PIFs and phytochromes is a fundamental process for repressing skotomorphogenesis and promoting photomorphogenesis (Franklin and Quail, 2010). All PIFs have at least one or both N-terminal active phytochrome B-binding (APB)- and/or active phytochrome A-binding (APA)-domains, necessary and sufficient for interaction with phys (Zhu et al., 2000; Khanna et al., 2004; Al-Sady et al., 2006; Shen et al., 2008; Leivar and Monte, 2014), appearing with varying affinities (Khanna et al., 2004; Castillon et al., 2007; Leivar and Quail, 2011). Among the PIFs, only PIF1 and PIF3 possess both domains (Ni et al., 1998; Ni et al., 1999; Zhu et al., 2000; Huq, 2004), whereas PIF2, 4-8 only have the APB domain (Huq and Quail, 2002; Khanna et al., 2004; Leivar et al., 2008; Luo et al., 2014). While for all PIFs, interactions with either phyA and/or phyB have been confirmed (Leivar and Quail, 2011; Lee and Choi, 2017), interaction of PIF8 and phyB was not confirmed until 2020. Even though it does not possess an APA, little evidence for binding of

Introduction

phyA was demonstrated (Oh et al., 2020). The physical interaction with phyB was shown to eliminate PIF1 and 3 from a specific promoter, repressing their transcriptional activation (Park et al., 2012). Furthermore, it initiates phosphorylation and subsequent ubiquitination and degradation of PIFs, promoting photomorphogenesis (Al-Sady et al., 2006; Lorrain et al., 2008; Shen et al., 2008; Leivar and Quail, 2011; Ni et al., 2014).

To date, it is still unclear whether other members of the PIF family are involved in the nuclear transport of phyB (Lee and Choi, 2017). Since the nuclear translocation of phyB is a crucial step for their signal transduction of responses to R and FR light, the investigation of this mechanism and identification of involved components, as in this study, is of immense relevance.

1.2 Synthetic biology

A multitude of groundbreaking findings in modern cell biology over the last decades equipped scientists with an extraordinary understanding of cellular signaling and the influence of external stimuli on cell fate and properties (Pryciak, 2009). Beyond understanding and deciphering linear signaling pathways and their conjunction to complex signaling networks, the advancing identification and characterization of key components led to highly novel approaches of rearranging and combining these elements into completely novel, custom-made synthetic signaling circuits (Pryciak, 2009; Kiel et al., 2010; Lim, 2010). The fundamental idea of the discipline, nowadays referred to as “synthetic biology” is stated back to Jacob and Monod and their description of the lac operon (Jacob and Monod, 1961b). Further, they postulated genetic regulatory networks, as they envisioned the possibility of remodeling regulatory components into new systems (Jacob and Monod, 1961a). Realization of these ideas, was achieved as recently as the beginning of this century (Cameron et al., 2014). After decades of identification and characterization of building blocks, the first simple regulatory circuits, implementing the concepts of electrical engineering, were created. Guided by the pioneering works on the first genetic toggle-switch (Gardner et al., 2000), an oscillating circuit of transcriptional regulation (Elowitz and Leibler, 2000) and autoregulatory gene networks (Becskei and Serrano, 2000) in bacteria, the concepts and ideas were adapted to mammalian and other eukaryotic systems. A crucial step for the development of synthetic circuits, was the construction of the first inducible synthetic gene switch in mammalian cells, adapted from the tetracycline regulated promoter of *E. coli*. A chimeric transcription factor, combining the DNA-binding tetracycline repressor (TetR) and the transcriptional activation domain VP16 from *Herpes simplex*, in combination with the appendant tetO operator motif, in close proximity to a minimal promoter, binding of TetR-VP16 induces the tetracycline-dependent expression of a downstream gene (Gossen and Bujard, 1992). Following studies even showed, the combination of various bacterial regulators (TetR, Pristinmycin repressor, Pip; macrolide repressor, E) fused to transactivation or the eukaryotic Krüppel associated box (KRAB) transrepressor domain, generating transcription control based on boolean logic gates (Kramer et al., 2004). Following these simple molecular engineering principles (illustrated in Figure 1.5), many chemical inducible switches were developed for mammalian cells (Hörner and Weber, 2012). Further, quantitative characterization of the used building blocks, as well as implementation of mathematical modeling, helped optimizing synthetic gene switches for tailored operation within their respective applications (Andres et al., 2019). Today, the field of synthetic biology offers a large tool box of applications from the modification or recombination of existing genetic elements, to the rebuilding of sensitive and complex biological circuits such as signaling pathways in orthogonal systems isolated from their native context (Lienert et al., 2014).

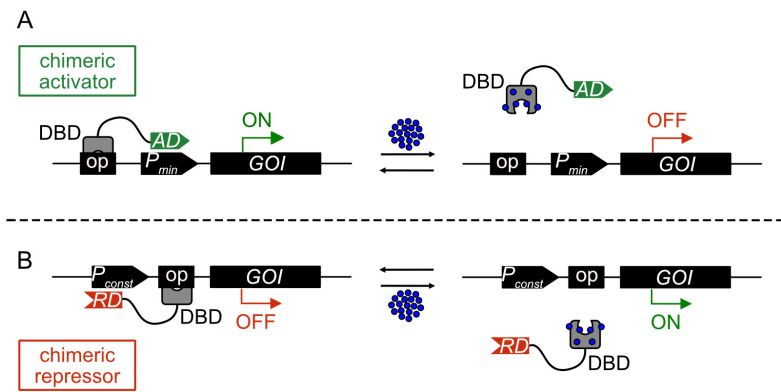


Figure 1.5: Scheme of the configuration and function of chimeric transcriptional regulators. (A) Transcriptional activator. A chimeric transcriptional activator consists out of a DNA-binding domain (DBD) fused to transcriptional activation domain (AD). Mediated by the DBD it binds to its cognate operator site (op) in close proximity to a minimal promoter (P_{min}) and activates expression of the gene of interest (GOI). Supplementation of small molecules (e.g. antibiotics like tetracycline in case of choice of TetR as DBD) removes the chimeric activator from its operator site and switches off the gene expression. **(B)** Transcriptional repressor. Contrary to (A), the DBD is fused to a repressor domain (RD) and the minimal promoter is exchanged by a constitutively active promoter (P_{const}). Binding to the operator site creates a close proximity of the promoter and the repressor domain, which inhibits the transcription of the GOI. In presence of the mentioned small molecules, the chimeric repressor dissociates from the operator site and no longer represses the expression of the GOI.

1.2.1 Application of CRISPR/Cas systems for genetic modification

The discovery of restriction enzymes, a class of prokaryotic endonucleases with the ability of cleaving DNA into fragments at specific restriction sites, marks a meaningful milestone for gene editing (Danna and Nathans, 1971), placing the fundament for a plurality of DNA-modifying tools developed since then (Pickar-Oliver and Gersbach, 2019). More recently, Zinc-finger nucleases (ZFNs), transcription activator-like effector nucleases (TALENs) and the RNA-guided clustered regularly interspaced short palindromic repeats – CRISPR associated (CRISPR-Cas) nucleases were, among others, the first described programmable DNA-modifying tools. Target recognition of TALENs and ZFNs depends on their DNA-binding domain. Therefore, engineering for pairing with custom DNA-sequences highly involves protein-engineering, increasing the level of complexity of generating modular DNA-modification (Chandrasegaran and Carroll, 2016; Pickar-Oliver and Gersbach, 2019). Lacking the need of protein engineering for targeting DNA anywhere in the sequence, CRISPR-Cas nucleases have revolutionized genetic engineering. It binds DNA depending on single guide RNAs (sgRNA), pairing with the sequence of choice (Marraffini, 2015; Pickar-Oliver and Gersbach, 2019). After discovery of the CRISPR-Cas system, with the type II Cas9 from *Streptococcus pyogenes* as the most prominent one, the identification of several other Cas-variants derived from a multiplicity of microorganisms led to development of multifaceted Cas-based systems with application ranging from fundamental science to medicine (Hsu et al., 2014; Fellmann et al., 2017). Alongside with adaption for functionality in the most relevant model organisms, a catalytically inactive Cas9 version (dead Cas9, dCas9) enabled a new

Introduction

level of customized RNA-guided manipulation of transcription by fusing it to positive or negative effector domains (Gilbert et al., 2013; Qi et al., 2013). Further, Cas-variants targeting RNA instead of DNA have been discovered, expanding the toolbox of CRISPR-Cas dependent genetic modification to the level of translation (Cox et al., 2017; Strutt et al., 2018). Amid those, Cas13 proteins utilize precise knockdown or modification of RNAs in mammalian or bacterial cell systems (Abudayyeh et al., 2016; Cox et al., 2017; Strutt et al., 2018). They are part of the type VI CRISPR effector family and, contrary to Cas9, function independent of short protospacer adjacent motif (PAM) sequences at the target site (Cox et al., 2017; Strutt et al., 2018).

1.2.2 Optogenetics

Despite their broad application and fundamental role in origin of the discipline of synthetic biology (Khalil and Collins, 2010), gene switches, based on chemical induction, have some crucial draw-backs in terms of spatiotemporal resolution, diffusion and toxicity of the inducer, as well as slow, mostly non-reversible induction kinetics (Müller et al., 2015). Subsequent to the discovery of microbial opsins and the introduction of the first light-controlled ion channel, channelrhodopsin, into mammalian neurons, a new discipline, later known as optogenetics, was established (Deisseroth et al., 2006; Hegemann and Möglich, 2011; Deisseroth, 2015). Beyond revolutionizing neuroscience in the early 2000s, nowadays the toolbox of genetically encoded, light-regulated proteins, switches and other tools based on plant and bacterial-derived photoreceptors ranges from UV-B to far-red wavelengths activated variants, controlling a multitude of processes in bacteria, fungi, animal or plant systems reviewed elsewhere (Beyer et al., 2015b; Fan and Lin, 2015; Müller et al., 2015; Kolar and Weber, 2017; Salinas et al., 2017; Kolar et al., 2018; Liu et al., 2018; Krueger et al., 2019). Compared to chemical inducers, light as an input offers a tight quantitative control with minimized invasiveness and superb control of spatiotemporal induction (Andres et al., 2019).

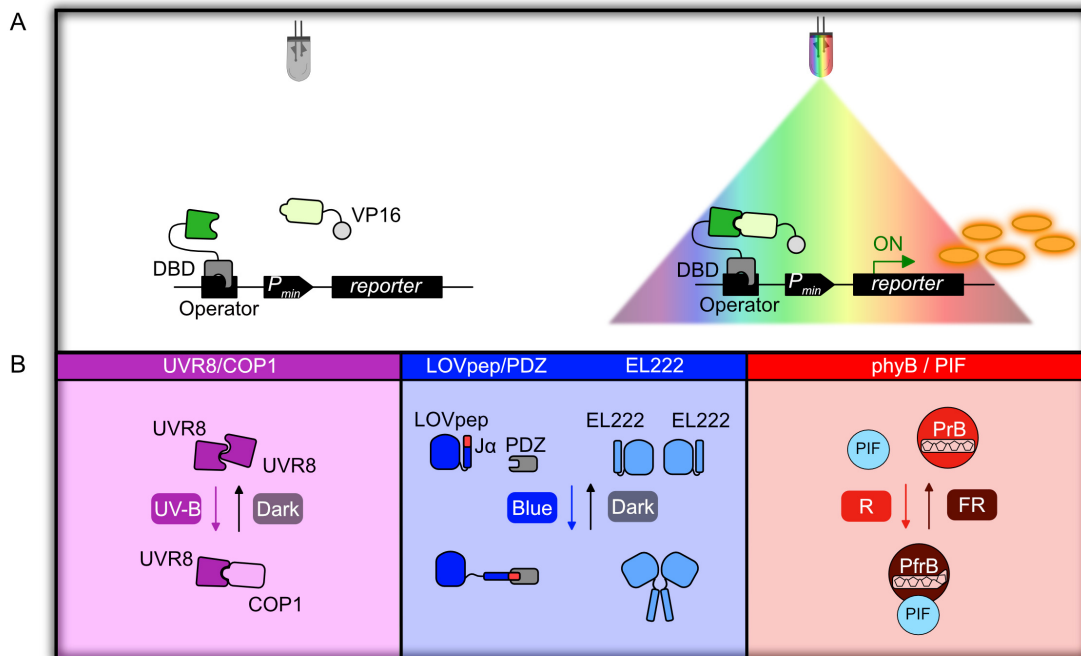


Figure 1.6: Illustration of the general principle of an optogenetic “light-switch” for transcriptional activation and switches used in the frame of this thesis. (A) Schematic overview of the general configuration of an optogenetic switch for transcriptional activation. One part of the split-transcription factor consists out of a DNA-binding domain (DBD) fused to one of the two light-dependent interaction partners. Mediated by the DBD it binds to its cognate operator site (op) in close proximity to a minimal promoter (P_{min}), without being able to activate gene expression. The other interaction partner is fused to a transcriptional activation domain (AD) and compiles the other half of the split transcription factor. Exposure to light of a specific wavelength (depending on the used light-responsive elements), leads to complex formation of the split transcription factor and induces a close proximity of the AD and the minimal promoter, recruiting the transcriptional machinery and subsequently activates gene expression. Depending on the used components, complex formation can revert in the dark or be reverted by exposure to another wavelength of light, resulting in the dissociation of the complex and termination of gene expression. **(B)** Illustration of the function of the “light-switches” used in the frame of this thesis. In the dark, UVR8 homodimerizes. Illumination with light of UV-B wavelengths, leads to dissociation of the homodimers and induces heterodimerization with COP1 (For the optogenetic switch in chapter 3.2.2. a truncated version of COP1, consisting out of its WD40-domain was used) (left). One part of the split transcription factor, a modified light-oxygen-voltage domain from phototropin 1 of *Avena sativa* (AsLOV2), harbors a C-term epitope tag, which is covered by the folded $J\alpha$ -Helix in darkness. Upon illumination with blue light, the $J\alpha$ -Helix unwinds. The now exposed tag enables recruitment of ePDZ (adapted from Blomeier et al., 2021a). EL222 is a blue-light sensitive transcription factor from the gram-negative bacterium *Erythrobacter litoralis*, consisting out of a light-sensitive LOV2- and a DNA-binding helix-turn-helix (HTH) domain. Under dark conditions, the HTH is attached to the LOV domain. Exposure to blue light disrupts the interaction of the HTH and the LOV domain and exposes the HTH. Now, EL222 is able to homodimerize and bind to a specific C120-DNA motif (Nash et al., 2011) (middle). In darkness, the non-active PrB-conformer is not able to interact with PIFs. Red light-dependent conformational change to its biological active PfrB form induces the interaction with PIFs. Irradiation of far red light reverts the conformational change back to PrB and aborts interaction with PIFs (right).

1.2.2.1 Optogenetic switches in mammalian cells

Due to the fact that light is an dispensable factor for growth of mammalian cells, application of optogenetic tools in mammalian cells led to development of a multitude of systems controlling processes ranging from gene expression, genome engineering, subcellular translocation of proteins, or even whole organelles, to manipulation of protein or RNA stability and kinase or receptor activity (Kolar and Weber, 2017). On the level of gene expression control, optogenetic switches are mostly based on the “two hybrid principle” of recruiting a transcriptional activation or repression domain to a DNA-bound protein (Figure 1.6). Here, specific light stimuli elicit structural reorganization of the components leading to homo- or hetero-association or dissociation of two components (Kolar and Weber, 2017). Expression or reconstitution of split

variants of DNA-modifying tools like CRISPR/Cas (as presented in chapter 1.2.1) under the control of optogenetic switches, genomic engineering or transcriptional activation of any gene of choice can be controlled by stimuli of light (Koner mann et al., 2013; Nihongaki et al., 2015; Polstein and Gersbach, 2015; Nihongaki et al., 2017; Bubeck et al., 2018; Zhou et al., 2018; Chen et al., 2020; Yu et al., 2020). Contrary to DNA-directed tools, only a small number of light-regulated RNA-targeting tools for controlling RNA localization or levels have been developed until now (Blomeier et al., 2021; Vogel et al., 2017; Weber et al., 2019; Kim et al., 2020; Pilsl et al., 2020).

1.2.2.2 Optogenetics in plants

Continuous exposure to light is essentially anchored into the life cycle of plants. Indispensability of illumination impedes the simple adaption of optogenetic tools, developed for application in other organisms. Hence, the list of synthetic light-controlled approaches is relatively short. The design of optogenetic tools for experimental use in plant systems demands sophisticated engineering, avoiding activation by wavelengths essential for plant growth in growth chambers and interference with the endogenous photosynthetic circuitry or light-triggered signal transduction (Andres et al., 2019; Christie and Zurbriggen, 2020). For a limited range of time, for example for transient transformation as a preliminary step for testing functionality of developed systems, plants or plant cells can be kept in darkness. Contrary, stable transformation for expression of the required components, is a very time-demanding process with the unavoidable need for light (Andres et al., 2019; Ochoa-Fernandez et al., 2020). Compared to the short alternation of generations in bacterial, yeast or mammalian systems, the slower characteristics of plant reproduction decelerates implementation and characterization of tools in plants (Andres et al., 2019).

Despite the mentioned obstacles, several optogenetic systems for application in plants or plant cell systems, following varying strategies to achieve orthogonality to endogenous plant signaling, have been developed in the last decade (Christie and Zurbriggen, 2020): The first described tool in *A. thaliana* mesophyll protoplasts is based on the R activated and FR deactivated phyB-PIF6 system. Supplementation of low intensities of FR to the ambient light of greenhouses or grow chambers provides repression of the system, while exposure to R activates gene expression (Müller et al., 2014b; Ochoa-Fernandez et al., 2016). PULSE (plant usable light-switch elements), a recently published tool combines two different light-inducible switches for enabling optogenetic control of gene expression, even under ambient white light conditions (Ochoa-Fernandez et al., 2020). It combines the R-inducible phyB-PIF6 switch for gene expression (red on module) with a blue light-inducible repressor, based on the bacterial photosensitive EL222 DNA-binding protein (blue off module). This combination of switches allows gene expression exclusively under irradiation of R, while it remains inactive in white

light or darkness. Besides the characterization in *A. thaliana* protoplasts, functionality of PULSE was demonstrated in transgenic plants. Another approach uses the bacterial-derived green light-sensitive photoreceptor CarH in *A. thaliana* protoplast (Chatelle et al., 2018), minimizing interference with plant photoreceptors, which usually have marginal activity at this range of the light spectrum. Being inactivated by green light and only active in the dark, the characteristics of the system are not substantially influenced by standardized growth conditions. A drawback of the system is the need for supplementation of the chromophore (AdoB12), which might impede *in vivo* application, especially in full plants (Christie and Zurbriggen, 2020; Ochoa-Fernandez et al., 2020). Applying orthogonal tools to already light-dependent processes, can be a strategy for optimizing endogenous physiological signaling. The BLINK1 system comprises a synthetic, blue light-gated K^+ channel, modifying K^+ flux in stomatal guard cells for accelerated kinetics of the stomatal aperture (Papanatsiou et al., 2019). Overall, BLINK1 improved gas exchange, water usage and biomass production compared to wild type plants. Further, another approach of optogenetically manipulating ion fluxes in plants was achieved by introducing the first opsin-based tool into plant cells. Study of the blue light-dependent membrane depolarization by channelrhodopsin2 (ChR2), identified the plant plasma membrane H^+ -ATPase to hold a major role in controlling repolarization of membrane potential during plant electrical signaling (Reyer et al., 2020). However, alongside with blue light, activity of ChR2 depends on addition of the co-factor retinal, hindering the *in vivo* application of the tool. Recently, Zhou et al. solved this problem by implementing the *in planta* production of retinal (Urquiza-Garcia and Zurbriggen, 2021; Zhou et al., 2021b). Moreover, they extended the channelrhodopsin-based toolbox for application in plants by engineering additional channelrhodopsins with shifted absorption spectra or induction kinetics (Zhou et al., 2021a).

1.2.3 Study of plant signaling in the orthogonal system of mammalian cells

Ideally, protein behavior and interactions are analyzed in their endogenous organism under the control of the proteins own promoters, highly benefiting from the availability of their natural environment and (interaction) context (Stynen et al., 2012). Nevertheless, the indispensable complexity and redundancy of plant signaling networks (described in chapter 1.1), hampers the isolated study of single proteins and selected interactions (Samodelov and Zurbriggen, 2017). One common approach of creating orthogonality but sticking to a plant-based system, is the transient expression of proteins in evolutionary distant plants like *Nicotiana bethamiana* leaves, followed by protein extraction and immunoprecipitation (Muñoz and Castellano, 2018), fluorescence-based techniques such as biomolecular fluorescence complementation (BiFC) (Walter et al., 2004) or Förster resonance energy transfer (FRET) (Stahl et al., 2013; Weidtkamp-Peters and Stahl, 2017; Long et al., 2018). However, plant systems might still

possess many homologous or genetically related proteins. The most extensively applied *in vivo* platforms for analyzing plant protein-protein-interactions (PPIs) are orthogonal yeast-two-hybrid (Y2H) approaches (Matiolli and Melotto, 2018).

Compared to *in vitro* or other heterologous *in vivo* systems like Y2H, mammalian cells mimic the natural cellular environment of the monitored plant-originated processes more closely in many cases, because conserved post translational modification of proteins or the presence of co-factors, reduces the occurrence of false positive results (Fiebitz et al., 2008; Hou et al., 2011; Beyer et al., 2015a). The application of mammalian cells as an orthogonal system for the synthetic construction of gene networks has progressively gained interest in recent research. A plurality of tools controlling cellular processes has been developed (Weber and Fussenegger, 2010) and many approaches for the heterologous, orthogonal reconstruction and analysis of complex plant signaling pathways in a simplified, optimized environment have been generated (Wend et al., 2013; Beyer et al., 2015a; Abbas et al., 2018; Blanco-Touriñán et al., 2020; Gratz et al., 2020). They may only provide the step-by-step-analysis of isolated components in initial studies, but can possibly facilitate the sharpening of today's knowledge of plant signaling pathways as a whole (illustrated in Figure 1.7).

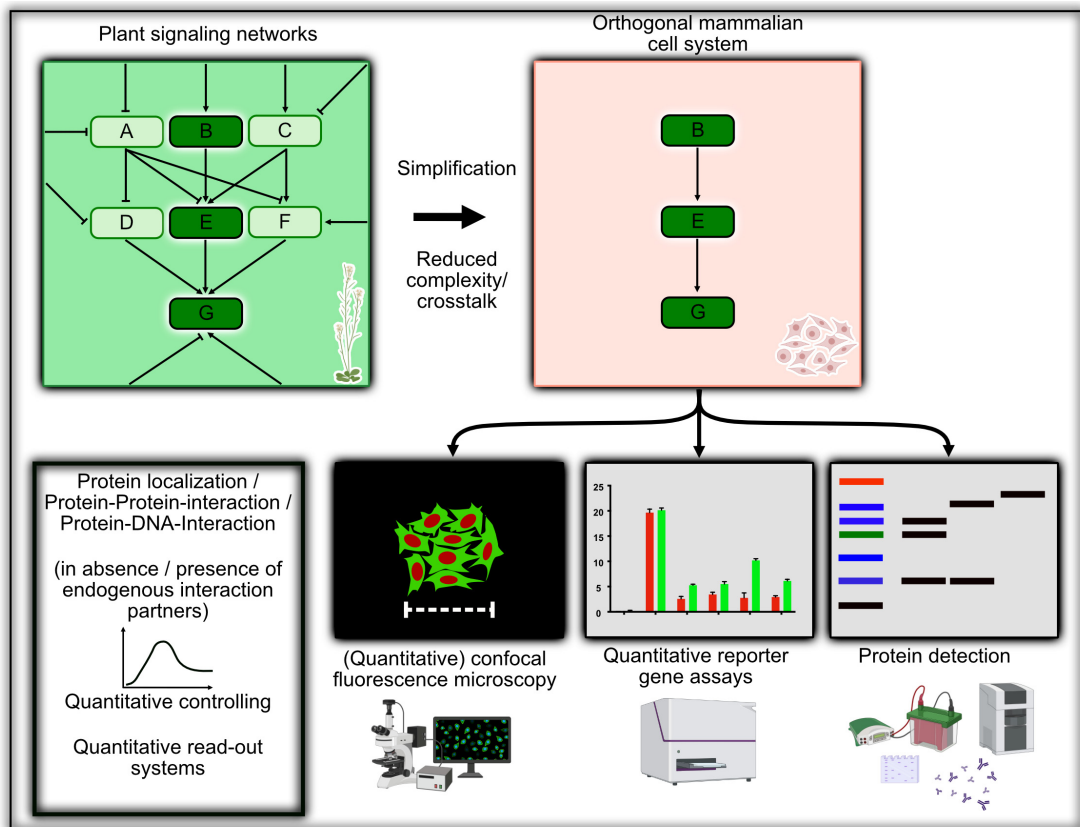


Figure 1.7: Illustration of the principle of studying plant signaling pathway components in the orthogonal system of mammalian cells and possible applications. The highly complex and intertwined structure of plant signaling networks impedes the study of single proteins, as well as chosen interactions of wanted components. Transferring the components of interest into the orthogonal system of mammalian cells allows the reconstruction or protein localization, protein-protein-interaction (PPI) or protein-DNA-interaction in a simplified environment with reduced complexity of the interaction network and crosstalk to unwanted endogenous plant factors. The plurality of available approaches spans from (quantitative) microscopy for protein localization or interaction up to quantitative reporter gene assays for studying PPIs or protein-DNA-interactions, as well as protein detection with e.g. western blot experiments. In general, the availability of mathematical modeling in connection with the mentioned approaches, allows the quantitative control and reconstruction of the plant-derived components of choice. This figure was created with BioRender.

1.2.3.1 Förster resonance energy transfer (FRET) approaches for analysis of protein interactions

Among the techniques used within the framework of this thesis for studying plant-originated PPIs, FRET-based techniques were established for supporting and validating the other applied approaches. They are an effective resources for expanding the value of conventional microscopical approaches by quantification of dynamic protein-protein interactions (PPIs) *in vivo* (Weidtkamp-Peters and Stahl, 2017). All FRET-based approaches depend on the physical effect of energy transfer from an excited donor-fluorophore, to a second, energy accepting fluorophore (acceptor) by dipole-dipole coupling. Requirements for this energy-transfer are spatial proximity of only a few nanometers and an optimal angle between the dipolar moments of both fluorophores (Förster, 1948; illustrated in Figure 1.8). To investigate if two candidate proteins interact, they are fused to fluorophores with overlapping emission- of the donor and excitation-wavelength of the acceptor-fluorophore (for example EGFP and mCherry). In case both fusion proteins fulfill all FRET-requirements, the emission intensity of the donor decreases, while the fluorescence-emission of the acceptor is elevated due to the energy transfer (Kremers et al., 2006; Long et al., 2018). Even small changes can directly be translated into a quantitative magnitude of the strength of the PPI. The simplest way of determining FRET is the photobleaching of the acceptor-protein (FRET-APB) and subsequent measurement of the donor intensity (Gu et al., 2004; Adjobo-Hermans et al., 2011). This technique does not need any special equipment and can therefore be performed with most confocal fluorescence microscopes. Despite the downsides of the need of high protein concentrations and a good signal-to-noise-ratio of both fluorophores (Long et al., 2018), it is perfectly applicable for a quick first screening of PPIs.

The mentioned disadvantages of FRET-APB approaches exclude this technique from being applicable for the analysis of interactions between poorly expressed interaction-partners or simply the need for the most native conditions. For this kind of applications, FRET-analysis by measuring the fluorescence lifetime (FRET- fluorescence lifetime imaging microscopy; FLIM) is the method of choice, since no high fluorescence intensity of both fluorophores is needed (Bucherl et al., 2013; Long et al., 2018). Here, FRET efficiency is determined by differences in fluorescence lifetime of the donor fluorophore due to quenching by the acceptor, compared to the non-quenched donor. Changes in fluorescence lifetime can easily be monitored by simultaneous fluorescence excitation of both fluorophores and measurement of their photon emission by Time Correlated Single Photon Counting (TCSPC). FRET-FLIM measurements need special and very expensive equipment, but allow an even more sensitive analysis of PPI-induced FRET.

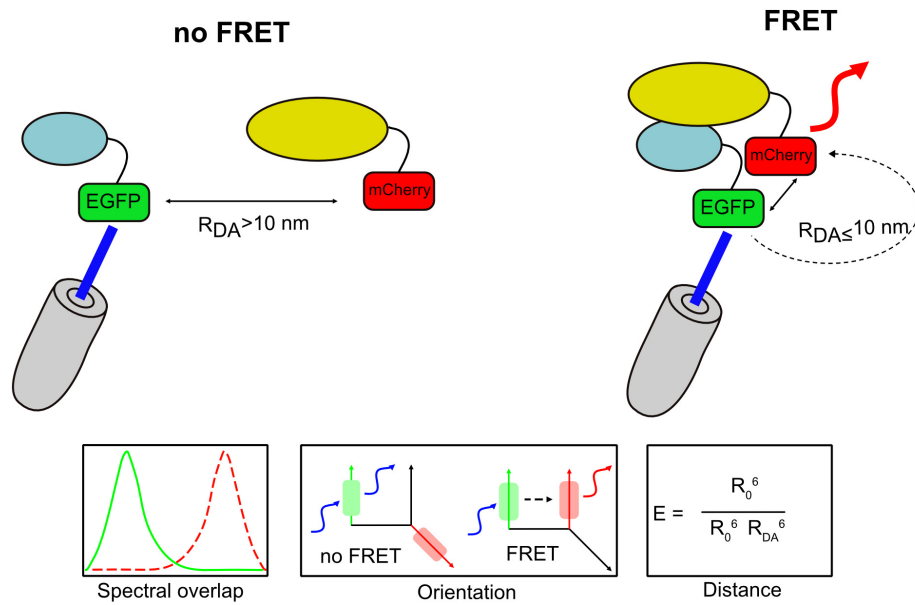


Figure 1.8: Illustration of the FRET measurement of a mCherry- and an EGFP-fused protein and factors essential for such a measurement. In case of no interaction between both proteins, the fused fluorescent proteins EGFP and mCherry are not localized within a close proximity to each other and no radiation free energy transfer occurs. Upon interaction of both proteins, close proximity of EGFP and mCherry is generated, inducing energy-transfer from the donor fluorophore EGFP to the acceptor fluorophore mCherry. FRET highly depends on the spectral overlap of the emission spectrum of the donor fluorophore and the excitation spectrum of the acceptor, as well as the distance and the orientation of both fluorophores to each other. This figure and the figure legend are adapted from the manuscript of Blomeier et al., 2021b, Appendix 7.1.1.

2 Aims

This study combines the development, characterization and application of diverse synthetic biology tools with the overall aim to monitor, quantify and control signaling processes in (orthogonal) mammalian or plant systems. It is split into two parts:

1. Understanding and quantification. The first part of this thesis aims to develop tools for the quantitative reconstruction of plant signaling in the orthogonal system of mammalian cells. Here, the superior goal was to be able to answer open questions, which are very difficult or nearly impossible to solve in their natural environment. Collaborative generation of mammalian-x-hybrid and (quantitative) microscopy approaches, described herein, allowed the synthetic reconstitution of plant signaling processes with the application on complex formation during perception of the phytohormone gibberellin, as well as analysis of selected downstream processes. These tools were then applied quantitatively understand the phytochrome-PIF interaction network with mammalian-3-hybrid approaches and investigation on possible unknown, PIF-mediated nuclear transport mechanisms of phytochromes with confocal fluorescence microscopy. Here, particular attention is given to the light-dependence of the analyzed processes.

2. Manipulation and control. The second part deals with the construction of novel optogenetic tools for spatiotemporal manipulation and control of signaling processes in mammalian and plant systems. Blue light-dependent control of expression of the RNA-cleaving CRISPR/Cas13b was achieved for downregulation of mRNA levels in different mammalian cells lines. Lastly, a UV-B activated optogenetic switch for induction of gene expression in mammalian cells was adapted for functionality in plant systems and quantitatively characterized in *A. thaliana* mesophyll protoplasts.

3 Results and Discussion

3.1 Quantitative reconstruction of plant signaling networks in the orthogonal system of mammalian cells

3.1.1 Quantitative reconstruction of the gibberellin perception mechanism

The chapter 3.1.1 is based on a manuscript in preparation with equal contribution of Jennifer Andres, Institute of Synthetic Biology, University of Düsseldorf (Blomeier et al., *in preparation* 2021b; Appendix 7.1.1) and contains selected results thereof.

As described in chapter 1.2.3, the study of plant signaling networks is highly impeded by the complexity and intertwined structure of the signaling cascades, with many components of redundant or overlapping function. Thereby, the isolated analysis in plants, especially in a quantitative fashion, is particularly complicated. Here, the study of such processes in orthogonal systems, with highly reduced crosstalk to other plant specific signaling processes gained interest in the last years and helped sharpening the understanding of such processes by offering a platform for analysis of, for example protein-DNA, protein-protein interaction (PPI) or protein localization (Beyer et al., 2015a; Abbas et al., 2018; Blanco-Touriñán et al., 2020; Gratz et al., 2020).

In this chapter, the design, development and characterization of a toolbox of (quantitative) approaches for the reconstruction of plant signaling processes in an orthogonal, cross-talk reduced environment are described. Mammalian-1-hybrid (M1H) were developed for investigation on the transactivation ability of transcription factors, as well as the influence of other transcription factors on these processes. Further, M2H up to M4H approaches were combined with quantitative microscopy-based FRET techniques for analyzing simple PPIs and their dependence on the supplementation of phytohormones. Subsequently, our findings were transferred on the analysis of the order of interaction events during complex formation of more than two proteins.

For establishment of our systems, we focused on the reconstruction of signal transduction processes during the gibberellic acid perception and selected downstream signaling events in human embryonic kidney cells (HEK-293T).

3.1.1.1 Mammalian-x-hybrid (MxH) approaches

The first approach, in the following referred as M1H (Mammalian-1-Hybrid), investigated on the relative strength of transcriptional activation activity of transcription factors after binding to their target DNA sequences. Since DELLA proteins lack a characteristic DNA binding domain, their influence on the regulation of signaling events is mediated by the interaction with transcription factors (Davière et al., 2008; Feng et al., 2008; de Lucas et al., 2008; Schwechheimer, 2012; Locascio et al., 2013). Therefore, we first tested the previously described activation of gene expression of ARABIDOPSIS RESPONSE REGULATOR1 (ARR1) by binding to synthetic cis-element sequences containing B-type ARR-binding motifs (TCS target element) on DNA (Müller and Sheen, 2008). Since the additive promotion of ARR1's transactivation ability by DELLAs was already shown in *Nicotiana benthamina* leaves (Marín-de la Rosa et al., 2015), our next step was to analyze the influence of DELLA proteins on these processes (M1H⁺; Mammalian-1-Hybrid⁺; Figure 2.1 A). For functionality in mammalian cells, we used the ARR1 Δ DDK mutant (lacking the CK-responsive DDK domain), which was shown to possess increased activity in the absence of plant-specific CKs (Sakai et al., 2000). Repetitions of the TCS element were placed in close proximity to the human cytomegalovirus minimal promoter (P_{hCMVmin}), controlling the expression of the human secreted alkaline phosphates (SEAP) gene on the reporter plasmid. While the transfection of the reporter construct did not induce any SEAP expression, the co-expression of ARR1 significantly increased the SEAP production, independent on fusion of an additional transactivation domain (VP16). Further, supplementation of either of the DELLA proteins RGA or GAI led to an additive rise in gene expression, with significant differences in most cases (M1H⁺) (Figure 2.1 B).

In summary, these results successfully support previous studies by demonstrating the binding of ARR1 to the TCS element and its capability of activating transcription, without the need of an additional transactivation domain. Further, DELLA proteins were observed to promote this effect by co-activating the activation of gene expression, supporting former Y2H and ChIP approaches (Marín-de la Rosa et al., 2015).

Next, we adapted and optimized a previously described split transcription factor system, based on the macrolide repressor (E-protein) and its target DNA motif (erythromycin resistance operator; *etr*₈) (Müller et al., 2013b). In brief, one transcription factor was N-terminally fused to the DNA binding E-protein, while a possible interaction partner was coupled to a transactivation domain (VP16) on its C-terminal. The *etr*₈ motif was placed upstream of the P_{hCMVmin} promoter, controlling the expression of SEAP. Interaction of both proteins draws the VP16 domain, fused to the interaction partner, in close proximity to the minimal promoter, recruiting the transcriptional machinery and thereby inducing expression of SEAP. For the study of interactions events during the gibberellin perception, we first designed and constructed

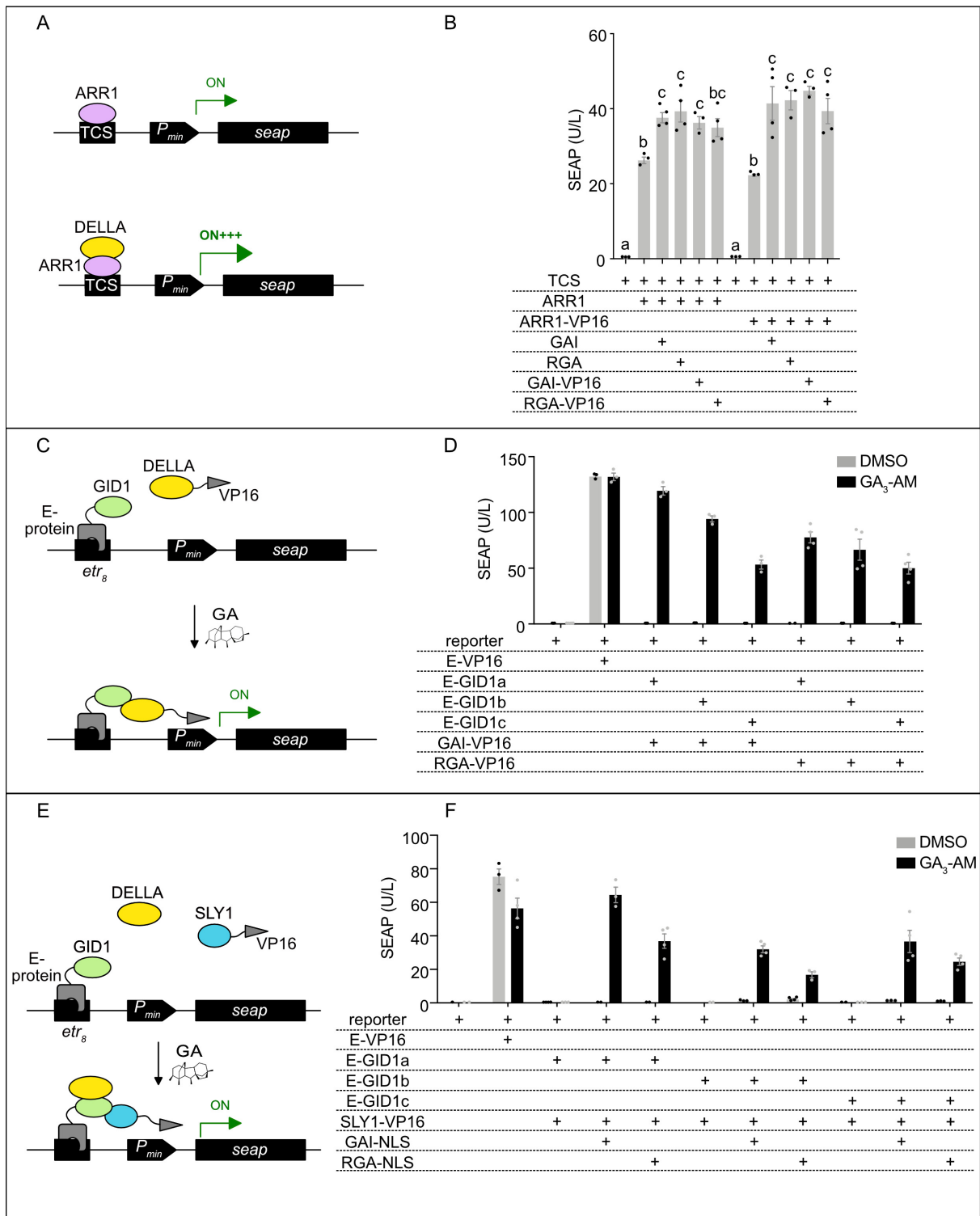
bicistronic vectors containing the DELLA proteins RGA or GAI fused to VP16 and the GA-receptors GID1a, b or c bound to the E-protein, respectively (Figure 2.1 C). For generation of two independent translational initiation sites, both were separated by a polioviral internal ribosome entry site (IRES_{PV}). While the interactions of the mentioned factors were studied in the absence of GA (M2H), supplementation of GA₃-AM was performed to test their hormone dependence (M3H).

Since previous studies showed the functionality of the gibberellin analog GA₃-AM in mammalian cells at a concentration of 10 μ M (Miyamoto et al., 2012), the same concentration was used in this study. For technical validation of the system, single transfection of the reporter construct was performed to analyze its background activity in the mammalian cell environment, while a fusion of E-VP16 was co-transfected to be able to compare the fitness of the cells after GA supplementation and under control conditions.

In all analyzed combinations no interaction of DELLA and GID1 was observed under control conditions (Figure 2.1 C). However, supplementation of GA₃-AM to the cell medium induced the interaction of DELLA and GID1 in all six tested combinations, while the set-ups with the GA-receptor GID1a generated the strongest induction of SEAP production (Figure 2.1 D). For exclusion of false negatives generated by the direction of protein fusion, the orientation of E-GID1 and DELLA-VP16 was inverted to E-DELLA and GID1-VP16. This orientation showed the same tendency of GA₃-AM induced interaction of all DELLA-GID1 combination, but with an overall lower SEAP production (data not shown, see Appendix 7.1.1). Combination of either the respective DELLAs or the GID1s with the F-Box Protein SLY1 did not lead to expression of the SEAP reporter gene in all tested combinations and orientations (data not shown, see Appendix 7.1.1). With the established M3H system we could show a hormone-dependent interaction for all six DELLA-GID1 combinations. Nevertheless, we underlined the importance of investigation on preferred fusion sites of proteins for either improving the dynamic range of the system, or exclude false negative results. In case of the DELLA-GID1 analysis, both orientations displayed the same tendency, but E-GID + DELLA-VP16 outperformed the reversed fusion sites in this approach.

Previous studies highlighted the role of the SCF^{SLY1} complex of targeting DELLA proteins in a GA-dependent manner (Dill et al., 2004; Fu et al., 2004). Nevertheless, the order of events was, so far, only studied by using yeast-three-hybrid assays. Here, the recognition of the already formed GA-GID1-DELLA complex by SLY1 was shown for the example of RGA and GID1a (Griffiths et al., 2006). In order to be able to recapitulate the order interaction during GA-perception in our mammalian system, we further co-transfected the third component to the respective M2H and M3H set-ups (Figure 2.1 E). No supportive effect on already detected interaction between DELLA and GID1 was observed, while the combination of E-DELLA/SLY1-VP16 did not show any SEAP expression after supplementation of SLY1-NLS (data not shown,

see Appendix 7.1.1). Interestingly, the treatment with GA₃-AM induced the SEAP expression for the E-GID1/SLY1-VP16 combination, when co-transfected with either RGA- or GAI-NLS, indicating a DELLA-mediated interaction of both parts of the split transcription factor system (Figure 2.1 F).



Results and Discussion

Figure 2.1: Synthetic reconstruction of DELLA-mediated regulation of transcriptional activation and comparison of mammalian-x-hybrid experiments analyzing the order of complex-formation during GA-perception in human embryonic kidney cells (HEK-293T). (A) Mode of function of mammalian one hybrid (M1H) and mammalian one hybrid⁺ (M1H⁺) experiments. The plant transcription factor ARR1 activates transcription of the SEAP reporter gene upon binding to repetitions of the TCS element (M1H). The presence of DELLA proteins further enhances this activation (M1H⁺). The reporter construct consisting out of the human secreted alkaline phosphates (SEAP) under the control of the human cytomegalovirus minimal promoter ($P_{hCMVmin}$), positioned downstream of repetitions of the TCS-element. The reporter plasmid was co-transfected with ARR1 (ARR1 Δ DDK) with or without being fused to the VP16 transactivation domain (M1H). Additional co-transfection of either GAI or RGA, as well as VP16-fused versions of both DELLAs was performed (M1H⁺). (B) 24 h post-transfection of the listed components, SEAP activity was quantified by a colorimetric assay. $n = 4$, error bars represent one standard error of the mean (SEM). One-way analyzes of variance (ANOVA) were performed with $p < 0.05$. (C) Scheme of the mammalian-hybrid detection system, investigating the possible interaction of GID1-receptors and DELLA proteins in the presence (M3H) or absence (M2H) of gibberellic acid (GA_3 -AM). GID1a, b or c were N-terminally fused to the DNA-binding macrolide repressor (E-protein), tethering it to the etr_8 operator site on the reporter plasmid. Recruitment of GAI or RGA, C-terminally fused to the VP16 transactivation domain, recruits the transcriptional activation machinery to the cytomegalovirus minimal promoter (P_{CMVmin}) and induces the expression of the secreted alkaline phosphatase reporter gene. (D) Macrolide repressor-based split-transcription factor system for analysis of GA-dependent interactions between E-GID1 and DELLA-VP16. 50,000 HEK-293T cells were seeded in 24-well plates and transfected 24 hours later with a reporter plasmid, containing the human secreted alkaline phosphatase (SEAP) under control of the human cytomegalovirus minimal promoter, positioned downstream of repetitions of an operator sequence for E (etr_8). A constitutively expressed fusion of both, the DNA-binding domain (E-Protein) and the Herpes simplex-derived transactivation domain (VP16) acted as positive control for gene expression, while single transfection of the reporter was used as negative control for controlling leakiness of the system in the different conditions. For quantitative analysis of GA-dependent interactions, a bicistronic vector containing the mentioned protein combinations, was co-transfected. 24 hours post transfection, the medium was exchanged by fresh medium containing either 10 μ M GA_3 -AM, dissolved in DMSO, or DMSO as control. Another 24 hours SEAP production was quantified using a colorimetric assay. $n = 4$, error bars represent one standard error of the mean (SEM). (E) Molecular design of the mammalian-hybrid detection system, investigating the order of possible interaction of SLY1, GID1-receptors and DELLA proteins in the presence (M4H) or absence (M3H) of gibberellic acid (GA). The DELLA proteins were fused to the E DNA-binding domain, tethering it to the etr_8 operator side on the reporter plasmid. In case of interaction, recruitment of SLY1 fused to the VP16 transactivation domain recruits the transcriptional activation machinery and induces the activation of the secreted alkaline phosphatase reporter gene under the control of the cytomegalovirus minimal promoter. Co-transfection of GID1a, b or c further analyzes if it is necessary for mediating the interaction of both parts of the split transcription factor. 50,000 HEK-293T cells were seeded in 24-well plates and transfected 24 hours later with the indicated components 24 hours post transfection, the medium was exchanged by fresh medium containing either 10 μ M GA_3 -AM, dissolved in DMSO, or DMSO as control. Another 24 hours SEAP production was quantified using a colorimetric assay. $n = 4$, error bars represent one standard error of the mean (SEM). This figure and the figure legend are adapted from the manuscript of Blomeier et al., 2021b, Appendix 7.1.1.

The obtained results could give new insights on the structure of the GA-GID1-DELLA-SLY1 complex, responsible for GA-perception and signal transmission, since not all orientations indicate the capability of all three involved proteins to bind to each other, or only show a relative affinity for each other below the threshold of the performed methods. Summed up, the results obtained in this part, support former studies indicating the GA-dependent interaction between GID1s and DELLAs as initiation of increased affinity of SLY1 for the GA-GID1-DELLA complex in yeast (Griffiths et al., 2006), determining the order of complex formation upon GA-perception. Here, a yeast-three-hybrid assay revealed the interaction between RGA and SLY1 only in the presence of GA_3 and the co-expression of GID1a. This study expands this investigation to all three GID1s and the two DELLA proteins RGA and GAI. It further indicates the recruitment of SLY1 to the respective DELLA protein, after previous GID1-DELLA complex formation upon GA-perception by the GID1 receptors. If this prediction is true, it could explain SEAP induction in case of co-expression of the DELLAs as no part of the split transcription-factor (Figure 2.1 D). This protein complex might guarantee a more beneficial orientation or smaller proximity of the transactivation domain to the minimal promoter in the M4H assays. However, a reason for the absence of SEAP expression in case of supplemental GID1 expression could be the low stability of the complex in this composition.

3.1.1.2 Microscopy based approaches

Lastly, we aimed on the development of independent approaches for validating the analyzed protein-protein interactions (PPIs) from the previously described MxH experiments.

First localization studies of the co-transfection of fluorescently tagged DELLA and GID1 proteins revealed the GA₃-AM dependent recruitment of EGFP-tagged GID1b to a nuclear localized mCherry-GAI (data not shown, see Appendix 7.1.1).

To be able to review if the discovered translocation of proteins was induced by interaction with another protein, the fixed cell samples were subsequently used for the establishment of FRET approaches, being highly valuable techniques for the quantitative analysis of such PPIs (Weidtkamp-Peters and Stahl, 2017). As explained in chapter 1.2.3.1, FRET describes the radiation free energy transfer from an excited donor-fluorophore to an acceptor fluorophore, depending on overlapping emission spectrum of the donor and excitation spectrum of the acceptor, as well as the proximity and angle of the dipolar moments of the fluorophores (Förster, 1948; illustrated in Figure 1.8).

Since the chosen fluorescent proteins EGFP and mCherry, for studying protein localization of the GID1s and GAI, are known to fulfill the requirements of overlapping spectra for FRET, we were able to use the same constructs for the analysis of possible FRET effects (Lam et al., 2012). In case of GA induced interaction between both, EGFP and mCherry are located in close proximity to each other. Ideal angles between the fluorophores induces energy transfer from the donor EGFP to the acceptor mCherry (illustrated in Figure 2.2 D).

With the exception of having access to a confocal fluorescence microscope with lasers and emission filters of the required wavelengths, FRET-APB (FRET- acceptor photobleaching) approaches are independent of special equipment. Therefore, we chose this simple method as our first experimental set-up of FRET measurements. Following 30 seconds of recording the fluorescence intensity of the donor and the acceptor fluorophore, bleaching of the acceptor was performed for two seconds. Following the bleaching step, the fluorescence of both was measured for another 30 seconds (illustrated in Figure 2.2 A-B). Since the bleaching of the acceptor terminates the energy transfer, evaluation of the recovery of donor fluorescence intensity after bleaching, allows the calculation of the FRET efficiency of both interaction partners (exemplified in Figure 2.2 C).

Results and Discussion

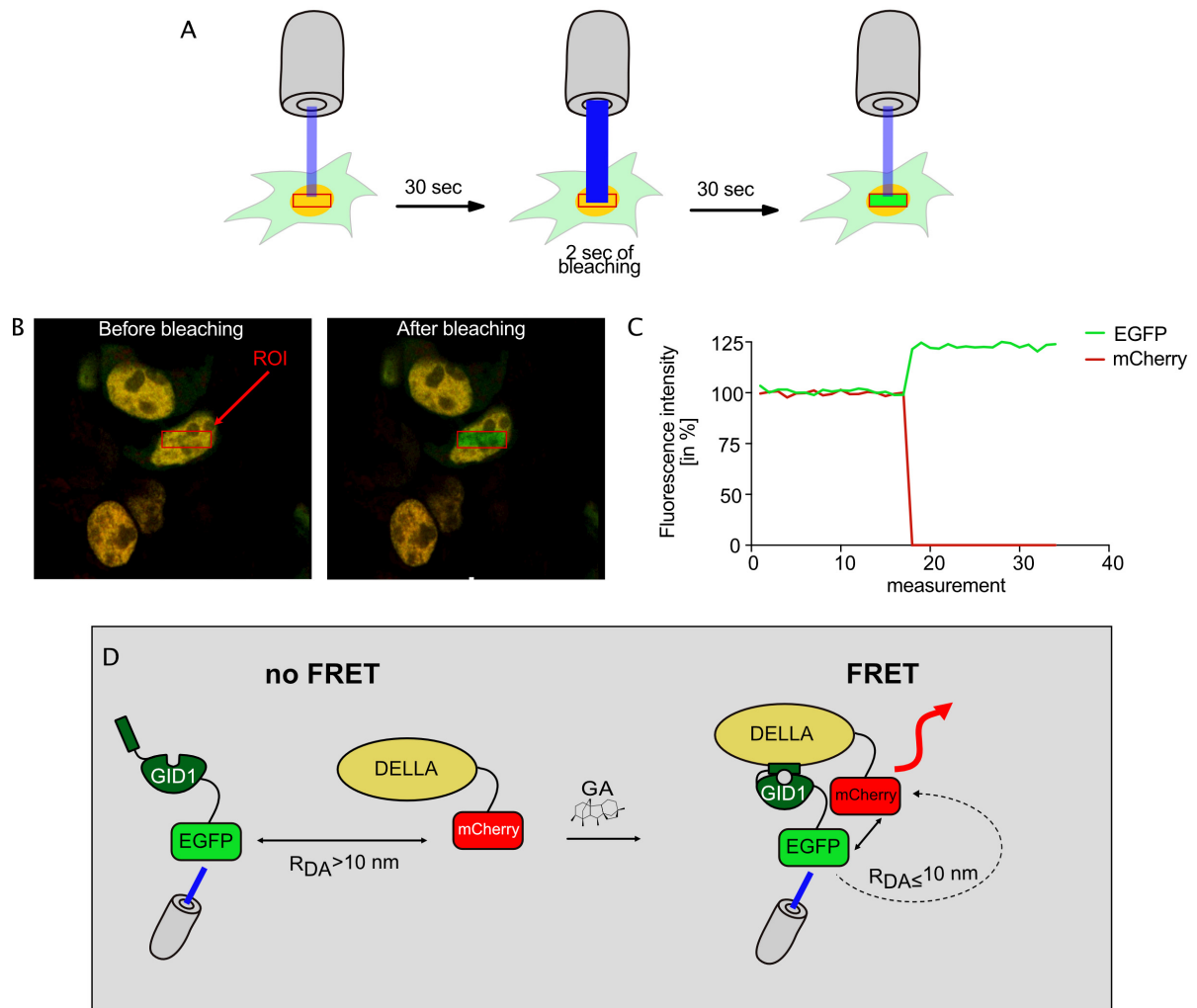


Figure 2.2: Overview of the principles of FRET measurements by acceptor photo-bleaching (FRET-APB) on the example of EGFP fused GID1b and mCherry tagged GAI constructs in mammalian HEK-293T cells. (A) Experimental set-up of FRET-APB measurements performed in this report. After 30 seconds of constant measurement of the fluorescence-intensity, the laser power of the 561 nm laser was raised up to 100 percent, bleaching the mCherry fluorescence in the area of the red rectangle (ROI). After two seconds of bleaching, fluorescence was measured for another 30 seconds. To calculate the efficiency of the FRET-APB measurement, the average fluorescence of the five seconds before and after bleaching were compared to each other. (B) Image of a mammalian HEK-293T cell, expressing EGFP-GID1b and NLS-mCherry-GAI, before (left) and after (right) the bleaching step of a FRET-APB measurement in the region of interest (ROI). (C) Visualization of exemplary fluorescence intensities of EGFP (green) and mCherry (red) before and after bleaching of the mCherry acceptor fluorophore in case of FRET between both fluorophores, within a regular FRET-APB measurement. (D) Illustration of the GA-dependent FRET measurement of a DELLA-mCherry and a GID1-EGFP protein. In the absence of GA, both proteins do not interact and are not localized within a close proximity to each other. No radiation free energy transfer occurs. Upon supplementation of GA, both proteins interact to each other, generating a close proximity of EGFP and mCherry, inducing energy-transfer from the donor fluorophore EGFP to the acceptor fluorophore mCherry. FRET highly depends on the spectral overlap of the emission spectrum of the donor fluorophore and the excitation spectrum of the acceptor, as well as the distance and the orientation of both fluorophores to each other. This figure and the figure legend are adapted from the manuscript of Blomeier et al., 2021b, Appendix 7.1.1.

For the optimization of constructs in terms FRET efficiency, reliability and time-consumption of the measurements, extensive characterization of the quantitative FRET efficiency of a plurality of construct combinations was performed. As FRET is highly influenced by independent factors like the proximity and flexibility of the individual components within the constructs or the environment in the artificially induced protein localizations (illustrated in Figure 1.8), different localization strategies, as well as N- and C-terminal fusion of fluorescent protein with varying linker lengths were compared. For simplification of the time demanding process of construct

optimization, only constructs containing the GA receptor GID1b and the DELLA protein GAI were examined (Figure 2.3 A-D). The cumulative result of the characterization revealed a nuclear localization strategy of GAI as beneficial for the measurements by increasing the FRET efficiency compared to the non-tagged variant. Accumulation of the protein inside of the nucleus created a strong and evenly distributed signal accelerated the measurement while it decreased the variance of the measured FRET efficiencies, when compared to the membrane-recruited variant (CAAX prenylation sequence). Comparisons between the different linker lengths connecting GAI or GID1b to the fluorescent protein and fusion sites thereof, as well the exchange of the fused fluorescent proteins EGFP and mCherry, identified the combination of EGFP-GID1b with a two amino acid linker with NLS-mCherry-GAI with a nine amino acid linker as the FRET pair with the strongest measured dynamic range between FRET efficiencies in the GA₃-AM induced and the DMSO control condition (Figure 2.3 A-D). The emerging construct combination of EGFP-2aa-GID1 and NLS-mCherry-9aa-GAI was subsequently analyzed on its induction kinetics and sensitivity to the treatment with GA₃-AM. While hormone incubation of 4 hours led to the strongest generated FRET efficiency (Figure 2.3 E), we detected FRET down to a sensitivity of 1 nM GA₃-AM (Figure 2.3 F).

As previously for the MxH experiments, interactions of all three proteins involved in GA perception-dependent signaling events were analyzed on possible PPIs. Here, no FRET effect was measured for the respective interactions of GAI or GID1b with SLY1, and supplementation of the third component did not induce any measurable rise in FRET efficiency. Moreover, the FRET efficiency of the GAI-GID1b pair was not increased by addition of SLY1 (data not shown, see Appendix 7.1.1).

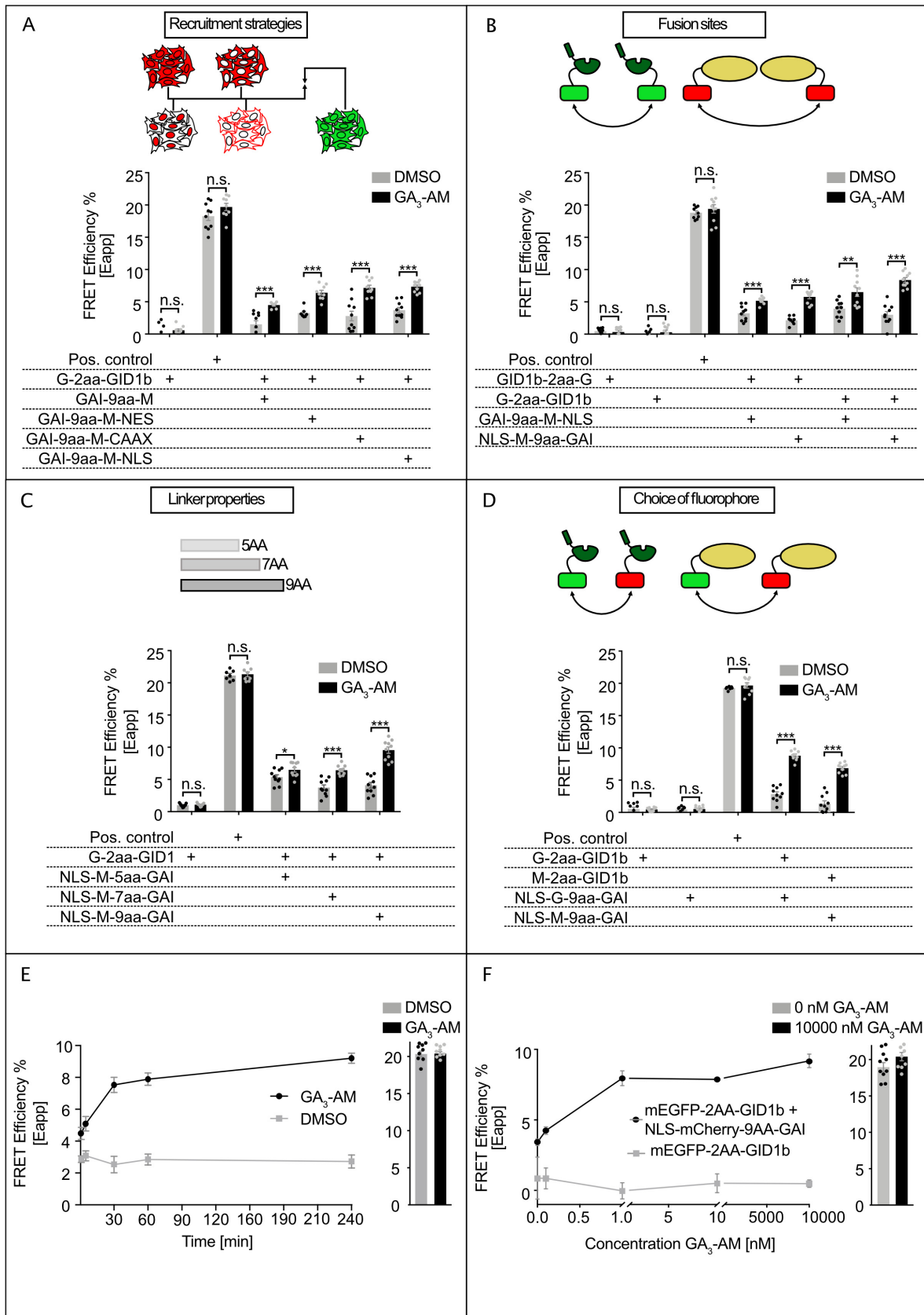


Figure 2.3: Comparison of apparent FRET efficiencies between fluorescently-tagged GAI and GID1b protein constructs in mammalian HEK-293T cells. (A) FRET-APB measurements of N- or C-terminally EGFP-tagged GID1b fusion proteins in co-transfection with N- or C-terminally mCherry-tagged GAI fusion proteins in the absence (grey bars) or presence (black bars) of GA₃-AM. (B) FRET-APB measurements of N-terminally mEGFP-tagged GID1b, co-transfected with different constructs of mCherry-GAI-fusions, with or without additional fusion to a localization tag, recruiting the protein to the nucleus (NLS), cytoplasm (NES) or plasma-membrane (CAAX), after supplementation of DMSO (grey bars) or GA₃-AM (black bars). (C) FRET-APB measurements of N-terminally EGFP-tagged GID1b fusion proteins in co-transfection with N-terminally mCherry-tagged GAI fusion proteins with different linker length between the fluorescent protein and GAI in the absence (grey bars) or presence (black bars) of GA₃-AM. (D) FRET-APB measurements of N-terminally EGFP- or mCherry-tagged GID1b fusion proteins in co-transfection with N-terminally mCherry- or EGFP-tagged GAI fusion proteins in the absence (grey bars) or presence (black bars) of GA₃-AM. 24 h after transfection, the cell culture medium was exchanged with fresh medium, supplemented with 0.5 μL DMSO or 10 μM of GA₃-AM solved in DMSO, per well. After four hours of incubation and subsequent fixation of the cells, potential protein-protein-interactions between GID1b- and GAI-constructs, were measured by bleaching the fluorescence signal of the acceptor-fluorophore mCherry and monitoring a potential increase in fluorescence emission of the donor fluorophore EGFP (FRET-APB). Intramolecular fusion of EGFP and mCherry to GID1b served as positive control for FRET, while the single transfection of EGFP-GID1b was used as negative control. *n* = 10, error bars represent one standard error of the mean (SEM). Significance was calculated with a paired students t-test (**P* < 0.05; ***P* < 0.01; ****P* < 0.001). (E) Kinetics of FRET-APB measurements of N-terminally EGFP-tagged GID1b fusion proteins in co-transfection with N-terminally mCherry-tagged GAI fusion proteins in the absence (grey labels) or presence (black labels) of GA₃-AM at different time-intervals after the respective treatment. Intramolecular fusion of EGFP and mCherry to GID1b served as positive control for FRET. *n* = 10 error bars represent one standard error of the mean (SEM). (F) Dose response of FRET-APB measurements of N-terminally EGFP-tagged GID1b fusion proteins in single transfection (grey labels) or in co-transfection with N-terminally mCherry-tagged GAI fusion proteins (black labels) after supplementation of different concentrations of GA₃-AM. Intramolecular fusion of EGFP and mCherry to GID1b served as positive control for FRET in the absence (grey bars) or presence (black bars) of GA₃-AM. *n* = 10, error bars represent one standard error of the mean (SEM). This figure and the figure legend are adapted from the manuscript of Blomeier et al., 2021b, Appendix 7.1.1.

Lastly, the construct design was transferred to the two other GID1s, GID1a and GID1c (Figure 2.4). All three combination of the respective GID1 with NLS-mCherry-GAI generated a significant increase in FRET efficiency after supplementation of GA₃-AM to the cell medium with the strongest measured effect for GID1b (Figure 2.4 A). Further, the live-cell-measurement of fluorescence lifetime by FRET-FLIM supported these results by revealing the strongest reduction of fluorescence lifetime for the co-transfection of the EGFP-GID1b donor and the NLS-mCherry-GAI acceptor (Figure 2.4 B).

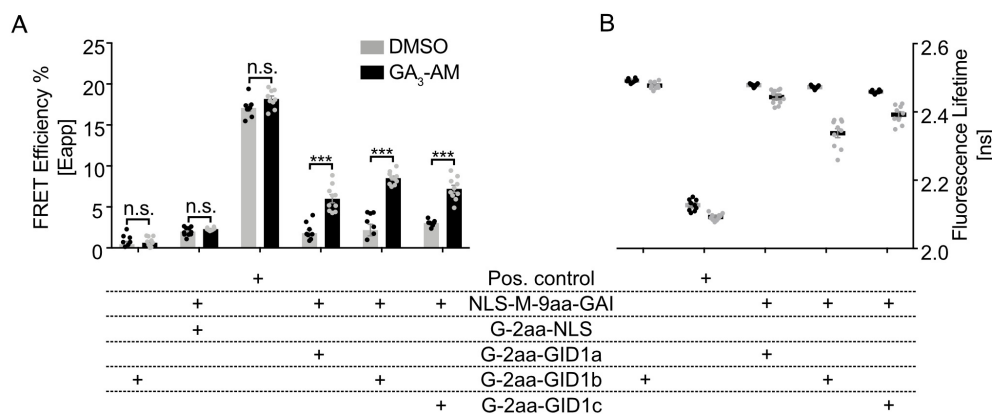


Figure 2.4: Visualization of apparent FRET efficiencies of FRET-APB measurements and visualization of fluorescence lifetime of fluorescently tagged GID1 fusion proteins in different experimental conditions in mammalian HEK-293T cells. mEGFP-GID1a, b or c were co-transfected with NLS-mCherry-GAI fusion proteins. Single transfection of EGFP-GID1b served as negative control, while fusion of GID1b to EGFP and mCherry functioned as positive control for intramolecular energy transfer. 24 h after transfection, the cell culture medium was exchanged with fresh medium (A) or live cell imaging solution (B), supplemented with 0.5 μL DMSO or 10 μM of GA₃-AM solved in DMSO, per well. Four hours later, cells were fixed for FRET-APB measurements (A) or kept alive for analysis of potential shifts in fluorescence lifetime of mEGFP-GID1b, caused by interaction with the GAI-constructs (B). *n* = 10, error bars represent one standard error of the mean (SEM). Significance in A was calculated with a paired students t-test (**P* < 0.05; ***P* < 0.01; ****P* < 0.001). This figure and the figure legend are adapted from the manuscript of Blomeier et al., 2021b, Appendix 7.1.1.

Our microscopy-based approaches strongly support the previously generated information from the MxH approaches. Here we validated the previously interactions of GAI and GID1a-c to be hormone-dependent, while we could detect the interaction of GID1b and GAI down to a sensitivity of 1 nM GA₃-AM. Unfortunately, we could not detect the interaction of SLY1 and any other component. Here, the distribution of the components within the GA-GID1-DELLA-SLY1 complex might possibly be disadvantageous for fulfilling the requirements for FRET.

Summarized, our results support previous *in vitro*, other orthogonal *in vivo* systems like yeast, or *in planta* studies reporting the transactivation ability of ARR1 and the influence of DELLAs on the induction of gene expression (Marín-de la Rosa et al., 2014; Marín-de la Rosa et al., 2015) and the GA-dependent interaction events during formation of the GA-perception complex (Griffiths et al., 2006; Nakajima et al., 2006; Suzuki et al., 2009).

The established methods and the orthogonal platform of mammalian cells itself, provide a system for expression of plant proteins in a crosstalk-reduced environment and offers an *in vivo* system for the quantitative reconstruction of:

- 1.) The recapitulation of transcriptional activation in interplay with other selected plant proteins.
- 2.) Protein-Protein-Interactions between at least two and up to three expressed factors in a phytohormone dependent fashion. Two independent methods have been developed and already demonstrate reliable and comparable recapitulation of the GA-dependent interaction between DELLA and GID1 proteins, while expanding the current understanding of protein affinities and the order of the complex formation during GA-perception in a broader and more quantitative manner.

Since the analysis of these kinds of interaction and transactivation assays are tough to perform in their natural plant environment, the usage of the orthogonal platform of mammalian cells, acts as a powerful complementary approach, supporting the understanding of signal transduction mechanisms in plants.

3.1.2 Synthetic reconstruction of the phytochrome-PIF interaction network in the orthogonal system of mammalian cells

Some of the established approaches described in chapter 3.1.1, were adapted for the analysis of *Arabidopsis thaliana* phytochrome and PIF interactions in the orthogonal system of mammalian cells. Despite light-dependent nuclear migration of phytochromes (phys) being essential for their biological activity and signal transduction *in planta*, the molecular mechanisms mediating this process are still poorly characterized. Therefore, the mammalian platform was used to analyze the nuclear transport mechanism of the phytochromes in interplay with the PHYTOCHROME INTERACTING FACTORS (PIFs) of the bHLH superfamily of transcription factors and quantify the relative strength of phy-PIF interactions upon illumination with red light (660 nm) or in darkness.

In brief, the split transcription factor system based on the bacterial tetracycline resistance mechanism, previously described by Müller et al., 2013a, was adapted for studying possible interactions of the respective full-length proteins of phyA-D in interaction with PIF1-8 after exposure to red light (660 nm; 20 $\mu\text{mol m}^{-2} \text{s}^{-1}$) or in the dark (Figure 2.5 A). Moreover, the microscopical approach of Beyer et al., 2015, for analysis of the nuclear transport mechanism of phyB was expanded to phyA-D. Here, co-transfection with one member of the PIF family (PIF1-8), was conducted to analyze changes in cellular localization of the phytochromes in the presence or absence of red light (660 nm; 20 $\mu\text{mol m}^{-2} \text{s}^{-1}$) (Figure 2.5 B).

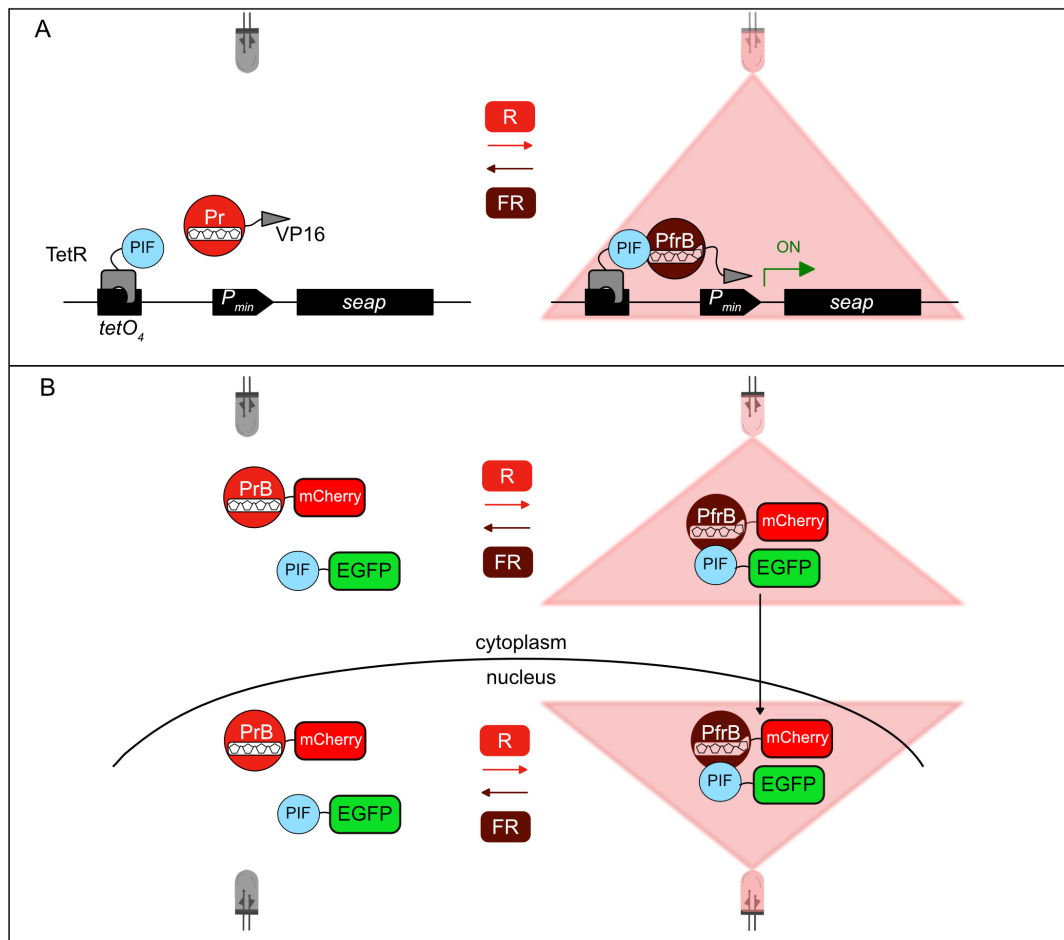


Figure 2.5: Overview of used approaches for the analysis of possible phytochrome-PIF interactions in mammalian cells. (A) Scheme of the mammalian-hybrid detection system, investigating the possible interaction of phytochromes and PIFs in the presence (M3H) or absence (M2H) of red light of 660 nm. PIFs were N-terminally fused to the DNA-binding tetracycline repressor (TetR), tethering it to the $tetO_4$ operator site on the reporter plasmid. Recruitment of phys, C-terminally fused to the VP16 transactivation domain, recruits the transcriptional activation machinery to the cytomegalovirus minimal promoter (P_{CMVmin}) and induces the expression of the secreted alkaline phosphatase reporter gene. (B) Illustration of the microscopic analysis of localization of phytochromes and PIFs on the example of phyB. While phyB was fused to mCherry, PIFs were fused to EGFP. In the dark, the biological inactive PrB conformer of phyB is localized at the cytoplasm of the cell. Illumination with red light of 660 nm induces the photoisomerization of the chromophore PCB and subsequent the conformational change of phyB to its active PfrB conformer. PfrB is able to bind to PIFs, mediating the nuclear transport of the phy-PIF complex. Illumination with red light or dark reversion reverts PfrB back to the inactive PrB, interruption the interaction with PIFs.

3.1.2.1 Mammalian-3-hybrid assays for investigation on interaction of phytochromes and PIFs

While the PIF proteins were N-terminally fused to the tetracycline repressor (TetR), binding the specific tetracycline operator sequence $tetO_4$ on the reporter plasmid, phyA-D were fused to the VP16 transactivation sequence. In case of interaction between PIF and phy, the transactivation domain recruits the transcriptional machinery to the minimal human cytomegalovirus immediate early promoter (P_{CMVmin}), inducing the expression of the SEAP reporter gene. In order to analyze phy-PIF combinations, bicistronic vectors containing a phytochrome fused to VP16 and a PIF fused to TetR, separated by a polioviral internal ribosome entry site ($IRES_{PV}$) were created. This plasmid design allows the initiation of two independent translations. Since previous studies already demonstrated the functionality of both proteins in this orientation of fusion (Beyer et al., 2015a), it was not exchanged in this

part. Our approach enables the quantitative characterization of the conditions and relative strength of the respective interactions.

Combinations of phyA-D with the eight PIF family members were tested on possible interactions in presence or absence of red light: 24 h after transfection, the cell medium was exchanged with fresh medium containing 15 μM phycocyanobilin (PCB). After one hour of incubation with PCB, the cells were illuminated with red light (660 nm ; $20\ \mu\text{mol m}^{-2}\text{ s}^{-1}$) or kept in the dark for 24 hours. Subsequent, 200 μl of the supernatant was transferred to a 96-well plate and incubated at 60°C for one hour, before the SEAP production was measured in a micro plate-reader. To guarantee optimal experimental conditions, transfection of the TetR-VP16 fusion acted as positive control for cellular fitness in both light conditions, while single transfection of the reporter plasmid served as negative control for indicating the background activity of the synthetic promoter construct. In both selected experiments the positive controls generated a strong SEAP production of at least 80 U/L, with similar levels under red light illumination and in the dark, while the reporter constructs showed minimal activation (Figure 2.6 A and Figure 2.7 A). In the conducted experiments with phyA containing vectors, only the combinations of phyA with PIF1 and PIF3 lead to a SEAP production above the background level, with activation in both conditions, under red light illumination and in darkness. Interestingly, the SEAP production after exposure to red light exceeds the level of the production in the dark by the factor of two, with a SEAP level of almost 30 U/L for the combination with PIF1 and around 17 U/L in interaction with PIF3 (Figure 2.6 B). These results suggest, the interaction of both PIFs and phyA being not strictly limited to the active PfrA conformer. In case of phyB, red light-dependent interactions with PIF1-3, PIF6 and PIF8 were observed. Contrary to phyA, no strong SEAP activity was measured in the dark in most cases, assuming a rather light-specific interaction in all cases. While the combinations with PIF1 and 3 led to an induction of SEAP production after red light illumination, with a total SEAP level of around 10 U/L, respectively, the weakest red light-induced SEAP production was measured for the combinations with PIF2 and PIF8. Even though the generated SEAP level after exposure to red light was at only 2.5 and 3.8 U/L, similar to the levels of combinations with PIF1 and 3 in the absence of red light, the low activation in darkness below 0.5 U/L generated an induction fold of around 9 for both combinations. Bicistronic expression of phyB with PIF6 induced the strongest measured SEAP levels after red light illumination of 14.7 U/L, with an induction fold of 18, compared to the non-illuminated counterparts (Figure 2.6 C).

Results and Discussion

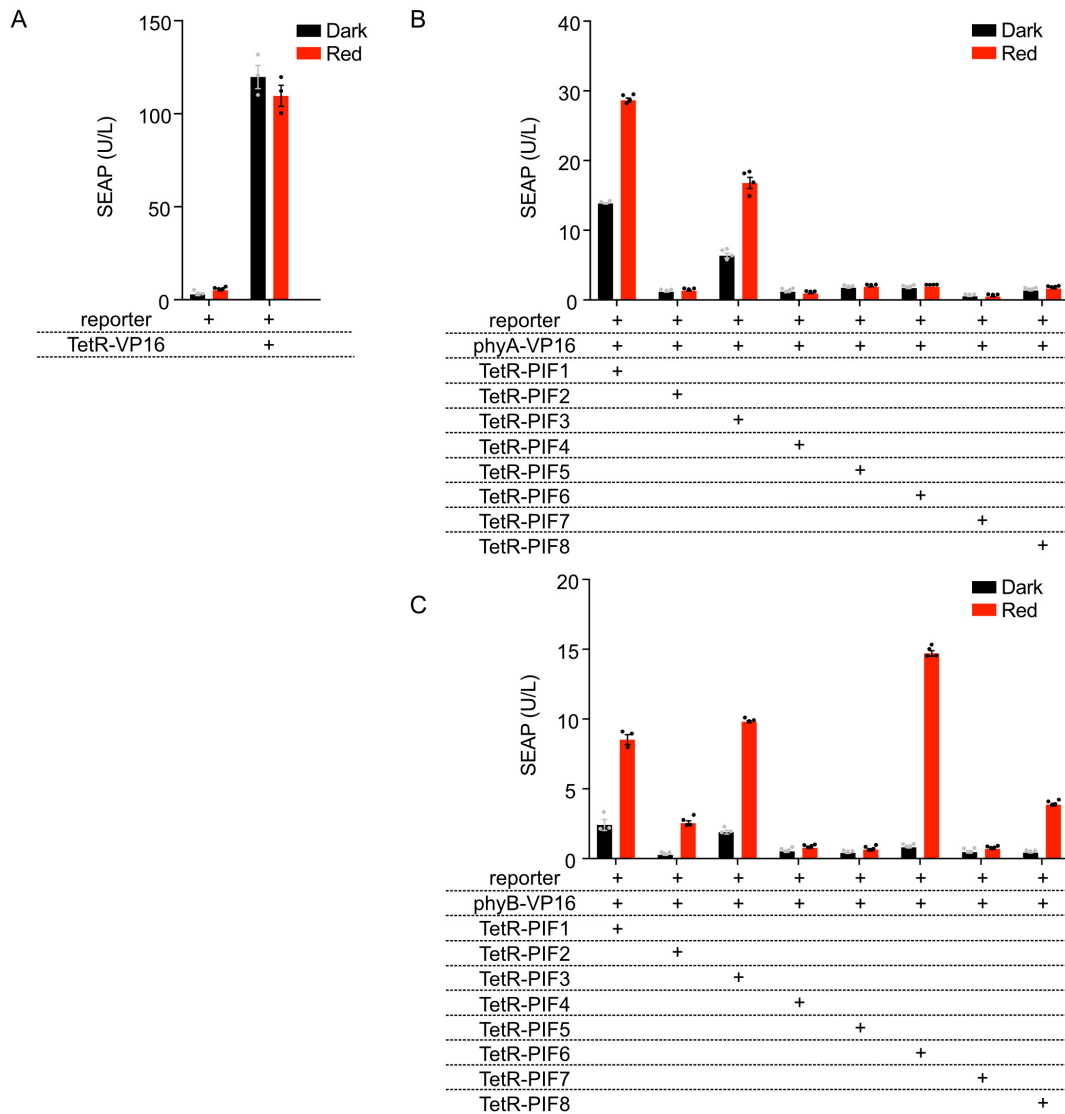


Figure 2.6: Mammalian-3-hybrid experiments analyzing interactions of phytochrome A or B and PIF proteins of *A. thaliana* in Chinese hamster ovary cells (CHO-K1). Tetracycline repressor-based split-transcription factor system for analysis of light-dependent interactions between TetR-PIF and phyA-VP16 (**B**) or TetR-PIF and phyB-VP16 (**C**). 50,000 CHO-K1 cells were seeded in 24-well plates and transfected 24 hours later with a reporter plasmid, containing the human secreted alkaline phosphatase (SEAP) under control of the human cytomegalovirus minimal promoter, positioned downstream of repetitions of an operator sequence for TetR ($tetO_4$). (**A**) A constitutively expressed fusion of both, the DNA-binding domain (TetR) and the Herpes simplex-derived transactivation domain (VP16) acted as positive control for gene expression, while single transfection of the reporter was used as negative control for controlling leakiness of the system in the different conditions. For quantitative analysis of red light-dependent interactions, a bicistronic vector containing the mentioned protein combinations, was co-transfected. 24 hours post transfection, the medium was exchanged by fresh medium containing 15 μM phycocyanobilin (PCB), dissolved in DMSO. After one hour, the cells were illuminated with red light (660 nm ; $20\ \mu\text{mol m}^{-2}\text{ s}^{-1}$; red bars) or kept in the dark (black bars). Another 24 hours later, SEAP production was quantified using a colorimetric assay. $n = 4$, error bars represent one standard error of the mean (SEM).

As observed for the bicistronic expression of phyA and the eight PIFs, combinations with phyC and D only showed a SEAP production above the background level in the presence of PIF1 and PIF3. Opposed to phyA, no red light-induced increase in SEAP production was measured. While the combination of phyC and PIF1 generated a SEAP level of slightly above 10 U/L in both light conditions, bicistronic expression of PIF3 led to a SEAP production of around 5 U/L after red light illumination and incubation in the dark (Figure 2.7 B). Overall, the

Results and Discussion

measured SEAP level of combination of PIF1 and PIF3 with phyD were lower than the one for co-expression of phyC. Bistronic expression of phyD and PIF1 led to a SEAP expression of around 4 U/L in darkness and around 3 U/L after red light. In case of the combination with PIF3 the levels were slightly higher at around 5.5 U/L after incubation in the dark and around 4.5 after exposure to red light (Figure 2.7 C).

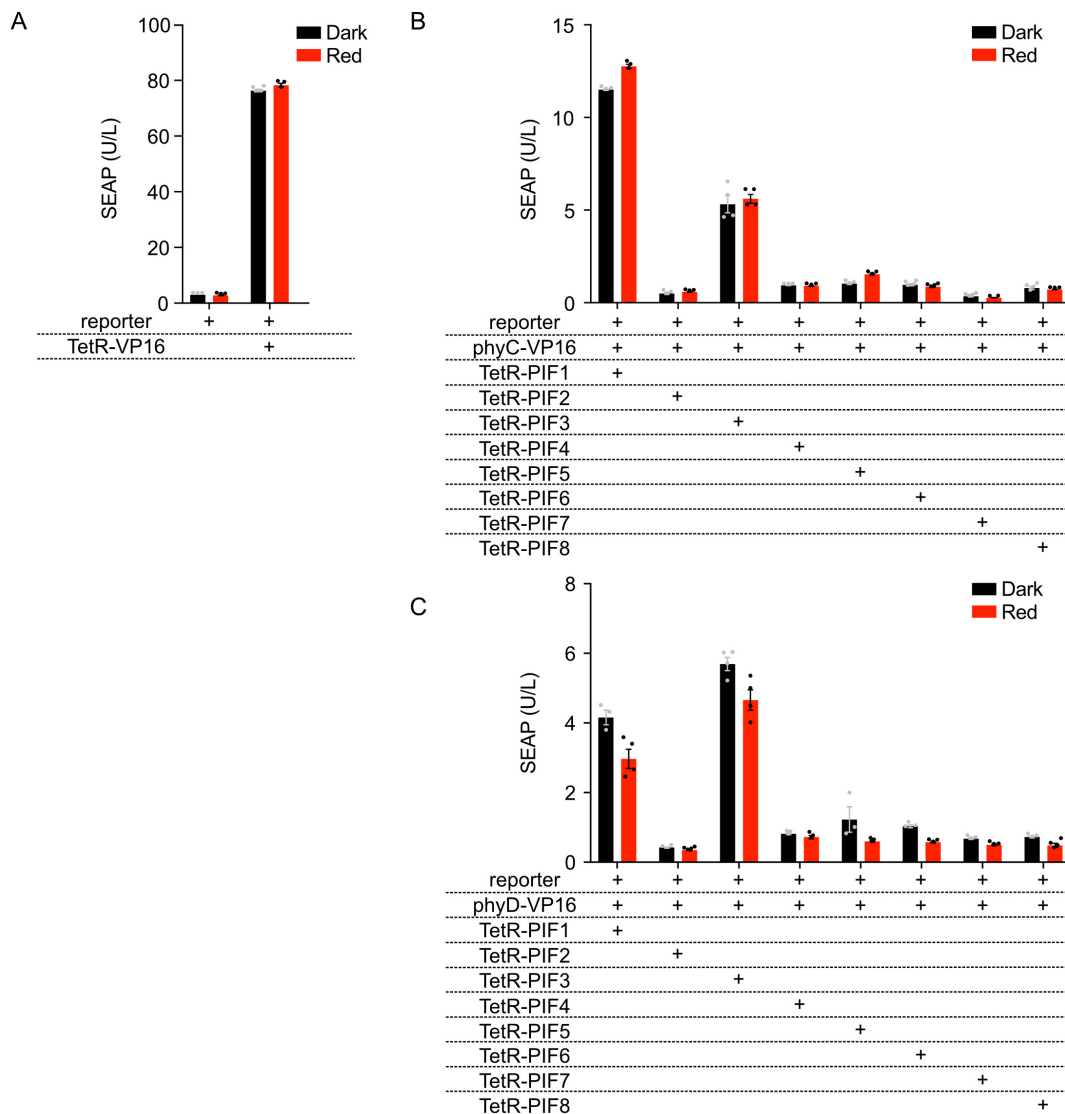


Figure 2.7: Mammalian-3-hybrid experiments analyzing interactions of phytochrome C or D and PIF proteins of *A. thaliana* in Chinese hamster ovary cells (CHO-K1). Tetracycline repressor-based split-transcription factor system for analysis of light-dependent interactions between TetR-PIF and phyC-VP16 (B) or TetR-PIF and phyD-VP16 (C). 50,000 CHO-K1 cells were seeded in 24-well plates and transfected 24 hours later with a reporter plasmid, containing the human secreted alkaline phosphatase (SEAP) under control of the human cytomegalovirus minimal promoter, positioned downstream of repetitions of an operator sequence for TetR (tetO₄). (A) A constitutively expressed fusion of both, the DNA-binding domain (TetR) and the Herpes simplex-derived transactivation domain (VP16) acted as positive control for gene expression, while single transfection of the reporter was used as negative control for controlling leakiness of the system in the different conditions. For quantitative analysis of red light-dependent interactions, a bistrionic vector containing the mentioned protein combinations, was co-transfected. 24 hours post transfection, the medium was exchanged by fresh medium containing 15 μ M phycocyanobilin (PCB), dissolved in DMSO. After one hour, the cells were illuminated with red light (660 nm; 20 μ mol m⁻² s⁻¹; red bars) or kept in the dark (black bars). Another 24 hours later, SEAP production was quantified using a colorimetric assay. $n = 4$, error bars represent one standard error of the mean (SEM).

3.1.2.2 Confocal fluorescence microscopy studies for analysis of PIF-dependent nuclear transport mechanisms of phytochromes

The nuclear import mechanisms of the different phytochromes and their light- and PIF-dependency was the objective of the second part of this study: all PIFs were fluorescently tagged with EGFP on their C-terminal, while the respective phytochromes were C-terminally fused to mCherry. Here, the experimental set-up is adapted from Beyer et al., 2015a: 24 h after co-expression of the single phytochromes and PIFs was performed, the chromophore phycocyanobilin (PCB) was added to the cultivation medium. After one hour of incubation in the dark, cells were either illuminated with red light of 660 nm or kept in the dark for another hour. Subsequent fixation of the cells allowed the confocal imaging of the protein localizations.

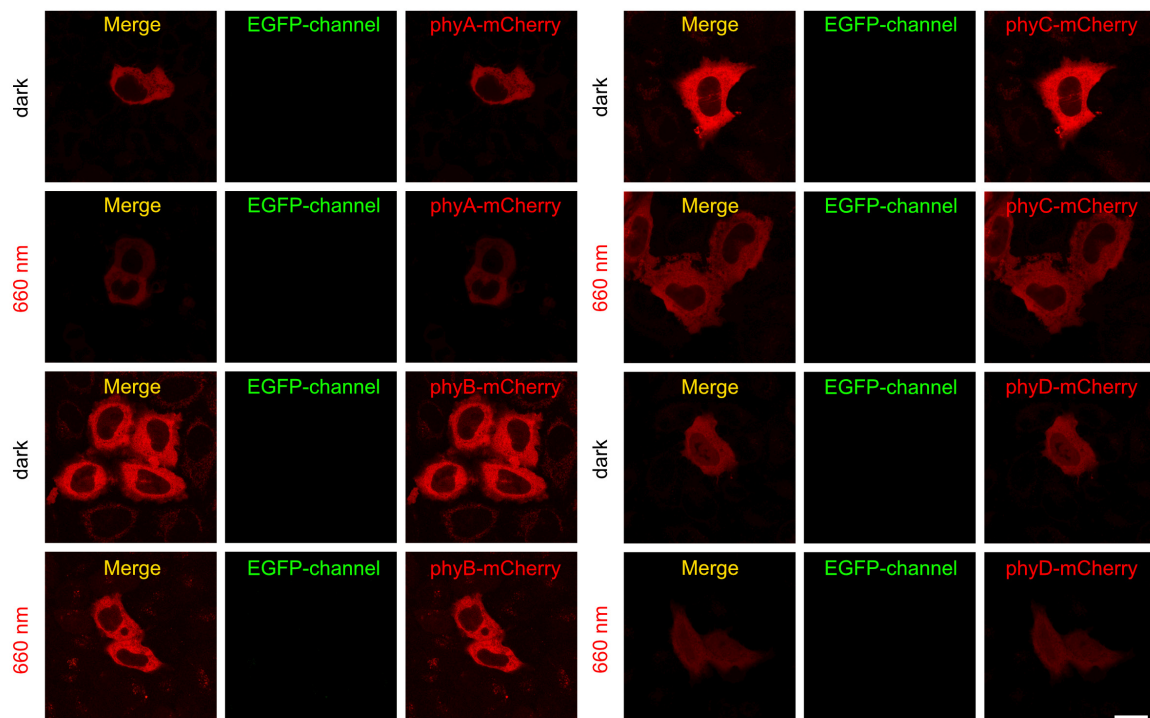


Figure 2.8: Confocal fluorescence microscopy imaging of intracellular localizations of phyA-D fused to mCherry in mammalian HeLa cells under different light conditions. phyA-D were fused to mCherry and single transfected. 24 h after transfection, the cell culture medium was exchanged with fresh medium, supplemented with 15 μM phycocyanobilin (PCB). After one hour of incubation in darkness, half of the samples were irradiated with red light (660 nm; 20 $\mu\text{mol m}^{-2} \text{s}^{-1}$, 1 h), while the other half remained in darkness. Subsequent to illumination/darkness, cells were fixed and the subcellular localization of the proteins was analyzed by confocal fluorescence microscopy. Scale bar, 20 μM .

Results and Discussion

With the exception of phyD, all phytochromes indicated mostly cytoplasmatic localization in both light conditions. However, phyD could be observed in equally distributed expression patterns all over the cell (Figure 2.8). The signal of all PIF-EGFP fusion indicated a nuclear localization of the proteins in speckle-like structures of bigger size as for PIF2, PIF3 or PIF6 or smaller structures as for PIF1, PIF4-5 and PIF7-8. Compared to all other PIFs with strictly nuclear localization, the expression pattern of PIF7-EGFP was not restricted to the nucleus, even though the cytoplasmatic signal was much weaker than the one of the nuclear proteins (Figure 2.9 - 2.12).

In case of phyA, only the co-transfection with PIF3-EGFP led to a red light-dependent nuclear translocation, generating nuclear speckle-like structures co-localizing with the ones of PIF (Figure 2.9). All other phyA-PIF combinations did not change the localization of phyA, independent on the light conditions.

Results and Discussion

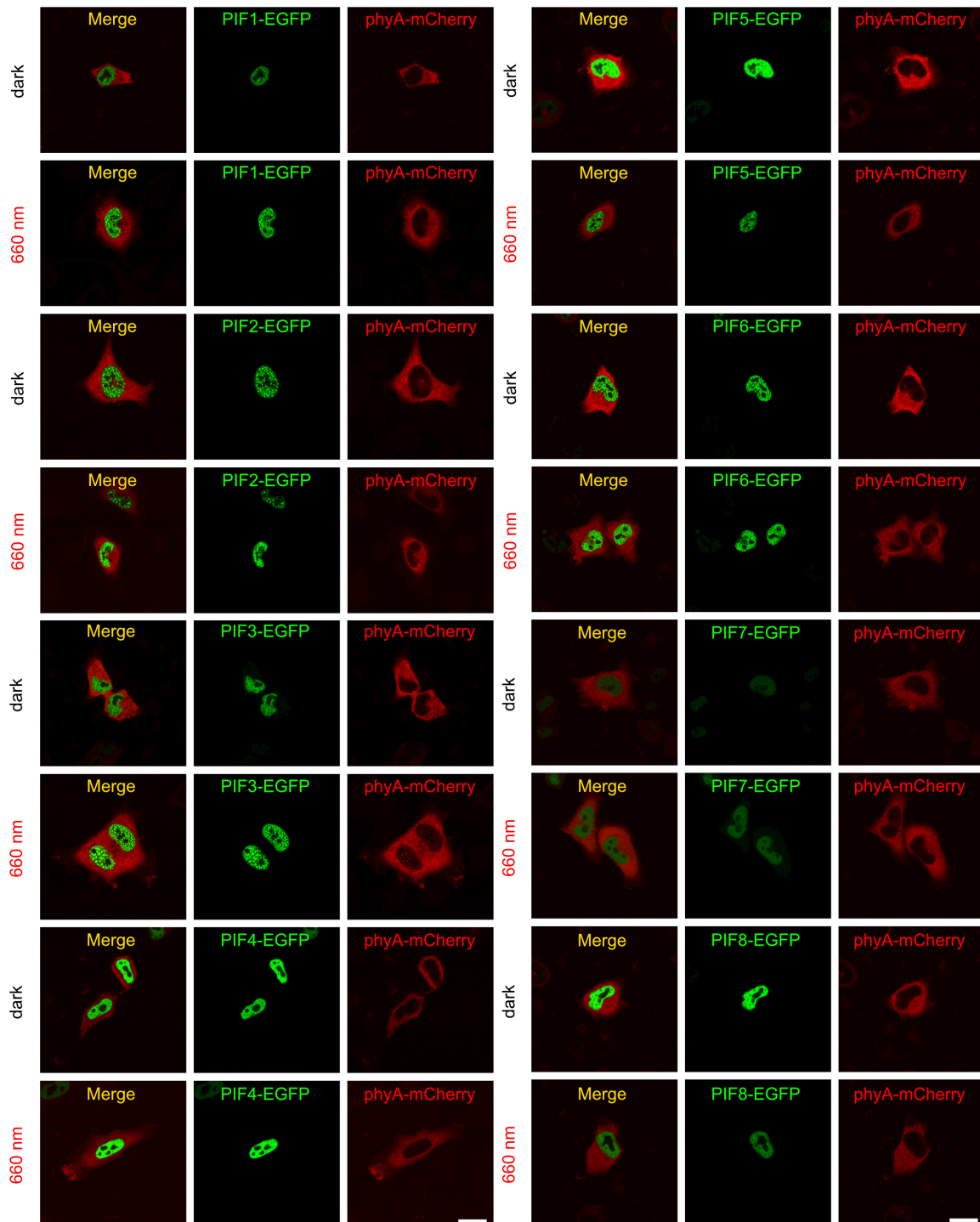


Figure 2.9: Confocal fluorescence microscopy imaging of intracellular localizations of phyA-mCherry and PIF1-8 fused to EGFP in mammalian HeLa cells under different light conditions. phyA-mCherry was co-transfected with PIF1-8 fused to EGFP. 24 h after transfection, the cell culture medium was exchanged with fresh medium, supplemented with 15 μM phycocyanobilin (PCB). After one hour of incubation in darkness, half of the samples were irradiated with red light (660 nm; 20 $\mu\text{mol m}^{-2} \text{s}^{-1}$, 1 h), while the other half remained in darkness. Subsequent to illumination/darkness, cells were fixed and the subcellular localization of the proteins analyzed by confocal fluorescence microscopy. Scale bar, 20 μM .

As already described by Beyer et al., co-transfection of phyB-mCherry and PIF3-EGFP was sufficient for a red light-dependent nuclear transport of the phytochrome. Among all other remaining PIFs, only the co-transfection with PIF2 led to a similar translocation of phyB: Upon illumination with red light, the cytoplasmatic phyB-mCherry partially translocated into nuclear speckle-like structures, which co-localize with the expression pattern of PIF2-EGFP. Co-transfection with PIF1 or PIF4-8 did not change the spatial distribution of phyB-mCherry within the analyzed cells (Figure 2.10).

Results and Discussion

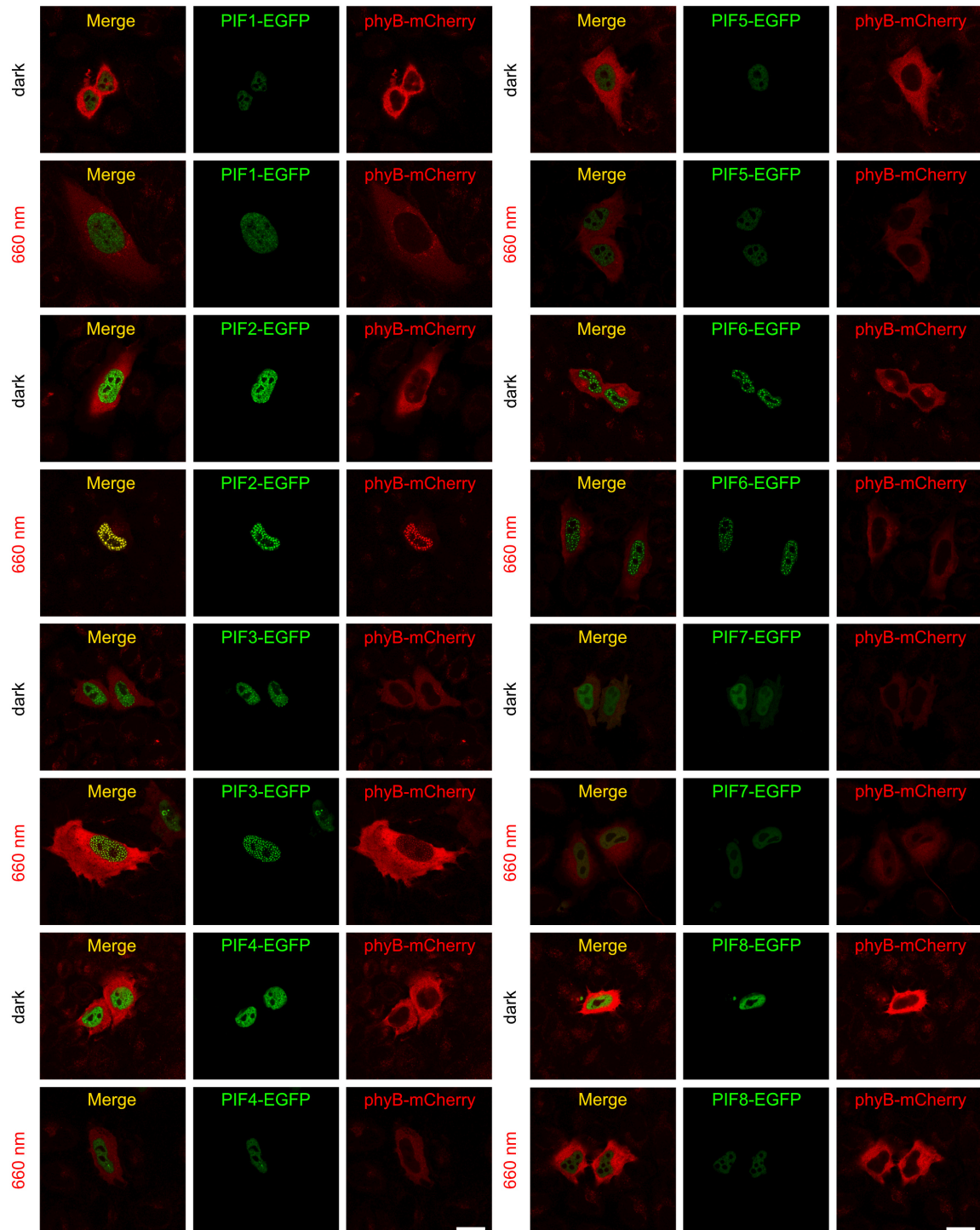


Figure 2.10: Confocal fluorescence microscopy imaging of intracellular localizations of phyB-mCherry and PIF1-8 fused to EGFP in mammalian HeLa cells under different light conditions. phyB-mCherry was co-transfected with PIF1-8 fused to EGFP. 24 h after transfection, the cell culture medium was exchanged with fresh medium, supplemented with 15 μM phycocyanobilin (PCB). After one hour of incubation in darkness, half of the samples were irradiated with red light (660 nm; 20 $\mu\text{mol m}^{-2} \text{s}^{-1}$, 1 h), while the other half remained in darkness. Subsequent to illumination/darkness, cells were fixed and the subcellular localization of the proteins analyzed by confocal fluorescence microscopy. Scale bar, 20 μM .

Results and Discussion

As for phyA, only in co-transfection with PIF3-EGFP a nuclear translocation of phyC-mCherry was observed. Contrary to phyA, the nuclear colocalization with the speckles / nuclear bodies of PIF3 appeared independent of the applied light conditions. Subsequent to both, illumination with red light or incubation in darkness, a nuclear translocation of phyC was monitored. All seven other phyC-PIF combinations did not lead to any shifts in the distribution of the fluorescence signal of phyC-mCherry (Figure 2.11).

Results and Discussion

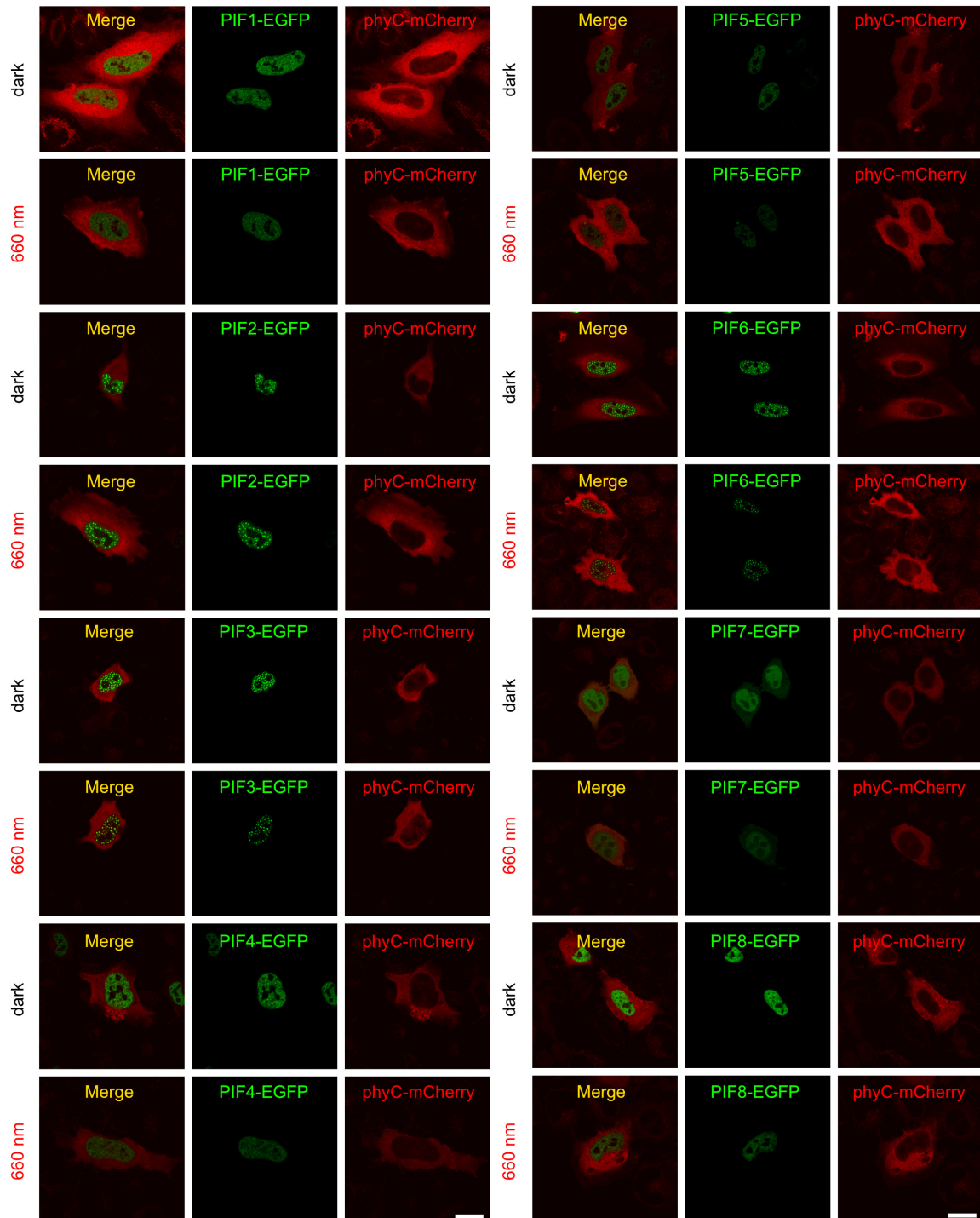


Figure 2.11: Confocal fluorescence microscopy imaging of intracellular localizations of phyC-mCherry and PIF1-8 fused to EGFP in mammalian HeLa cells under different light conditions. phyC-mCherry was co-transfected with PIF1-8 fused to EGFP. 24 h after transfection, the cell culture medium was exchanged with fresh medium, supplemented with 15 μM phycocyanobilin (PCB). After one hour of incubation in darkness, half of the samples were irradiated with red light (660 nm; 20 $\mu\text{mol m}^{-2} \text{s}^{-1}$, 1 h), while the other half remained in darkness. Subsequent to illumination/darkness, cells were fixed and the subcellular localization of the proteins analyzed by confocal fluorescence microscopy. Scale bar, 20 μM .

Results and Discussion

Since phyD-mCherry already possessed nuclear localization without being co-transfected with any PIF, a redistribution of its nuclear signal after co-transfection with the respective PIF constructs was analyzed. Despite all PIF are distributed in bigger or smaller nuclear speckle-like distributions, only the co-transfection of phyD-mCherry and PIF3-EGFP led to the formation of nuclear phyD-mCherry speckles. In all other cases, the expression pattern of phyD-mCherry remained evenly distributed within the analyzed cells (Figure 2.12).

Results and Discussion

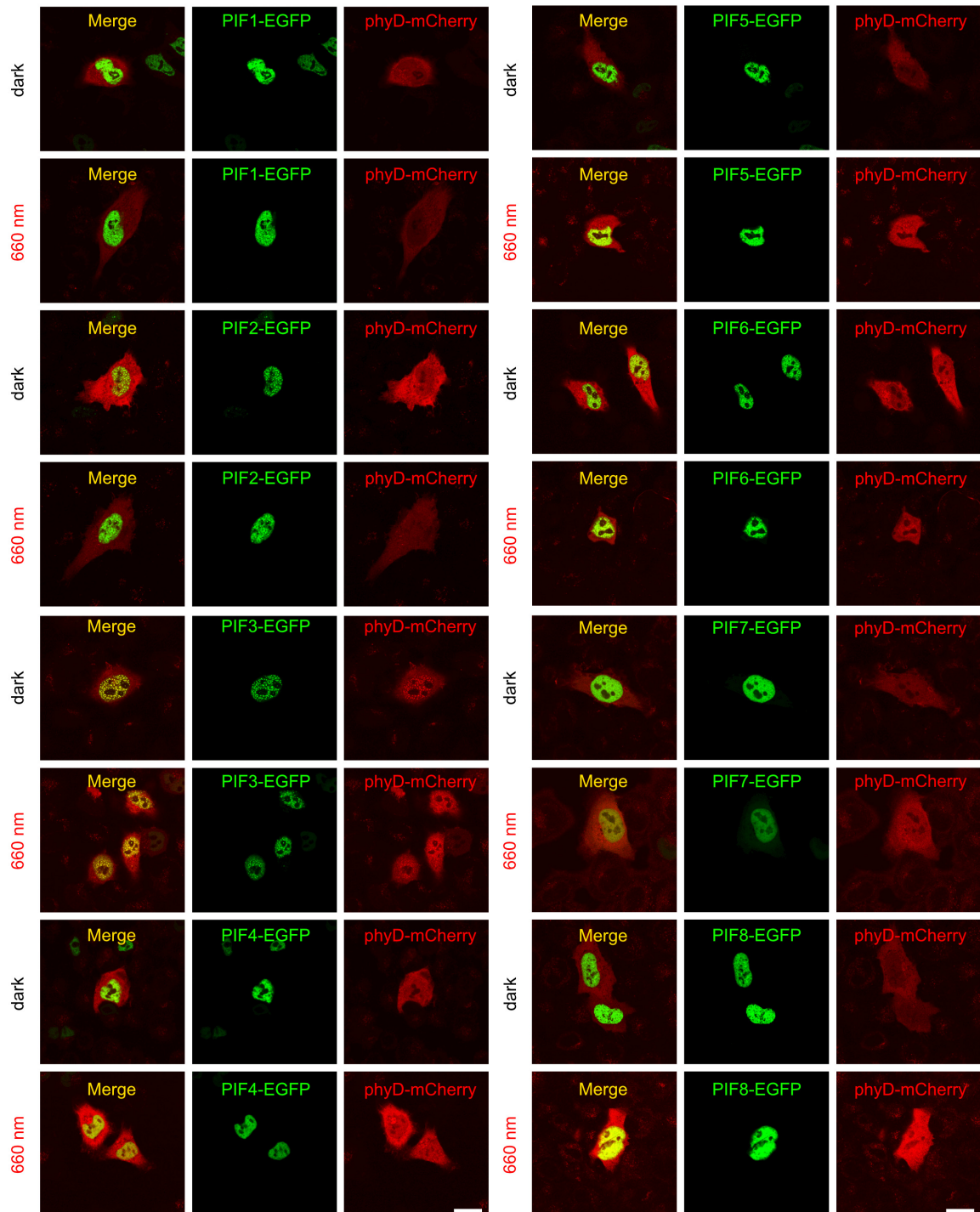


Figure 2.12: Confocal fluorescence microscopy imaging of intracellular localizations of phyD-mCherry and PIF1-8 fused to EGFP in mammalian HeLa cells under different light conditions. phyD-mCherry was co-transfected with PIF1-8 fused to EGFP. 24 h after transfection, the cell culture medium was exchanged with fresh medium, supplemented with 15 μM phycocyanobilin (PCB). After one hour of incubation in darkness, half of the samples were irradiated with red light (660 nm; 20 $\mu\text{mol m}^{-2} \text{s}^{-1}$, 1 h), while the other half remained in darkness. Subsequent to illumination/darkness, cells were fixed and the subcellular localization of the proteins analyzed by confocal fluorescence microscopy. Scale bar, 20 μM .

The combinatorial approach of localization and PPI analysis allows the differentiation between the possibility of phy-PIF interactions, once both proteins are localized in the same cellular compartment (mammalian-hybrid approaches, chapter 3.1.2.1), and the ability of the PIFs of interacting with the respective phys or even transporting them into the nucleus, while being present in their non-modified localization (microcopy analysis, chapter 3.1.2.2). The results of both applied approaches are summarized in Table 2.1.

While the mammalian-hybrid approach revealed interactions of all four tested phytochromes with PIF1, it was not sufficient for nuclear transport of phyA-C. While PIF1 and phyD interacted in both light conditions in the M3H assays, after red light illumination or after incubation in the dark, no changes in its already nuclear and cytoplasmatic localization were observed when co-transfected with PIF1-EGFP. Since PIF1-EGFP did not show distinct nuclear speckle-like structures, a possible co-localization with phyD-mCherry was hard to identify (Figure 2.12). PIF3 showed an interaction pattern similar to PIF1: Red light-dependent interaction with phyA-B and light-independent interaction with phyC-D. Contrary to PIF1, PIF3-EGFP was sufficient for the red light-dependent nuclear transport of phyA and B fused to mCherry, while phyC-mCherry displayed nuclear co-localization with PIF3, independent of the light conditions. Further, the nuclear fraction of phyD-mCherry showed co-localization with PIF3-EGFP. Although PIF1 and PIF3 were reported to bear both, an APA and an APB domain for binding phyA and phyB (Zhu et al., 2000; Khanna et al., 2004; Al-Sady et al., 2006; Shen et al., 2008), our results demonstrate the additional interaction with phyC and phyD. Contrary to phyA and B, no higher affinity for the Pfr form of phyC and D was observed (Figure 2.7 C and D, Figure 2.11 and Figure 2.12), indicating a red light-independent interaction.

Besides PIF1 and PIF3, only phyB indicated interaction with other PIFs in the experiments carried out. The mammalian-hybrid experiments additionally revealed red light-induced interactions with PIF2, PIF6 and PIF8 (Figure 2.6 C). Nevertheless, besides PIF3, only co-expression of PIF2-EGFP generated a nuclear transport of phyB-mCherry (Figure 2.10).

Since only PIF1 and PIF3 have known phytochrome interaction domains beside the ABP domain for interaction with phyB, our results support this assumption. Additional events, like the possible interaction of PIF8 and phyA, as in a previous study (Oh et al., 2020) could not be observed in our experiments.

While redundancy of the components and interconnectivity with other pathways impede the analysis of the phy-PIF network *in planta*, this study might help to decode the behavior of the single components and their connection more precisely. In case of phyA and B, extensive studies on their interactome have been performed, but nevertheless isolated interaction analyses are still rarely seen. Yeast-based approaches reported interactions of phyA with PIF1 and 3, but were only able to use the first 621 amino acids of phyB, since the full-length variant led to autoactivation in the yeast-hybrid assays (Li et al., 2021).

Results and Discussion

With our mammalian-based platform we were able to test the full-length proteins of phyA-D in combination with all known PIFs. Further we were able to combine the simple interaction analysis with localization studies, revealing novel insights into the nuclear transport of the tested phytochromes. This conjointly performed experiments highlight the importance of a many-sided view on the objective, since interaction might only occur once both proteins are located in the same compartment, but their nuclear transport is only carried out by a shorter list of interactors. Nevertheless, the established approaches need subsequent validation in their native environment.

Table 2.1: Summary of phytochrome interaction and localization studies. Color-fillings of the table cells indicate the light condition with detectable interaction (**A**) or nuclear transport / occurrence of nuclear phytochrome speckle-like structures (**B**). In case of phyA, an interaction with PIF1 and 3 was monitored after incubation in darkness, which was not as strong as after red light illumination.

		Interaction SEAP-assay							
A		PIF1	PIF2	PIF3	PIF4	PIF5	PIF6	PIF7	PIF8
	phyA	✓		✓					
	phyB	✓	✓	✓			✓		✓
	phyC	✓		✓					
	phyD	✓		✓					

		nuclear transport / speckles							
B		PIF1	PIF2	PIF3	PIF4	PIF5	PIF6	PIF7	PIF8
	phyA			✓					
	phyB		✓	✓					
	phyC			✓					
	phyD			✓					

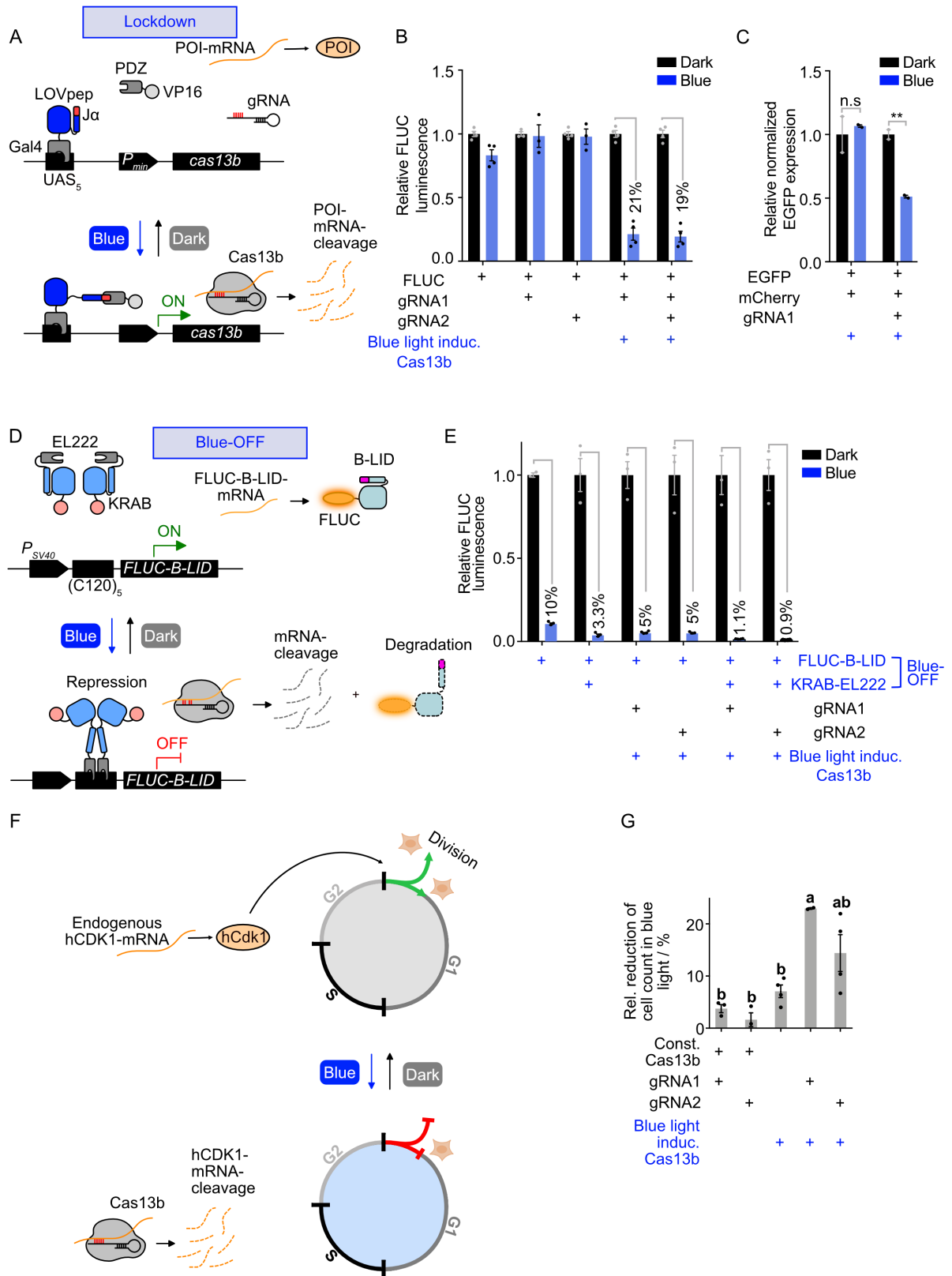
3.2 Tools for controlling signaling in plant and mammalian cells

3.2.1 Blue Light-Operated CRISPR/Cas13b-mediated mRNA Knockdown (Lockdown)

This chapter is based on the publication Blomeier et al., 2021a with equal contribution of Patrick Fischbach, Institute of Synthetic Biology, University of Düsseldorf (Appendix 7.1.2) and represents selected results.

Manipulation of mRNA levels is predominantly performed using inducible RNA interference (RNAi), short regulatory RNAs, or more recently RNA-targeting CRISPR/Cas systems (Chang et al., 2016; Unniyampurath et al., 2016). These approaches are very efficient but lack crucial characteristics, like spatiotemporal control. Optogenetic tools provide these unique properties by utilizing light to precisely control cellular processes within a complex network. However, optogenetic tools for the regulation of mRNA levels are still rarely seen (Vogel et al., 2017; Weber et al., 2019; PilsI et al., 2020). The here described novel Blue Light-Operated, CRISPR/Cas13b-Mediated mRNA Knockdown (Lockdown) system, combines optogenetic control with precise RNA destabilization. Lockdown is composed out of a blue light-inducible split transcription factor, based on the TULIP system, for expression of the recently identified type VI Cas-effector *PspCas13b* (Strickland et al., 2012; Müller et al., 2014a; Cox et al., 2017). The sequence of *PspCas13b* was inserted downstream of a minimal promoter and five adjacent repeats of the GAL4 upstream activating sequence (UAS₅). In darkness, one part of the split transcription factor, GAL4 fused to a modified light-oxygen-voltage domain from phototropin 1 of *Avena sativa* (*AsLOV2*), binds the UAS₅ on the reporter plasmid, without activating transcription. The complex harbors a C-term epitope tag, which is covered by the folded J α -Helix. Upon illumination with blue light, the J α -Helix unwinds. The now exposed tag enables recruitment of ePDZ, which is fused to a transcriptional activation domain (VP16), activating expression of Cas13b. Guided by a constitutively co-expressed gRNA, Cas13b targets and cleaves the mRNA of interest. Inversely, after switching off the illumination, the system rapidly turns off due to the half life time of the excited state of the *AsLOV2* domain (Strickland et al., 2012; Müller et al., 2014a). Dissociation of the split transcription factor stops the expression of Cas13b and discontinues mRNA-cleavage (Figure 2.13 A).

Results and Discussion



Results and Discussion

Figure 2.13: Design and characterization of the Lockdown system. (A) Lockdown architecture. The blue light-responsive split transcription factor, bound to DNA via Gal4, activates expression of the gene encoding Cas13b upon illumination. Blue light illumination recruits the transcriptional activator VP16 via exposition of a PDZ-interacting epitope embedded in the Ja helix. A specific gRNA guides Cas13b to cleave a target mRNA encoding a protein of interest (POI). (B) Co-expression of FLUC-specific gRNA1 or gRNA2 and their influence on FLUC levels in HEK-293T cells using Lockdown to control the expression of Cas13b. The cells were either illuminated with 460 nm light for 24 h (blue bars) or kept in the dark (black bars). Values from illuminated samples were normalized to the corresponding sample kept in the dark. $n = 4$; error bars represent one standard error of the mean. (C) Quantification of EGFP expression via qRT-PCR. HEK-293T cells were co-transfected with the blue light switch, P_{PGK}-EGFP, and P_{SV40}-mCherry. An EGFP-specific gRNA was included. Illumination for 48 h was started 4 h post transfection, or cells were kept in the dark. $n = 2$; error bars represent one standard error of the mean (SEM). Significance was calculated with a paired students t-test (*P < 0.05; **P < 0.01; ***P < 0.001). (D) Combined repression of protein levels using Lockdown and Blue-OFF. In the dark, Lockdown and Blue-OFF are inactive, leading to usual expression levels of target proteins (FLUC). Under blue light, Cas13b (Lockdown) cleaves the target mRNA, whereas the KRAB-EL222 repressor protein and the B-LID degraon (Blue-OFF) repress FLUC production on the transcriptional and post-translational level, respectively. Under blue light, the Blue-OFF system acts by recruiting the KRAB repressor to the promoter by binding of EL222 to 5 repeats of the C120 sequence. B-LID is fused to the FLUC target protein and exposes a RRRG-degron sequence upon illumination, leading to proteasomal degradation. (E) Combinatorial analysis of the Lockdown and Blue-OFF components shown in D. FLUC bioluminescence was determined from lysates of HEK-293T cell expressing the indicated components. The gRNAs from Figure A were used. Cells were illuminated with 460 nm light for 24 h, or kept in the dark. Values were normalized to the corresponding dark sample. $n = 4$, error bars indicate one standard error of the mean. (F) Guided by a hCDK1-specific gRNA, Cas13b binds to the mRNA of hCDK1 for subsequent cleavage. hCDK1 cannot operate at the G2 checkpoint, inducing the transition from G2 to mitosis, causing a G2-arrest and no proliferation of the transfected cells. (G) HEK-293T cells were transiently transfected with the constitutively expressed Cas13b or the Lockdown system and in combination with one of two hCDK1-specific gRNAs, respectively. 4 h post transfection, the cells were either illuminated with $10 \mu\text{mol m}^{-2} \text{s}^{-1}$ of blue light of 460 nm (blue bars) or kept in dark conditions (black bars) for 24 h. Cells were detached from the cell culture plate and measured for total number of cells with a CASY counter (automated cell counting device). The relative reduction of total cells of each transfection set-up were calculated, comparing the mean number of cells grown in dark conditions to cells illuminated with $10 \mu\text{mol m}^{-2} \text{s}^{-1}$ of blue light of 460 nm. The error bars represent the standard error of the mean, $n = 4$. One-way analyzes of variance (ANOVA) were performed with $p < 0.01$. Reprinted (adapted) from Blomeier et al., 2021a (Appendix 7.1.2).

As a proof of principle, two gRNAs targeting the firefly luciferase (FLUC) were designed and co-expressed with a SV40-promoter driven FLUC in human embryonic kidney cells (HEK-293T), respectively. Using Lockdown in combination with each gRNA, comparable results were obtained: In the presence of blue light ($10 \mu\text{mol m}^{-2} \text{s}^{-1}$ at 460 nm, 24 h), the FLUC-levels were reduced to about 20 percent, compared to levels of cells kept in dark (Figure 2.13 B). Experiments with the constitutively expressed Cas13b (data not shown, see Appendix 7.1.2), suggested Lockdown to function in a similar range as the constitutively active variant (Cox et al., 2017).

In order to show the functionality of Lockdown on the mRNA level, quantitative real-time PCR was performed to quantify mRNA cleavage of the fluorescent protein EGFP (Figure 2.13 C). Therefore, HEK-293T cells were transfected with EGFP, constitutively expressed from a PGK promoter, an EGFP-specific gRNA and Lockdown. Further, co-transfection of mCherry was carried out to demonstrate gRNA-specificity. 24 h post transfection, the cells were either illuminated with $10 \mu\text{mol m}^{-2} \text{s}^{-1}$ of blue light (460 nm) or kept continuously under dark conditions. In absence of a respective gRNA, light-dependent reduction of the EGFP level could not be detected. In contrast, combination of gRNA1 and Lockdown, significantly reduced the EGFP signal in blue light conditions, while the mRNA level of mCherry remained comparable to the one under dark conditions. In summary, a reduction of the EGFP-level was monitored, while the level of mCherry remained consistent throughout both conditions,

indicating a blue light-dependent and gRNA-sequence-specific knockdown of the chosen mRNA.

Even though the gene expression process includes diverse steps from initiation of gene transcription to messenger RNA and finally its translation to the final protein (Crick, 1970; Fellmann et al., 2017), methods for protein down-regulation predominantly target only one of the mentioned processes. Hence, targeting multiple processes could increase the efficiency of reducing the expressed amount of the protein of interest. For this purpose, Lockdown was combined with the recently published optogenetic Blue-OFF system for blue light-induced dual-controlled downregulation of protein levels (Baaske et al., 2018; Fischbach et al., 2020) for conjointly accomplishing reduction of protein abundance on three regulatory stages. The Blue-OFF system functions on the level of inhibition of transcriptional initiation with the light-activated KRAB-EL222 repressor module and protein degradation by fusion of a blue light-inducible degradation domain (B-LID) to the protein of interest. Combined, the system immensely reduces the amount of targeted protein, but does not target the already transcribed mRNA. The combination of Blue-OFF and Lockdown could potentially reduce the level protein of interest down to minimum by simultaneously repressing the initiation of its expression, targeting and cleaving its mRNA and degrading the protein itself (Figure 2.13 D).

At first, HEK-293T cells were transfected with a B-LID fused FLUC and incubated in darkness for 24 h, followed by 24 h of illumination with $10 \mu\text{mol m}^{-2} \text{s}^{-1}$ at 460 nm. The relative FLUC expression of cells illuminated with blue light was decreased down to 10 % compared to cells kept under dark conditions. Co-transfection with KRAB-EL222 enabled assembly of the full Blue-OFF system, which should inhibit initiation of the Firefly-B-LID expression (Baaske et al., 2018). This combination reduced the relative expression of the protein down to only 3.3 % after illumination with blue light. While co-transfection with single components of Lockdown did not further decrease the measured protein levels, a combination of FLUC-B-LID and Lockdown with any of the gRNAs, reduced the relative protein levels down to 5 % upon blue light illumination, compared to non-light-treated cells. To analyze the additive effect of all previously mentioned modules, the full Blue-OFF system and Lockdown with each of the designed gRNAs were co-transfected. Combining the individual tool features to down-regulate protein levels, moreover decreased the measured relative reporter expression to around 1 % of the detected level in the dark (Figure 2.13 E).

To demonstrate the functionality of the system to be able to knockdown endogenous mRNA, the human cyclin-dependent kinase 1 (CDK1) was selected for blue light-inducible mRNA downregulation. The Cdk-family of kinases is one of the main regulators of integrating external and internal stimuli for modulating expression of genes and cell division (Morgan, 1997; Malumbres and Carnero, 2003; Lim and Kaldis, 2013; Malumbres, 2014; Leopold et al., 2018). Cdk1 plays a superior role at the checkpoint of coordinating the transition from G2-phase into

mitosis (Malumbres and Barbacid, 2009; Malumbres, 2014; de Gooijer et al., 2017; Prevo et al., 2018). Inhibition of Cdk1 in human cells discontinues the cell cycle through a G2/M arrest, while most proteins connected to the control of Cdks are related to tumor development, making the manipulation and understanding of these regulators of cell proliferation of highest interest (Malumbres and Carnero, 2003). In order to be able to manipulate the cell cycle by down-regulating the mRNA of endogenous hCDK1 in a highly spatiotemporal resolution, HEK-293T cells were co-transfected with one of two designed hCdk1 targeting gRNAs and Lockdown (Figure 2.13 F). Four hours after transfection the cells were illuminated with $10 \mu\text{mol m}^{-2} \text{s}^{-1}$ at 460 nm for 24 h or kept under dark conditions. The combination of Lockdown and each of the gRNAs led to significantly decreased total cell count, when exposed to blue light (Figure 2.13 G), indicating the applicability of Lockdown for the blue light-dependent down-regulation of mRNA of endogenous genes. Since this approach does not require further protein engineering and simply relies on a suitable gRNA design, this strategy can be easily transferred to any other endogenous protein of interest.

In conclusion, the Lockdown system provides highly spatiotemporal regulation of transcription by providing optogenetic control of expression of *PspCas13b* and degradation of RNA, accordingly. Further it can be combined with other systems for synergistic downregulation of protein and mRNA levels. Lockdown can be reprogrammed precisely for targeting any mRNA of interest (exogenous or endogenous) by designing a sequence-specific gRNA.

3.2.2 UV-B light-inducible system (UV-B_{ON}) for the control of gene expression in *A. thaliana* mesophyll protoplasts

This chapter is based on Blomeier et al., 2021c, *in preparation* (Appendix 7.1.3) and represents selected results.

Since the continuing exposure to daylight is indispensable for the life cycle of plants, optogenetic systems for application in plants or plant systems need to bypass the activation by daylight. Applied examples are the strict activation by a single range of wavelengths, while exposure to white light deactivates the systems, as for PULSE (Ochoa-Fernandez et al., 2020) or using light of a wavelength with minimal interference to the plants photoreceptors like the CarH-based system, which is inactivated by green light and only active in the dark (Chatelle et al., 2018). For the purpose of expanding the toolbox of optogenetic switches for application in plant systems, we repurposed a UV-B responsive split transcription factor system, based on the interaction of *A. thaliana* UV-B photoreceptor UVR8 and COP1 for application in mammalian cells (Müller et al., 2013b), for functionality in plant systems. As plant protoplasts offer a platform for the fast and reliable prototyping, which has extensively been applied for plant synthetic biological approaches (Schaumberg et al., 2016; Lin et al., 2020; Ochoa-Fernandez et al., 2020; Lin et al., 2021), we characterized our system in this platform.

In the absence of UV-B, UV RESISTANCE LOCUS 8 (UVR8) homodimerizes, while exposure to UV-B disrupts the dimerization (Rizzini et al., 2011). The now monomeric UVR8 is the active conformer and enables interaction with the E3-ubiquitin ligase CONSTITUTIVE PHOTOMORPHOGENIC 1 (COP1). Point of the interaction is the conserved WD40 domain (residues 336-674) of COP1 (Favory et al., 2009). Mediated by direct interaction with REPRESSOR OF UV-B PHOTOMORPHOGENESIS 1 (RUP1) and RUP2, UVR8 homodimerizes again in the dark, inhibiting the interaction with COP1 (Gruber et al., 2010; Heijde and Ulm, 2013). Since mammals have a counterpart of COP1 with 50 % similarity, only the WD40-domain of COP1, necessary and sufficient for interaction with UVR8 (Rizzini et al., 2011) was used in the previous study. To avoid any interaction with endogenous pathways, the truncated version of UVR8, with removed N- and C-terminal tails, was utilized. In order to create a UV-B light inducible split transcription factor system, COP was C-terminally fused to a transactivation domain (VP16), while UVR8 was bound to the DNA-binding macrolide repressor (E) on its N-terminal. E is bound to a specific DNA-motif (erythromycin resistance operator; *etr₈*) on the reporter plasmid, containing the reporter gene under control of a minimal human cytomegalovirus immediate early promoter ($P_{hCMVmin}$). In the dark, UVR8 homodimerizes without activating gene expression. Upon illumination with light of the UV-B range of wavelengths, UVR8 monomerizes and is able to interact with COP1, generating close proximity of VP16 to the minimal promoter. Subsequent, the transcriptional machinery is

recruited, inducing expression of the reporter gene. Reconversion of UVR8 to the homodimerized state in the absence of UV-B terminates the gene expression.

In order to adapt the switch designed for usage in mammalian cells, E-UVR8 and COP1-VP16 were expressed under control of the CaMV35S promoter, functioning in *A. thaliana*. Further, the SEAP reporter gene was exchanged by the highly sensitive Firefly luciferase (FLUC; Figure 2.14 A). To avoid influence of light from other wavelengths than UV-B, a filter glass with an emission spectrum of 260 – 390 nm, was placed between the light source and the protoplasts. *A. thaliana* mesophyll protoplasts were isolated and transformed as described (Ochoa-Fernandez et al., 2016). Transformation with the indicated components was followed by four hours of incubation in the dark and by another 18 hours of illumination with light of 311 nm ($7 \mu\text{mol m}^{-2} \text{s}^{-1}$) or incubation in the dark. Co-transformation of a constitutively expressed renilla luciferase (RLUC) served as normalization element. After exposure to the described light conditions, luciferase activity was determined by calculating the FLUC/RLUC ratio.

At first the original switch with the required changes for application in plant cells was tested. While a fusion of E-VP16 acted as positive control of the E-based system, single transformation of the reporter plasmid was used for determining the background activation of the synthetic promoter. Further, both proteins were fused to a nuclear localization, guaranteeing the nuclear abundance of all needed components, to compare their function. Nuclear localization of UVR8 reduced leakiness in combination with both variants of COP1, but also decreased the activity of the system in UV-B illumination. Both combinations possessed a comparable dynamic range between protoplasts kept in the dark and UV-B exposed counterparts of 16- and 13-fold, respectively. The UVR8 variant without NLS showed stronger activation in co-transformation with the non-tagged COP1, with comparable induction fold of 13x, while co-expression of COP1-VP16-NLS led to a weaker activation of the system in UV-B, with the lowest measured induction fold of 8.

Since the non-tagged variant of UVR8(12-381) displayed the strongest UV-B induced activation, a full-length version of UVR8 was further compared to the truncated version. In relation to the previously described combinations, co-transformation of the complete UVR8 protein and both COP1 version, led to a much stronger activation of the system with induction folds of 38 (COP1-VP16) and 28 (COP1-VP16-NLS) (Figure 2.14 B).

Since previous studies reported the homodimerization of UVR8 in darkness to be promoted by RUP1 and RUP2 (Gruber et al., 2010; Heijde and Ulm, 2013), functionality of the system in protoplast isolated from wild type (Col-0) plants was compared to *rup1/rup2* double mutant protoplasts. Interestingly, the combinations of COP1 with the full length UVR8 generated even stronger induction folds as in the wild type background (data not shown, see Appendix 7.1.3). Nevertheless, the functionality of the system was not drastically improved, leading to the decision of continuing the characterization of the system in the wild type background.

Results and Discussion

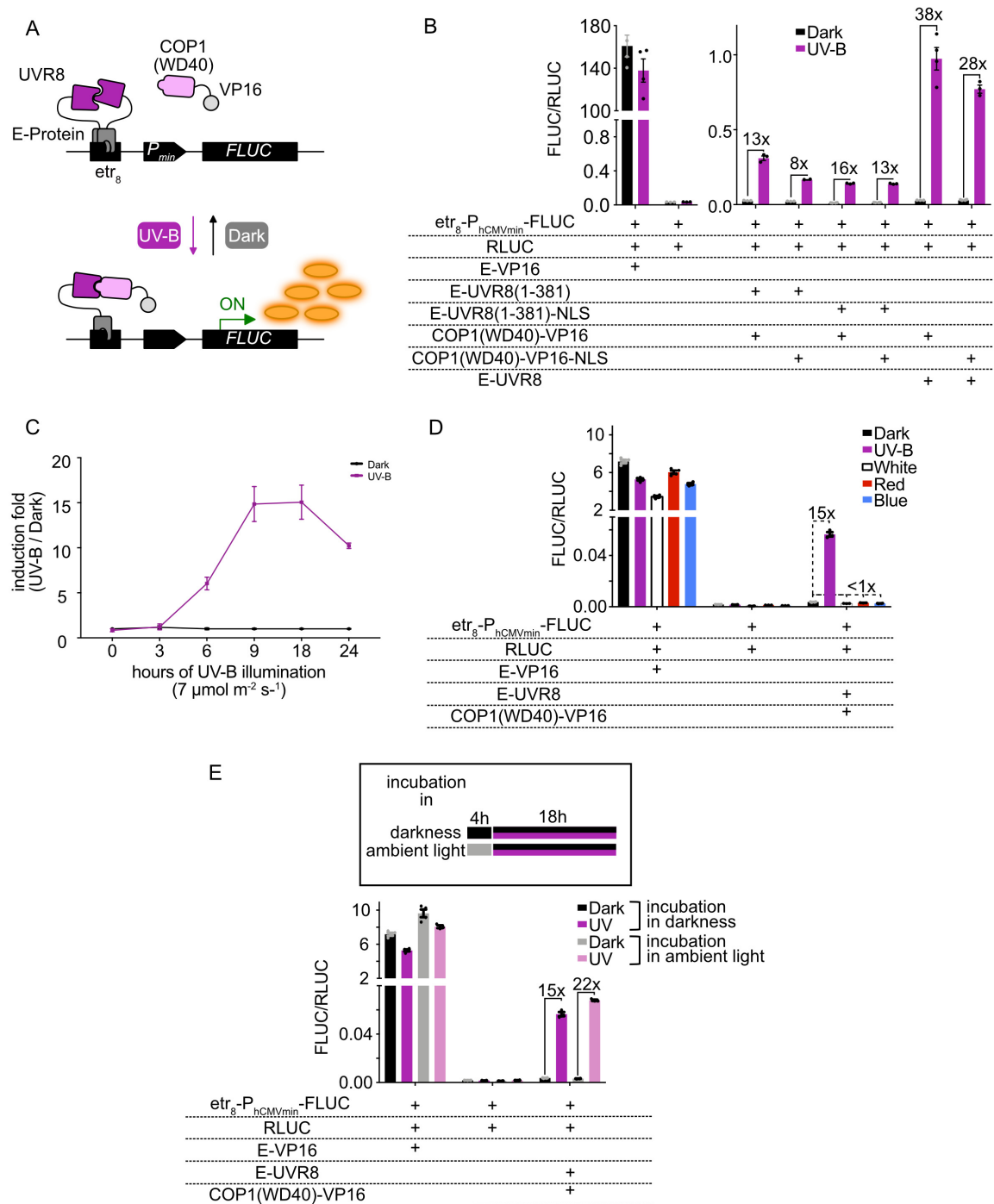


Figure 2.14: Mode of function and characterization of the UV-B light-induced gene expression system (UV-B_{ON}) for application in *A. thaliana* protoplasts. (A) Mode of function. Under dark conditions, UVR8 dimers fused to the macrolide repressor E are bound to the octameric *etr*₈ operator sequence on the reporter plasmid without activating gene expression. Upon illumination with UV-B light (311 nm) dimerization of UVR8 is disrupted by conformational change of UVR8 to its open state. The open, non-dimerized state is able to bind to COP1(WD40) and recruits it to the reporter plasmid. COP1(WD40) is fused to the VP16 transactivation domain, now in close proximity to the minimal promoter, initiating gene expression of the firefly luciferase (FLUC) reporter gene. In absence of UV-B illumination, UVR8 spontaneously reverts back to the closed state, terminating the gene expression (adapted from Müller et al., 2013b). (B) Characterization of the UV-B inducible gene expression system in wild type protoplasts of *A. thaliana*. Protoplasts were isolated and transformed with the indicated components. After transformation and four hours of incubation in the dark, protoplasts were exposed to light of 311 nm ($7 \mu\text{mol m}^{-2} \text{s}^{-1}$) for 18 hours (purple bars) or kept in the dark (black/grey bars) before the FLUC expression, normalized to constitutively expressed renilla luciferase (RLUC), was determined. $n = 4$, error bars indicate one standard error of the mean (SEM). (C) Kinetics of the UV-B inducible gene expression system (UV-B_{ON}). Protoplasts were isolated and transformed with E-UVR8 and COP1(WD40)-VP16 and the reporter

Results and Discussion

plasmid ($\text{etr}_8\text{-P}_{\text{CMVmin}}\text{-FLUC}$). After transformation and four hours of incubation in the dark, protoplasts were exposed to light of 311 nm ($7 \mu\text{mol m}^{-2} \text{s}^{-1}$) or kept in the dark for the indicated time intervals, before the FLUC expression, normalized to constitutively expressed renilla luciferase (RLUC), was determined. Values were normalized to the corresponding dark sample. $n=4$, error bars indicate one standard error of the mean (SEM). (D) Characterization of the UV-B light-induced gene expression system (UV-B_{ON}) for application in *A. thaliana* protoplasts in different light conditions. Protoplasts were isolated and transformed with the indicated components. After transformation and four hours of incubation in the dark, protoplasts were exposed to light of 311 nm ($7 \mu\text{mol m}^{-2} \text{s}^{-1}$; purple bars), white light ($10 \mu\text{mol m}^{-2} \text{s}^{-1}$ for the following wavelength ranges: blue 420–490 nm, red 620–680 nm, and far-red 700–750 nm white bars), blue light of 460 nm ($5 \mu\text{mol m}^{-2} \text{s}^{-1}$; blue bars), red light of 660 nm ($5 \mu\text{mol m}^{-2} \text{s}^{-1}$, red bars) for 18 hours or kept in the dark (black bars) before the FLUC expression, normalized to constitutively expressed renilla luciferase (RLUC), was determined. $n = 4$, error bars indicate one standard error of the mean (SEM). (E) Characterization of the UV-B light-induced gene expression system (UV-B_{ON}) for application in *A. thaliana* protoplasts after different incubation conditions. Protoplasts were isolated and transformed with the indicated components. After transformation and four hours of incubation in the dark or under ambient light, protoplasts were exposed to light of 311 nm ($7 \mu\text{mol m}^{-2} \text{s}^{-1}$; purple/rose bars) for 18 hours or kept in the dark (black/grey bars) before the FLUC expression, normalized to constitutively expressed renilla luciferase (RLUC), was determined. $n = 4$, error bars indicate one standard error of the mean (SEM). This figure and the figure legend are adapted from the manuscript of Blomeier et al., 2021c, Appendix 7.1.3.

Induction kinetics of the system further evaluated the dynamics of the UV-B_{ON} system (Figure 2.14 C). Here, the UVR8-COP1 combination with the biggest dynamic range, composed of the full length UVR8 and COP1-VP16, was transformed and revealed no activation of the systems in the first three hours of illumination, while the peak of activation seemed to be reached after 18 hours. A longer exposure to pure UV-B light might have influence on the fitness of the protoplasts.

In a following experiment the influence of light from other wavelengths on the induction of the described UV-B_{ON} system was evaluated (Figure 2.14 D). Therefore, the protoplasts were not only exposed to light of 311 nm, but additionally to simulated white ($10 \mu\text{mol m}^{-2} \text{s}^{-1}$ for the following wavelength ranges: blue 420–490 nm, red 620–680 nm, and far-red 700–750 nm, see Ochoa-Fernandez et al., 2020), red (660 nm; $5 \mu\text{mol m}^{-2} \text{s}^{-1}$) and blue light (460 nm; $5 \mu\text{mol m}^{-2} \text{s}^{-1}$). The duration of illumination was, as before, 18 hours, after 4 hours of incubation in the dark. In the described experiment, all other light conditions had an effect on the fitness of the protoplast, since the E-VP16 held a lower RLUC/FLUC ratio than protoplast kept in the dark, with the lowest measured value in white light. While the reporter alone did not indicate any changes in RLUC/FLUC ratios in all tested light conditions, illumination with UV-B led to an induction in RLUC/FLUC ratio of 15-fold for the UVR8-COP1 switch, compared to protoplasts kept in darkness. The three other light conditions led to no induction of the system, when compared to protoplasts of the control group, kept in the dark.

After fitting an ordinary differential equations (ODE) model to our obtained data from the kinetics experiment, we hypothesized endogenous COP1 to potentially inhibit the interaction of our E-UVR8 and COP1(WD40)-VP16 split transcription factor (data not shown, see Appendix 7.1.3). To test our hypothesis, protoplasts of the same transformation were analyzed on the influence of incubation in ambient light before exposure to UV-B light, in order to reduce the possible inhibitory effect of nuclear COP1 in darkness (von Arnim and Deng, 1994; Lau and Deng, 2012; Pacín et al., 2014; Yin et al., 2016). Here the previously applied incubation in darkness was compared to incubation under ambient light conditions in a growth chamber.

Since the protoplasts were from the same round of transformation as in the experiment diagrammed in Figure 2.14 D, the values of protoplasts incubated in darkness are the same. Interestingly, incubation under ambient light conditions increased the overall fitness of both, protoplasts subsequently kept in the dark, or UV-B exposed counterparts. It also led to a higher induction of the UV-B induced system from 15-fold after incubation in darkness, to 22-fold after incubation under ambient light conditions (Figure 2.14 E).

Summarized, we have successfully developed an UV-B responsive optogenetic switch for the use in *A. thaliana* mesophyll protoplasts cells by adapting the design of the UVR8-COP1 based system, previously described in mammalian cells. We further improved the dynamic range of the system by exchanging truncated versions of UVR8 with the full-length variant of UVR8 (Figure 2.14 B). Since the switch was not activated by any other tested light condition (Figure 2.14 D), the autonomy from another “OFF-module” for deactivation of the gene expression under other light conditions than UV-B and the thereby simpler organization and smaller size of the system, could be a benefit compared to other systems like PULSE (Ochoa-Fernandez et al., 2020). In addition, combination of UVR8_{ON} with other light-responsive modules like the Red_{ON} or the BLUE_{OFF} switches (Müller et al., 2014b; Ochoa-Fernandez et al., 2016; Ochoa-Fernandez et al., 2020) could expand the range of applications for multichromatic control of gene expression in plant systems. Further, we applied mathematical modeling to our obtained results, which led to the attempt of incubation our protoplasts in ambient light, which ultimately even indicated beneficial effects on protoplast fitness and induction of our system. Simple filtration of light of the UV range of wavelength might further allow the expression of the system in full plant systems, growing under ambient light conditions without activation of gene expression. Nevertheless, subsequent experiments of the functionality of UV-B_{ON} in ambient light conditions with supplemented UV-B irradiation need to be performed. However, the transfer of the system into stable plant lines expressing the switch will be needed to test if the indicated characteristics of the systems can be transferred from protoplasts to full plants.

4 Conclusion

This work combines the establishment and characterization of synthetic biology approaches for the (quantitative) analysis, control or manipulation of signaling processes in (orthogonal) mammalian and plant systems:

First, we adapted and redesigned various systems for analyzing protein-protein-interactions or protein-DNA-interactions originating from plants, in an orthogonal mammalian cell system. Isolated from their highly complex, redundant and intertwined signaling networks in plants, the behavior of single components and their interplay could be monitored in a quantitative manner. Among them, M1H to M4H systems were exemplary established on the gibberellin perception mechanism of *A. thaliana* and associated downstream signaling processes. Interactions of the corresponding proteins were tested on their phytohormone-dependency, while different configurations of the system helped to understand the complex-formation during GA-perception. Further, transcription factors were tested on their binding to specific DNA sequences and their ability of activation gene expression. (Quantitative) microscopy approaches were established for supporting the previously collected information on PPI in a highly sensitive manner and enabled monitoring localization and possible translocation of the respective proteins.

The established approaches were subsequently utilized for investigation on the phytochrome-PIF-interaction network. Here, we combined interaction analyses between phy and PIFs with M3H approaches and microscopical studies of possible PIF-mediated nuclear transport mechanisms and their dependence on red light. For the first time, full sets of isolated interaction and localization studies of phyA-D with all known PIFs were performed, giving new hints on these complex light- and localization-dependent signaling events. They could help to understand their function and role within signaling networks in the future.

Second, novel optogenetic tools were designed and characterized for their functionality in mammalian and plant systems. We developed the Lockdown system for spatiotemporal control of degradation of the exo- or endogenous RNA of choice, by using a blue light-responsive optogenetic switch (AsLOV2-ePDZ) for expression of the RNA-processing *PspCas13b*. Further, Lockdown was combined with other blue light-inducible switches for the triple-controlled downregulation of protein levels by inhibition of the transcriptional initiation, protein degrading and mRNA cleavage.

Finally, we engineered a UV-B light-induced optogenetic switch (UV-B_{ON}) for usage in *A. thaliana* mesophyll protoplasts on the base of UV-B induced interaction of COP1 and UVR8. Being activated exclusively by light of the UV-B range of wavelengths, this switch could be transferred for usage in full plants, growing under ambient light conditions with filtered UV-B irradiation in the future.

5 Materials and Methods

5.1 Mammalian cell experiments

5.1.1 Plasmid generation/construction

Plasmids and Oligonucleotides designed and constructed in the frame of this thesis are listed in Table 5.1 and 5.2

5.1.2 Mammalian cell cultivation and transfection

All experiments are based on transient plasmid transfection of the respective mammalian cells. human embryonic kidney cells (HEK-293T; DSMZ, Braunschweig, Germany), human epithelioid cervix carcinoma cells (HeLa; DSMZ, Braunschweig, Germany) and Chinese hamster ovary cells (CHO-K1; DSMZ) were cultivated seeded and transfected as described before (Müller et al., 2013b; Beyer et al., 2015a). Cells were either transfected in 24-well (5×10^4 cells) or 96-well (8×10^3 cells) plates using polyethyleneimine (PEI; Polysciences Inc. Europe, Hirschberg, Germany; no. 23966-1). If not indicated otherwise, all plasmids were transfected in equal amounts (w/w).

5.1.3 Phytohormone experiments

The GA substrate Gibberellic Acid Acetoxymethyl Ester (GA₃-AM) was obtained from Santa Cruz Biotech (Dallas, USA). 24 h post transfection the cultivation medium was exchanged with fresh cultivation medium, either containing 10 μM of GA₃-AM (if not indicated otherwise) or the equal amount of DMSO. Hormone incubation was performed for 24 h for SEAP reporter assays and for 4 h for microscopy experiments (if not indicated otherwise). As described in the manuscript of Blomeier et al., 2021b (Appendix 7.1.1).

5.1.4 Light experiments in mammalian cells

In order to prevent the cell samples from unintended activation of the light-sensitive systems, work was performed under safe light conditions (522 nm). 24 h post transfection, mammalian cells were illuminated using custom-built LED light-boxes housing LEDs of the respective wavelengths (460 nm for blue light experiments and 660 nm for red light experiments) for the indicated periods of time with a light intensity of 10 (blue) or 20 (red) $\mu\text{mol m}^{-2} \text{s}^{-1}$ or kept in darkness (typically for 24 h, unless indicated otherwise). 96-well experiments of Appendix 7.1.2 were done in optoPlate-96 illumination devices (Bugaj and Lim, 2019; Thomas et al., 2020).

Materials and Methods

5.1.5 SEAP reporter assay

SEAP production of the respective cells was performed as described elsewhere (Müller et al., 2013a). In brief, 24 h after light exposure or hormone induction, samples were heat-inactivated and transferred to 96 well assay plates. After supplementation of SEAP buffer (20 mM L-homoarginine, 1 mM MgCl₂ 21 % (v/v) diethanolamine), 20 µL of 120 nM para-Nitrophenylphosphate (pNPP, Sigma-Aldrich, St. Louis, USA) were added, before the absorbance was measured at 405 nm for one hour using a BMG Labtech CLARIOstar (BMG Labtech GmbH, Orthenberg Germany). Determination of the SEAP activity [U/L] was performed by calculating the slope of the absorbance values [OD/min] using Lambert-Beer's-law:

$$\frac{U}{L} = \frac{E}{\varepsilon \times d} \times 10^6 \times \frac{200}{80}$$

E = increase in optical density/para-nitrophenolate per minute

$\varepsilon = 18,600 \text{ M}^{-1}\text{cm}^{-1}$

d = length of the light path [cm], 0.6 cm

$\frac{200}{80}$ = amount of SEAP-containing supernatant / dilution factor of the sample.

5.1.6 Fixation and imaging of mammalian cells

Cells were seeded on glass coverslips and fixed with paraformaldehyde after the experiment was performed as described in Blomeier et al., 2021a (Appendix 7.1.2) and elsewhere (Beyer et al., 2015a)

5.1.7 Microscopy

Confocal imaging was performed with an Eclipse Ti microscope (Nikon, Tokyo, Japan) equipped with a C2plus confocal laser scanner and a 20x air objective, NA=0.45 or a 60x oil objective NA=1.40 as described in Blomeier et al., 2021a (Appendix 7.1.2) and the manuscript of Blomeier et al., 2021b (Appendix 7.1.1). EGFP and mCherry fluorescence were visualized using an excitation laser of 488 and 561 nm and emission filters from 505-545 and 570-620 nm, respectively.

5.1.8 FRET-APB experiments

FRET-APB measurements were operated with the NIS elements software (Nikon, Tokyo, Japan) using a laser power of 0.1 % of the 488 nm laser and 0.5% for the 561 nm laser to avoid acquisition bleaching of the fluorophores before bleaching, as described in the manuscript of Blomeier et al., 2021b (Appendix 7.1.1). The FRET efficiency was calculated by

Materials and Methods

analyzing the percentage of relative changes in EGFP intensity before and after bleaching (EFRET = $((EGFP_{\text{after}} - EGFP_{\text{before}}) / (EGFP_{\text{after}})) * 100$).

5.1.9 FRET-FLIM experiments

FRET-FLIM measurements were performed using a LSM 780 confocal laser-scanning microscope (Zeiss, Oberkochen, Germany) equipped with a single-photon counting device (PicoQuant Hydra Harp 400, PicoQuant, Berlin, Germany). HEK-293T cells were seeded into chambered 4-well glass bottom dishes, while cells were live-imaged covered with a live-cell imaging solution (Thermo fisher) as described in the manuscript of Blomeier et al., 2021b (Appendix 7.1.1).

5.1.10 Luminescence analysis of mammalian cell experiments

Firefly luciferase assays were performed as described in Blomeier et al. 2021a, (Appendix 7.1.2). The cells were lysed and incubated as previously described (Baaske et al., 2018), with the exception of cells grown in 96-well plates. Here, the supernatant was removed and the substrate was directly added to the cells without prior cell lysis. For detection of Luminescence a Centro XS3 LB960 Microplate Luminometer (Berthold Technologies, Bad Wildbad, Germany) was used.

5.1.11 Quantitative real time PCR

RNA isolation, conversion of RNA to cDNA and qRT-PCR experiments were performed as described in Blomeier et al., 2021a (Appendix 7.1.2)

5.1.12 Western Blot

Western Blot experiments for the detection of EGFP and Actin were performed as described in Blomeier et al., 2021a (Appendix 7.1.2)

5.1.13 Cell proliferation assays

For cell proliferation assays, HEK-293T cells (30,000 cells) were seeded, transfected and illuminated as described above. On the next day, cells were detached from the cultivation plate, before the cell concentration was determined with a Cell counter CASY (OMNI Life Science, Bremen, Germany) as described in Blomeier et al., 2021 (Appendix 7.1.2).

5.1.14 Statistics

Ordinary one-way ANOVAs and student's t-tests for determination of statistical significance were performed with GraphPad Prism 7 for Mac Os X version 10.13.1. Statistical outliers were determined and excluded as described elsewhere (Jacobs and Dinman, 2004).

5.2 Protoplast experiments

5.2.1 Protoplast isolation and transformation

Preparation of seedlings, plant growth conditions, protoplast isolation and transformation was performed as described by Ochoa-Fernandez et al., 2016. A total of 40 µg of DNA was transformed with ratios of 15 µg for COP1 and UVR8 containing plasmids, respectively and 7.5 µg of the $\text{etr}_8\text{-P}_{\text{hCMVmin}}$ -FLUC reporter, as well as 2.5 µg of the RLUC containing plasmid for normalization of FLUC luminescence.

5.2.2 UV-Light experiments in protoplasts

UV-B light experiments were performed as described in the manuscript of Blomeier et al., 2021c. 800 µL of each transformation set-up was transferred to a 24 well plate and incubated for 4 hours under the respective conditions. Afterwards, protoplasts were illuminated with light of 311 nm (UV-B) or kept in darkness (typically for 18 h, unless indicated otherwise).

5.2.3 Luminescence analysis of protoplast experiments

The luminescence analysis of the protoplast experiments was performed as described in the manuscript of Blomeier et al., 2021c. Firefly and renilla luminescence were measured in a Centro XS3 LB960 Microplate Luminometer (Berthold Technologies, Bad Wildbad, Germany).

5.2.4 Light source and illumination conditions

As described in the manuscript of Blomeier et al., 2021c, UV-B illumination of protoplast samples was performed with a UVB narrowband lamp (Philips, prod. no. PL-S 9W/01) covered by an ultraviolet transmitting, visible light absorbing filter (U340, Hoya, Tokio, Japan) at a light intensity of $7 \mu\text{mol m}^{-2} \text{s}^{-1}$ of 311 nm UV-B light, if not indicated otherwise.

5.3 Plasmids

Table 5.1: Construction and description of plasmids used in this work. (All plasmids were constructed using AQUA and Gibson assembly cloning methods.)

Plasmid	Description	Reference
pC0043	P_{U6}-PspCas13b DR-BbsI-BbsI-pA P _{U6} -driven mammalian expression vector for cloning of guide RNAs compatible with PspCas13b.	pC0043-PspCas13b crRNA was a gift from Feng Zhang (Addgene #103854) (Cox et al., 2017)
pC0046	P_{EF1α}-PspCas13b-NES-HIV P _{EF1α} driven mammalian expression vector for expression of PspCas13b for knockdown of target RNAs in combination with compatible gRNAs.	pC0046-EF1α-PspCas13b-NES-HIV was a gift from Feng Zhang (Addgene #103862) (Cox et al., 2017)
pGB109	P_{CaMV35S}-RLUC-pA P _{CaMV35S} -driven plant expression vector encoding the renilla luciferase.	GoldenBraid Database
pJA086	P_{SV40}-mEGFP-pA P _{SV40} -driven mammalian expression vector encoding the fluorescent protein mEGFP.	Jennifer Andres (unpublished)
pLKTBP001	P_{CMV}-FLUC-pA P _{CMV} -driven mammalian expression vector encoding the firefly luciferase.	Unpublished
pLJM1-GFP	5'LTR-RRE-P_{CMV}-EGFP-P_{PGK}-Puro'-3'LTR 3 rd generation lentiviral vector for EGFP fusion; PGK-driven puromycin resistance.	pLJM1-EGFP was a gift from David Sabatini (Addgene #19319) (Sancak et al., 2008)
pKM081	etr₈-P_{CMVmin}-SEAP-pA Vector encoding SEAP under control of a modified P _{ETR} .	(Müller et al., 2013b)
pKM195	(pifO)₄-P_{hCMVmin}-SEAP-pA Vector encoding SEAP under control of a pif operator-CMVmin promoter.	Konrad Müller, unpublished
pKM083	UAS₅-TATA-GLUC-pA Vector encoding Gaussia luciferase (GLUC) under control of P _{Gal4} .	(Müller et al., 2014a)

Materials and Methods

pKM516	P_{SV40}-Gal4BD-LOVpep[T406A,T407A,I532A]-IRESPV-ePDZb-VP16-NLS-pA P _{SV40} -driven bicistronic mammalian vector encoding Gal4BD-LOVpep[T406A,T407A,I532A] and ePDZb-VP16-NLS.	(Müller et al., 2014a)
pKM565	P_{SV40}-KRAB-EL222-pA P _{SV40} -driven mammalian expression vector encoding the light-responsive repressor KRAB-EL222.	(Baaske et al., 2018)
pMZ333	P _{SV40} driven mammalian expression vector derived from <i>XbaI/NotI</i> digested pSAM200.	(Beyer et al., 2015a)
pMZ725	P_{SV40}-PIF3-mEGFP-pA P _{SV40} -driven mammalian expression vector encoding <i>A. thaliana</i> PIF3 fused to the fluorescent protein mEGFP.	(Beyer et al., 2015a)
pMZ820	P_{CaMV35S}-E-UVR8(12-381)-pA P _{CaMV35S} -driven plant expression vector encoding <i>A. thaliana</i> UVR8(12-381) fused to the macrolide repressor E.	Matias Zurbriggen (unpublished)
pMZ821	P_{CaMV35S}-COP1(WD40)-VP16-pA P _{CaMV35S} -driven plant expression vector encoding the WD40 domain of <i>A. thaliana</i> COP1 fused to the VP16 transactivation domain.	Matias Zurbriggen (unpublished)
pMZ824	P_{CaMV35S}-E-VP16-NLS-pA P _{CaMV35S} -driven plant expression vector encoding the macrolide repressor E fused to the VP16 transactivation domain and a nuclear localization domain.	Matias Zurbriggen (unpublished)
pMZ1173	P_{SV40}-phyA-mCherry-pA P _{SV40} -driven mammalian expression vector encoding <i>A. thaliana</i> phytochrome A fused to the fluorescent protein mCherry.	Matias Zurbriggen (unpublished)
pMZ1203	P_{SV40}-(C120)₅-FLUC-B-LID-pA P _{SV40} -driven mammalian expression vector encoding the firefly luciferase fused to a blue light-inducible degron (B-LID), containing the EL222-DNA-binding site (C120) ₅ .	(Baaske et al., 2018)
pMZ1214	P_{SV40}-VTC2-VP16-IRES-TetR-PAS-LOV_{WT}-pA	Matias Zurbriggen (unpublished)
pPF002	tetO₄-P_{CMVmin}-SEAP-BGHTA; P_{SV40}-RLUC-SV40TA	Patrick Fischbach (unpublished)
pPF131	P_{SV40}-phyB-VP16-IRES-TetR-PIF1-pA	Patrick Fischbach (unpublished)
pHB018	P_{SV40}-phyE-mCherry-pA P _{SV40} -driven mammalian expression vector encoding <i>A. thaliana</i> phytochrome E fused to the fluorescent protein mCherry.	Hannes Beyer (unpublished)
pHB090	P_{SV40}-PIF1-mEGFP-pA P _{SV40} -driven mammalian expression vector encoding <i>A. thaliana</i> PIF1 fused to the fluorescent protein mEGFP.	Hannes Beyer (unpublished)

Materials and Methods

pHB091	P_{SV40}-PIF4-mEGFP-pA P _{SV40} -driven mammalian expression vector encoding <i>A. thaliana</i> PIF4 fused to the fluorescent protein mEGFP.	Hannes Beyer (unpublished)
pHB092	P_{SV40}-PIF5-mEGFP-pA P _{SV40} -driven mammalian expression vector encoding <i>A. thaliana</i> PIF5 fused to the fluorescent protein mEGFP.	Hannes Beyer (unpublished)
pHB093	P_{SV40}-PIF6-mEGFP-pA P _{SV40} -driven mammalian expression vector encoding <i>A. thaliana</i> PIF6 fused to the fluorescent protein mEGFP.	Hannes Beyer (unpublished)
pHB094	P_{SV40}-PIF7-mEGFP-pA P _{SV40} -driven mammalian expression vector encoding <i>A. thaliana</i> PIF7 fused to the fluorescent protein mEGFP.	Hannes Beyer (unpublished)
pRD093	P_{SV40}-PIF3-mVenus-pA P _{SV40} -driven mammalian expression vector encoding <i>A. thaliana</i> PIF3 fused to the fluorescent protein mVenus.	Rebecca Driesch (unpublished)
pROF052	(etr)₈-P_{hCMVmin}-FLUC-pA	Rocio Ochoa-Fernandez
pROF150	P_{CaMV35S}-E-UVR8(12-381)-NLS-pA E-UVR8 was amplified from pMZ820 with oligos oROF003/157. pMZ827 was linearized by <i>EcoRI/NdeI</i> . Both fragments were assembled by AQUA cloning.	This work
pROF151	P_{CaMV35S}-COP1(WD40)-VP16-NLS-pA COP1(WD40)-VP16 was amplified from pMZ821 with oligos oROF003/158. pMZ827 was linearized by <i>EcoRI/NdeI</i> . Both fragments were assembled by AQUA cloning.	This work
pRSET	PT7-driven bacterial expression vector	Novagen
pSAM	P_{SV40}-TetR-VP16-pA	(Fussenegger et al., 1997)
pSJ025	P_{SV40}-phyB-mCherry-pA P _{SV40} -driven mammalian expression vector encoding <i>A. thaliana</i> phytochrome B fused to the fluorescent protein mCherry.	(Beyer et al., 2015a)
pSJ050	P_{SV40}-phyC-mCherry-pA P _{SV40} -driven mammalian expression vector encoding <i>A. thaliana</i> phytochrome C fused to the fluorescent protein mCherry.	Samuel Julliot (unpublished)
pSJ051	P_{SV40}-phyD-mCherry-pA P _{SV40} -driven mammalian expression vector encoding <i>A. thaliana</i> phytochrome D fused to the fluorescent protein mCherry.	Samuel Julliot (unpublished)
pSJ080	P_{SV40}-PIF8-mEGFP-pA P _{SV40} -driven mammalian expression vector encoding <i>A. thaliana</i> PIF8 fused to the fluorescent protein mEGFP.	Samuel Julliot (unpublished)

Materials and Methods

pSLS404	P_{CaMV35S}-Renilla-2A-GAI-Firefly-myc-pA Ratiometric gibberellin sensor plasmid with <i>A. thaliana</i> DELLA protein GAI as SM for use in plant cells.	Lisa Schmunk/ Sophia Samodelov (unpublished)
pSLS405	P_{CaMV35S}-Renilla-2A-RGA-Firefly-myc-pA Ratiometric gibberellin sensor plasmid with the <i>A. thaliana</i> DELLA protein RGA as SM for use in plant cells.	Lisa Schmunk/ Sophia Samodelov (unpublished)
pSLS411	P_{SV40}-GID1a-pA Expression vector encoding the <i>A.thaliana</i> gibberellin receptor GID1a under control of P _{SV40} .	Lisa Schmunk/ Sophia Samodelov (unpublished)
pSLS412	P_{SV40}-GID1b-pA Expression vector encoding the <i>A.thaliana</i> gibberellin receptor GID1b under control of P _{SV40} .	Lisa Schmunk/ Sophia Samodelov (unpublished)
pSLS413	P_{SV40}-GID1c-pA Expression vector encoding the <i>A.thaliana</i> gibberellin receptor GID1c under control of P _{SV40} .	Lisa Schmunk/ Sophia Samodelov (unpublished)
pSLS414	P_{SV40}-SLY1-pA Expression vector encoding <i>A.thaliana</i> F-Box protein SLY1 under control of P _{SV40} .	Lisa Schmunk/ Sophia Samodelov (unpublished)
pSLS433	P_{SV40}-GID1a-NLS-HA-pA The <i>A.thaliana</i> gibberellin receptor GID1a was amplified from pSLS411 with oSLS414/oSLS438. pMZ333 was amplified with oSLS436/oSLS442. Both fragments were assembled using Gibson cloning.	Lisa Schmunk/ Sophia Samodelov (Appendix 7.1)
pSLS434	P_{SV40}-GID1b-NLS-HA-pA The <i>A.thaliana</i> gibberellin receptor GID1b was amplified from pSLS412 with oSLS416/oSLS439. pMZ333 was amplified with oSLS436/oSLS442. Both fragments were assembled using Gibson cloning.	Lisa Schmunk/ Sophia Samodelov (Appendix 7.1)
pSLS435	P_{SV40}-GID1c-NLS-HA-pA The <i>A.thaliana</i> gibberellin receptor GID1c was amplified from pSLS413 with oSLS418/oSLS440. pMZ333 was amplified with oSLS436/oSLS442. Both fragments were assembled using Gibson cloning.	Lisa Schmunk/ Sophia Samodelov (Appendix 7.1)
pSLS436	P_{SV40}-SLY1-NLS-HA-pA The <i>A.thaliana</i> F-Box protein SLY1 was amplified from pSLS414 with oSLS420/oSLS441. pMZ333 was amplified with oSLS436/oSLS442. Both fragments were assembled using Gibson cloning.	Lisa Schmunk/ Sophia Samodelov (Appendix 7.1)
pSLS437	P_{SV40}-GAI-NLS-FLAG-pA The <i>A.thaliana</i> DELLA protein GAI was amplified from a GAI containing plasmid (ABRC) with oSLS444/oSLS445. pMZ333 was amplified with oSLS448/oSLS442. Both fragments were assembled using Gibson cloning.	Lisa Schmunk/ Sophia Samodelov (Appendix 7.1)

Materials and Methods

pSLS438	P_{SV40}-RGA-NLS-FLAG-pA The <i>A.thaliana</i> DELLA protein RGA was amplified from a RGA containing plasmid (ABRC) with oSLS446/oSLS447. pMZ333 was amplified with oSLS448/oSLS442. Both fragments were assembled using Gibson cloning.	Lisa Schmunk/ Sophia Samodelov (Appendix 7.1)
pSLS443	P_{SV40}-ARR1DDDK-NLS-HA-pA ARR1 Δ DDDK-NLS-HA was amplified from a plasmid received from the Alabadi/Blázquez lab, IBMCP Valencia and amplified with oSLS454/455. pMZ333 was amplified with oSLS436/oSLS442. Both fragments were assembled using Gibson cloning.	Lisa Schmunk/ Sophia Samodelov (Appendix 7.1)
pSLS446	P_{SV40}-ARR1DDDK-VP16-NLS-HA-pA ARR1 Δ DDDK-NLS-HA was amplified from a plasmid received from the Alabadi/Blázquez lab, IBMCP Valencia and amplified with oSLS454/463. VP16-NLS-HA was amplified from pKM018 with oSLS443/oSLS466. pMZ333 was amplified with oSLS436/oSLS442. All fragments were assembled using Gibson cloning.	Lisa Schmunk/ Sophia Samodelov (Appendix 7.1)
pSLS454	TCS-P_{hCMVmin}-SEAP-pA The repetitive TCS motif was amplified from a plasmid received from the Alabadi/Blázquez lab, IBMCP Valencia and amplified with oSLS470/oSLS471. pKM195 was linearized with <i>NruI/EcoRV</i> . Both fragments were assembled using Gibson cloning.	Lisa Schmunk/ Sophia Samodelov (Appendix 7.1)
pSLS470	P_{CaMV35S}-Renilla-2A-RGAΔ17-Firefly-myc-pA	Lisa Schmunk/ Sophia Samodelov (unpublished)
pWW035	P_{SV40}-E-VP16-pA	(Weber et al., 2002)
pJATB001	P_{SV40}-GAI-VP16-IRES-TetR-PIF6(1-100)-pA GAI was PCR amplified from pSLS404 with oJATB001/oJATB002. pPF001 was linearized with <i>SpeI/EcoRV</i> . Both fragments were assembled using AQUA cloning.	This work
pJATB002	P_{SV40}-RGA-VP16-IRES-TetR-PIF6(1-100)-pA RGA was PCR amplified from pSLS405 with oJATB003/oJATB004. pPF001 was linearized with <i>SpeI/EcoRV</i> . Both fragments were assembled using AQUA cloning.	This work
pJATB003	P_{SV40}-GAI-VP16-IRES-TetR-Gid1a-pA GID1a was PCR amplified from pSLS411 with oJATB005/oJATB006. pJATB001 was linearized with <i>BsrGI/Ascl</i> . Both fragments were assembled using AQUA cloning.	This work
pJATB004	P_{SV40}-GAI-VP16-IRES-TetR-Gid1b-pA GID1b was PCR amplified from pSLS412 with oJATB007/oJATB008. pJATB001 was linearized with <i>BsrGI/Ascl</i> . Both fragments were assembled using AQUA cloning.	This work
pJATB005	P_{SV40}-GAI-VP16-IRES-TetR-Gid1c-pA GID1c was PCR amplified from pSLS413 with oJATB009/oJATB010. pJATB001 was linearized with <i>BsrGI/Ascl</i> . Both fragments were assembled using AQUA cloning.	This work
pJATB006	P_{SV40}-RGA-VP16-IRES-TetR-Gid1a-pA GID1a was PCR amplified from pSLS411 with oJATB005/oJATB006. pJATB002 was linearized with <i>BsrGI/Ascl</i> . Both fragments were assembled using AQUA cloning.	This work

Materials and Methods

pJATB007	P_{SV40}-RGA-VP16-IRES-TetR-Gid1b-pA GID1b was PCR amplified from pSLS412 with oJATB007/oJATB008. pJATB002 was linearized with <i>BsrGI</i> / <i>Ascl</i> . Both fragments were assembled using AQUA cloning.	This work
pJATB008	P_{SV40}-RGA-VP16-IRES-TetR-Gid1c-pA GID1c was PCR amplified from pSLS413 with oJATB009/oJATB010. pJATB002 was linearized with <i>BsrGI</i> / <i>Ascl</i> . Both fragments were assembled using AQUA cloning.	This work
pJATB023	P_{SV40}-GAI-VP16-IRES-TetR-SLY1-pA SLY1 was PCR amplified from pSLS414 with oJATB029/oJATB030. pJATB001 was linearized with <i>BsrGI</i> / <i>Ascl</i> . Both fragments were assembled using AQUA cloning.	This work
pJATB024	P_{SV40}-RGA-VP16-IRES-TetR-SLY1-pA SLY1 was PCR amplified from pSLS414 with oJATB029/oJATB030. pJATB002 was linearized with <i>BsrGI</i> / <i>Ascl</i> . Both fragments were assembled using AQUA cloning.	This work
pJATB025	P_{SV40}-SLY1-VP16-IRES-TetR-Gid1a-pA SLY1 was PCR amplified from pSLS414 with oJATB031/oJATB032. pJATB003 was linearized with <i>SpeI</i> / <i>EcoRV</i> . Both fragments were assembled using AQUA cloning.	This work
pJATB026	P_{SV40}-SLY1-VP16-IRES-TetR-Gid1b-pA SLY1 was PCR amplified from pSLS414 with oJATB031/oJATB032. pJATB004 was linearized with <i>SpeI</i> / <i>EcoRV</i> . Both fragments were assembled using AQUA cloning.	This work
pJATB027	P_{SV40}-SLY1-VP16-IRES-TetR-Gid1c-pA SLY1 was PCR amplified from pSLS414 with oJATB031/oJATB032. pJATB005 was linearized with <i>SpeI</i> / <i>EcoRV</i> . Both fragments were assembled using AQUA cloning.	This work
pJATB028	P_{SV40}-GAI-VP16-IRES-TetR-RGA-pA RGA was PCR amplified from pSLS405 with oJATB033/oJATB034. pJATB001 was linearized with <i>BsrGI</i> / <i>Ascl</i> . Both fragments were assembled using AQUA cloning.	This work
pJATB029	P_{SV40}-RGA-VP16-IRES-TetR-GAI-pA GAI was PCR amplified from pSLS404 with oJATB035/oJATB036. pJATB002 was linearized with <i>BsrGI</i> / <i>Ascl</i> . Both fragments were assembled using AQUA cloning.	This work
pJATB030	P_{SV40}-Gid1a-VP16-IRES-TetR-GAI-pA GID1a was PCR amplified from pSLS411 with oJATB037/oJATB038. pJATB029 was linearized with <i>SpeI</i> / <i>EcoRV</i> . Both fragments were assembled using AQUA cloning.	This work
pJATB031	P_{SV40}-Gid1b-VP16-IRES-TetR-GAI-pA GID1b was PCR amplified from pSLS412 with oJATB039/oJATB040. pJATB029 was linearized with <i>SpeI</i> / <i>EcoRV</i> . Both fragments were assembled using AQUA cloning.	This work
pJATB032	P_{SV40}-Gid1c-VP16-IRES-TetR-GAI-pA GID1c was PCR amplified from pSLS413 with oJATB041/oJATB042. pJATB029 was linearized with <i>SpeI</i> / <i>EcoRV</i> . Both fragments were assembled using AQUA cloning.	This work

Materials and Methods

pJATB033	P_{SV40}-Gid1a-VP16-IRES-TetR-RGA-pA GID1a was PCR amplified from pSLS411 with oJATB037/oJATB038. pJATB028 was linearized with <i>SpeI/EcoRV</i> . Both fragments were assembled using AQUA cloning.	This work
pJATB034	P_{SV40}-Gid1b-VP16-IRES-TetR-RGA-pA GID1b was PCR amplified from pSLS412 with oJATB039/oJATB040. pJATB028 was linearized with <i>SpeI/EcoRV</i> . Both fragments were assembled using AQUA cloning.	This work
pJATB035	P_{SV40}-Gid1c-VP16-IRES-TetR-RGA-pA GID1c was PCR amplified from pSLS413 with oJATB041/oJATB042. pJATB028 was linearized with <i>SpeI/EcoRV</i> . Both fragments were assembled using AQUA cloning.	This work
pJATB057	P_{SV40}-SLY1-VP16-IRES-TetR-GAI-pA GAI was PCR amplified from pSLS404 with oJATB035/oJATB036. pJATB025 was linearized with <i>BsrGI/Ascl</i> . Both fragments were assembled by AQUA cloning.	This work
pJATB058	P_{SV40}-SLY1-VP16-IRES-TetR-RGA-pA RGA was PCR amplified from pSLS405 with oJATB033/oJATB034. pJATB025 was linearized with <i>BsrGI/Ascl</i> . Both fragments were assembled by AQUA cloning.	This work
pJATB059	P_{SV40}-GID1a-VP16-IRES-TetR-SLY1-pA GID1a was PCR amplified from pSLS411 with oJATB037/oJATB038. pJATB023 was linearized with <i>SpeI/EcoRV</i> . Both fragments were assembled using AQUA cloning.	This work
pJATB060	P_{SV40}-GID1b-VP16-IRES-TetR-SLY1-pA GID1b was PCR amplified from pSLS412 with oJATB039/oJATB040. pJATB023 was linearized with <i>SpeI/EcoRV</i> . Both fragments were assembled using AQUA cloning.	This work
pJATB061	P_{SV40}-GID1c-VP16-IRES-TetR-SLY1-pA GID1c was PCR amplified from pSLS413 with oJATB041/oJATB042. pJATB023 was linearized with <i>SpeI/EcoRV</i> . Both fragments were assembled using AQUA cloning.	This work
pJATB066	P_{SV40}-GAI-VP16-IRES-E-GID1a-pA E-Protein was PCR-amplified from pWW035 with oJATB074/075. pJATB003 was linearized with <i>NotI/BsrGI</i> . Both fragments were assembled using AQUA cloning.	This work
pJATB067	P_{SV40}-GAI-VP16-IRES-E-GID1b-pA E-Protein was PCR-amplified from pWW035 with oJATB074/076. pJATB004 was linearized with <i>NotI/BsrGI</i> . Both fragments were assembled using AQUA cloning.	This work
pJATB068	P_{SV40}-GAI-VP16-IRES-E-GID1c-pA E-Protein was PCR-amplified from pWW035 with oJATB074/077. pJATB005 was linearized with <i>NotI/BsrGI</i> . Both fragments were assembled using AQUA cloning.	This work
pJATB069	P_{SV40}-RGA-VP16-IRES-E-GID1a-pA E-Protein was PCR-amplified from pWW035 with oJATB074/075. pJATB006 was linearized with <i>NotI/BsrGI</i> . Both fragments were assembled using AQUA cloning.	This work

Materials and Methods

pJATB070	P_{SV40}-RGA-VP16-IRES-E-GID1b-pA E-Protein was PCR-amplified from pWW035 with oJATB074/076. pJATB007 was linearized with <i>NotI/BsrGI</i> . Both fragments were assembled using AQUA cloning.	This work
pJATB071	P_{SV40}-RGA-VP16-IRES-E-GID1c-pA E-Protein was PCR-amplified from pWW035 with oJATB074/077. pJATB008 was linearized with <i>NotI/BsrGI</i> . Both fragments were assembled using AQUA cloning.	This work
pJATB072	P_{SV40}-GID1a-VP16-IRES-E-GAI-pA E-Protein was PCR-amplified from pWW035 with oJATB074/078. pJATB030 was linearized with <i>NotI/BsrGI</i> . Both fragments were assembled using AQUA cloning.	This work
pJATB073	P_{SV40}-GID1b-VP16-IRES-E-GAI-pA E-Protein was PCR-amplified from pWW035 with oJATB074/078. pJATB031 was linearized with <i>NotI/BsrGI</i> . Both fragments were assembled using AQUA cloning.	This work
pJATB074	P_{SV40}-GID1c-VP16-IRES-E-GAI-pA E-Protein was PCR-amplified from pWW035 with oJATB074/078. pJATB032 was linearized with <i>NotI/BsrGI</i> . Both fragments were assembled using AQUA cloning.	This work
pJATB075	P_{SV40}-GID1a-VP16-IRES-E-RGA-pA E-Protein was PCR-amplified from pWW035 with oJATB074/079. pJATB033 was linearized with <i>NotI/BsrGI</i> . Both fragments were assembled using AQUA cloning.	This work
pJATB076	P_{SV40}-GID1b-VP16-IRES-E-RGA-pA E-Protein was PCR-amplified from pWW035 with oJATB074/079. pJATB034 was linearized with <i>NotI/BsrGI</i> . Both fragments were assembled using AQUA cloning.	This work
pJATB077	P_{SV40}-GID1c-VP16-IRES-E-RGA-pA E-Protein was PCR-amplified from pWW035 with oJATB074/079. pJATB035 was linearized with <i>NotI/BsrGI</i> . Both fragments were assembled using AQUA cloning.	This work
pJATB078	P_{SV40}-SLY1-VP16-IRES-E-GID1a-pA E-Protein was PCR-amplified from pWW035 with oJATB074/075. pJATB025 was linearized with <i>NotI/BsrGI</i> . Both fragments were assembled using AQUA cloning.	This work
pJATB079	P_{SV40}-SLY1-VP16-IRES-E-GID1b-pA E-Protein was PCR-amplified from pWW035 with oJATB074/076. pJATB026 was linearized with <i>NotI/BsrGI</i> . Both fragments were assembled using AQUA cloning.	This work
pJATB080	P_{SV40}-SLY1-VP16-IRES-E-GID1c-pA E-Protein was PCR-amplified from pWW035 with oJATB074/077. pJATB027 was linearized with <i>NotI/BsrGI</i> . Both fragments were assembled using AQUA cloning.	This work
pJATB081	P_{SV40}-SLY1-VP16-IRES-E-GAI-pA E-Protein was PCR-amplified from pWW035 with oJATB074/078. pJATB057 was linearized with <i>NotI/BsrGI</i> . Both fragments were assembled using AQUA cloning.	This work

Materials and Methods

pJATB082	P_{SV40}-SLY1-VP16-IRES-E-RGA-pA E-Protein was PCR-amplified from pWW035 with oJATB074/079. pJATB058 was linearized with <i>NotI</i> / <i>BsrGI</i> . Both fragments were assembled using AQUA cloning.	This work
pJATB083	P_{SV40}-GID1a-VP16-IRES-E-SLY1-pA E-Protein was PCR-amplified from pWW035 with oJATB074/080. pJATB059 was linearized with <i>NotI</i> / <i>BsrGI</i> . Both fragments were assembled using AQUA cloning.	This work
pJATB084	P_{SV40}-GID1b-VP16-IRES-E-SLY1-pA E-Protein was PCR-amplified from pWW035 with oJATB074/080. pJATB060 was linearized with <i>NotI</i> / <i>BsrGI</i> . Both fragments were assembled using AQUA cloning.	This work
pJATB085	P_{SV40}-GID1c-VP16-IRES-E-SLY1-pA E-Protein was PCR-amplified from pWW035 with oJATB074/080. pJATB061 was linearized with <i>NotI</i> / <i>BsrGI</i> . Both fragments were assembled using AQUA cloning.	This work
pJATB086	P_{SV40}-GAI-VP16-IRES-E-SLY1-pA E-Protein was PCR-amplified from pWW035 with oJATB074/080. pJATB023 was linearized with <i>NotI</i> / <i>BsrGI</i> . Both fragments were assembled using AQUA cloning.	This work
pJATB087	P_{SV40}-RGA-VP16-IRES-E-SLY1-pA E-Protein was PCR-amplified from pWW035 with oJATB074/080. pJATB024 was linearized with <i>NotI</i> / <i>BsrGI</i> . Both fragments were assembled using AQUA cloning.	This work
pTBPF001	UAS₅-PspCas13b-NES-HA-pA Plasmid pKM083 was PCR-amplified with oTBPF003 and oTBPF004. <i>PspCas13b</i> was amplified from pC0046 with oTBPF001 and oTBPF002. Both fragments were assembled using AQUA cloning.	This work
pTBPF003	P_{U6}-FLUC gRNA1-PspCas13bDR-pA pC0043 was linearized by digestion with <i>BbsI</i> and assembled with oTBPF009 using AQUA cloning.	This work
pTBPF004	P_{U6}-FLUC gRNA2-PspCas13bDR-pA Plasmid pC0043 was linearized by digestion with <i>BbsI</i> and assembled with oTBPF010 using AQUA cloning.	This work
pTBPF005	P_{U6}-EGFP gRNA1-PspCas13bDR-pA Plasmid pC0043 was linearized by digestion with <i>BbsI</i> and assembled with oTBPF011 using AQUA cloning.	This work
pTBPF006	P_{U6}-EGFP gRNA2-PspCas13bDR-pA Plasmid pC0043 was linearized by digestion with <i>BbsI</i> -HF and assembled with oTBPF012 using AQUA cloning.	This work

Materials and Methods

pTBPF014	<p>P_{SV40}-mCherry-pA</p> <p>Plasmid pJA086 was linearized with <i>NotI</i> and <i>XbaI</i>, mCherry was PCR-amplified from pSJ025 with oTBPF034 and oTB035. Both fragments were assembled using AQUA cloning.</p>	This work
pTBPF015	<p>P_{SV40}-FLUC-pA</p> <p>Plasmid pLKPTBPF001 was linearized with <i>XhoI</i> and <i>BamHI</i>, the P_{SV40} promoter was PCR-amplified from pMZ1203 with oTBPF036 and oTBPF037. Both fragments were assembled by AQUA cloning.</p>	This work
pTBPF018	<p>P_{PGK}-EGFP-pA</p> <p>Plasmid pJA086 was linearized with <i>NheI</i> and <i>XhoI</i>, P_{PGK} was PCR-amplified from pLJM1-GFP with oTBPF041 and oTBPF042. Both fragments were assembled using AQUA cloning.</p>	This work
pTBPF020	<p>P_{U6}-hCDK1 gRNA2-PspCas13bDR-pA</p> <p>Plasmid pC0043 was linearized with <i>BbsI</i> and assembled with oTBPF0047 using Gibson cloning.</p>	This work
pTBPF021	<p>P_{U6}-hCDK1 gRNA1-PspCas13bDR-pA</p> <p>Plasmid pC0043 was linearized with <i>BbsI</i> and assembled with oTBPF048 using Gibson cloning.</p>	This work
pTB023	<p>P_{SV40}-PIF3-mVenus-pA</p> <p>PIF3-mVenus was PCR-amplified from pRD093 with oTB129/130. pMZ333 was linearized by <i>NotI/XbaI</i>. Both fragments were assembled using AQUA cloning.</p>	This work
pTB034	<p>P_{SV40}-phyB-VP16-IRES-TetR-PIF4-pA</p> <p>PIF4 was PCR-amplified from pHB091 with oTB153/154. pPF009 was linearized by <i>AsiSI/Ascl</i>. Both fragments were assembled using AQUA cloning.</p>	This work
pTB035	<p>P_{SV40}-phyB-VP16-IRES-TetR-PIF5-pA</p> <p>PIF5 was PCR-amplified from pHB092 with oTB155/156. pPF009 was linearized by <i>AsiSI/Ascl</i>. Both fragments were assembled using AQUA cloning.</p>	This work
pTB036	<p>P_{SV40}-phyB-VP16-IRES-TetR-PIF6-pA</p> <p>PIF6 was PCR-amplified from pHB093 with oTB157/158. pPF009 was linearized by <i>AsiSI/Ascl</i>. Both fragments were assembled using AQUA cloning.</p>	This work
pTB037	<p>P_{SV40}-phyB-VP16-IRES-TetR-PIF7-pA</p> <p>PIF7 was PCR-amplified from pHB094 with oTB159/160. pPF009 was linearized by <i>AsiSI/Ascl</i>. Both fragments were assembled using AQUA cloning.</p>	This work
pTB038	<p>P_{SV40}-phyB-VP16-IRES-TetR-PIF8-pA</p> <p>PIF8 was PCR-amplified from pSJ080 with oTB161/162. pPF009 was linearized by <i>AsiSI/Ascl</i>. Both fragments were assembled using AQUA cloning.</p>	This work

Materials and Methods

pTB053	P_{SV40}-PIF3-9AA-Linker-mEGFP-pA EGFP was amplified from pTB210 with oTB201/202. pTB023 was PCR-amplified with oTB223/212. Both fragments were assembled using AQUA cloning.	This work
pTB073	P_{SV40}-phyC-VP16-IRES-TetR-PIF1-pA phyC was PCR-amplified from pSJ050 with oTB323/324. pPF131 was PCR-amplified with oTB321/322. Both fragments were assembled using AQUA cloning.	This work
pTB074	P_{SV40}-phyC-VP16-IRES-TetR-PIF2-pA phyC was PCR-amplified from pSJ050 with oTB323/324. pTB105 was PCR-amplified with oTB321/322. Both fragments were assembled using AQUA cloning.	This work
pTB075	P_{SV40}-phyC-VP16-IRES-TetR-PIF3-pA phyC was PCR-amplified from pSJ050 with oTB323/324. pTB106 was PCR-amplified with oTB321/322. Both fragments were assembled using AQUA cloning.	This work
pTB076	P_{SV40}-phyC-VP16-IRES-TetR-PIF4-pA phyC was PCR-amplified from pSJ050 with oTB323/324. pTB034 was PCR-amplified with oTB321/322. Both fragments were assembled using AQUA cloning.	This work
pTB077	P_{SV40}-phyC-VP16-IRES-TetR-PIF5-pA phyC was PCR-amplified from pSJ050 with oTB323/324. pTB035 was PCR-amplified with oTB321/322. Both fragments were assembled using AQUA cloning.	This work
pTB078	P_{SV40}-phyC-VP16-IRES-TetR-PIF6-pA phyC was PCR-amplified from pSJ050 with oTB323/324. pTB036 was PCR-amplified with oTB321/322. Both fragments were assembled using AQUA cloning.	This work
pTB079	P_{SV40}-phyC-VP16-IRES-TetR-PIF7-pA phyC was PCR-amplified from pSJ050 with oTB323/324. pTB037 was PCR-amplified with oTB321/322. Both fragments were assembled using AQUA cloning.	This work
pTB080	P_{SV40}-phyC-VP16-IRES-TetR-PIF8-pA phyC was PCR-amplified from pSJ050 with oTB323/324. pTB038 was PCR-amplified with oTB321/322. Both fragments were assembled using AQUA cloning.	This work
pTB081	P_{SV40}-phyD-VP16-IRES-TetR-PIF1-pA phyD was PCR-amplified from pSJ051 with oTB325/326. pPF131 was PCR-amplified with oTB321/322. Both fragments were assembled using AQUA cloning.	This work
pTB082	P_{SV40}-phyD-VP16-IRES-TetR-PIF2-pA phyD was PCR-amplified from pSJ051 with oTB325/326. pTB105 was PCR-amplified with oTB321/322. Both fragments were assembled using AQUA cloning.	This work

Materials and Methods

pTB083	P_{SV40}-phyD-VP16-IRES-TetR-PIF3-pA phyD was PCR-amplified from pSJ051 with oTB325/326. pTB106 was PCR-amplified with oTB321/322. Both fragments were assembled using AQUA cloning.	This work
pTB084	P_{SV40}-phyD-VP16-IRES-TetR-PIF4-pA phyD was PCR-amplified from pSJ051 with oTB325/326. pTB034 was PCR-amplified with oTB321/322. Both fragments were assembled using AQUA cloning.	This work
pTB085	P_{SV40}-phyD-VP16-IRES-TetR-PIF5-pA phyD was PCR-amplified from pSJ051 with oTB325/326. pTB035 was PCR-amplified with oTB321/322. Both fragments were assembled using AQUA cloning.	This work
pTB086	P_{SV40}-phyD-VP16-IRES-TetR-PIF6-pA phyD was PCR-amplified from pSJ051 with oTB325/326. pTB036 was PCR-amplified with oTB321/322. Both fragments were assembled using AQUA cloning.	This work
pTB087	P_{SV40}-phyD-VP16-IRES-TetR-PIF7-pA phyD was PCR-amplified from pSJ051 with oTB325/326. pTB037 was PCR-amplified with oTB321/322. Both fragments were assembled using AQUA cloning.	This work
pTB088	P_{SV40}-phyD-VP16-IRES-TetR-PIF8-pA phyD was PCR-amplified from pSJ051 with oTB325/326. pTB038 was PCR-amplified with oTB321/322. Both fragments were assembled using AQUA cloning.	This work
pTB097	P_{SV40}-phyA-VP16-IRES-TetR-PIF1-pA phyA was PCR-amplified from pMZ1173 with oTB329/330. pPF131 was PCR-amplified with oTB321/322. Both fragments were assembled using AQUA cloning.	This work
pTB098	P_{SV40}-phyA-VP16-IRES-TetR-PIF2-pA phyA was PCR-amplified from pMZ1173 with oTB329/330. pTB105 was PCR-amplified with oTB321/322. Both fragments were assembled using AQUA cloning.	This work
pTB099	P_{SV40}-phyA-VP16-IRES-TetR-PIF3-pA phyA was PCR-amplified from pMZ1173 with oTB329/330. pTB106 was PCR-amplified with oTB321/322. Both fragments were assembled using AQUA cloning.	This work
pTB100	P_{SV40}-phyA-VP16-IRES-TetR-PIF4-pA phyA was PCR-amplified from pMZ1173 with oTB329/330. pTB034 was PCR-amplified with oTB321/322. Both fragments were assembled using AQUA cloning.	This work
pTB101	P_{SV40}-phyA-VP16-IRES-TetR-PIF5-pA phyA was PCR-amplified from pMZ1173 with oTB329/330. pTB035 was PCR-amplified with oTB321/322. Both fragments were assembled using AQUA cloning.	This work

Materials and Methods

pTB102	P_{SV40}-phyA-VP16-IRES-TetR-PIF6-pA phyA was PCR-amplified from pMZ1173 with oTB329/330. pTB036 was PCR-amplified with oTB321/322. Both fragments were assembled using AQUA cloning.	This work
pTB103	P_{SV40}-phyA-VP16-IRES-TetR-PIF7-pA phyA was PCR-amplified from pMZ1173 with oTB329/330. pTB037 was PCR-amplified with oTB321/322. Both fragments were assembled using AQUA cloning.	This work
pTB104	P_{SV40}-phyA-VP16-IRES-TetR-PIF8-pA phyA was PCR-amplified from pMZ1173 with oTB329/330. pTB038 was PCR-amplified with oTB321/322. Both fragments were assembled using AQUA cloning.	This work
pTB105	P_{SV40}-phyB-VP16-IRES-TetR-PIF2-pA PIF2 was PCR-amplified from PIF2 containing plasmid (ABRC) with oTB331/332. pTB034 was linearized by AsiSI/Ascl. Both fragments were assembled using AQUA cloning.	This work
pTB106	P_{SV40}-phyB-VP16-IRES-TetR-PIF3-pA PIF3 was PCR-amplified from pTB023 with oTB151/152. pTB034 was linearized by AsiSI/Ascl. Both fragments were assembled using AQUA cloning.	This work
pTB107	P_{SV40}-PIF2-EGFP-pA PIF2 was PCR-amplified from PIF2 containing plasmid (ABRC) with oTB367/368. pTB204 was PCR-amplified with oTB073/210. Both fragments were assembled using AQUA cloning.	This work
pTB200	P_{SV40}-GAI-mCherry-pA GAI was amplified from pSLS405 with oligos oTB064/065. mCherry was amplified from pSJ050 with oligos oTB066/067. pMZ333 was linearized by <i>NotI/XbaI</i> . Fragments were assembled using AQUA cloning.	This work
pTB204	P_{SV40}-GID1b-EGFP-pA GID1b was amplified from pSLS412 with oligos oTB077/083. mEGFP was amplified from pHB090 with oligos oTB085/061. pMZ333 was linearized by <i>NotI/XbaI</i> . Fragments were assembled using AQUA cloning.	This work
pTB210	P_{SV40}-ARR1ΔDKK-mEGFP-pA ARR1ΔDKK was amplified from pSLS443 with oligos oTB099/100. mEGFP was amplified from pTB204 with oligos oTB101/102. pMZ333 was linearized by <i>NotI/XbaI</i> . Fragments were assembled using AQUA cloning.	This work
pTB227	P_{SV40}-GID1b-9AA-Linker-mEGFP-pA GID1b was PCR-amplified from pSLS434 with oTB203/204. pTB053 was linearized by <i>NotI/AfeI</i> . Both fragments were assembled using AQUA cloning.	This work

Materials and Methods

pTB228	P_{SV40}-GID1b-9AA-Linker-mEGFP-9AA-Linker-mCherry-pA mCherry was amplified from pTB200 with oTB255/256. pTB227 was PCR-amplified with oTB212/254. Both fragments were assembled using AQUA cloning.	This work
pTB233	P_{SV40}-GAI-9AA-Linker-mCherry-CAAX(unphosphorylatable)-pA GAI was PCR-amplified from pTB200 with oTB064/244. pTB216 was PCR-amplified with oTB210/246. Both fragments were assembled using AQUA cloning.	This work
pTB235	P_{SV40}-mEGFP-GID1b-pA GID1b was PCR-amplified from pTB204 with oTB248/249. pTB400 was PCR-amplified with oTB212/247. Both fragments were assembled using AQUA cloning.	This work
pTB239	P_{SV40}-GAI-9AA-Linker-mCherry-NLS-pA GAI-9AA-Linker-mCherry was PCR-amplified from pTB233 with oTB064/257. pMZ333 was linearized by <i>NotI/XbaI</i> . Both fragments were assembled using AQUA cloning.	This work
pTB240	P_{SV40}-GAI-9AA-Linker-mCherry-NES-pA GAI-9AA-Linker-mCherry was PCR-amplified from pTB233 with oTB064/258. pMZ333 was linearized by <i>NotI/XbaI</i> . Both fragments were assembled using AQUA cloning.	This work
pTB243	P_{SV40}-GAI-9AA-Linker-mCherry-pA GAI-9AA-Linker-mCherry was PCR-amplified from pTB233 with oTB064/261. pMZ333 was linearized by <i>NotI/XbaI</i> . Both fragments were assembled using AQUA cloning.	This work
pTB245	P_{SV40}-mCherry-9AA-Linker-GAI-pA mCherry was PCR-amplified from pTB200 with oTB263/264. GAI was PCR-amplified from pTB216 with oTB265/266. pMZ333 was linearized by <i>NotI/XbaI</i> . Fragments were assembled using AQUA cloning.	This work
pTB258	P_{SV40}-NLS-mCherry-5AA-Linker-GAI-pA GAI was PCR-amplified from pTB200 with oTB296/266. pTB262 was PCR-amplified with oTB212/247. Both fragments were assembled using AQUA cloning.	This work
pTB259	P_{SV40}-NLS-mCherry-7AA-Linker-GAI-pA GAI was PCR-amplified from pTB200 with oTB297/266. pTB262 was PCR-amplified with oTB212/247. Both fragments were assembled using AQUA cloning.	This work
pTB262	P_{SV40}-NLS-mCherry-9AA-Linker-GAI-pA mCherry-GAI was PCR-amplified from pTB245 with oTB291/266. pMZ333 was linearized by <i>NotI/XbaI</i> . Both fragments were assembled using AQUA cloning.	This work
pTB263	P_{SV40}-mCherry-GID1b-pA GID1b was PCR-amplified from pTB204 with oTB249/292. pTB245 was PCR-amplified with oTB212/247. Both fragments were assembled using AQUA cloning.	This work

Materials and Methods

pTB264	P_{SV40}-NLS-mEGFP-9AA-Linker-GAI-pA mEGFP was PCR-amplified from pTB210 with oTB291/264. pTB262 was PCR-amplified with oTB265/293. Both fragments were assembled using AQUA cloning.	This work
pTB265	P_{SV40}-mEGFP-NLS-pA mEGFP was PCR-amplified from pTB210 with oTB299/300. pMZ333 was linearized by <i>NotI/XbaI</i> . Both fragments were assembled using AQUA cloning.	This work
pTB267	P_{SV40}-mEGFP-GID1a-pA GID1a was PCR-amplified from pJATB006 with oTB301/302. pTB400 was PCR-amplified with oTB212/247. Both fragments were assembled using AQUA cloning.	This work
pTB268	P_{SV40}-mEGFP-GID1c-pA GID1c was PCR-amplified from pJATB008 with oTB303/304. pTB400 was PCR-amplified with oTB212/247. Both fragments were assembled using AQUA cloning.	This work
pTB271	P_{SV40}-mCherry-SLY1-pA SLY1 was PCR-amplified from pJATB023 with oTB318/320. pTB263 was PCR-amplified with oTB212/247. Both fragments were assembled using AQUA cloning.	This work
pTB272	P_{SV40}-mEGFP-SLY1-pA SLY1 was PCR-amplified from pJATB023 with oTB319/320. pTB400 was PCR-amplified with oTB212/247. Both fragments were assembled using AQUA cloning.	This work
pTB400	P_{SV40}-mEGFP-PAS-LOV_{wt}-pA mEGFP was amplified from pTB210 with oTB226/227, PASLOV was amplified from pMZ1214 with oTB228/229. pMZ333 was linearized by <i>NotI/XbaI</i> . Fragments were assembled using AQUA cloning.	This work
pTB511	P_{35S}-E-UVR8-pA UVR8 was amplified from synthesized UVR8 from IDT and amplified with oTB216/217. pMZ820 was linearized by <i>EcoRI/SgrAI</i> . Both fragments were assembled using AQUA cloning.	This work

All pJATB plasmids were designed and constructed together with Jennifer Andres.

All pTBPF plasmids were designed and constructed together with Patrick Fischbach.

5.4 Oligonucleotides

Table 5.2: Oligonucleotides used for cloning in this work.

Oligonucleotide	Sequence (5' → 3')
oJATB001	GTCTTTTATTTTCAGGTCCCGGATCGGAATTGACTAGTCCACCATGAAGAGAGATCAT
oJATB002	CTACCAGCACTACCAGCACTATCGAATTCGATATCATTGGTGGAGAGTTTCCAAG
oJATB003	GTCTTTTATTTTCAGGTCCCGGATCGGAATTGACTAGTCCACCATGAAGAGAGATCATCA CCAATTCC
oJATB004	CTACCAGCACTACCAGCACTATCGAATTCGATATCGTACGCCGCCGTCGA
oJATB005	AGGCGGTGGAAGTGGTGGCGGAGGTAGCGATTGTACAATGGCTGCGAGCGAT
oJATB006	TATCTTATCATGTCTGGATCGAAGCTTTTAGGCGCGCCTTAACATTCCGCGTTTACAAAC G
oJATB007	AGGCGGTGGAAGTGGTGGCGGAGGTAGCGATTGTACAATGGCTGGTGGTAACGA
oJATB008	TATCTTATCATGTCTGGATCGAAGCTTTTAGGCGCGCCTTAAGGAGTAAGAAGCACAGG A
oJATB009	GAGGCGGTGGAAGTGGTGGCGGAGGTAGCGATTGTACAATGGCTGGAAGTGAAGAAG
oJATB010	TATCTTATCATGTCTGGATCGAAGCTTTTAGGCGCGCCTCATTGGCATTCTGCGTTTA
oJATB029	GGCGGTGGAAGTGGTGGCGGAGGTAGCGATTGTACAATGAAGCGCAGTACTACC
oJATB030	TATCTTATCATGTCTGGATCGAAGCTTTTAGGCGCGCCTTATTGGATTCTGGAAGAGG TC
oJATB031	TCTTTTATTTTCAGGTCCCGGATCGGAATTGACTAGTCCACCATGAAGCGCAGT
oJATB032	ACTACCAGCACTACCAGCACTATCGAATTCGATATCTTTGGATTCTGGAAGAGGTCTCTT A
oJATB033	GGCGGTGGAAGTGGTGGCGGAGGTAGCGATTGTACAATGAAGAGAGATCATCACC TCCAAGGT
oJATB034	TATCTTATCATGTCTGGATCGAAGCTTTTAGGCGCGCCTAGTACGCCGCCGTCGA
oJATB035	GGCGGTGGAAGTGGTGGCGGAGGTAGCGATTGTACAATGAAGAGAGATCATCATCATC ATC
oJATB036	TATCTTATCATGTCTGGATCGAAGCTTTTAGGCGCGCCTAATTGGTGGAGAGTTTCCA AG
oJATB037	ACTACCAGCACTACCAGCACTATCGAATTCGATATCACATTCCGCGTTTACAAACGC
oJATB038	CTTTTATTTTCAGGTCCCGGATCGGAATTGACTAGTCCACCATGGCTGCGAGCGAT
oJATB039	ACTACCAGCACTACCAGCACTATCGAATTCGATATCAGGAGTAAGAAGCACAGGACTTG
oJATB040	CTTTTATTTTCAGGTCCCGGATCGGAATTGACTAGTCCACCATGGCTGGTGG
oJATB041	CTTTTATTTTCAGGTCCCGGATCGGAATTGACTAGTCCACCATGGCTGGAAG
oJATB042	ACTACCAGCACTACCAGCACTATCGAATTCGATATCTTGGCATTCTGCGTTTACAAATG
oJATB074	ACAGATTGTATCATAAAGCGAATTGGATTGCGGCCGCGAATTCATATGCCCCGCCCA AG
oJATB075	AATAAGATTAACCTTCATCGCTCGCAGCCATTCTGCGGAACCAGCACTGCCGGCGCTG TTATGTACAATTAAGCTGTACGCGGACG
oJATB076	GTTAAGGTTGACTTCGTTACCACCAGCCATTCTGCGGAACCAGCACTGCCGGCGCTG TTATGTACAATTAAGCTGTACGCGGACG
oJATB077	AATAAGATTAACCTTCACCTTCCAGCCATTCTGCGGAACCAGCACTGCCGGCGCTGT TATGTACAATTAAGCTGTACGCGGACG
oJATB078	ATGATGATGATGATGATGATCTCTCTTCATACCAGCACTACCAGCACTACCAGCACTGTT ATGTACAATTAAGCTGTACGCGGACG
oJATB079	CGTCCGCGTACAGCTTAATTGTACATAACAGTGCTGGTAGTGCTGGTAGTGCTGGTATG AAGAGAGATCATCACC AATTCCAAGGT
oJATB080	CAAATCAGAGTCGGTAGTACTGCGCTTATTCTGCGGAACCAGCACTGCCGGCGCTG TTATGTACAATTAAGCTGTACGCGGACG
oROF003	AGGTAAGCTTGGTACCACC
oROF157	TGGATCCAAGCTTCTCGAGCCCGGGGAATTCCTACACCTTCTTCTTCTTTGGTCCA TCGACGCTGAGT
oROF158	TGGATCCAAGCTTCTCGAGCCCGGGGAATTCCTACACCTTCTTCTTCTTTGGCCA CCGTA CTCGTCAAT
oSLS414	CAGGTCCCGGATCGAATTGCGGCCGAGGAGGCGCCACCATGGCTGCGAGCGATGAA GTTAATCTTATTG
oSLS416	CAGGTCCCGGATCGAATTGCGGCCGAGGAGGCGCCACCATGGCTGGTGGTAAACGAA GTCAACC
oSLS418	CAGGTCCCGGATCGAATTGCGGCCGAGGAGGCGCCACCATGGCTGGAAGTGAAGAA GTTAATCTTATTGAG
oSLS420	CAGGTCCCGGATCGAATTGCGGCCGAGGAGGCGCCACCATGAAGCGCAGTACTACC GACTCTG

Materials and Methods

oSLS436 TACCCATACGATGTTCCAGATTACGCTTAGTCTAGAGTCGACCTGCAGCCCAAG
oSLS438 AGCGTAATCTGGAACATCGTATGGGTACACCTTCCGCTTTTTCTGGGACATTCCGCGT
TTACAAACGCCGAAATC
oSLS439 AGCGTAATCTGGAACATCGTATGGGTACACCTTCCGCTTTTTCTGGGAGGAGTAAGAA
GCACAGGACTTGACTTG
oSLS440 AGCGTAATCTGGAACATCGTATGGGTACACCTTCCGCTTTTTCTGGGTTGGCATTCTG
CGTTTACAAATGCAGCTATC
oSLS441 AGCGTAATCTGGAACATCGTATGGGTACACCTTCCGCTTTTTCTGGGTTGGATTCTG
GAAGAGGTCTCTTAGTG
oSLS442 CCGCAATTCGATCCGGGACCTG
oSLS443 GAATTCGATAGTGCTGGTAGTGCTGGTAG
oSLS444 CAGGTCCCGGATCGAATTGCGGCCGAGGAGGCCACCATGAAGAGAGATCATCAT
CATCATCATCAAGATAAG
oSLS445 CTACTTGCATCGTCGTCCTTGTAGTCCACCTTCCGCTTTTTCTGGGATTGGTGGAGA
GTTTCCAAGCCGAG
oSLS446 CAGGTCCCGGATCGAATTGCGGCCGAGGAGGCCACCATGAAGAGAGATCATCAC
CAATTCGAAGTTC
oSLS447 CTACTTGCATCGTCGTCCTTGTAGTCCACCTTCCGCTTTTTCTGGGTACGCCGCCG
TCGAGAGTTTC
oSLS448 GACTACAAGGACGACGATGACAAGTAGTCTAGAGTCGACCTGCAGCCCAAG
oSLS454 CAGGTCCCGGATCGAATTGCGGCCGAGGAGGCCACCATGTACGGAAGAGGAAA
GACGAGG
oSLS455 AGCGTAATCTGGAACATCGTATGGGTACACCTTCCGCTTTTTCTGGGAACCGGAATGT
TATCGATGGAGTATGCG
oSLS463 CTACCAGCACTACCAGCACTATCGAATTCAACCGGAATGTTATCGATGGAGTATGCG
oSLS466 AGCGTAATCTGGAACATCGTATGGGTACACCTTCCGCTTTTTCTGGGCC
oSLS470 GAAAAGTGCCACCTGACGTCGTCGACGATATCGGCCAGTGCCAAGCTTATGCTAGC
oSLS471 ACGAGCTCTGCTTATATAGGGCTAGCTCGCGAGAGGAAGGGTCTTGGCTAGAAAATCC
oTBPF001 CGTTCGAGATCTGCGATCTAAGTAAGCTTGGCCACCATGAACATCCCCGCTCTGGTGG
AAAAC
oTBPF002 CTCCCATTATAAGTTCCATAGGATGGGCGGCCGCTTAGGCATAGTCGGGGACATCAT
ATGG
oTBPF003 GCGGCCGCCCATCCTATGG
oTBPF004 GGTGGCCAAGCTTACTTAGATCGCAG
oTBPF009 ATAGCCCCTCAAACCTGGACCTTCCACAACGAGGTGGACATTACCTACGCCGAGTACTT
CGGTGTTTCGTCCTTTCCACAAGATATATA
oTBPF010 ATAGCCCCTCAAACCTGGACCTTCCACAACCACGGTAAAACCATGACCGAGAAGGAGA
TCGGTGTTTCGTCCTTTCCA
oTBPF011 ATAGCCCCTCAAACCTGGACCTTCCACAACCTGGACGGCGACGTAAACGGCCACAAGT
TCGGTGTTTCGTCCTTTCCACAAGA
oTBPF012 ATAGCCCCTCAAACCTGGACCTTCCACAACACCCAGTCCAAGCTGAGCAAAGACCCCA
ACCGGTGTTTCGTCCTTTCCACAAGATATATA
oTBPF034 TTTTGTCTTTATTTTCAGGTCCCGGATCGAATTGCGGCCGATGGTGGAGCAAGGGCGA
GGAGG
oTBPF035 CTGGATCGAAGCTTGGGCTGCAGGTGCACTTCTAGACTACTTGTACAGCTCGTCCATG
CCG
oTBPF036 CATGTTTGACAGCTTATCATCGATAAGCTAGCTTGGATCCCTGTGGAATGTGTGTCAGT
TAGGGTG
oTBPF037 TTACCAGTAACTTTCTGGTTTTCCAGTTCCTCGAGAGCTTTTTGCAAAGCCTAGGCCT
CC
oTBPF041 TTCTCATGTTTGACAGCTTATCATCGATAAGCTAGCTTGGGGTTGCGCCTTTTCCAAGG
C
oTBPF042 TTACCAGTAACTTTCTGGTTTTCCAGTTCCTCGAGCTGGGGAGAGAGGTGCGTGATTC
oTBPF047 ATAGCCCCTCAAACCTGGACCTTCCACAACGCCAGAGCTTTTGAATACCTATCAGAGT
AGGTGTTTCGTCCTTTCCACAAGATATATA
oTBPF048 ATAGCCCCTCAAACCTGGACCTTCCACAACGGGCACTCCAATAATGAAGTGTGGCCA
GAGGTGTTTCGTCCTTTCCACAAGATATATA
oTB061 CTGGATCGAAGCTTGGGCTGCAGGTGCACTGATATCTTACTTGTACAGCTCGTCCATGC
oTB064 TCTTTTATTTTCAGGTCCCGATCGAATTGCGCGGCCGCCACCATGAAGAGAGATCAT
oTB065 ATCCTCCTCGCCCTTGCTCACCATTGCTGAATTGGTGGAGAGTTTCAA
oTB066 GCCACCTCGGCTTGGAACTCTCCACCAATTCAGCAATGGTGGAGCAAGGG
oTB067 CTGGATCGAAGCTTGGGCTGCAGGTGCACTTCTAGACTACTTGTACAGCTCGTCCATG
C
oTB073 GGCAGCATGGTGAGCAAG
oTB077 TCTTTTATTTTCAGGTCCCGGATCGAATTGCACCGGTCCACCATGGCTGGTGG
oTB083 CAGCTCCTCGCCCTTGCTCACCATGCTGCCAGGAGTAAGAAGCACAGGACTTG
oTB085 AGCAAGTCAAGTCTGTGCTTCTACTCCTGGCAGCATGGTGGAGCAAG
oTB099 TCTTTTATTTTCAGGTCCCGGATCGAATTGCGCGGCCGCCACCATGTACGGAA

Materials and Methods

oTB100 CAGCTCCTCGCCCTTGCTCACCATGCTGCCAACCGAATGTTATCGATGG
oTB101 GACGCATACTCCATCGATAACATTCCGGTTGGCAGCATGGTGAGCAAG
oTB102 GATCGAAGCTTGGGCTGCAGGTCGACTCTAAGCGCTTTACTTGTACAGCTCGTCCATG
C
oTB129 TCTTTTATTTTCAGGTCCCGGATCGAATTGCGCGGCCGCCACCATGCCTCTGTTTGAGC
TTTTCAG
oTB130 CTGGATCGAAGCTTGGGCTGCAGGTCGACTAGCGCTTTACTTGTACAGCTCGTCCA
oTB151 GGCGGTGGAAGTGGTGGCGGAGGTAGCGATGCGATCGCTATGCCTCTGTTTGAGCTTT
T
oTB152 TATCTTATCATGTCTGGATCGAAGCTTTTAGGCGCGCCCTACGACGATCCACAAAAGT
AT
oTB153 GGCGGTGGAAGTGGTGGCGGAGGTAGCGATGCGATCGCTATGGAACACCAAGGTTGG
oTB154 TATCTTATCATGTCTGGATCGAAGCTTTTAGGCGCGCCCTAGTGGTCCAACGAGAACC
oTB155 GGCGGTGGAAGTGGTGGCGGAGGTAGCGATGCGATCGCTATGGAACAAGTGTGCT
GA
oTB156 TATCTTATCATGTCTGGATCGAAGCTTTTAGGCGCGCCCTACGCTATTTTACCCATATGA
AGACT
oTB157 GGCGGTGGAAGTGGTGGCGGAGGTAGCGATGCGATCGCTATGATGTTCTTACCAACC
GATTATT
oTB158 TATCTTATCATGTCTGGATCGAAGCTTTTAGGCGCGCCCTCATCTGTTAGTTTTCTTGAT
TTCTTGT
oTB159 GGCGGTGGAAGTGGTGGCGGAGGTAGCGATGCGATCGCTATGTCGAATTATGGAGTTA
AAGAGC
oTB160 TATCTTATCATGTCTGGATCGAAGCTTTTAGGCGCGCCCTAATCTCTTTTCTCATGATTC
GAAGAAC
oTB161 GGCGGTGGAAGTGGTGGCGGAGGTAGCGATGCGATCGCTATGAGCCAATGTGTTCCA
AA
oTB162 TATCTTATCATGTCTGGATCGAAGCTTTTAGGCGCGCCCTATTTTGGATTGCAAGGAGG
AG
oTB201 GGGTCTTCTGATCAGTTTTGTGGATCGTCGGGCGCCAGCGCTGGCAGCGCCAGCGGC
ATGGTGAGCAAGGGCGA
oTB202 CTGGATCGAAGCTTGGGCTGCAGGTCGACTGCGATCGCTTACTTGTACAGCTCGTCCA
TGC
oTB203 TCTTTTATTTTCAGGTCCCGGATCGAATTGCGCGGCCGCCACCATGGCTGGTGG
oTB204 CTTGCTCACCATGCCGCTGGCGCTGCCAGCGCTGGCGCCAGGAGTAAGAAGCACAGG
ACTTGA
oTB210 GCAATTCGATCCGGGACCT
oTB212 AGTCGACCTGCAGCCC
oTB216 CACATGCGTCCGCGTACAGCGGTACCGGCGGCGGCCGCATGGCGGAGGATATGGCT
oTB217 CCGGTGGATCCAAGCTTCTCGAGCCCCGGGGGAATTCTCAAATTCGTACACGCTTGACA
TCA
oTB223 CGACGATCCACAAAAGTATCAG
oTB226 AGTCTTTTTGTCTTTTATTTTCAGGTCCCGGATCGAATTGCGCGGCCGCCACCATGGTG
AGCAAGGGCG
oTB227 TTTTTCAATTAACCCAGTTGTGATTCCATGCTGCCCTTGTACAGCTCGTCCATGC
oTB228 ATCACTCTCGGCATGGACGAGCTGTACAAGGGCAGCATGGAATCACAAGTGGTTTAA
TT
oTB229 CTGGATCGAAGCTTGGGCTGCAGGTCGACTTCTAGACTAGGAGGTAAGTGCACCC
oTB244 CATGTTATCCTCCTCGCCCTTGCTCACCATGCCGCTGGCGCTGCCAGCGCTGGCGCCA
TTGGTGGAGAGTTTCAA
oTB246 ATGGTGAGCAAGGGCGAG
oTB247 CTTGTACAGCTCGTCCATGCC
oTB248 ATCACTCTCGGCATGGACGAGCTGTACAAGGGCAGCATGGCTGGTGGTAACGAAGT
oTB249 CTGGATCGAAGCTTGGGCTGCAGGTCGACTGCGATCGCCTAAGGAGTAAGAAGCACAG
GACTT
oTB254 GGCGCCGCTGCCGCGCTGCCGCTGGCCTTGTACAGCTCGTCCATGCC
oTB255 GCCAGCGGCAGCGCCGCGAGCGGCCATGGTGAGCAAGGGCGA
oTB256 CTGGATCGAAGCTTGGGCTGCAGGTCGACTGCGATCGCCTACTTGTACAGCTCGTCCA
TGC
oTB257 CTGGATCGAAGCTTGGGCTGCAGGTCGACTGATATCCTACACCTTCTCTTCTTTG
GCTTGTACAGCTCGTCCAT
oTB258 CTGGATCGAAGCTTGGGCTGCAGGTCGACTGATATCCTAGATGGTCAGGGTGCCGAAC
TTCTTGGTCATCTTGTACAGCTCGTCCAT
oTB261 CTGGATCGAAGCTTGGGCTGCAGGTCGACTGATATCCTACTTGTACAGCTCGTCCAT
oTB263 TCTTTTATTTTCAGGTCCCGGATCGAATTGCGCGGCCGCCACCATGGTGGAGCAAGGGC
GA
oTB264 GCCGCTGGCGCTGCCAGCGCTGGCGCCCTTGTACAGCTCGTCCATGC
oTB265 GGCGCCAGCGCTGGCAGCGCCAGCGGCATGAAGAGAGATCATCATCATC
oTB266 CTGGATCGAAGCTTGGGCTGCAGGTCGACTGCGATCGCCTAATTGGTGGAGAGTTTCC
AA

Materials and Methods

oTB291 TCTTTTATTTTCAGGTCCCGGATCGAATTGCGCGGCCGCCACCATGCCAAAGAAGAAG
AGGAAGGTGATGGTGAGCAAGGGCG
oTB292 TCCACCGCGGCATGGACGAGCTGTACAAGGGCAGCATGGCTGGTGGTAACGAAGT
oTB293 GCAATTGCATCCGGGA
oTB296 CCACCGCGGCATGGACGAGCTGTACAAGGGCGCCAGCGCTGGCATGAAGAGAGATC
ATCATCATCATC
oTB297 CCACCGCGGCATGGACGAGCTGTACAAGGGCGCCAGCGCTGGCAGCGCCATGAAGA
GAGATCATCATCATCATC
oTB299 TCTTTTATTTTCAGGTCCCGGATCGAATTGCGCGGCCGCCACCATGGTGAGCAAGGGC
GA
oTB300 CTGGATCGAAGCTTGGGCTGCAGGTGCGACTGATATCCTACACCTTCTTCTTCTTTG
GCTTGTACAGCTCGTCCATGC
oTB301 ATCACTCTCGGCATGGACGAGCTGTACAAGGGCAGCATGGCTGCGAGCGATG
oTB302 CTGGATCGAAGCTTGGGCTGCAGGTGCGACTGCGATCGCTTAACATTCCGCGTTTACAA
ACGC
oTB303 ATCACTCTCGGCATGGACGAGCTGTACAAGGGCAGCATGGCTGGAAGTGAAGAAG
oTB304 CTGGATCGAAGCTTGGGCTGCAGGTGCGACTGCGATCGCTCATTGGCATTCTGCGTTTA
oTB318 TCCACCGCGGCATGGACGAGCTGTACAAGGGCAGCATGAAGCGCAGTACTACC
oTB319 ATCACTCTCGGCATGGACGAGCTGTACAAGGGCAGCATGAAGCGCAGTACTACC
oTB320 CTGGATCGAAGCTTGGGCTGCAGGTGCGACTGCGATCGCTTATTTGGATTCTGGAAGAG
GT
oTB321 GATATCGAATTGCATAGTGCTGG
oTB322 GGTGGACTAGTCAATTCCG
oTB323 AGGTCCCGGATCGGAATTGACTAGTCCACCATGTCATCGAACACTTCACG
oTB324 AGCACTACCAGCACTATCGAATTCGATATCAATCAAGGGAAATTCTGTGAGG
oTB325 AGGTCCCGGATCGGAATTGACTAGTCCACCATGGTCTCCGGAGGTGG
oTB326 AGCACTACCAGCACTATCGAATTCGATATCTGAAGAGGGCATCATCATCATTAGAGG
oTB329 AGGTCCCGGATCGGAATTGACTAGTCCACCATGTCAGGCTCTAGGCCG
oTB330 AGCACTACCAGCACTATCGAATTCGATATCCTTGTTTGCTGCAGCGAGTT
oTB331 GGCGGTGGAAGTGGTGGCGGAGGTAGCGATGCGATCGCTATGGAAGCAAACCCCTTA
GC
oTB332 TATCTTATCATGTCTGGATCGAAGCTTTTAGGCGCGCCTTAGTTTGGCGAGCGATAATA
ACT
oTB367 TCTTTTATTTTCAGGTCCCGGATCGAATTGCGCGGCCGCCACCATGGAAGCAAACCCCT
TAGC
oTB368 CAGCTCCTCGCCCTTGCTCACCATGCTGCCGTTTGGCGAGCGATAATAAC

Materials and Methods

Table 5.3: Oligonucleotides designed and used for RT-qPCR experiments in this work

Oligonucleotide		Sequence (5'→3')
oTB351	GAPDH Fwd	GTCTCCTCTGACTTCAACAGCG
oTB352	GAPDH Rev	ACCACCCTGTTGCTGTAGCCAA
oTB359	EGFP Fwd	GGGCACAAGCTGGAGTACAA
oTB360	EGFP Rev	GTCCTCGATGTTGTGGCG
oTB361	mCherry Fwd	AAGCAGAGGCTGAAGCTGAAGG
oTB362	mCherry rev	GCGTTCGTA CTGTTCCACGATG

Table 5.4: Guide RNAs designed and used in this work.

gRNA	Sequence (5'→3')
Firefly 1	GAGGTGGACATTACCTACGCCGAGTACTTC
Firefly 2	CACGGTAAAACCATGACCGAGAAGGAGATC
EGFP 1	CTGGACGGCGACGTAACGGCCACAAGTTC
EGFP 2	ACCCAGTCCAAGCTGAGCAAAGACCCCAAC
hCDK1 1	GGGCACTCCCAATAATGAAGTGTGGCCAGA
hCDK1 2	GCCAGAGCTTTTGAATACCTATCAGAGTA

6 References

- Abbas M, Hernández-García J, Pollmann S, Samodelov SL, Kolb M, Friml J, Hammes UZ, Zurbriggen MD, Blázquez MA, Alabadi D** (2018) Auxin methylation is required for differential growth in Arabidopsis. *Proc Natl Acad Sci* **115**: 6864–6869
- Abudayyeh OO, Gootenberg JS, Konermann S, Joung J, Slaymaker IM, Cox DBT, Shmakov S, Makarova KS, Semenova E, Minakhin L, et al** (2016) C2c2 is a single-component programmable RNA-guided RNA-targeting CRISPR effector. *Science* (80-) **353**: aaf5573
- Ádám É, Hussong A, Bindics J, Wüst F, Viczián A, Essing M, Medzihradzky M, Kircher S, Schäfer E, Nagy F** (2011) Altered Dark- and Photoconversion of Phytochrome B Mediate Extreme Light Sensitivity and Loss of Photoreversibility of the phyB-401 Mutant. *PLoS One* **6**: e27250
- Ádám É, Kircher S, Liu P, Mérai Z, González-Schain N, Hörner M, Viczián A, Monte E, Sharrock RA, Schäfer E, et al** (2013) Comparative functional analysis of full-length and N-terminal fragments of phytochrome C, D and E in red light-induced signaling. *New Phytol* **200**: 86–96
- Adjobo-Hermans MJW, Goedhart J, van Weeren L, Nijmeijer S, Manders EMM, Offermanns S, Gadella TWJ** (2011) Real-time visualization of heterotrimeric G protein Gq activation in living cells. *BMC Biol.* doi: 10.1186/1741-7007-9-32
- Al-Sady B, Kikis EA, Monte E, Quail PH** (2008) Mechanistic duality of transcription factor function in phytochrome signaling. *Proc Natl Acad Sci U S A* **105**: 2232–7
- Al-Sady B, Ni W, Kircher S, Schäfer E, Quail PH** (2006) Photoactivated phytochrome induces rapid PIF3 phosphorylation prior to proteasome-mediated degradation. *Mol Cell* **23**: 439–46
- Andres J, Blomeier T, Zurbriggen MD** (2019) Synthetic Switches and Regulatory Circuits in Plants. *Plant Physiol* **179**: 862–884
- Appleford NEJ, Evans DJ, Lenton JR, Gaskin P, Croker SJ, Devos KM, Phillips AL, Hedden P** (2006) Function and transcript analysis of gibberellin-biosynthetic enzymes in wheat. **223**: 568–582
- Arana M V, Sánchez-Lamas M, Strasser B, Ibarra SE, Cerdán PD, Botto JF, Sánchez RA** (2014) Functional diversity of phytochrome family in the control of light and gibberellin-mediated germination in Arabidopsis. *Plant Cell Environ* **37**: 2014–23
- Ariizumi T, Lawrence PK, Steber CM** (2011) The Role of Two F-Box Proteins, SLEEPY1 and SNEEZY, in Arabidopsis Gibberellin Signaling. *Plant Physiol* **155**: 765–775
- Ariizumi T, Murase K, Sun T -p., Steber CM** (2008) Proteolysis-Independent Downregulation of DELLA Repression in Arabidopsis by the Gibberellin Receptor GIBBERELLIN INSENSITIVE DWARF1. *Plant Cell Online* **20**: 2447–2459
- von Arnim AG, Deng X-W** (1994) Light inactivation of arabidopsis photomorphogenic repressor COP1 involves a cell-specific regulation of its nucleocytoplasmic partitioning. *Cell* **79**: 1035–1045
- Baaske J, Gonschorek P, Engesser R, Dominguez-Monedero A, Raute K, Fischbach P, Müller K, Cachat E, Schamel WWA, Minguet S, et al** (2018) Dual-controlled optogenetic system for the rapid down-regulation of protein levels in mammalian cells. *Sci Rep* **8**: 15024
- Bae G, Choi G** (2008) Decoding of Light Signals by Plant Phytochromes and Their Interacting Proteins. *Annu Rev Plant Biol* **59**: 281–311
- Becskei A, Serrano L** (2000) Engineering stability in gene networks by autoregulation. *Nature* **405**: 590–593
- Bernier G, Périlleux C** (2005) A physiological overview of the genetics of flowering time control. *Plant Biotechnol J* **3**: 3–16
- Beyer HM, Juillot S, Herbst K, Samodelov SL, Müller K, Schamel WW, Römer W, Schäfer E, Nagy F, Strähle U, et al** (2015a) Red Light-Regulated Reversible Nuclear Localization of Proteins in Mammalian Cells and Zebrafish. *ACS Synth Biol* **4**: 951–958
- Beyer HM, Naumann S, Weber W, Radziwill G** (2015b) Optogenetic control of signaling in

References

- mammalian cells. *Biotechnol J* **10**: 273–283
- Blanco-Touriñán N, Legris M, Minguet EG, Costigliolo-Rojas C, Nohales MA, Iniesto E, García-León M, Pacín M, Heucken N, Blomeier T, et al** (2020) COP1 destabilizes DELLA proteins in *Arabidopsis*. *Proc Natl Acad Sci U S A* **117**: 13792–13799
- Blomeier T, Fischbach P, Koch L, Andres J, Miñambres M, Beyer HM, Zurbriggen MD** Blue Light-Operated CRISPR/Cas13b-Mediated mRNA Knockdown (Lockdown). *Adv Biol* 2000307
- Blumenstein A, Vienken K, Tasler R, Purschwitz J, Veith D, Frankenberg-Dinkel N, Fischer R** (2005) The *Aspergillus nidulans* Phytochrome FphA Represses Sexual Development in Red Light. *Curr Biol* **15**: 1833–1838
- Bubeck F, Hoffmann MD, Hartevelde Z, Aschenbrenner S, Bietz A, Waldhauer MC, Börner K, Fakhiri J, Schmelas C, Dietz L, et al** (2018) Engineered anti-CRISPR proteins for optogenetic control of CRISPR–Cas9. *Nat Methods* **15**: 924–927
- Bucherl CA, van Esse GW, Kruis A, Luchtenberg J, Westphal AH, Aker J, van Hoek A, Albrecht C, Borst JW, de Vries SC** (2013) Visualization of BRI1 and BAK1(SERK3) Membrane Receptor Heterooligomers during Brassinosteroid Signaling. *Plant Physiol* **162**: 1911–1925
- Bugaj LJ, Lim WA** (2019) High-throughput multicolor optogenetics in microwell plates. *Nat Protoc* **14**: 2205–2228
- Burgie ES, Vierstra RD** (2014) Phytochromes: an atomic perspective on photoactivation and signaling. *Plant Cell* **26**: 4568–83
- Van Buskirk EK, Decker P V, Chen M** (2012) Photobodies in light signaling. *Plant Physiol* **158**: 52–60
- Cameron DE, Bashor CJ, Collins JJ** (2014) A brief history of synthetic biology. *Nat Rev Microbiol* **12**: 381–390
- Casal JJ** (2013) Photoreceptor Signaling Networks in Plant Responses to Shade. *Annu Rev Plant Biol* **64**: 403–427
- Casal JJ, Fankhauser C, Coupland G, Blázquez MA** (2004) Signalling for developmental plasticity. *Trends Plant Sci* **9**: 309–314
- Casal JJ, Luccioni LG, Oliverio KA, Boccacalandro HE** (2003) Light, phytochrome signalling and photomorphogenesis in *Arabidopsis* †. doi: 10.1039/b300094j
- Casal JJ, Sánchez RA** (1998) Phytochromes and seed germination. *Seed Sci Res* **8**: 317–329
- Castillon A, Shen H, Huq E** (2007) Phytochrome Interacting Factors: central players in phytochrome-mediated light signaling networks. *Trends Plant Sci* **12**: 514–521
- Chandrasegaran S, Carroll D** (2016) Origins of Programmable Nucleases for Genome Engineering. *J Mol Biol* **428**: 963–89
- Chang H, Yi B, Ma R, Zhang X, Zhao H, Xi Y** (2016) CRISPR/cas9, a novel genomic tool to knock down microRNA in vitro and in vivo. *Sci Rep* **6**: 22312
- Chatelle C, Ochoa-Fernandez R, Engesser R, Schneider N, Beyer HM, Jones AR, Timmer J, Zurbriggen MD, Weber W** (2018) A Green-Light-Responsive System for the Control of Transgene Expression in Mammalian and Plant Cells. *ACS Synth Biol* **7**: 1349–1358
- Chen M, Chory J** (2011) Phytochrome signaling mechanisms and the control of plant development. *Trends Cell Biol* **21**: 664–671
- Chen M, Schwab R, Chory J** (2003) Characterization of the requirements for localization of phytochrome B to nuclear bodies. *Proc Natl Acad Sci U S A* **100**: 14493–8
- Chen M, Tao Y, Lim J, Shaw A, Chory J** (2005) Regulation of Phytochrome B Nuclear Localization through Light-Dependent Unmasking of Nuclear-Localization Signals. *Curr Biol* **15**: 637–642
- Chen X, Chen Y, Xin H, Wan T, Ping Y** (2020) Near-infrared optogenetic engineering of photothermal nanoCRISPR for programmable genome editing. *Proc Natl Acad Sci* **117**: 2395–2405
- Christie JM, Zurbriggen MD** (2020) Optogenetics in plants. *New Phytol* nph.17008
- Clack T, Shokry A, Moffet M, Liu P, Faul M, Sharrock RA** (2009) Obligate heterodimerization of *Arabidopsis* phytochromes C and E and interaction with the PIF3 basic helix-loop-helix transcription factor. *Plant Cell* **21**: 786–99

- Cox DBT, Gootenberg JS, Abudayyeh OO, Franklin B, Kellner MJ, Joung J, Zhang F** (2017) RNA editing with CRISPR-Cas13. *Science* (80-) **358**: 1019–1027
- Crick F** (1970) Central Dogma of Molecular Biology. *Nature* **227**: 561–563
- Danna K, Nathans D** (1971) Specific Cleavage of Simian Virus 40 DNA by Restriction Endonuclease of Hemophilus Influenzae* (gel electrophoresis/electron microscopy/DNA mapping/DNA fragments/tumor virus).
- Daviere J-M, Achard P** (2013) Gibberellin signaling in plants. *Development* **140**: 1147–1151
- Davière J-M, de Lucas M, Prat S** (2008) Transcriptional factor interaction: a central step in DELLA function. *Curr Opin Genet Dev* **18**: 295–303
- Deisseroth K** (2015) Optogenetics: 10 years of microbial opsins in neuroscience. *Nat Neurosci* **18**: 1213–1225
- Deisseroth K, Feng G, Majewska AK, Miesenböck G, Ting A, Schnitzer MJ** (2006) Next-generation optical technologies for illuminating genetically targeted brain circuits. *J Neurosci* **26**: 10380–6
- Depuydt S, Hardtke CS** (2011) Hormone Signalling Crosstalk in Plant Growth Regulation. *Curr Biol* **21**: R365–R373
- Dill A, Sun T-P** (2001) Synergistic Derepression of Gibberellin Signaling by Removing RGA and GAI Function in *Arabidopsis thaliana*.
- Dill A, Thomas SG, Hu J, Steber CM, Sun T** (2004) The *Arabidopsis* F-Box Protein SLEEPY1 Targets Gibberellin Signaling Repressors for Gibberellin-Induced Degradation. *Plant Cell* **16**: 1392–1405
- Donohue K, Heschel MS, Butler CM, Barua D, Sharrock RA, Whitelam GC, Chiang GCK** (2008) Diversification of phytochrome contributions to germination as a function of seed-maturation environment. *New Phytol* **177**: 367–79
- Elowitz MB, Leibler S** (2000) A synthetic oscillatory network of transcriptional regulators. *Nature* **403**: 335–338
- Evans L** (1996) Crop evolution, adaptation and yield.
- Fan LZ, Lin MZ** (2015) Optical control of biological processes by light-switchable proteins. *Wiley Interdiscip Rev Dev Biol* **4**: 545–54
- Farrow SC, Facchini PJ** (2014) Functional diversity of 2-oxoglutarate/Fe(II)-dependent dioxygenases in plant metabolism. *Front Plant Sci* **5**: 524
- Favory J-J, Stec A, Gruber H, Rizzini L, Oravecz A, Funk M, Albert A, Cloix C, Jenkins GI, Oakeley EJ, et al** (2009) Interaction of COP1 and UVR8 regulates UV-B-induced photomorphogenesis and stress acclimation in *Arabidopsis*. *EMBO J* **28**: 591–601
- Fedorov R, Schlichting I, Hartmann E, Domratcheva T, Fuhrmann M, Hegemann P** (2003) Crystal structures and molecular mechanism of a light-induced signaling switch: The Phot-LOV1 domain from *Chlamydomonas reinhardtii*. *Biophys J* **84**: 2474–82
- Fellmann C, Gowen BG, Lin P-C, Doudna JA, Corn JE** (2017) Cornerstones of CRISPR–Cas in drug discovery and therapy. *Nat Rev Drug Discov* **16**: 89–100
- Feng S, Martinez C, Gusmaroli G, Wang Y, Zhou J, Wang F, Chen L, Yu L, Iglesias-Pedraz JM, Kircher S, et al** (2008) Coordinated regulation of *Arabidopsis thaliana* development by light and gibberellins. *Nature* **451**: 475–9
- Fernández AP, Gil P, Valkai I, Nagy F, Schäfer E** (2005) Analysis of the Function of the Photoreceptors Phytochrome B and Phytochrome D in *Nicotiana plumbaginifolia* and *Arabidopsis thaliana*. *Plant Cell Physiol* **46**: 790–796
- Fiebitz A, Nyarsik L, Haendler B, Hu YH, Wagner F, Thamm S, Lehrach H, Janitz M, Vanhecke D** (2008) High-throughput mammalian two-hybrid screening for protein-protein interactions using transfected cell arrays. *BMC Genomics* **9**: 1–10
- Fischbach P, Gonschorek P, Baaske J, Davies JA, Weber W, Zurbriggen MD** (2020) Optogenetic Downregulation of Protein Levels to Control Programmed Cell Death in Mammalian Cells with a Dual Blue-Light Switch. pp 159–170
- Fischer AJ, Rockwell NC, Jang AY, Ernst LA, Waggoner AS, Duan Y, Lei H, Lagarias JC** (2005) Multiple roles of a conserved GAF domain tyrosine residue in cyanobacterial and plant phytochromes. *Biochemistry* **44**: 15203–15
- Förster T** (1948) Zwischenmolekulare Energiewanderung und Fluoreszenz. *Ann Phys* **437**: 55–75

References

- Franklin KA, Quail PH** (2010) Phytochrome functions in Arabidopsis development. *J Exp Bot* **61**: 11–24
- Froehlich AC, Noh B, Vierstra RD, Loros J, Dunlap JC** (2005) Genetic and molecular analysis of phytochromes from the filamentous fungus *Neurospora crassa*. *Eukaryot Cell* **4**: 2140–52
- Fu X, Richards DE, Fleck B, Xie D, Burton N, Harberd NP** (2004) The Arabidopsis mutant *sleepy1gar2-1* protein promotes plant growth by increasing the affinity of the SCF^{SLY1} E3 ubiquitin ligase for DELLA protein substrates. *Plant Cell* **16**: 1406–18
- Furuya M, Schäfer E** (1996) Photoperception and signalling of induction reactions by different phytochromes. *Trends Plant Sci* **1**: 301–307
- Fussenegger M, Moser S, Mazur X, Bailey JE** (1997) Autoregulated multicistronic expression vectors provide one-step cloning of regulated product gene expression in mammalian cells. *Biotechnol Prog* **13**: 733–740
- Gale MD, Youssefian S** (1985) Dwarfing genes in wheat. *Prog Plant Breeding*–1 1–35
- Galvão VC, Fankhauser C** (2015) Sensing the light environment in plants: photoreceptors and early signaling steps. *Curr Opin Neurobiol* **34**: 46–53
- Gardner TS, Cantor CR, Collins JJ** (2000) Construction of a genetic toggle switch in *Escherichia coli*. *Nature*. doi: 10.1038/35002131
- Gartner W, Braslavsky SE** (2003) The phytochromes: spectroscopy and function. pp 136–180
- Gazzarrini S, Tsai AY-L, Gazzarrini S, Tsai AY-L** (2015) Hormone cross-talk during seed germination. *Essays Biochem* **58**: 151–164
- Genoud T, Schweizer F, Tscheuschler A, Debrieux D, Casal JJ, Schäfer E, Hiltbrunner A, Fankhauser C** (2008) FHY1 Mediates Nuclear Import of the Light-Activated Phytochrome A Photoreceptor. *PLOS Genet* **4**: e1000143
- Gilbert LA, Larson MH, Morsut L, Liu Z, Brar GA, Torres SE, Stern-Ginossar N, Brandman O, Whitehead EH, Doudna JA, et al** (2013) CRISPR-Mediated Modular RNA-Guided Regulation of Transcription in Eukaryotes. *Cell* **154**: 442–451
- de Gooijer MC, van den Top A, Bockaj I, Beijnen JH, Würdinger T, van Tellingen O** (2017) The G2 checkpoint—a node-based molecular switch. *FEBS Open Bio* **7**: 439–455
- Gossen M, Bujard H** (1992) Tight control of gene expression in mammalian cells by tetracycline-responsive promoters. *Proc Natl Acad Sci* **89**: 5547–5551
- Gratz R, Brumbarova T, Ivanov R, Trofimov K, Tünnermann L, Ochoa-Fernandez R, Blomeier T, Meiser J, Weidtkamp-Peters S, Zurbriggen MD, et al** (2020) Phospho-mutant activity assays provide evidence for alternative phospho-regulation pathways of the transcription factor FER-LIKE IRON DEFICIENCY-INDUCED TRANSCRIPTION FACTOR. *New Phytol* **225**: 250–267
- Griffiths J, Murase K, Rieu I, Zentella R, Zhang Z-L, Powers SJ, Gong F, Phillips AL, Hedden P, Sun T, et al** (2006) Genetic Characterization and Functional Analysis of the GID1 Gibberellin Receptors in Arabidopsis. *Plant Cell* **18**: 3399–3414
- Gruber H, Heijde M, Heller W, Albert A, Seidlitz HK, Ulm R** (2010) Negative feedback regulation of UV-B-induced photomorphogenesis and stress acclimation in Arabidopsis. *Proc Natl Acad Sci U S A* **107**: 20132–7
- Gu Y, Di WL, Kellsell DP, Zicha D** (2004) Quantitative fluorescence resonance energy transfer (FRET) measurement with acceptor photobleaching and spectral unmixing. *J Microsc* **215**: 162–173
- Gyula P, Schäfer E, Nagy F** (2003) Light perception and signalling in higher plants. *Curr Opin Plant Biol* **6**: 446–452
- Hedden P** (2003) The genes of the Green Revolution. *Trends Genet* **19**: 5–9
- Hedden P, Thomas SG** (2012) Gibberellin biosynthesis and its regulation. *Biochem J* **444**: 11–25
- Hegemann P, Möglich A** (2011) Channelrhodopsin engineering and exploration of new optogenetic tools. *Nat Methods* **8**: 39–42
- Heijde M, Ulm R** (2013) Reversion of the Arabidopsis UV-B photoreceptor UVR8 to the homodimeric ground state. *Proc Natl Acad Sci U S A* **110**: 1113–8
- Hennig L, Stoddart WM, Dieterle M, Whitelam GC, Schäfer E** (2002) Phytochrome E

References

- controls light-induced germination of Arabidopsis. *Plant Physiol* **128**: 194–200
- Heschel MS, Butler CM, Barua D, Chiang GCK, Wheeler A, Sharrock RA, Whitelam GC, Donohue K** (2008) New Roles of Phytochromes during Seed Germination. *Int J Plant Sci* **169**: 531–540
- Heschel MS, Selby J, Butler C, Whitelam GC, Sharrock RA, Donohue K** (2007) A new role for phytochromes in temperature-dependent germination. *New Phytol* **174**: 735–741
- Hiltbrunner A, Tscheuschler A, Viczián A, Kunkel T, Kircher S, Schäfer E** (2006) FHY1 and FHL Act Together to Mediate Nuclear Accumulation of the Phytochrome A Photoreceptor. *Plant Cell Physiol* **47**: 1023–1034
- Hiltbrunner A, Viczián A, Bury E, Tscheuschler A, Kircher S, Tóth R, Honsberger A, Nagy F, Fankhauser C, Schäfer E** (2005) Nuclear Accumulation of the Phytochrome A Photoreceptor Requires FHY1. *Curr Biol* **15**: 2125–2130
- Hörner M, Weber W** (2012) Molecular switches in animal cells. *FEBS Lett* **586**: 2084–2096
- Hou BH, Takanaga H, Grossmann G, Chen LQ, Qu XQ, Jones AM, Lalonde S, Schweissgut O, Wiechert W, Frommer WB** (2011) Optical sensors for monitoring dynamic changes of intracellular metabolite levels in mammalian cells. *Nat Protoc* **6**: 1818–1833
- Hsu PD, Lander ES, Zhang F** (2014) Development and applications of CRISPR-Cas9 for genome engineering. *Cell* **157**: 1262–1278
- Huang H, Yoo CY, Bindbeutel R, Goldsworthy J, Tielking A, Alvarez S, Naldrett MJ, Evans BS, Chen M, Nusinow DA** (2016) PCH1 integrates circadian and light-signaling pathways to control photoperiod-responsive growth in Arabidopsis. *Elife*. doi: 10.7554/eLife.13292
- Huang X, Zhang Q, Jiang Y, Yang C, Wang Q, Li L** (2018) Shade-induced nuclear localization of PIF7 is regulated by phosphorylation and 14-3-3 proteins in Arabidopsis. *Elife*. doi: 10.7554/eLife.31636
- Huq E** (2004) PHYTOCHROME-INTERACTING FACTOR 1 Is a Critical bHLH Regulator of Chlorophyll Biosynthesis. *Science* (80-) **305**: 1937–1941
- Huq E, Quail PH** (2002) PIF4, a phytochrome-interacting bHLH factor, functions as a negative regulator of phytochrome B signaling in Arabidopsis. *EMBO J* **21**: 2441–50
- Jacob F, Monod J** (1961a) On the Regulation of Gene Activity. *Cold Spring Harb Symp Quant Biol* **26**: 193–211
- Jacob F, Monod J** (1961b) Genetic regulatory mechanisms in the synthesis of proteins. *J Mol Biol* **3**: 318–356
- Jacobs JL, Dinman JD** (2004) Systematic analysis of bicistronic reporter assay data. *Nucleic Acids Res* **32**: e160
- Jiao Y, Lau OS, Deng XW** (2007) Light-regulated transcriptional networks in higher plants. *Nat Rev Genet* **8**: 217–230
- Jung J-H, Domijan M, Klose C, Biswas S, Ezer D, Gao M, Khattak AK, Box MS, Charoensawan V, Cortijo S, et al** (2016) Phytochromes function as thermosensors in Arabidopsis. *Science* (80-) **354**: 886–889
- Khalil AS, Collins JJ** (2010) Synthetic biology: applications come of age. *Nat Rev Genet* **11**: 367–379
- Khanna R, Huq E, Kikis EA, Al-Sady B, Lanzatella C, Quail PH** (2004) A novel molecular recognition motif necessary for targeting photoactivated phytochrome signaling to specific basic helix-loop-helix transcription factors. *Plant Cell* **16**: 3033–44
- Kiel C, Yus E, Serrano L** (2010) Engineering Signal Transduction Pathways. *Cell* **140**: 33–47
- Kim NY, Lee S, Yu J, Kim N, Won SS, Park H, Heo W Do** (2020) Optogenetic control of mRNA localization and translation in live cells. *Nat Cell Biol* **22**: 341–352
- Kircher S, Gil P, Kozma-Bognár L, Fejes E, Speth V, Husselstein-Muller T, Bauer D, Ádám É, Schäfer E, Nagy F** (2002) Nucleocytoplasmic Partitioning of the Plant Photoreceptors Phytochrome A, B, C, D, and E Is Regulated Differentially by Light and Exhibits a Diurnal Rhythm. *Plant Cell* **14**: 1541–1555
- Kircher S, Kozma-Bognar L, Kim L, Adam E, Harter K, Schafer E, Nagy F** (1999) Light quality-dependent nuclear import of the plant photoreceptors phytochrome A and B. *Plant Cell* **11**: 1445–56

- Klose C, Venezia F, Hussong A, Kircher S, Schäfer E, Fleck C** (2015) Systematic analysis of how phytochrome B dimerization determines its specificity. *Nat Plants* **1**: 15090
- Kolar K, Knobloch C, Stork H, Žnidarič M, Weber W** (2018) OptoBase: A Web Platform for Molecular Optogenetics. *ACS Synth Biol* **7**: 1825–1828
- Kolar K, Weber W** (2017) Synthetic biological approaches to optogenetically control cell signaling. *Curr Opin Biotechnol* **47**: 112–119
- Konermann S, Brigham MD, Trevino AE, Hsu PD, Heidenreich M, Le Cong L, Platt RJ, Scott DA, Church GM, Zhang F** (2013) Optical control of mammalian endogenous transcription and epigenetic states. *Nature* **500**: 472–476
- Koornneef A, Pieterse CMJ** (2008) Cross Talk in Defense Signaling. *Plant Physiol* **146**: 839–844
- Kramer BP, Fischer C, Fussenegger M** (2004) BioLogic gates enable logical transcription control in mammalian cells. *Biotechnol Bioeng* **87**: 478–484
- Kremers GJ, Goedhart J, Van Munster EB, Gadella TWJ** (2006) Cyan and yellow super fluorescent proteins with improved brightness, protein folding, and FRET Förster radius. *Biochemistry* **45**: 6570–6580
- Krueger D, Izquierdo E, Viswanathan R, Hartmann J, Pallares Cartes C, De Renzis S** (2019) Principles and applications of optogenetics in developmental biology. *Development*. doi: 10.1242/dev.175067
- Lai EC** (2004) Development. *Development* **112**: 231–240
- Lam AJ, St-Pierre F, Gong Y, Marshall JD, Cranfill PJ, Baird MA, McKeown MR, Wiedenmann J, Davidson MW, Schnitzer MJ, et al** (2012) Improving FRET dynamic range with bright green and red fluorescent proteins. *Nat Methods* **9**: 1005–1012
- Lau OS, Deng XW** (2012) The photomorphogenic repressors COP1 and DET1: 20 years later. *Trends Plant Sci* **17**: 584–93
- Lee N, Choi G** (2017) Phytochrome-interacting factor from Arabidopsis to liverwort. *Curr Opin Plant Biol* **35**: 54–60
- Legris M, Klose C, Burgie ES, Rojas CCR, Neme M, Hiltbrunner A, Wigge PA, Schäfer E, Vierstra RD, Casal JJ** (2016) Phytochrome B integrates light and temperature signals in Arabidopsis. *Science* (80-) **354**: 897–900
- Leivar P, Monte E** (2014) PIFs: systems integrators in plant development. *Plant Cell* **26**: 56–78
- Leivar P, Monte E, Al-Sady B, Carle C, Storer A, Alonso JM, Ecker JR, Quail PH** (2008) The Arabidopsis phytochrome-interacting factor PIF7, together with PIF3 and PIF4, regulates responses to prolonged red light by modulating phyB levels. *Plant Cell* **20**: 337–52
- Leivar P, Quail PH** (2011) PIFs: pivotal components in a cellular signaling hub. *Trends Plant Sci* **16**: 19–28
- Leopold A V., Chernov KG, Verkhusha V V.** (2018) Optogenetically controlled protein kinases for regulation of cellular signaling. *Chem Soc Rev* **47**: 2454–2484
- Li H, Qin X, Song P, Han R, Li J** (2021) A LexA-based yeast two-hybrid system for studying light-switchable interactions of phytochromes with their interacting partners. *aBIOTECH* **1**–12
- Li L, Ljung K, Breton G, Schmitz RJ, Pruneda-Paz J, Cowing-Zitron C, Cole BJ, Ivans LJ, Pedmale U V, Jung H-S, et al** (2012) Linking photoreceptor excitation to changes in plant architecture. *Genes Dev* **26**: 785–90
- Lienert F, Lohmueller JJ, Garg A, Silver PA** (2014) Synthetic biology in mammalian cells: next generation research tools and therapeutics. *Nat Rev Mol Cell Biol* **15**: 95–107
- Lim S, Kaldis P** (2013) Cdks, cyclins and CKIs: roles beyond cell cycle regulation. *Development* **140**: 3079–93
- Lim WA** (2010) Designing Customized Cell Signaling Circuits. *Nat Rev Mol Cell Biol* **11**: 393–403
- Lin Q, Jin S, Zong Y, Yu H, Zhu Z, Liu G, Kou L, Wang Y, Qiu J-L, Li J, et al** (2021) High-efficiency prime editing with optimized, paired pegRNAs in plants. *Nat Biotechnol* **1**–5
- Lin Q, Zong Y, Xue C, Wang S, Jin S, Zhu Z, Wang Y, Anzalone A V., Raguram A, Doman JL, et al** (2020) Prime genome editing in rice and wheat. *Nat Biotechnol* **38**: 582–585

References

- Liu P, Sharrock RA** (2017) Biological activity and dimerization state of modified phytochrome A proteins. doi: 10.1371/journal.pone.0186468
- Liu Z, Zhang J, Jin J, Geng Z, Qi Q, Liang Q** (2018) Programming Bacteria With Light-Sensors and Applications in Synthetic Biology. *Front Microbiol* **9**: 2692
- Locascio A, Blázquez MA, Alabadí D** (2013) Genomic analysis of della protein activity. *Plant Cell Physiol* **54**: 1229–1237
- Long Y, Stahl Y, Weidtkamp-Peters S, Smet W, Du Y, Gadella TWJ, Goedhart J, Scheres B, Bliilou I** (2018) Optimizing FRET-FLIM Labeling Conditions to Detect Nuclear Protein Interactions at Native Expression Levels in Living Arabidopsis Roots. *Front Plant Sci* **9**: 1–13
- Lorrain S, Allen T, Duek PD, Whitelam GC, Fankhauser C** (2008) Phytochrome-mediated inhibition of shade avoidance involves degradation of growth-promoting bHLH transcription factors. *Plant J* **53**: 312–23
- de Lucas M, Davière J-M, Rodríguez-Falcón M, Pontin M, Iglesias-Pedraz JM, Lorrain S, Fankhauser C, Blázquez MA, Titarenko E, Prat S** (2008) A molecular framework for light and gibberellin control of cell elongation. *Nature* **451**: 480–484
- Luo Q, Lian H-L, He S-B, Li L, Jia K-P, Yang H-Q** (2014) COP1 and phyB Physically Interact with PIL1 to Regulate Its Stability and Photomorphogenic Development in Arabidopsis. *Plant Cell* **26**: 2441–2456
- Malumbres M** (2014) Cyclin-dependent kinases. *Genome Biol* **15**: 122
- Malumbres M, Barbacid M** (2009) Cell cycle, CDKs and cancer: a changing paradigm. *Nat Rev Cancer* **9**: 153–166
- Malumbres M, Carnero A** (2003) Cell cycle deregulation: a common motif in cancer. *Prog Cell Cycle Res* **5**: 5–18
- Marín-de la Rosa N, Pfeiffer A, Hill K, Locascio A, Bhalerao RP, Miskolczi P, Grønlund AL, Wanchoo-Kohli A, Thomas SG, Bennett MJ, et al** (2015) Genome Wide Binding Site Analysis Reveals Transcriptional Coactivation of Cytokinin-Responsive Genes by DELLA Proteins. *PLoS Genet* **11**: e1005337
- Marín-de la Rosa N, Sotillo B, Miskolczi P, Gibbs DJ, Vicente J, Carbonero P, Oñate-Sánchez L, Holdsworth MJ, Bhalerao R, Alabadí D, et al** (2014) Large-scale identification of gibberellin-related transcription factors defines group VII ETHYLENE RESPONSE FACTORS as functional DELLA partners. *Plant Physiol* **166**: 1022–32
- Marraffini LA** (2015) CRISPR-Cas immunity in prokaryotes. *Nature* **526**: 55–61
- Martel C, Blair LK, Donohue K** (2018) PHYD prevents secondary dormancy establishment of seeds exposed to high temperature and is associated with lower PIL5 accumulation. *J Exp Bot* **69**: 3157–3169
- Martínez-García JF, Huq E, Quail PH** (2000) Direct targeting of light signals to a promoter element-bound transcription factor. *Science* **288**: 859–63
- Massari ME, Murre C** (2000) Helix-loop-helix proteins: regulators of transcription in eucaryotic organisms. *Mol Cell Biol* **20**: 429–40
- Matiolli CC, Melotto M** (2018) A Comprehensive Arabidopsis Yeast Two-Hybrid Library for Protein-Protein Interaction Studies: A Resource to the Plant Research Community. *Mol Plant-Microbe Interact* **31**: 899–902
- Matsushita T, Mochizuki N, Nagatani A** (2003) Dimers of the N-terminal domain of phytochrome B are functional in the nucleus. *Nature* **424**: 571–574
- McGinnis KM, Thomas SG, Soule JD, Strader LC, Zale JM, Sun T, Steber CM** (2003) The Arabidopsis SLEEPY1 gene encodes a putative F-box subunit of an SCF E3 ubiquitin ligase. *Plant Cell* **15**: 1120–30
- Miyamoto T, DeRose R, Suarez A, Ueno T, Chen M, Sun T, Wolfgang MJ, Mukherjee C, Meyers DJ, Inoue T** (2012) Rapid and orthogonal logic gating with a gibberellin-induced dimerization system. *Nat Chem Biol* **8**: 465–70
- Montgomery BL, Lagarias JC** (2002) Phytochrome ancestry: sensors of bilins and light. *Trends Plant Sci* **7**: 357–366
- Morgan DO** (1997) CYCLIN-DEPENDENT KINASES: Engines, Clocks, and Microprocessors. *Annu Rev Cell Dev Biol* **13**: 261–291
- Müller B, Sheen J** (2008) Cytokinin and auxin interplay in root stem-cell specification during

References

- early embryogenesis. *Nature* **453**: 1094–1097
- Müller K, Engesser R, Metzger S, Schulz S, Kämpf MM, Busacker M, Steinberg T, Tomakidi P, Ehrbar M, Nagy F, et al** (2013a) A red/far-red light-responsive bi-stable toggle switch to control gene expression in mammalian cells. *Nucleic Acids Res* **41**: e77–e77
- Müller K, Engesser R, Schulz S, Steinberg T, Tomakidi P, Weber CC, Ulm R, Timmer J, Zurbriggen MD, Weber W** (2013b) Multi-chromatic control of mammalian gene expression and signaling. *Nucleic Acids Res* **41**: e124–e124
- Müller K, Engesser R, Timmer J, Zurbriggen MD, Weber W** (2014a) Orthogonal Optogenetic Triple-Gene Control in Mammalian Cells. *ACS Synth Biol* **3**: 796–801
- Müller K, Naumann S, Weber W, Zurbriggen MD** (2015) Optogenetics for gene expression in mammalian cells. *Biol Chem* **396**: 145–152
- Müller K, Siegel D, Jahnke FR, Gerrer K, Wend S, Decker EL, Reski R, Weber Abce W, Zurbriggen MD** (2014b) A red light-controlled synthetic gene expression switch for plant systems †. *Mol BioSyst* **10**: 1679
- Muñoz A, Castellano MM** (2018) Coimmunoprecipitation of Interacting Proteins in Plants. *Methods Mol. Biol. Methods Mol Biol*, pp 279–287
- Murase K, Hirano Y, Sun TP, Hakoshima T** (2008) Gibberellin-induced DELLA recognition by the gibberellin receptor GID1. *Nature* **456**: 459–463
- Murre C, Bain G, van Dijk MA, Engel I, Furnari BA, Massari ME, Matthews JR, Quong MW, Rivera RR, Stuiver MH** (1994) Structure and function of helix-loop-helix proteins. *Biochim Biophys Acta - Gene Struct Expr* **1218**: 129–135
- Murre C, McCaw PS, Baltimore D** (1989) A new DNA binding and dimerization motif in immunoglobulin enhancer binding, daughterless, MyoD, and myc proteins. *Cell* **56**: 777–783
- Nagy F, Kircher S, Schafer E** (2001) Intracellular trafficking of photoreceptors during light-induced signal transduction in plants. *J. Cell Sci.* 114:
- Nakajima M, Shimada A, Takashi Y, Kim YC, Park SH, Ueguchi-Tanaka M, Suzuki H, Katoh E, Iuchi S, Kobayashi M, et al** (2006) Identification and characterization of Arabidopsis gibberellin receptors. *Plant J* **46**: 880–889
- Nash AI, McNulty R, Shillito ME, Swartz TE, Bogomolni RA, Luecke H, Gardner KH** (2011) Structural basis of photosensitivity in a bacterial light-oxygen-voltage/helix-turn-helix (LOV-HTH) DNA-binding protein. *Proc Natl Acad Sci U S A* **108**: 9449–54
- Ni M, Tepperman JM, Quail PH** (1998) PIF3, a phytochrome-interacting factor necessary for normal photoinduced signal transduction, is a novel basic helix-loop-helix protein. *Cell* **95**: 657–67
- Ni M, Tepperman JM, Quail PH** (1999) Binding of phytochrome B to its nuclear signalling partner PIF3 is reversibly induced by light. *Nature* **400**: 781–784
- Ni W, Xu S-L, Tepperman JM, Stanley DJ, Maltby DA, Gross JD, Burlingame AL, Wang Z-Y, Quail PH** (2014) A mutually assured destruction mechanism attenuates light signaling in Arabidopsis. *Science* (80-) **344**: 1160–1164
- Nihongaki Y, Furuhashi Y, Otabe T, Hasegawa S, Yoshimoto K, Sato M** (2017) CRISPR–Cas9-based photoactivatable transcription systems to induce neuronal differentiation. *Nat Methods* **14**: 963–966
- Nihongaki Y, Kawano F, Nakajima T, Sato M** (2015) Photoactivatable CRISPR-Cas9 for optogenetic genome editing. *Nat Biotechnol* **33**: 755–760
- Ochoa-Fernandez R, Abel NB, Wieland F-G, Schlegel J, Koch L-A, Miller JB, Engesser R, Giuriani G, Brandl SM, Timmer J, et al** (2020) Optogenetic control of gene expression in plants in the presence of ambient white light. *Nat Methods* **17**: 717–725
- Ochoa-Fernandez R, Samodelov SL, Brandl SM, Wehinger E, Müller K, Weber W, Zurbriggen MD** (2016) Optogenetics in Plants: Red/Far-Red Light Control of Gene Expression. *Methods Mol. Biol.* pp 125–139
- Oh J, Park E, Song K, Bae G, Choi G** (2020) PHYTOCHROME INTERACTING FACTOR8 Inhibits Phytochrome A-Mediated Far-Red Light Responses in Arabidopsis. *Plant Cell* **32**: 186–205
- Pacín M, Legris M, Casal JJ** (2014) Rapid decline in nuclear constitutive

References

- photomorphogenesis1 abundance anticipates the stabilization of its target elongated hypocotyl5 in the light. *Plant Physiol* **164**: 1134–8
- Papanatsiou M, Petersen J, Henderson L, Wang Y, Christie JM, Blatt MR** (2019) Optogenetic manipulation of stomatal kinetics improves carbon assimilation, water use, and growth. *Science* **363**: 1456–1459
- Park E, Park J, Kim J, Nagatani A, Lagarias JC, Choi G** (2012) Phytochrome B inhibits binding of phytochrome-interacting factors to their target promoters. *Plant J* **72**: 537–546
- Peng J, Richards DE, Hartley NM, Murphy GP, Devos KM, Flintham JE, Beales J, Fish LJ, Worland AJ, Pelica F, et al** (1999) ‘Green revolution’ genes encode mutant gibberellin response modulators. *Nature* **400**: 256–261
- Pfeiffer A, Nagel M-K, Popp C, Wüst F, Bindics J, Viczián A, Hiltbrunner A, Nagy F, Kunkel T, Schäfer E** (2012) Interaction with plant transcription factors can mediate nuclear import of phytochrome B. *Proc Natl Acad Sci U S A* **109**: 5892–7
- Pickar-Oliver A, Gersbach CA** (2019) The next generation of CRISPR–Cas technologies and applications. *Nat Rev Mol Cell Biol* **20**: 490–507
- Pilsel S, Morgan C, Choukeife M, Möglich A, Mayer G** (2020) Optoribogenetic control of regulatory RNA molecules. *Nat Commun* **11**: 4825
- Polstein LR, Gersbach CA** (2015) A light-inducible CRISPR-Cas9 system for control of endogenous gene activation. *Nat Chem Biol* **11**: 198–200
- Prevo R, Pirovano G, Puliyadi R, Herbert KJ, Rodriguez-Berriguete G, O’Docherty A, Greaves W, McKenna WG, Higgins GS** (2018) CDK1 inhibition sensitizes normal cells to DNA damage in a cell cycle dependent manner. *Cell Cycle* **17**: 1513–1523
- Pryciak PM** (2009) Designing new cellular signaling pathways. *Chem Biol* **16**: 249
- Qi LS, Larson MH, Gilbert LA, Doudna JA, Weissman JS, Arkin AP, Lim WA** (2013) Repurposing CRISPR as an RNA-Guided Platform for Sequence-Specific Control of Gene Expression. *Cell* **152**: 1173–1183
- Rausenberger J, Hussong A, Kircher S, Kirchenbauer D, Timmer J, Nagy F, Schäfer E, Fleck C** (2010) An Integrative Model for Phytochrome B Mediated Photomorphogenesis: From Protein Dynamics to Physiology. *PLoS One* **5**: e10721
- Rausenberger J, Tscheuschler A, Nordmeier W, Wüst F, Timmer J, Schäfer E, Fleck C, Hiltbrunner A** (2011) Photoconversion and Nuclear Trafficking Cycles Determine Phytochrome A’s Response Profile to Far-Red Light. *Cell* **146**: 813–825
- Reyer A, Häßler M, Scherzer S, Huang S, Pedersen JT, Al-Rascheid KAS, Bamberg E, Palmgren M, Dreyer I, Nagel G, et al** (2020) Channelrhodopsin-mediated optogenetics highlights a central role of depolarization-dependent plant proton pumps. *Proc Natl Acad Sci U S A* **117**: 20920–20925
- Rizzini L, Favory J-J, Cloix C, Faggionato D, O’Hara A, Kaiserli E, Baumeister R, Schafer E, Nagy F, Jenkins GI, et al** (2011) Perception of UV-B by the Arabidopsis UVR8 Protein. *Science* (80-) **332**: 103–106
- Rockwell NC, Su Y-S, Lagarias JC** (2006) PHYTOCHROME STRUCTURE AND SIGNALING MECHANISMS. *Annu Rev Plant Biol* **57**: 837–858
- Sakai H, Aoyama T, Oka A** (2000) Arabidopsis ARR1 and ARR2 response regulators operate as transcriptional activators. *Plant J* **24**: 703–11
- Sakamoto K, Nagatani A** (1996) Nuclear localization activity of phytochrome B. *Plant J* **10**: 859–868
- Salinas F, Rojas V, Delgado V, Agosin E, Larrondo LF** (2017) Optogenetic switches for light-controlled gene expression in yeast. *Appl Microbiol Biotechnol* **101**: 2629–2640
- Samodelov SL, Beyer HM, Guo X, Augustin M, Jia K-P, Baz L, Ebenhöf O, Beyer P, Weber W, Al-Babili S, et al** (2016) StrigoQuant: A genetically encoded biosensor for quantifying strigolactone activity and specificity. *Sci Adv* **2**: e1601266
- Samodelov SL, Zurbruggen MD** (2017) Quantitatively Understanding Plant Signaling: Novel Theoretical–Experimental Approaches. *Trends Plant Sci* **22**: 685–704
- Sancak Y, Peterson TR, Shaul YD, Lindquist RA, Thoreen CC, Bar-Peled L, Sabatini DM** (2008) The Rag GTPases bind raptor and mediate amino acid signaling to mTORC1. *Science* **320**: 1496–501
- Santner A, Calderon-Villalobos LIA, Estelle M** (2009) Plant hormones are versatile chemical

References

- regulators of plant growth. *Nat Chem Biol* **5**: 301–307
- Schaumberg KA, Antunes MS, Kassaw TK, Xu W, Zalewski CS, Medford JI, Prasad A** (2016) Quantitative characterization of genetic parts and circuits for plant synthetic biology. *Nat Methods* **13**: 94–100
- Schwechheimer C** (2012) Gibberellin Signaling in Plants – The Extended Version. *Front Plant Sci* **2**: 107
- Sharrock RA, Quail PH** (1989) Novel phytochrome sequences in *Arabidopsis thaliana*: structure, evolution, and differential expression of a plant regulatory photoreceptor family. *Genes Dev* **3**: 1745–1757
- Sheen J** (2010) Discover and Connect Cellular Signaling. *Plant Physiol* **154**: 562–566
- Shen H, Zhu L, Castillon A, Majee M, Downie B, Huq E** (2008) Light-induced phosphorylation and degradation of the negative regulator PHYTOCHROME-INTERACTING FACTOR1 from *Arabidopsis* depend upon its direct physical interactions with photoactivated phytochromes. *Plant Cell* **20**: 1586–602
- Shimada A, Ueguchi-Tanaka M, Nakatsu T, Nakajima M, Naoe Y, Ohmiya H, Kato H, Matsuoka M** (2008) Structural basis for gibberellin recognition by its receptor *GID1*. *Nature* **456**: 520–523
- Shinomura T, Uchida K, Furuya M** (2000) Elementary processes of photoperception by phytochrome A for high-irradiance response of hypocotyl elongation in *Arabidopsis*. *Plant Physiol* **122**: 147–56
- Silverstone AL, Ciampaglio CN, Sun T, Kitano H, Koshioka M, Futsuhara Y, Matsuoka M, Yamaguchi J** (1998) The *Arabidopsis RGA* Gene Encodes a Transcriptional Regulator Repressing the Gibberellin Signal Transduction Pathway. *Plant Cell* **10**: 155–169
- Sineshchekov VA** (1995) Photobiophysics and photobiochemistry of the heterogeneous phytochrome system. *Biochim Biophys Acta - Bioenerg* **1228**: 125–164
- Stahl Y, Grabowski S, Bleckmann A, Kühnemuth R, Weidtkamp-Peters S, Pinto KG, Kirschner GK, Schmid JB, Wink RH, Hülsewede A, et al** (2013) Moderation of *Arabidopsis* root stemness by *CLAVATA1* and *ARABIDOPSIS CRINKLY4* receptor kinase complexes. *Curr Biol* **23**: 362–71
- Strickland D, Lin Y, Wagner E, Hope CM, Zayner J, Antoniou C, Sosnick TR, Weiss EL, Glotzer M** (2012) TULIPs: tunable, light-controlled interacting protein tags for cell biology. *Nat Methods* **9**: 379–84
- Strutt SC, Torrez RM, Kaya E, Negrete OA, Doudna JA** (2018) RNA-dependent RNA targeting by CRISPR-Cas9. *Elife*. doi: 10.7554/eLife.32724
- Stynen B, Tournu H, Tavernier J, Van Dijck P** (2012) Diversity in Genetic In Vivo Methods for Protein-Protein Interaction Studies: from the Yeast Two-Hybrid System to the Mammalian Split-Luciferase System. *Microbiol Mol Biol Rev* **76**: 331–382
- Sun T, Gubler F** (2004) Molecular Mechanism of Gibberellin Signaling in Plants. *Annu Rev Plant Biol* **55**: 197–223
- Suzuki H, Park SH, Okubo K, Kitamura J, Ueguchi-Tanaka M, Iuchi S, Katoh E, Kobayashi M, Yamaguchi I, Matsuoka M, et al** (2009) Differential expression and affinities of *Arabidopsis* gibberellin receptors can explain variation in phenotypes of multiple knock-out mutants. *Plant J* **60**: 48–55
- Thomas OS, Hörner M, Weber W** (2020) A graphical user interface to design high-throughput optogenetic experiments with the optoPlate-96. *Nat Protoc* **15**: 2785–2787
- Thomas SG, Phillips AL, Hedden P** (1999) Molecular cloning and functional expression of gibberellin 2- oxidases, multifunctional enzymes involved in gibberellin deactivation. *Proc Natl Acad Sci* **96**: 4698–4703
- Toledo-Ortiz G, Huq E, Quail PH** (2003) The *Arabidopsis* Basic/Helix-Loop-Helix Transcription Factor Family. *Plant Cell* **15**: 1749–1770
- Ueguchi-Tanaka M, Ashikari M, Nakajima M, Itoh H, Katoh E, Kobayashi M, Chow TY, Hsing YIC, Kitano H, Yamaguchi I, et al** (2005) GIBBERELLIN INSENSITIVE DWARF1 encodes a soluble receptor for gibberellin. *Nature* **437**: 693–698
- Ueguchi-Tanaka M, Nakajima M, Katoh E, Ohmiya H, Asano K, Saji S, Hongyu X, Ashikari M, Kitano H, Yamaguchi I, et al** (2007) Molecular Interactions of a Soluble Gibberellin

References

- Receptor, *GID1*, with a Rice *DELLA* Protein, *SLR1*, and Gibberellin. *Plant Cell* **19**: 2140–2155
- Unniyampurath U, Pilankatta R, Krishnan MN** (2016) RNA Interference in the Age of CRISPR: Will CRISPR Interfere with RNAi? *Int J Mol Sci* **17**: 291
- Urquiza-Garcia U, Zurbruggen MD** (2021) Biofortifying green optogenetics. *Nat Plants* **7**: 104–105
- Vanstraelen M, Benková E** (2012) Hormonal Interactions in the Regulation of Plant Development. *Annu Rev Cell Dev Biol* **28**: 463–487
- Verma V, Ravindran P, Kumar PP** (2016) Plant hormone-mediated regulation of stress responses. *BMC Plant Biol* **16**: 86
- Viczián A, Ádám É, Staudt A, Lambert D, Klement E, Romero Montepaone S, Hiltbrunner A, Casal J, Schäfer E, Nagy F, et al** (2020) Differential phosphorylation of the N-terminal extension regulates phytochrome B signaling. *New Phytol* **225**: 1635–1650
- Vierstra RD** (2009) The ubiquitin–26S proteasome system at the nexus of plant biology. *Nat Rev Mol Cell Biol* **10**: 385–397
- Vogel P, Hanswillemenke A, Stafforst T** (2017) Switching Protein Localization by Site-Directed RNA Editing under Control of Light. *ACS Synth Biol* **6**: 1642–1649
- Vu TQ, de Castro RMB, Qin L** (2017) Bridging the gap: microfluidic devices for short and long distance cell–cell communication. *Lab Chip* **17**: 1009–1023
- Walter M, Chaban C, Schütze K, Batistic O, Weckermann K, Näke C, Blazevic D, Grefen C, Schumacher K, Oecking C, et al** (2004) Visualization of protein interactions in living plant cells using bimolecular fluorescence complementation. *Plant J* **40**: 428–438
- Wang Y, Deng D** (2014) Molecular basis and evolutionary pattern of *GA-GID1-DELLA* regulatory module. *Mol Genet Genomics* **289**: 1–9
- Weber AM, Kaiser J, Ziegler T, Pilsel S, Renzl C, Sixt L, Pietruschka G, Moniot S, Kakoti A, Juraschitz M, et al** (2019) A blue light receptor that mediates RNA binding and translational regulation. *Nat Chem Biol* **15**: 1085–1092
- Weber W, Fussenegger M** (2010) Synthetic gene networks in mammalian cells. *Curr Opin Biotechnol* **21**: 690–696
- Weber W, Fux C, Daoud-El Baba M, Keller B, Weber CC, Kramer BP, Heinzen C, Aubel D, Bailey JE, Fussenegger M** (2002) Macrolide-based transgene control in mammalian cells and mice. doi: 10.1038/nbt731
- Weidtkamp-Peters S, Stahl Y** (2017) The Use of FRET/FLIM to Study Proteins Interacting with Plant Receptor Kinases. *Methods Mol. Biol.* pp 163–175
- Wend S, Wagner HJ, Müller K, Zurbruggen MD, Weber W, Radziwill G** (2013) Optogenetic Control of Protein Kinase Activity in Mammalian Cells. *ACS Synth Biol*. doi: 10.1021/sb400090s
- Willige BC, Ghosh S, Nill C, Zourelidou M, Dohmann EMN, Maier A, Schwechheimer C** (2007) The *DELLA* Domain of *GA INSENSITIVE* Mediates the Interaction with the *GA INSENSITIVE DWARF1A* Gibberellin Receptor of *Arabidopsis*. *Plant Cell Online* **19**: 1209–1220
- Xu X, Paik I, Zhu L, Huq E** (2015) Illuminating Progress in Phytochrome-Mediated Light Signaling Pathways. *Trends Plant Sci* **20**: 641–650
- Yabuta T, Sumiki Y** (1938) On the crystal of gibberellin, a substance to promote plant growth. *J Agric Chem Soc Japan* **14**: 1526
- Yamaguchi R, Nakamura M, Mochizuki N, Kay SA, Nagatani A** (1999) Light-dependent Translocation of a Phytochrome B-GFP Fusion Protein to the Nucleus in Transgenic *Arabidopsis*. *J Cell Biol* **145**: 437–445
- Yamaguchi S** (2008) Gibberellin Metabolism and its Regulation. *Annu Rev Plant Biol* **59**: 225–251
- Yanovsky MJ, Casal JJ, Luppi JP** (1997) The *VLF* loci, polymorphic between ecotypes *Landsberg erecta* and *Columbia*, dissect two branches of phytochrome A signal transduction that correspond to very-low-fluence and high-irradiance responses. *Plant J* **12**: 659–67
- Yanovsky MJ, Casal JJ, Whitelam GC** (1995) Phytochrome A, phytochrome B and *HY4* are involved in hypocotyl growth responses to natural radiation in *Arabidopsis*: weak de-

References

- etiolation of the phyA mutant under dense canopies. *Plant, Cell Environ* **18**: 788–794
- Yeom M, Kim H, Lim J, Shin A-Y, Hong S, Kim J-I, Gil Nam H** (2014) How Do Phytochromes Transmit the Light Quality Information to the Circadian Clock in Arabidopsis? *Mol Plant* **7**: 1701–1704
- Yin R, Skvortsova MY, Loubéry S, Ulm R** (2016) COP1 is required for UV-B-induced nuclear accumulation of the UVR8 photoreceptor. *Proc Natl Acad Sci U S A* **113**: E4415-22
- Yu Y, Wu X, Guan N, Shao J, Li H, Chen Y, Ping Y, Li D, Ye H** (2020) Engineering a far-red light-activated split-Cas9 system for remote-controlled genome editing of internal organs and tumors. *Sci Adv* **6**: eabb1777
- Zeidler M, Zhou Q, Sarda X, Yau C, Chua N** (2004) The nuclear localization signal and the C-terminal region of FHY1 are required for transmission of phytochrome A signals. *Plant J* **40**: 355–365
- Zhang Y, Mayba O, Pfeiffer A, Shi H, Tepperman JM, Speed TP, Quail PH** (2013) A Quartet of PIF bHLH Factors Provides a Transcriptionally Centered Signaling Hub That Regulates Seedling Morphogenesis through Differential Expression-Patterning of Shared Target Genes in Arabidopsis. *PLoS Genet* **9**: e1003244
- Zhang Y, Pfeiffer A, Tepperman JM, Dalton-Roesler J, Leivar P, Gonzalez Grandio E, Quail PH** (2020) Central clock components modulate plant shade avoidance by directly repressing transcriptional activation activity of PIF proteins. *Proc Natl Acad Sci U S A* **117**: 3261–3269
- Zhou XX, Zou X, Chung HK, Gao Y, Liu Y, Qi LS, Lin MZ** (2018) A Single-Chain Photoswitchable CRISPR-Cas9 Architecture for Light-Inducible Gene Editing and Transcription. *ACS Chem Biol* **13**: 443–448
- Zhou Y, Ding M, Duan X, Konrad KR, Nagel G, Gao S** (2021a) Extending the Anion Channelrhodopsin-Based Toolbox for Plant Optogenetics. *Membranes (Basel)* **11**: 287
- Zhou Y, Ding M, Gao S, Yu-Strzelczyk J, Krischke M, Duan X, Leide J, Riederer M, Mueller MJ, Hedrich R, et al** (2021b) Optogenetic control of plant growth by a microbial rhodopsin. *Nat Plants* **7**: 144–151
- Zhu Y, Tepperman JM, Fairchild CD, Quail PH** (2000) Phytochrome B binds with greater apparent affinity than phytochrome A to the basic helix-loop-helix factor PIF3 in a reaction requiring the PAS domain of PIF3. *Proc Natl Acad Sci U S A* **97**: 13419–24

7 Appendix

7.1 Original publications and manuscripts

Tim Blomeier*, Jennifer Andres*, Julia Kapr, Lisa Schmunk, Miguel A. Blázquez, Matias D. Zurbriggen. Mammalian cell-based platform for quantitative reconstruction of plant signaling pathways *In preparation*, May 2021
*equal contribution

Contribution: Design, execution and analysis of all experiments with Jennifer Andres. Preparation of all figures. Participation in planning and writing of the manuscript.

Tim Blomeier*, Patrick Fischbach*, Leonie-Alexa Koch, Jennifer Andres, Miguel Miñambres, Hannes M. Beyer, Matias D. Zurbriggen. Blue Light-Operated CRISPR/Cas13b-Mediated mRNA Knockdown (Lockdown) *Advanced Biology* 2000307, February 2021
*equal contribution

Contribution: Design, execution and analysis of all experiments with Patrick Fischbach. Preparation of all figures. Participation in planning and writing of the manuscript.

Tim Blomeier, Uriel Urquiza-Garcia, Giovanni Giuriani, Matias D. Zurbriggen. UV-B light-inducible system for the transcriptional control of gene expression in *A. thaliana* mesophyll protoplasts *In preparation*, May 2021

Contribution: Design, execution and analysis of all experiments, with the exception of the experiments of Figure 2.14 B and C, which were performed by G. Giuriani und my supervision. Preparation of all figures and writing of the manuscript.

7.1.1 Mammalian cell-based platform for quantitative reconstruction of plant signaling pathways

1 **Mammalian cell-based platform for quantitative** 2 **reconstruction of plant signaling pathways**

3

4 Tim Blomeier^{1,#}, Jennifer Andres^{1,#}, Julia Kapr¹, Lisa Schmunk², Sophia L. Samodelov³,
5 Miguel A. Blázquez⁴, Matias D. Zurbriggen^{1,*}

6

7 ¹Institute of Synthetic Biology, University of Düsseldorf and CEPLAS, Düsseldorf, Germany

8 ²Cardiovascular Strategic Research Initiative, University of Cambridge

9 ³Department of Clinical Pharmacology and Toxicology, University Hospital Zurich, Zurich, Switzerland

10 ⁴Instituto de Biología Molecular y Celular de Plantas (IBMCP), CSIC-Universidad Politécnica de Valencia, Campus UPV CPI
11 8E, Valencia, Spain

12

13 [#]These authors contributed equally to this work

14 ^{*}Corresponding author: Email: matias.zurbriggen@uni-duesseldorf.de

15

16 **ABSTRACT**

17

18 **Plant signaling networks are build out of highly complex and intertwined sequences of**
19 **events for the integration of internal and external stimuli. Since many of the individual**
20 **components possess redundant or overlapping function, their isolated analysis in**
21 **plants, especially in a quantitative fashion, is particularly complicated. Here, the study**
22 **of such signaling events in orthogonal systems, with highly reduced crosstalk to other**
23 **plant specific signaling processes, like yeast or *in vitro* systems, gained interest in the**
24 **last years and helped sharpening the understanding of such processes. Nevertheless,**
25 **especially yeast systems demonstrate some major drawbacks in terms of generation**
26 **of false assumptions. In many cases, mammalian cells mimic the natural cellular**
27 **environment of the monitored processes more closely by providing conserved post-**
28 **translational modifications or co-factors essential for interaction of proteins. Here we**
29 **present the design and characterization of a toolbox of quantitative tools for the**
30 **analysis of plant signaling processes in the orthogonal system of mammalian cells.**
31 **Focusing on the recapitulation of interaction events during the formation of the**
32 **gibberellic acid perception complex and selected downstream signaling events,**
33 **described in previous studies, our platform allowed us optimization of our approaches**
34 **and even expand the knowledge for supporting the future analysis of such processes**
35 **in their endogenous organism.**

36

37

38

39

40

41

42

43 **Introduction**

44

45 Plants as sessile organisms employ phytohormones to constantly adapt their behavior to
46 changing environmental conditions. These phytohormones represent structurally unrelated
47 molecular compounds collectively regulating diverse processes of the plants' life cycle
48 (Santner et al., 2009). Vital growth and developmental movements and mechanisms are i.a.
49 controlled and regulated by diterpenoid phytohormones called gibberellins (GAs) (Yamaguchi
50 and Kamiya, 2000; Ueguchi-Tanaka et al., 2005). Their perception by specific intracellular
51 receptors activates a signal relay leading to changes in gene expression. GA perception and
52 signaling involves three main components: GA receptors, F-Box proteins belonging to a SCF
53 E3 protein ligase complex and GA regulator proteins. In *Arabidopsis thaliana*, all of these
54 components have undergone multiplication events resulting in 3 GA receptors (GA
55 INSENSITIVE DWARF1 (GID1) a, b and c), two F-Box proteins (SLEEPY1 (SLY1) and
56 SNEEZY (SNZ)) and five DELLA regulators of GA response belonging to the GRAS-family of
57 transcriptional regulators in plants (GA-INSENSITIVE,GAI; REPRESSOR-of-ga1-3, RGA;
58 RGA-like1, RGL1; RGL2 and RGL3) (Dill et al., 2004; Murase et al., 2008). GAs are perceived
59 by GID1 leading to a conformational change of the latter which allows their interaction with
60 DELLA regulators. The GA-GID1-DELLA cluster associates to the SCF complex via the F-Box
61 SLY1/SNZ and DELLA becomes polyubiquitinated and consequently degraded by the 26S
62 proteasome resulting in GA downstream signaling responses (Daviere and Achard, 2013).
63 The above-mentioned combinatorial complexity and redundancy of signaling components
64 makes it particularly difficult to analyze GA signaling *in planta*. Already established methods
65 such as knock-out mutant plants, reporter assays, western blots and Yeast-2-Hybrids (as
66 orthogonal systems) unveiled many aspects of GA signaling (Dill et al., 2004; Griffiths et al.,
67 2006). Nevertheless, they display some limitations regarding the roles of individual proteins
68 and interactions thereof as well as kinetic aspects. In order to tackle these obstacles of
69 functional redundancy and interdependence of GA-dependent signaling components,
70 synthetic biology approaches offer a large toolbox of applications from the modification or the
71 recombination of existing genetic elements up to rebuilding of sensitive and complex biological
72 circuits such as signaling pathways in orthogonal systems, isolated from their native context
73 (Lienert et al., 2014). Mammalian cells as a platform for the analysis of plant signaling events
74 mimic the natural cellular environment of such processes more closely, when compared to
75 other *in vivo* systems like yeast or *in vitro* approaches. Parameters like conserved post
76 translational modifications of proteins or the availability of cofactors, essential for interaction

77 of the analyzed components, reduces the likelihood of observing wrongly drawn conclusions
78 (Fiebitz et al., 2008; Hou et al., 2011; Beyer et al., 2015). Further, the availability of
79 quantitatively described building-blocks enables the implementation of mathematical
80 modeling. This allows successive standardization of newly discovered components or their
81 expression levels (Endy, 2005; Mutalik et al., 2013). In recent years, a plurality of approaches
82 for the heterologous, orthogonal reconstruction and analysis of complex plant signaling
83 pathways in a simplified, optimized mammalian environment have been generated (Wend et
84 al., 2013; Beyer et al., 2015; Abbas et al., 2018; Blanco-Touriñán et al., 2020; Gratz et al.,
85 2020), illustrating their importance. This platform allows the step-by-step-analysis of isolated
86 components in initial studies, but further in facilitating the sharpening of today 's knowledge of
87 plant signaling pathways as a whole and even provides the availability of independent
88 methods for verifying the generated hypothesis.

89 In this study, we aimed on the development and characterization of a toolbox of (quantitative)
90 approaches for the quantitative reconstruction of plant signaling events in our platform of
91 mammalian cells. While we analyzed the transactivation ability of transcription factors with a
92 mammalian-1-hybrid (M1H) approach, the influence of additional transcription factors on these
93 processes was observed. In addition, we established M2H up to M4H approaches and
94 microscopy-based FRET techniques for the quantification of protein-protein interactions
95 (PPIs) and the investigation on the order of interaction events during the formation of
96 complexes of more than two proteins. In order to have a centralized objective for the
97 establishment of the mentioned approaches, we focused our efforts on the analysis of PPIs
98 and selected downstream signaling events connected to the GA perception induced signal
99 transduction.

100

101 **Results**

102

103 **Mammalian-1-hybrid (M1H) approach for the analysis of the transactivation ability of** 104 **transcription factors**

105 DELLAs are transcriptional regulators and hubs for integration of different signaling pathways
106 of plant development and stress-responses (Locascio et al., 2013; Marín-de la Rosa et al.,
107 2014). Nevertheless, they lack the typical DNA binding domains. Their influence on
108 transcriptional regulation therefore is mainly mediated by influencing other transcription factors
109 (e.g. PIFs) (Davière et al., 2008; Feng et al., 2008; de Lucas et al., 2008; Schwechheimer,
110 2012; Locascio et al., 2013). As a proof of principle for recapitulating the transcriptional
111 regulation of a plant derived transcription factor in our mammalian platform, related to GA-
112 dependent signaling processes, we have chosen the transactivation ability of the transcription

113 factor ARABIDOPSIS RESPONSE REGULATOR1 (ARR1). While its binding to synthetic cis-
114 element sequences containing B-type ARR-binding motifs (TCS target element) on DNA was
115 shown (Müller and Sheen, 2008), Y2H and ChIP approaches indicated the promotion of
116 DELLAs on transcriptional activation of ARR1 to the mentioned DNA-element (Marín-de la
117 Rosa et al., 2015). In plants, ARR1 is usually activated through cytokinin-dependent
118 phosphorylation. For functionality in mammalian cells, the ARR1 Δ DDK mutant (lacking the
119 CK-responsive DDK domain) was used, which showed increased activity in the absence of
120 CKs (Sakai et al., 2000).

121 ARR1 was co-transfected with the TCS element, incorporated into a reporter gene construct,
122 upstream of a minimal version of the human cytomegalovirus promoter ($P_{hCMVmin}$). Single
123 transfection of the reporter acted as negative control to exclude interference with
124 transcriptional regulators endogenous to the human cells. Upon binding of the transcriptional
125 activator to the respective element, transcription of the human secreted alkaline phosphatase
126 (SEAP) is initiated. For identifying transcriptional regulators which are able to bind to the
127 specific motifs but lacking the capability of transcriptional activation, fusion of the VP16
128 transactivation-domain was additionally performed. Analyzing the influence of DELLA proteins
129 on transcriptional activation capability of ARR1, the DELLA proteins RGA and GAI were co-
130 transfected (Figure 1 A). 24 hours after transfection, the determination of the SEAP production
131 was quantitatively analyzed by a previously described colorimetric assay (Müller et al., 2014a;
132 Beyer et al., 2015). In the first set-up with the objective of the transactivation ability of ARR1
133 to the synthetic TCS element (M1H), no autoactivation of the reporter construct was identified,
134 while the co-expression of ARR1 induced a significant increase in expression of the SEAP
135 reporter of about 26 U/L. Co-expression of the DELLA proteins RGA or GAI and ARR1 (M1H⁺)
136 led to another significant gain of SEAP expression between 35 and 40 U/L, while the fusion of
137 VP16 to both DELLAs did not further increase the gene expression. Moreover, the VP16-fused
138 ARR1 led to comparable results as with the non-fused variant, but with slightly higher SEAP
139 values in case of co-transfection of the DELLA proteins of around 40-45 U/L for the four
140 combinations (Figure 1 B). The performed experiments highlight the applicability of the
141 orthogonal platform of mammalian cells for investigation on transcriptional activation of plant
142 transcription factors (M1H) and further the influence of additional proteins on their behavior in
143 a crosstalk-reduced environment (M1H⁺).

144 145 **Mammalian-x-hybrid (MxH) assays analyzing gibberellic acid-induced DELLA-GID-** 146 **interactions**

147 In order to analyze the existence and order of protein interactions during GA perception in the
148 orthogonal system of mammalian cells, we adapted and optimized a previously described
149 macrolide repressor-based split transcription factor system (Müller et al., 2013) for the analysis

150 of GA-induced interactions. In brief, one transcription factor is fused to a transactivation
151 domain (VP16), while the possible interaction partner is bound to the DNA-binding macrolide
152 repressor protein (E). E binds to a specific DNA-motif (erythromycin resistance operator; etr_8)
153 adjacent to a minimal human cytomegalovirus immediate early promoter ($P_{hCMVmin}$), controlling
154 expression of the SEAP (human secreted alkaline phosphatase) reporter gene. Lacking
155 transactivation ability, the E-fused protein is recruited to the etr_8 motif in the reporter plasmid
156 without activating gene expression. Only in case of protein-protein-interaction (PPI) the
157 transactivation-domain VP16, fused to the interaction partner, recruits the transcriptional
158 machinery to promote expression of SEAP. This approach allows the fast and quantitative
159 analysis of the respective interactions.

160 At first, bicistronic vectors containing one of the DELLA proteins RGA or GAI, and the GA-
161 receptors GID1a, b or c, separated by a polioviral internal ribosome entry site ($IRES_{PV}$) to
162 create two independent initiation points of translation, were cloned. While the DELLA proteins
163 were C-terminally fused to the VP16-transactivation domain, the macrolide repressor (E
164 protein) was N-terminally fused to either GID1a, b or c (Figure 2 A). In order to eliminate false
165 negative results, caused by either N- or C-terminal fusion of the natural proteins, the positions
166 of the DELLA and GID1 proteins were inverted (Figure 2 B). HEK-293T-cells were transfected
167 with a combination of reporter- and the bicistronic split-transcription factor construct. Single
168 transfection of the reporter acted as negative control for endogenous activation of SEAP
169 production, while a fusion of E and VP16 was used as positive control for cellular fitness in the
170 different conditions. Previous studies identified the gibberellin analog GA_3 -AM as being able
171 to diffuse into mammalian cells, where it is cleaved by esterases, releasing a functional GA_3 .
172 At a concentration of 10 μ M it was sufficient to induce an interaction between a GID1-receptor
173 protein and a truncated version of GAI (Miyamoto et al., 2012). Therefore, GA_3 -AM at this
174 concentration was used in this study.

175 In a first experiment, the mentioned two orientations of protein fusion were compared: 24 h
176 after transfection the cell medium was exchanged, containing either 0.5 μ l of a 10 μ M solution
177 of GA_3 -AM or 0.5 μ l of DMSO, per well. Another 24 hours later, 200 μ l of the supernatant was
178 transferred to a 96-well plate and incubated at 60°C for one hour, before the SEAP production
179 was measured in a micro plate-reader. SEAP production of both orientations of all six
180 combinations were compared to each other (Figure 2 C and D). Pairs of DELLA-VP16 and E-
181 GID1 (Figure 2 C) revealed a GA-dependent induction in SEAP production of more than 50
182 U/L for all combinations, with a higher level in combination with GAI, respectively. Both DELLA
183 combinations with GID1a possessed the highest production of the reporter protein. Reversed
184 orientations of protein-fusion indicated a much weaker SEAP production of less than 50 U/L,
185 with comparable induction among the three GID1 combinations with the respective DELLAs.
186 As for the inverted protein fusions, combinations with GAI possessed higher SEAP values of

187 around 40 U/L, compared to 10-20 U/L for the combinations with RGA (Figure 2 D). Although
188 we successfully demonstrated GA-dependent interactions of the DELLAs and GID1s for both
189 variants of protein fusion, our results highlight the importance for validation of construct
190 functionality. Since the E-GID1/DELLA-VP16 generated a much stronger induction of GA-
191 dependent SEAP production, we continued with these constructs in the following experiments.

192

193 **Mammalian-3- and 4-hybrid assays for the investigation on the order of complex-**
194 **formation during GA-perception**

195 Although previous studies revealed that the SCF^{Sly1} complex targets DELLA proteins for
196 degradation in the presence of GA (Dill et al., 2004; Fu et al., 2004), only a study performed
197 in yeast revealed a direct recognition of the GA-GID1-DELLA complex by the F-box protein
198 SLY1 in yeast three-hybrid assays (Griffiths et al., 2006). To address this question,
199 mammalian 3- and 4-hybrid assays were performed. In order to have combinations of all
200 components of the GA-perception mechanism tested, the interaction assays were expanded
201 to analyze the interaction of the F-Box Protein SLY1, responsible for recruitment of the SCF
202 degradation complex. Thus, combinations of E-SLY1 and DELLA-VP16, as well as E-GID1
203 and SLY1-VP16, and vice versa, were tested (Figure S1 and Figure S2). In all assays, no
204 increase in SEAP production was monitored. Neither in the DMSO-supplemented control, nor
205 in the GA₃-AM-condition.

206 Lastly, the interplay of all three different protein-families was tested in mammalian-4-hybrid
207 assays. The already existing bicistronic vectors of all possible interaction partner combinations
208 were transfected and SEAP production in the presence and absence of GA₃-AM was
209 quantified subsequently. Other than in the previous experiments, nuclear localized variants of
210 the missing third component, without being fused to E or VP16, was co-transfected to analyze
211 its influence on the SEAP production (illustrated in Figure 3 A, B and C). With small variations,
212 the combinations of DELLA-VP16 and E-GID1 showed the same pattern of GA₃-AM induced
213 SEAP production as described in the previous experiments. All combinations indicated a GA-
214 dependent increase in SEAP production, with a highest measured SEAP-level in case of
215 GID1a, respectively. The additive transfection of SLY led to no further increase in SEAP-
216 activity of all measured protein combinations (Figure 3 E). In the presence of GA₃-AM, co-
217 transfection with either GAI or RGA boosted the SEAP production of the E-GID1/SLY1-VP16
218 split transcription factor construct level in all six cases. Again, the combinations featuring
219 GID1a indicate the strongest level of reporter production, while co-transfection of GAI induced
220 a stronger SEAP expression than addition of RGA in case of all three different GA-receptor
221 variants (Figure 3 D). Supplementation of the three GID1s did not lead to any elevation of
222 SEAP-activity of the E-DELLA/SLY1-VP16-constructs in all cases (Figure 3 F).

223 In summary, our observations support the previously indicated order of events during the
224 formation of the GA-perception complex analyzed in yeast (Griffiths et al., 2006). The GA-
225 dependent interaction of the GID1s and DELLAs increases the affinity of the GA-GID1-DELLA
226 complex for SLY1, initiating the interaction with the F-Box protein. We not only expanded this
227 observation to the interaction of the two DELLA proteins GAI and RGA, in combination with
228 the three known GA-receptors of *A.thaliana*, but furthermore observed the mentioned
229 complex-formation for only one of the studied orientations of proteins in our mammalian-hybrid
230 system. These results might give insights on the structure and stability of the complex.

231

232 **Gibberellic acid induced co-localization of GAI and GID1b**

233 In order to be able to visualize possible GA-dependent translocation of co-transfected DELLA
234 and GID1 proteins in isolation from other plant signaling components, the DELLA protein GAI
235 was fused to the fluorescent protein mCherry and was expressed under the control of the
236 constitutive mammalian cell compatible SV40 promoter. In a similar design, the GA-receptor
237 GID1a, b and c were fused to the fluorescent protein EGFP, allowing combined observation
238 of the different emission wavelengths by confocal fluorescence microscopy. Since both,
239 fluorescently tagged GAI and the three GID1s were ubiquitously expressed all over the
240 mammalian cells (data not shown), we artificially created the nuclear localization of mCherry-
241 GAI by fusing it to a nuclear localization sequence (NLS). Creating spatially distinct expression
242 patterns, this configuration enabled the possibility of observing possible translocation events
243 (Figure 4 A). Mammalian cells were transfected with both, a GAI and a GID1-containing
244 plasmid. After 24 hours, supplementation of GA₃-AM was performed. Four hours after
245 treatment, fixation and mounting of the cells led to the possibility of observing the intracellular
246 localization of the fluorescently-tagged proteins under different conditions, to monitor possible
247 interaction events and their hormone dependency. Additional to GA₃-AM-treated cells,
248 localization behavior was observed in the absence of the hormone, using DMSO as a control
249 condition, since it served as hormone-solvent.

250 The fusion of the localization-tag successfully generated the expected localization of mCherry-
251 GAI proteins in the nucleus (Figure 4 B-D). In all combinations of co-transfection of mCherry-
252 GAI and EGFP-GID1, no translocation of any of the GID1s was monitored in the DMSO-
253 controls. All GID1 proteins were evenly distributed throughout the respective cells. However,
254 upon supplementation of GA₃-AM the main part of the EGFP-GID1b fusion protein was
255 recruited to the nucleus (Figure 4 C). In case of co-transfection with EGFP-GID1a, a stronger
256 nuclear signal was monitored (Figure 4 B), while the detected EGFP-GID1c did not change its
257 distribution, compared to the DMSO-control condition (Figure 4 D).

258

259

260
261 **Improvement and characterization of GA-induced interactions between GAI and GID1b**
262 **with FRET- acceptor photo bleaching (FRET-APB) experiments**

263 To expand the value of microscopical approaches to a quantitative level, FRET-based
264 techniques are effective resources for quantification of dynamic protein-protein interactions
265 (PPIs) *in vivo* (Weidtkamp-Peters and Stahl, 2017). All FRET-based approaches depend on
266 the physical effect of energy transfer from an excited donor-fluorophore, to a second, energy
267 accepting fluorophore (acceptor) by dipole-dipole coupling. Requirements for this energy-
268 transfer are the overlapping emission spectrum of the donor with the excitation spectrum of
269 the acceptor, spatial proximity of only a few nanometers and an optimal angle between the
270 dipolar moments of both fluorophores (Förster, 1948; illustrated in Figure 6 A).

271 FRET-APB experiments were performed using fixed cells of the previously described
272 experimental set-up with combination of different GAI-mCherry- and GID1b-EGFP-fusion
273 proteins, in order to optimize the reliability and time-consumption of the experimental set-up.
274 All with the superior aim of finding the construct-combination with the highest dynamic range
275 between control and GA₃-AM-induced FRET efficiency. Subsequently, this strategy will be
276 expanded to the other GAI-GID1 combinations. Additionally, a GID1b-EGFP-mCherry fusion
277 protein was constructed, from now on serving as FRET-positive control, enabling the tracking
278 of the influence of phytohormone on the general FRET efficiency, while guaranteeing the
279 comparability and reproducibility of independent experiments. In all performed experiments,
280 its FRET efficiency reached a level of around 20 percent. An experimental set-up, consisting
281 out of 30 seconds of recording fluorescence intensity previously and subsequently to a two
282 seconds lasting step of acceptor-bleaching, reduced the acquisition bleaching of the
283 fluorophores and allowed observation of constant fluorescence-intensity of the respective
284 fluorescent proteins (illustrated in Figure 5). As many independent factors, like fluorophore
285 proximity or angles, but also the different environments in the artificially induced protein
286 localizations, have an influence on the FRET efficiency, different constructs were designed
287 and constructed for comparison of their FRET-APB based interaction affinities. Here, not only
288 localization-tags, but C- and N-terminal fusion of the fluorescent proteins and varying linker-
289 length, influencing the proximity and flexibility of the components within the constructs, were
290 tested (Figure 6).

291 The very first experiment was conducted using different localization strategies of the GAI
292 construct. Therefore, the NLS-tag was removed or exchanged by either a nuclear exclusion
293 signal (NES) or prenylation tag (CAAX), recruiting the fused protein to the plasma membrane
294 (Figure 6 B). Overall, all GAI-GID1b combinations indicated a higher FRET efficiency in the
295 presence of GA₃-AM, compared to the DMSO control condition. The cells expressing the non-
296 tagged mCherry-GAI generated a FRET efficiency of 4.5 percent after GA₃-AM treatment and

297 1.5 percent after DMSO supplementation, while all tested localization strategies lifted the
298 dynamic range between GA-induced FRET and the DMSO-control condition. Here, the
299 prenylated and the nuclear mCherry-GAI fusions showed an even higher FRET efficiency of
300 7.1 percent (CAAX) and 7.3 percent (NLS), while the associated DMSO-controls displayed
301 comparable efficiencies of around 3 percent. Altogether, the combination of NLS as well as
302 the CAAX fused GAI, in combination with GID1b, generated the highest FRET efficiency in
303 presence of GA₃-AM with the biggest dynamic range between hormone treated and non-
304 treated conditions. If compared to each other, the choice of NLS-fusion distributes
305 independence of highly overexpressed areas at the plasma membrane for execution of FRET-
306 APB measurements, as well as the benefit of accelerated measurements. Here, the rounded
307 shape of the nuclei facilitated the possibility of bleaching a multiplicity of cells without the need
308 of rotating the measurement area until the plasma membrane reaches the designated position
309 for bleaching.

310 Since the previous experiment indicated the nuclear localized GAI-mCherry to induce the
311 highest FRET efficiency, GID1b-constructs with N- or C-terminal mEGFP-fusions connected
312 by a two amino acid linker, in combination with a nuclear localized N- or C-terminal nine amino
313 acid linker fusion of GAI and mCherry were tested to reveal the most beneficially orientation
314 of the components within the constructs. Here, the combination of both proteins with N-
315 terminal fusion of the respective fluorescent proteins, reached the highest FRET efficiency
316 after supplementation of GA₃-AM, as well as the biggest difference between hormone treated
317 and non-treated cells (Figure 6 C). Further, a decrease in length of the linker between GAI
318 and mCherry decreased the FRET efficiency from around 9.5 percent for 9 amino acids to
319 around 6.5 percent for both shorter variants of seven and five amino acids (Figure 6 D). Lastly,
320 the fluorophores fused to GAI and GID1b were exchanged, respectively. The variant of
321 mCherry-2aa-GID1b and NLS-EGFP-9aa-GAI reached a FRET efficiency of around 6.8
322 percent after GA₃-AM supplementation. Contrary, the previously described combination
323 possessed a stronger FRET-level of 8.8 percent in presence of GA₃-AM (Figure 6 E). Here,
324 the higher FRET efficiency of the mCherry-GAI and EGFP-GAI co-transfection led to the
325 decision of ultimately selecting this combination for the subsequent characterization and
326 transfer to the two other GA-receptors GID1a and c.

327 While in all previously described experiments, an incubation time of four hours with GA₃-AM
328 at a concentration of 10 mM was performed, the following experiments revealed the kinetics
329 and dose response of the FRET efficiency between the beforehand described protein
330 constructs (Figure 7). During the interval of 240 min of induction, the FRET efficiency did not
331 increase in the DMSO control condition and remained slightly below 3 percent. While GA₃-AM
332 treatment immediately increased the FRET efficiency to 4.5 percent, it rose to 7.5 percent after
333 30 minutes. From now on, the level further climbed with a smaller slope and reached the

334 highest level of about 9.2 percent after 240 min of hormone induction (Figure 7 A). Longer
335 time intervals were not measured. The dose response experiment revealed that already a
336 concentration of 1 nM of GA₃-AM was sufficient for an increase in FRET efficiency to around
337 8 percent. Higher concentrations of 10 nM kept the FRET efficiency on a comparable level,
338 while 10000 nM slightly further increased the level to about 9 percent (Figure 7 B).
339 Summarized, even shorter induction times and lower hormone concentrations induced the
340 interaction between GAI and GID1b in this approach, but the previously applied four hours of
341 induction at a concentration of 10 nM GA₃-AM led to the overall strongest measured FRET
342 efficiency throughout the performed study.

343

344 **FRET-4-hybrid approach for study of the order of protein interactions during GA** 345 **perception complex formation**

346 After the interaction between GAI and GID1b was extensively studied, the next step was to
347 add the third component to the FRET-APB approaches. Therefore, the F-box protein SLY1
348 was fluorescently tagged with either mCherry or EGFP to enable the FRET-APB measurement
349 in combination with the previously characterized GAI and GID1b constructs. In addition, a
350 nuclear localized, non-fluorescent variant of the third component was co-transfected,
351 respectively (Figure S3). While the combinations with fluorescently tagged SLY1 all possessed
352 a FRET efficiency below four percent, in presence or absence of GA₃-AM, co-transfection of
353 either GID1b-NLS or GAI-NLS did not increase the FRET level. Further, co-transfection of
354 SLY1-NLS did not increase the FRET efficiency of EGFP-2aa-GID1b and NLS-mCherry-9aa-
355 GAI in the performed study. Without SLY1-NLS, GA₃-AM treatment boosted the efficiency to
356 7.8 percent, while addition of the F-box protein resulted in a FRET level of 6.7 percent. In
357 conclusion, no direct interaction SLY1 with either GAI or GID1b could be measured with the
358 performed FRET-ABP analysis and co-transfection of SLY1-NLS did not further increase the
359 FRET efficiency of GAI and GID1b.

360

361 **FRET- acceptor photo bleaching (FRET-APB) and FRET – fluorescence lifetime imaging** 362 **microscopy (FLIM) approaches identify GA-dependent interactions between GAI and** 363 **GID1a, b and c**

364 Finally, the construct design of EGFP-2aa-GID1b was transferred to the two other GID1s.
365 Since all three sensors are highly similar in sequence, a comparable mode of interaction with
366 GAI was considered. Additionally, a nuclear localized EGFP was constructed for excluding
367 wrongly measured interactions caused by protein overexpression in the area of the cellular
368 nucleus. At first, possible interactions were analyzed with the already established FRET-APB
369 approach (Figure 8 A). While the donor-only control showed no FRET signal, the combination
370 of NLS-EGFP and the GAI-construct possessed a slightly higher level of around two percent

371 in both conditions. In all three GID1-GAI combinations, GA₃-AM supplementation significantly
372 increased the FRET efficiency with the highest measured value of 8.5 percent for the co-
373 transfection of GID1b.

374 In order to revise the results from the FRET-APB measurements, highly sensitive FRET-
375 fluorescence lifetime imaging microscopy (FLIM) measurements were mostly performed in the
376 same experimental set-up with the only difference of use living cells, without fixation.
377 Combinations of mEGFP-GID1a, b and c with NLS-mCherry-GAI constructs were tested on
378 potential fluorescence lifetime reduction of the EGFP-donor, with or without supplementation
379 of GA₃-AM. As before, single transfection of the mEGFP-GID1b donor and the fusion protein
380 of GID1b-mEGFP acted as negative and positive control in this assay (Figure 8 B; Table S1).
381 In the single transfection set-up, GID1b fused to mEGFP indicated a fluorescence lifetime of
382 around 2.49 ns after DMSO supplementation and 2.48 ns in the presence of GA₃-AM, while
383 the GID1b-mEGFP-mCherry fusion possessed an average lifetime of about 2.13 ns in the
384 DMSO supplemented cells and 2.10 ns in GA-treated counterparts. These two lifetimes
385 indicate the range from no FRET effect (donor only) to fusion of both fluorophores. Therefore,
386 both controls are marking the borders of the measurable lifetime decrease of these proteins
387 in this approach. Overall, these numbers indicate an influence of GA₃-AM on fluorescence
388 lifetime of 10-30 picoseconds. Combination of all three GID1s with NLS-mCherry-GAI led to
389 comparable fluorescence lifetimes of the donor at 2.48 ns for GID1a, 2.47 ns for GID1b and
390 2.46 ns for GID1c in the DMSO control condition. While the decrease in lifetime of the EGFP-
391 fused GID1a only slightly exceeded the measured drop caused by GA₃-AM, with a decrease
392 of 40 ps after GA₃-AM supplementation, combination with GID1c led to a decrease in lifetime
393 of 70 ps. In case of GID1b, even a decrease of 130 ps was measured (Figure 8 B, Table S1).
394 Both applied strategies of measuring the PPI of the three GID1s and the DELLA protein GAI
395 successfully revealed a GA₃-AM dependent interaction of both, supporting our data obtained
396 with the mammalian-hybrid approaches.

397

398 Discussion

399 In this study, we introduce a toolbox of synthetic biological tools for the quantitative analysis
400 of plant signaling processes in an orthogonal mammalian cell system. Moreover, combinatorial
401 application of the established mammalian-hybrid- and microscopy-approaches avoid a one-
402 sided view on the pathway of interest by relying on a single experimental approach.

403 M1H to M4H approaches robustly reveal possible PPI or Protein-DNA-interactions, with almost
404 no leakiness in the absence of either the activating transcription factor (M1H) or the interaction
405 inducing hormone (M3H). Further, the supplementation of additional factors was sufficient to
406 increase the activation capacity of a transcription factor in the M1H⁺ approaches, or even
407 mediated the interaction of the two parts of the split transcription factor system (M4H).

408 They highly underline the capability of this platform for recapitulating, supporting or even
409 extend the knowledge generated by previous *in vitro*, in yeast or *in vivo* studies in plants,
410 dealing with GA-affinities of the three gibberellin-receptor protein GID1a, b and c or the GA-
411 dependency of their interaction with the negatively influencing downstream regulators of the
412 DELLA family (Griffiths et al., 2006; Nakajima et al., 2006; Suzuki et al., 2009). This study
413 expands the investigation of the formation of the GA-perception complex, previously analyzed
414 in yeast (Griffiths et al., 2006), to all three GID1s and the two DELLA proteins RGA and GAI
415 and indicates the recruitment of SLY1 to the respective DELLA protein, after previous GID1-
416 DELLA complex formation upon GA-perception by the GID1 receptors. If this hypothesis is
417 true, it could explain SEAP-induction in case of co-expression of the DELLAs as no part of the
418 split transcription-factor (Figure 3 D), since this protein complex might guarantee a more
419 beneficial orientation or smaller proximity of the transactivation domain to the minimal
420 promoter in the M4H assays. However, a reason for the absence of SEAP-expression in case
421 of supplemental GID1 expression (Figure 3 F) could be the low stability of the complex in this
422 composition. Taken together, we have developed and established a range of powerful
423 mammalian-hybrid approaches for screening of protein-DNA or protein-protein interactions,
424 allowing extensive and fast studies of plant signaling networks in a quantitative manner.
425 The microscopy approaches not only allowed to analyze protein (co)localization, but moreover
426 enabled the quantitative study of interaction affinities with different approaches and added
427 knowledge to the attempt of deciphering the structure of a GA-GID1-DELLA-SLY1-complex.
428 Our FRET-based approaches not only supported the identification of GA-dependent
429 interactions between GAI and GIDa-c (Figure 8), but allowed the detailed analysis of the
430 interaction of GAI and GID1b, with induction at a hormone concentration of down to 1 nM
431 GA₃-AM (Figure 7 A). The much faster mammalian-hybrid approaches could be used for a first
432 screening of possible interaction partners, while transfer of detected interactors to microscopy
433 analyses might help deepen the understanding of the possible interactions by revealing protein
434 localizations and provide an independent second method for verifying PPIs in a highly
435 sensitive manner.
436 Our mammalian cell platform offers a versatile toolbox for quantitatively characterization of
437 plant signaling networks from analyzing simple PPIs to the order of complex-formation, to
438 mobility of single proteins or complexes (e.g. by combination with other approaches like
439 anisotropy or FRAP (fluorescence recovery after photobleaching) measurements in future
440 experiments. Taken together, our toolbox of quantitative approaches, could strongly support
441 the analysis of such processes in the originated plant system by providing a crosstalk-reduced
442 platform which mimics the natural cellular environment of the monitored plant-originated
443 processes more closely than yeast or *in vitro* systems.
444

445 **Materials and Methods:**

446

447 **Mammalian cell culture**

448 Human embryonic kidney cells (HEK-293T; DSMZ, Braunschweig, Germany) were cultivated
449 in Dulbecco's modified Eagle's medium (DMEM, PAN Biotech, cat. no. P04-03550)
450 supplemented with 10% (v/v) tetracycline-free fetal bovine serum (FBS; PAN Biotech; cat. no.
451 P30-3602; batch no. P080317TC) and 1.4% (v/v) penicillin/streptomycin (PAN Biotech; cat.
452 no. P06-07100).

453

454 **Hormones/Substrates/Chemicals**

455 The GA Gibberellic Acid Acetoxymethyl Ester (GA₃-AM) was purchased from Santa Cruz
456 Biotech.

457

458 **PEI transfection, hormone-induction and SEAP assays**

459 For Mammalian-Hybrid experiments, 50,000 HEK-293T cells were seeded in 500 µl DMEM
460 cell culture medium in 24-well cell culture dishes (Corning). Human embryonic kidney cells
461 (HEK-293T; DSMZ, Braunschweig, Germany) were cultivated in Dulbecco's modified Eagle's
462 medium (DMEM, PAN Biotech, cat. no. P04-03550) supplemented with 10% (v/v) tetracycline-
463 free fetal bovine serum (FBS; PAN Biotech; cat. no. P30-3602; batch no. P080317TC) and
464 1.4% (v/v) penicillin/streptomycin (PAN Biotech; cat. no. P06-07100).

465 The cells were transfected 24h post seeding as described before (Müller et al., 2013). Briefly,
466 0.75 µg DNA per well were diluted in 50 µL OptiMEM (Invitrogen, Thermo Fisher Scientific)
467 and mixed with a PEI/OptiMEM mix [2.5 µL PEI solution (1 mg/ml, Polysciences Europe GmbH
468 cat. no. 23966-1) in 50 µL OptiMEM]. After 15 min incubation at RT, 100 µl of the transfection
469 mixes were added to each well in a dropwise manner. The medium was exchanged 4 h post
470 transfection. Another 20 h later, the medium was exchanged with either GA₃-AM or DMSO
471 containing DMEM cell culture medium (10 µM GA₃-AM and 1/1000 DMSO). The reporter
472 SEAP was quantified using a colorimetric assay as described elsewhere (Müller et al., 2014b)

473

474 **Confocal Microscopy and FRET-APB measurements**

475 For confocal imaging, 50,000 mammalian HEK-293T cells in a density of 50,000 cells were
476 seeded onto glass cover slides and placed in 24- well cell culture dishes.

477 24 h after seeding, cells were transfected with the indicated plasmids. Another 24 h later, the
478 medium was exchanged, with either GA₃-AM or DMSO-containing DMEM (10µM of GA₃-AM
479 or 1/1000 of DMSO if not described differently). After incubation of 4 h (if not described
480 differently), the growing medium was removed and replaced by 4% Paraformaldehyde, while
481 the cell culture dish was put on ice for 10 min. After being incubated another 10 min at room

482 temperature, the PFA was removed and cells were washed with 500 μ L of 1 x PBS. The
483 coverslips were embedded in 8 μ L of Mowiol 4-88 (Roth) supplemented with 15 mg mL⁻¹ 1,4-
484 diazabicyclo[2.2.2]octane (DABCO, Roth) to be mounted onto microscope slides (as
485 described by Beyer et al., 2015; Blanco-Touriñán et al., 2020). In order to accelerate drying,
486 the microscope slides were incubated at 37°C for 30 min. The confocal imaging was performed
487 using a Nikon Instruments Eclipse Ti with a C2plus confocal laser scanner, 60Å oil objective,
488 NA = 1.40). While EGFP-fluorescence was excited with a diode laser of 488 nm and detected
489 between 505 and 545 nm, while the mCherry signal was excited with a laser of 561 nm and
490 detected between 570 and 620 nm.

491 FRET-APB measurements were operated with the NIS elements software (Nikon) using a
492 laser power of 0.1 % of the 488 nm laser and 0.5% for the 561 nm laser to avoid acquisition
493 bleaching of the fluorophores before bleaching. The frame size was kept at 512 x 512 pixels.
494 After 30 seconds of acquisition the mCherry signal was bleached in a region of interest (ROI)
495 with the 561 nm laser at a laser intensity of 100%. Subsequent to bleaching, the fluorescence
496 intensity of both signals was recorded for another 30 seconds. The FRET efficiency was
497 calculated by analyzing the percentage of relative changes in EGFP intensity before and after
498 bleaching: $EFRET = ((EGFP_{after} - EGFP_{before}) / (EGFP_{after})) * 100$. For each condition, 10 cells
499 were analyzed and the average EFRET was calculated.

500

501 **FRET-FLIM measurements**

502 For FRET-FLIM measurement, 100,000 HEK-293T cells were seeded into chambered 4-well
503 glass bottom dishes (Sarstedt). While the transfection was performed in the same way as
504 described before, here, living cells were imaged. They were covered with a live-cell imaging
505 solution (Thermo fisher) supplemented with either 10 μ M of GA₃-AM or 1/1000 of DMSO, 24 h
506 after transfection. After 4 hours of incubation with the hormone or DMSO containing solution,
507 FRET-FLIM was performed using a LSM 780 confocal laser-scanning microscope equipped
508 with a single-photon counting device (PicoQuant Hydra Harp 400). The EGFP signal was
509 excited at a wavelength of 485 nm using a linearly polarized pulsed laser (pulse rate: 32 MHz;
510 laser: LDH-D-C-485, PicoQuant). Before measurement, the pinhole was set to 1 airy unit (AU)
511 and the excitation power was adjusted to 1 μ W using the C-Apochromat objective (40x/1.2 W
512 Corr M27). The emission was detected with a by Tau-SPAD detectors (PicoQuant) with a
513 band-pass filter (520/35, AHF)). Fluorescence of mCherry was excited at 561 nm using a
514 continuous wave with the laser power set to 0,1%, while the emission was detected at with a
515 band pass filter between 572 and 642 nm (HC 607/70, AHF).

516 For image acquisition a resolution of 256 x 256 pixel with a zoom factor of 4 and 12.61 μ s of
517 pixel dwell time was chosen. For each measurement a series of 80 frames was taken and
518 further analyzed using SymphoTime64 (PicoQuant). For every measurement, only pixels with

519 a minimum of 100 photons per pixel were included and fitted with a bi-exponential decay
520 function model, incorporating the instrument response function and background contribution,
521 enabling the calculation of the fluorescence lifetime.

522

523 **Data analysis**

524 The data was, unless otherwise specified, analyzed using Microsoft Excel (Version 16.26 for
525 Mac Os X) and GraphPad Prism 7 for Mac Os X version 10.13.1. Ordinary one-way ANOVAs
526 and student's t-tests for determination of statistical significance were performed with
527 GraphPad Prism 7 for Mac Os X version 10.13.1. Statistical outliers were determined and
528 excluded as described elsewhere (Jacobs and Dinman, 2004).

529

530 **SUPPLEMENTARY INFORMATION**

531

532 Supplementary information are available on request.

533

534 **ACKNOWLEDGEMENTS**

535

536 The authors thank R. Wurm, M. Gerads and S. Kuschel for valuable technical assistance;
537 Leonie-Alexa Koch and Patrick Fischbach for helpful comments on the manuscript. This work
538 was supported in part by the Deutsche Forschungsgemeinschaft (DFG, German Research
539 Foundation) under Germany's Excellence Strategies CEPLAS – EXC-1028 project no.
540 194465578 and EXC-2048/1 – Project no. 390686111, the iGRAD Plant (IRTG 1525), Grant
541 ZU259/2-1, and the Collaborative Research Center SFB1208 (project no. 267205415) to MDZ;
542 the European Commission – Research Executive Agency (H2020 Future and Emerging
543 Technologies FET-Open project no. 801041 CyGenTig to MDZ; and the Human Frontiers
544 Scientific Program Project no. RGY0063 to MDZ. TB was supported for this research through
545 the International Max Planck Research School (IMPRS) on Understanding Complex Plant
546 Traits using Computational and Evolutionary Approaches at the Max Planck Institute for Plant
547 Breeding Research and the Universities of Düsseldorf and Cologne.

548

549 **COMPETING OF INTERESTS**

550

551 The authors declare no conflict of interest.

552

553

554 **AUTHOR CONTRIBUTION**

555

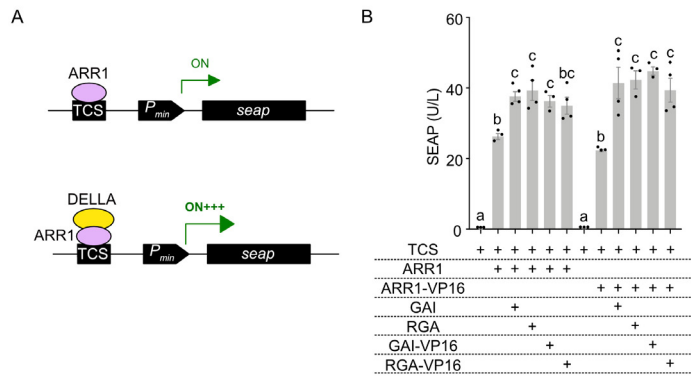
556 TB and JA designed and performed the experiments, analyzed the data and wrote the
557 manuscript. JK and LS designed constructs and performed preliminary experiments. MAB
558 and MDZ designed the experiments, analyzed the data and wrote the manuscript.

559 **References**

560

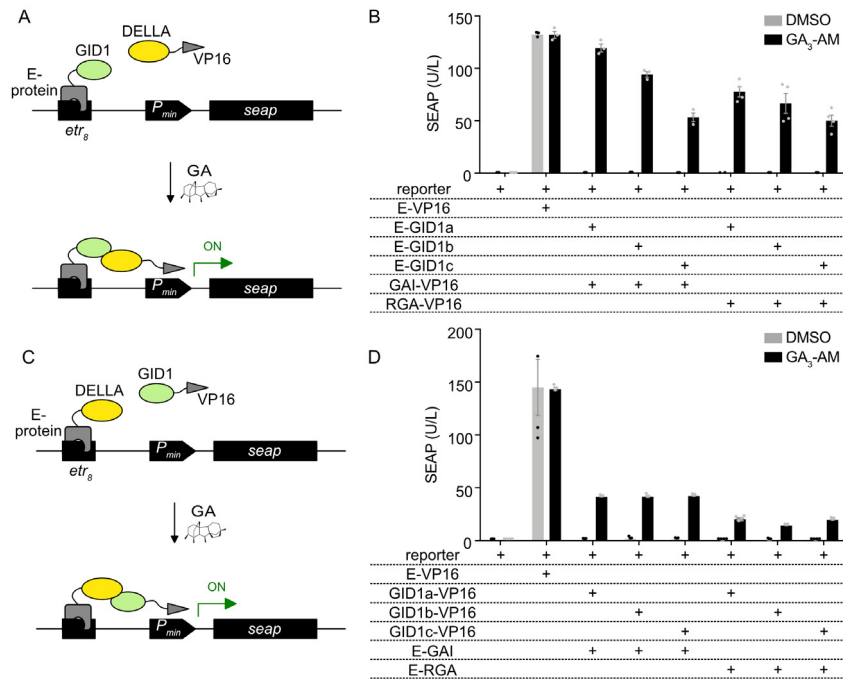
- 561 **Abbas M, Hernández-García J, Pollmann S, Samodelov SL, Kolb M, Friml J, Hammes**
562 **UZ, Zurbriggen MD, Blázquez MA, Alabadí D** (2018) Auxin methylation is required
563 for differential growth in Arabidopsis. *Proc Natl Acad Sci* **115**: 6864–6869
- 564 **Beyer HM, Juillot S, Herbst K, Samodelov SL, Müller K, Schamel WW, Römer W,**
565 **Schäfer E, Nagy F, Strähle U, et al** (2015) Red Light-Regulated Reversible Nuclear
566 Localization of Proteins in Mammalian Cells and Zebrafish. *ACS Synth Biol* **4**: 951–958
- 567 **Blanco-Touriñán N, Legris M, Minguet EG, Costigliolo-Rojas C, Nohales MA, Iniesto E,**
568 **García-León M, Pacín M, Heucken N, Blomeier T, et al** (2020) COP1 destabilizes
569 DELLA proteins in Arabidopsis. *Proc Natl Acad Sci U S A* **117**: 13792–13799
- 570 **Daviere J-M, Achard P** (2013) Gibberellin signaling in plants. *Development* **140**: 1147–1151
- 571 **Davière J-M, de Lucas M, Prat S** (2008) Transcriptional factor interaction: a central step in
572 DELLA function. *Curr Opin Genet Dev* **18**: 295–303
- 573 **Dill A, Thomas SG, Hu J, Steber CM, Sun T** (2004) The Arabidopsis F-Box Protein
574 SLEEPY1 Targets Gibberellin Signaling Repressors for Gibberellin-Induced
575 Degradation. *Plant Cell* **16**: 1392–1405
- 576 **Endy D** (2005) Foundations for engineering biology. *Nature* **438**: 449–453
- 577 **Feng S, Martinez C, Gusmaroli G, Wang Y, Zhou J, Wang F, Chen L, Yu L, Iglesias-**
578 **Pedraz JM, Kircher S, et al** (2008) Coordinated regulation of Arabidopsis thaliana
579 development by light and gibberellins. *Nature* **451**: 475–9
- 580 **Fiebitz A, Nyarsik L, Haendler B, Hu YH, Wagner F, Thamm S, Lehrach H, Janitz M,**
581 **Vanhecke D** (2008) High-throughput mammalian two-hybrid screening for protein-
582 protein interactions using transfected cell arrays. *BMC Genomics* **9**: 1–10
- 583 **Förster T** (1948) Zwischenmolekulare Energiewanderung und Fluoreszenz. *Ann Phys* **437**:
584 55–75
- 585 **Fu X, Richards DE, Fleck B, Xie D, Burton N, Harberd NP** (2004) The Arabidopsis mutant
586 *sleepy1gar2-1* protein promotes plant growth by increasing the affinity of the SCFSLY1
587 E3 ubiquitin ligase for DELLA protein substrates. *Plant Cell* **16**: 1406–18
- 588 **Gratz R, Brumbarova T, Ivanov R, Trofimov K, Tünnermann L, Ochoa-Fernandez R,**
589 **Blomeier T, Meiser J, Weidtkamp-Peters S, Zurbriggen MD, et al** (2020) Phospho-
590 mutant activity assays provide evidence for alternative phospho-regulation pathways of
591 the transcription factor FER-LIKE IRON DEFICIENCY-INDUCED TRANSCRIPTION
592 FACTOR. *New Phytol* **225**: 250–267
- 593 **Griffiths J, Murase K, Rieu I, Zentella R, Zhang Z-L, Powers SJ, Gong F, Phillips AL,**
594 **Hedden P, Sun T, et al** (2006) Genetic Characterization and Functional Analysis of the
595 GID1 Gibberellin Receptors in Arabidopsis. *Plant Cell* **18**: 3399–3414
- 596 **Hou BH, Takanaga H, Grossmann G, Chen LQ, Qu XQ, Jones AM, Lalonde S,**
597 **Schweissgut O, Wiechert W, Frommer WB** (2011) Optical sensors for monitoring
598 dynamic changes of intracellular metabolite levels in mammalian cells. *Nat Protoc* **6**:
599 1818–1833
- 600 **Jacobs JL, Dinman JD** (2004) Systematic analysis of bicistronic reporter assay data.
601 *Nucleic Acids Res* **32**: e160
- 602 **Lienert F, Lohmueller JJ, Garg A, Silver PA** (2014) Synthetic biology in mammalian cells:
603 next generation research tools and therapeutics. *Nat Rev Mol Cell Biol* **15**: 95–107
- 604 **Locascio A, Blázquez MA, Alabadí D** (2013) Genomic analysis of della protein activity.
605 *Plant Cell Physiol* **54**: 1229–1237
- 606 **de Lucas M, Davière J-M, Rodríguez-Falcón M, Pontin M, Iglesias-Pedraz JM, Lorrain**
607 **S, Fankhauser C, Blázquez MA, Titarenko E, Prat S** (2008) A molecular framework
608 for light and gibberellin control of cell elongation. *Nature* **451**: 480–484
- 609 **Marín-de la Rosa N, Pfeiffer A, Hill K, Locascio A, Bhalerao RP, Miskolczi P, Grønlund**
610 **AL, Wanchoo-Kohli A, Thomas SG, Bennett MJ, et al** (2015) Genome Wide Binding
611 Site Analysis Reveals Transcriptional Coactivation of Cytokinin-Responsive Genes by
612 DELLA Proteins. *PLoS Genet* **11**: e1005337

- 613 **Marín-de la Rosa N, Sotillo B, Miskolczi P, Gibbs DJ, Vicente J, Carbonero P, Oñate-**
614 **Sánchez L, Holdsworth MJ, Bhalerao R, Alabadí D, et al** (2014) Large-scale
615 identification of gibberellin-related transcription factors defines group VII ETHYLENE
616 RESPONSE FACTORS as functional DELLA partners. *Plant Physiol* **166**: 1022–32
- 617 **Miyamoto T, DeRose R, Suarez A, Ueno T, Chen M, Sun T, Wolfgang MJ, Mukherjee C,**
618 **Meyers DJ, Inoue T** (2012) Rapid and orthogonal logic gating with a gibberellin-
619 induced dimerization system. *Nat Chem Biol* **8**: 465–70
- 620 **Müller B, Sheen J** (2008) Cytokinin and auxin interplay in root stem-cell specification during
621 early embryogenesis. *Nature* **453**: 1094–1097
- 622 **Müller K, Engesser R, Schulz S, Steinberg T, Tomakidi P, Weber CC, Ulm R, Timmer J,**
623 **Zurbruggen MD, Weber W** (2013) Multi-chromatic control of mammalian gene
624 expression and signaling. *Nucleic Acids Res* **41**: e124–e124
- 625 **Müller K, Zurbruggen MD, Weber W** (2014a) Control of gene expression using a red- and
626 far-red light-responsive bi-stable toggle switch. *Nat Protoc* **9**: 622–632
- 627 **Müller K, Zurbruggen MD, Weber W** (2014b) Control of gene expression using a red- and
628 far-red light-responsive bi-stable toggle switch. *Nat Protoc* **9**: 622–632
- 629 **Murase K, Hirano Y, Sun TP, Hakoshima T** (2008) Gibberellin-induced DELLA recognition
630 by the gibberellin receptor *GID1*. *Nature* **456**: 459–463
- 631 **Mutalik VK, Guimaraes JC, Cambray G, Lam C, Christoffersen MJ, Mai Q-A, Tran AB,**
632 **Paull M, Keasling JD, Arkin AP, et al** (2013) Precise and reliable gene expression via
633 standard transcription and translation initiation elements. *Nat Methods* **10**: 354–360
- 634 **Nakajima M, Shimada A, Takashi Y, Kim YC, Park SH, Ueguchi-Tanaka M, Suzuki H,**
635 **Katoh E, Iuchi S, Kobayashi M, et al** (2006) Identification and characterization of
636 *Arabidopsis* gibberellin receptors. *Plant J* **46**: 880–889
- 637 **Sakai H, Aoyama T, Oka A** (2000) *Arabidopsis* *ARR1* and *ARR2* response regulators
638 operate as transcriptional activators. *Plant J* **24**: 703–11
- 639 **Santner A, Calderon-Villalobos LIA, Estelle M** (2009) Plant hormones are versatile
640 chemical regulators of plant growth. *Nat Chem Biol* **5**: 301–307
- 641 **Schwechheimer C** (2012) Gibberellin Signaling in Plants – The Extended Version. *Front*
642 *Plant Sci* **2**: 107
- 643 **Suzuki H, Park SH, Okubo K, Kitamura J, Ueguchi-Tanaka M, Iuchi S, Katoh E,**
644 **Kobayashi M, Yamaguchi I, Matsuoka M, et al** (2009) Differential expression and
645 affinities of *Arabidopsis* gibberellin receptors can explain variation in phenotypes of
646 multiple knock-out mutants. *Plant J* **60**: 48–55
- 647 **Ueguchi-Tanaka M, Ashikari M, Nakajima M, Itoh H, Katoh E, Kobayashi M, Chow TY,**
648 **Hsing YIC, Kitano H, Yamaguchi I, et al** (2005) GIBBERELLIN INSENSITIVE
649 DWARF1 encodes a soluble receptor for gibberellin. *Nature* **437**: 693–698
- 650 **Weidtkamp-Peters S, Stahl Y** (2017) The Use of FRET/FLIM to Study Proteins Interacting
651 with Plant Receptor Kinases. *Methods Mol. Biol.* pp 163–175
- 652 **Wend S, Wagner HJ, Müller K, Zurbruggen MD, Weber W, Radziwill G** (2013)
653 Optogenetic Control of Protein Kinase Activity in Mammalian Cells. *ACS Synth Biol*. doi:
654 10.1021/sb400090s
- 655 **Yamaguchi S, Kamiya Y** (2000) Gibberellin biosynthesis: its regulation by endogenous and
656 environmental signals. *Plant Cell Physiol* **41**: 251–7
- 657
658

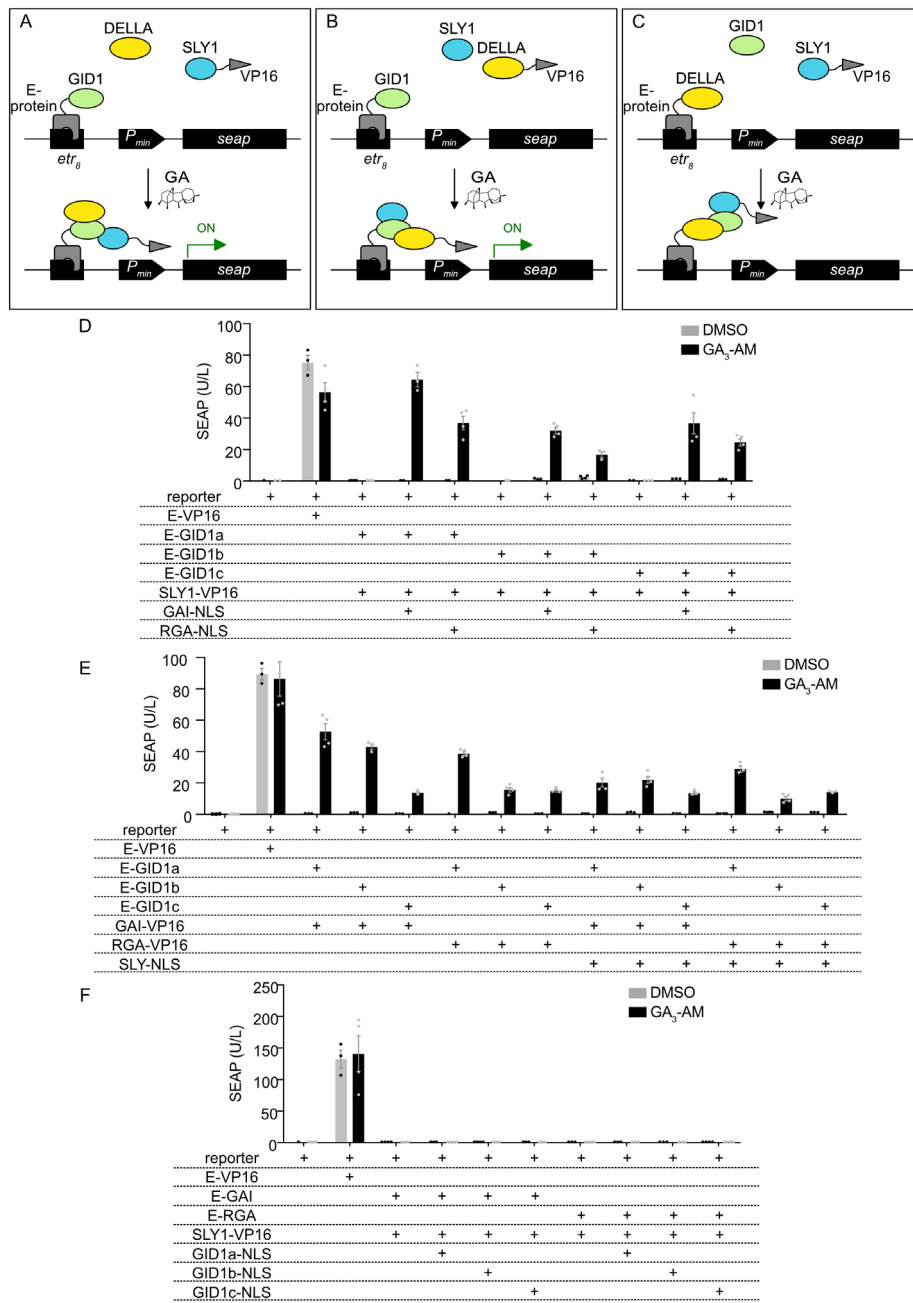


659
 660
 661
 662
 663
 664
 665
 666
 667
 668
 669
 670
 671

Figure 1: Synthetic reconstruction of DELLA-mediated regulation of transcriptional activation of ARR1 proteins in human embryonic kidney cells (HEK-293T). (A) Mode of function of mammalian one hybrid (M1H) and mammalian one hybrid* (M1H*) experiments. The plant transcription factor ARR1 activates transcription of the SEAP reporter gene upon binding to repetitions of the TCS element (M1H). The presence of DELLA proteins further enhances this activation (M1H*). The reporter construct consisting out of the human secreted alkaline phosphates (SEAP) under the control of the human cytomegalovirus minimal promoter ($P_{hCMVmin}$), positioned downstream of repetitions of the TCS-element. The reporter plasmid was co-transfected with ARR1 (ARR1 Δ DDK) with or without being fused to the VP16 transactivation domain (M1H). Additional co-transfection of either GAI or RGA, as well as VP16-fused versions of both DELLAs was performed (M1H*). (B) 24 h post transfection of the listed components, SEAP activity was quantified by a colorimetric assay. $n = 4$, error bars represent one standard error of the mean (SEM). One-way analyzes of variance (ANOVA) were performed with $p < 0.05$.



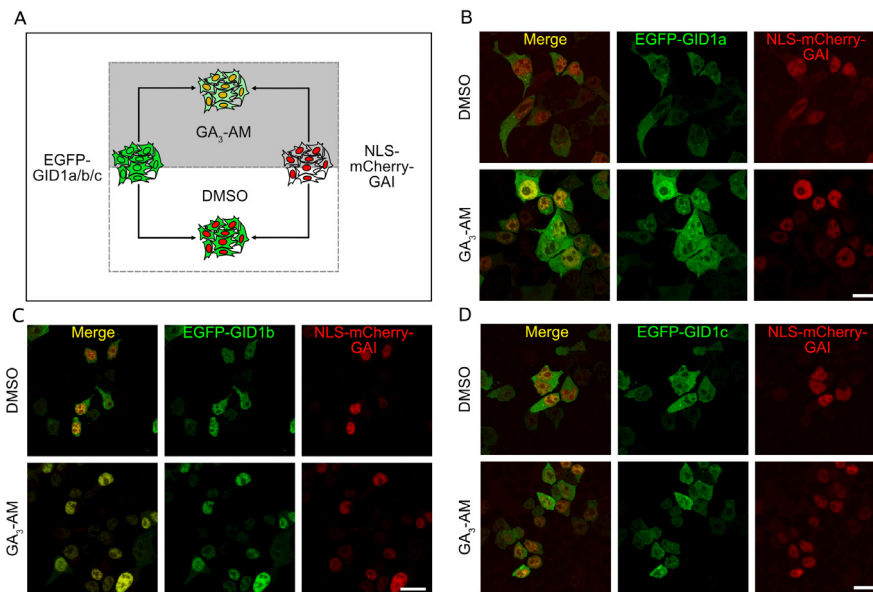
672
 673 **Figure 2: Comparison of mammalian-2 and 3-hybrid experiments analyzing interactions of DELLA and GID1 proteins of**
 674 ***A. thaliana* in human embryonic kidney cells (HEK-293T).** (A) and (C) Scheme of the mammalian-hybrid detection system,
 675 investigating the possible interaction of GID1-receptors and DELLA proteins in the presence (M3H) or absence (M2H) of
 676 gibberellic acid (GA₃-AM). GID1a, b or c (A) or DELLA proteins GAI or RGA (C) were N-terminally fused to the DNA-binding
 677 macrolide repressor (E), tethering it to the *etr*₈ operator site on the reporter plasmid. Recruitment of GAI or RGA (A) or GID1a, b,
 678 c (C), C-terminally fused to the VP16 transactivation domain, recruits the transcriptional activation machinery to the
 679 cytomegalovirus minimal promoter (*P*_{CMVmin}) and induces the expression of the secreted alkaline phosphatase reporter gene. (B)
 680 and (D) Macrolide repressor-based split-transcription factor system for analysis of GA-dependent interactions between E-GID1
 681 and DELLA-VP16 (B) or E-DELLA and GID1-VP16 (D). 50,000 HEK-293T cells were seeded in 24-well plates and transfected
 682 24 hours later with a reporter plasmid, containing the human secreted alkaline phosphatase (SEAP) under control of the human
 683 cytomegalovirus minimal promoter, positioned downstream of repetitions of an operator sequence for E (*etr*₈). A constitutively
 684 expressed fusion of both, the DNA-binding domain (E protein) and the Herpes simplex-derived transactivation domain (VP16)
 685 acted as positive control for gene expression, while single transfection of the reporter was used as a negative control for controlling
 686 leakiness of the system in the different conditions. For quantitative analysis of GA-dependent interactions, a bicistronic vector
 687 containing the mentioned protein combinations, was co-transfected. 24 hours post transfection, the medium was exchanged by
 688 fresh medium containing either 10 μM GA₃-AM, dissolved in DMSO, or DMSO as a control. Another 24 hours SEAP production
 689 was quantified using a colorimetric assay. *n* = 4, error bars represent one standard error of the mean (SEM).
 690



691
692
693
694
695
696

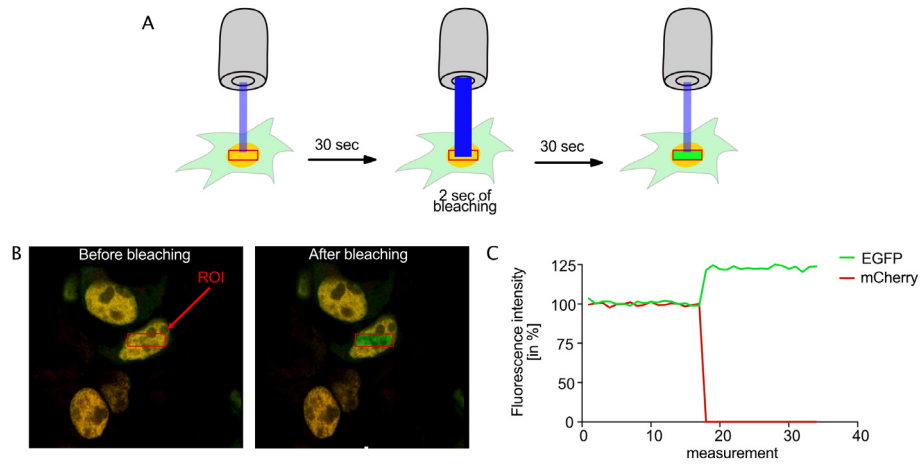
697
698
699
700
701
702
703
704
705
706
707
708
709
710

Figure 3: Mammalian-3 and 4-hybrid experiments analyzing the order of complex-formation during GA-perception in human embryonic kidney cells (HEK-293T). (A), (B) and (C) Molecular design of the mammalian-hybrid detection system, investigating the order of possible interaction of SLY1, GID1-receptors and DELLA proteins (right) in the presence or absence of gibberellic acid (GA). The GID1-receptors (A and B) or a DELLA protein (C) were fused to the E DNA-binding domain, tethering it to the etr_3 operator side on the reporter plasmid. In case of interaction, recruitment of SLY1 (A and C) or DELLAs (B) fused to the VP16 transactivation domain recruits the transcriptional activation machinery and induces the activation of the secreted alkaline phosphatase reporter gene under the control of the cytomegalovirus minimal promoter (M3H). Co-transfection of the third component (M4H) further analyzes if it is necessary for mediating the interaction of both parts of the split transcription factor. (C), (D) and (E) 50,000 HEK-293T cells were seeded in 24-well plates and transfected 24 hours later with the indicated components 24 hours post transfection, the medium was exchanged by fresh medium containing either 10 μ M GA₃-AM, dissolved in DMSO, or DMSO as a control. Another 24 hours SEAP production was quantified using a colorimetric assay. $n = 4$, error bars represent one standard error of the mean (SEM).

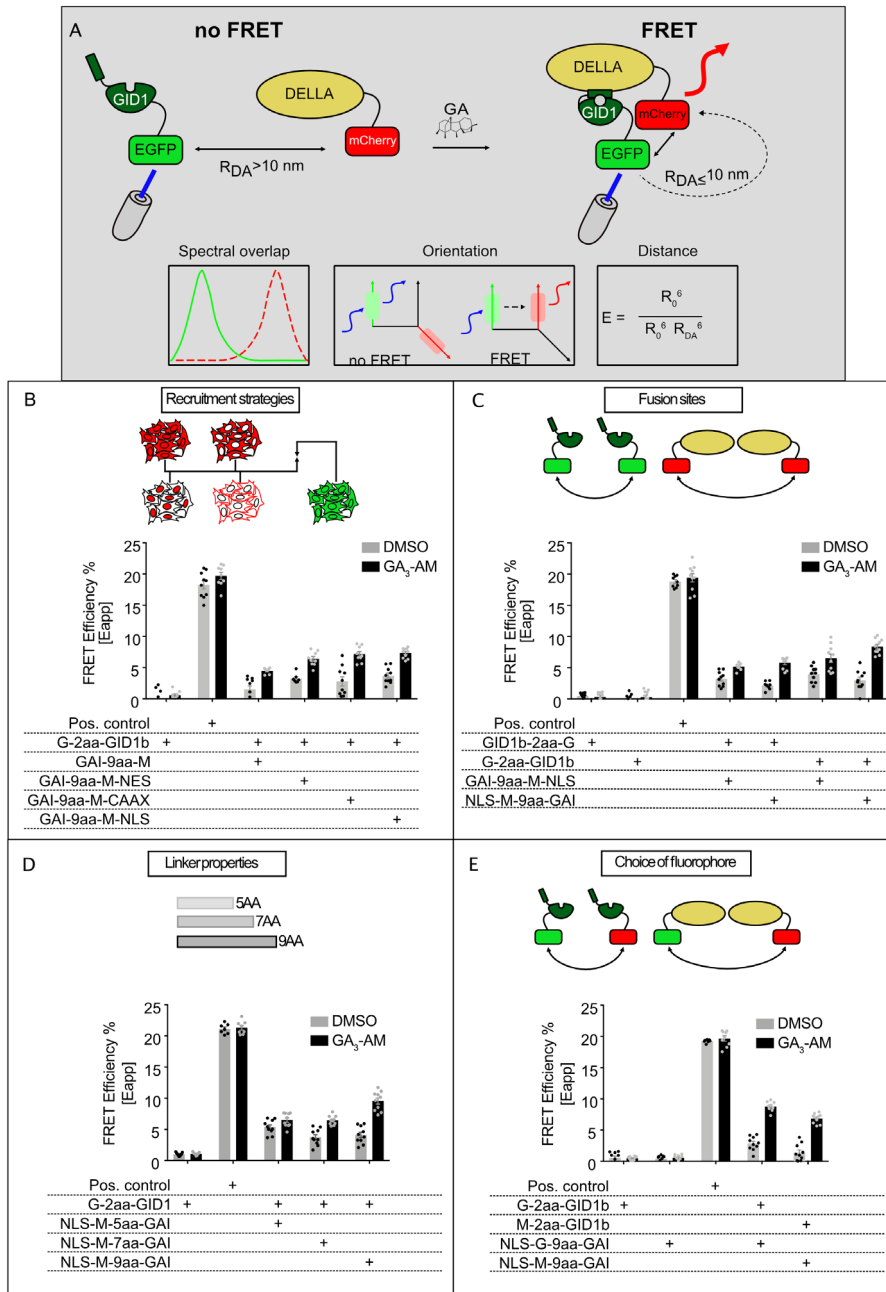


711
712
713
714
715
716
717
718
719
720
721
722
723

Figure 4: GA-dependent nuclear recruitment strategy for studying the interaction of DELLA- and GID1-fusion proteins. (A) Illustration of the GA-dependent nuclear recruitment. The DELLA fusion proteins were C-terminally linked to an NLS sequence, inducing their recruitment to the nucleus of the expressing cells, while the GA-receptor proteins GID1a, b and c were equally expressed in all cellular compartments. Upon supplementation of the phytohormone GA, a possible interaction between respective DELLA and GID1 proteins, induces a translocation of the EGFP-GID1 fusion proteins, generating a co-localization of both in the area of the nucleus. (B) Confocal fluorescence microscopy imaging of intracellular localization of EGFP-GID1a and GAI-mCherry-NLS in mammalian HEK-293T cells after GA₃-AM or DMSO supplementation. (C) Confocal fluorescence microscopy imaging of intracellular localization of EGFP-GID1b and GAI-mCherry-NLS in mammalian HEK-293T cells after GA₃-AM or DMSO supplementation. (D) Confocal fluorescence microscopy imaging of intracellular localization of EGFP-GID1c and GAI-mCherry-NLS in mammalian HEK-293T cells after GA₃-AM or DMSO supplementation. All constructs were expressed under the control of the constitutive promoter derived from the simian virus 40 (P_{SV40}).



724
 725 **Figure 5: Overview of the principles of FRET measurements by acceptor photo-bleaching (FRET-APB) on the example**
 726 **of EGFP-GID1b and NLS-mCherry-GAI constructs in mammalian HEK-293T cells. (A)** Experimental set-up of FRET-APB
 727 **measurements performed in this study. After 30 seconds of constant measurement of the fluorescence-intensity, the laser power**
 728 **of the 561 nm laser was raised up to 100 percent, bleaching the mCherry fluorescence in the area of the red rectangle (ROI).**
 729 **After 2 seconds of bleaching, fluorescence was measured for another 30 seconds. To calculate the efficiency of the FRET-APB**
 730 **measurement the average fluorescence of the five seconds before and after bleaching were compared to each other. (B)** Image
 731 **of a mammalian HEK-293T cells, expressing EGFP-GID1b and NLS-mCherry-GAI, before (left) and after (right) the bleaching**
 732 **step of a FRET-APB measurement in the region of interest (ROI). (C)** Visualization of exemplary fluorescence intensities of EGFP
 733 **(green) and mCherry (red) before and after bleaching of the mCherry acceptor fluorophore in case of FRET between both**
 734 **fluorophores, within a regular FRET-APB measurement.**
 735



736
737
738
739

740 **Figure 6: Comparison of apparent FRET efficiencies between fluorescently-tagged GAI and GID1b protein constructs in mammalian HEK-293T cells.** (A) Illustration of the GA-dependent FRET measurement of a DELLA-mCherry and a GID1-EGFP proteins and factors essential for such a measurement. In the absence of GA, both proteins do not interact and are not localized within a close proximity to each other. No radiation free energy transfer occurs. Upon supplementation of GA, both proteins interact to each other, generating a close proximity of EGFP and mCherry, inducing energy-transfer from the donor fluorophore EGFP to the acceptor fluorophore mCherry. FRET highly depends on the spectral overlap of the emission spectrum of the donor fluorophore and the excitation spectrum of the acceptor, as well as the distance and the orientation of both fluorophores to each other. (B) FRET-APB measurements of N- or C-terminally EGFP-tagged GID1b fusion proteins in co-transfection with N- or C-terminally mCherry-tagged GAI fusion proteins in the absence (grey bars) or presence (black bars) of GA₃-AM. (C) FRET-APB measurements of N-terminally mEGFP-tagged GID1b, co-transfected with different constructs of mCherry-GAI-fusions, with or without additional fusion to a localization tag, recruiting the protein to the nucleus (NLS), cytoplasm (NES) or plasma-membrane (CAAX), after supplementation of DMSO (grey bars) or GA₃-AM (black bars). (D) FRET-APB measurements of N-terminally EGFP-tagged GID1b fusion proteins in co-transfection with N-terminally NLS-mCherry-tagged GAI fusion proteins with different linker length between the fluorescent protein and GAI in the absence (grey bars) or presence (black bars) of GA₃-AM. (E) FRET-APB measurements of N-terminally EGFP- or mCherry-tagged GID1b fusion proteins in co-transfection with N-terminally mCherry- or EGFP-tagged GAI fusion proteins in the absence (grey bars) or presence (black bars) of GA₃-AM. 24 h after transfection, the cell culture medium was exchanged with fresh medium, supplemented with 0.5 μL DMSO or 10 μM of GA₃-AM solved in DMSO, per well. After four hours of incubation and subsequent fixation of the cells, potential protein-protein-interactions between GID1b- and GAI-constructs, were measured by bleaching the fluorescence signal of the acceptor-fluorophore mCherry and monitoring a potential increase in fluorescence emission of the donor fluorophore EGFP (FRET-APB). Intramolecular fusion of EGFP and mCherry to GID1b served as positive control for FRET, while the single transfection of EGFP-GID1b was used as negative control. *n* = 10, error bars represent one standard error of the mean (SEM). Significance was calculated with a paired students t-test (**P* < 0.05; ***P* < 0.01; ****P* < 0.001).

741
742
743
744
745
746
747
748
749
750
751
752
753
754
755
756
757
758
759
760
761
762
763

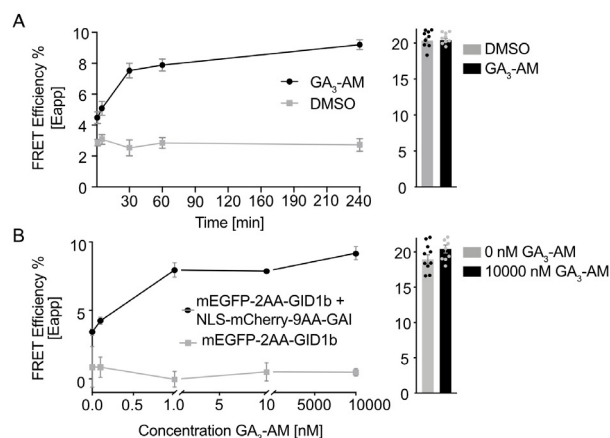
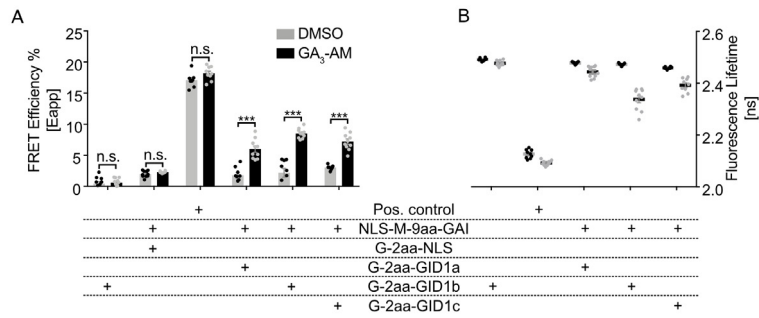


Figure 7: Dose-response and kinetics of apparent FRET efficiency between fluorescently-tagged GAI and GID1b protein constructs in mammalian HEK-293T cells. (A) Kinetics of FRET-APB measurements of N-terminally EGFP-tagged GID1b in co-transfection with N-terminally mCherry-tagged GAI in the absence (grey labels) or presence (black labels) of GA₃-AM at different time-intervals of the respective treatment. Intramolecular fusion of EGFP and mCherry to GID1b served as positive control for FRET. At different time-intervals after transfection, the cell culture medium was exchanged with fresh medium, supplemented with 0.5 μL DMSO or 10 μM of GA₃-AM solved in DMSO, per well. (B) Dose response of FRET-APB measurements of N-terminally EGFP-tagged GID1b in single transfection (grey labels) or in co-transfection with N-terminally mCherry-tagged GAI (black labels) after supplementation of different concentrations of GA₃-AM. Intramolecular fusion EGFP and mCherry to GID1b served as positive control for FRET in the absence (grey bars) or presence (black bars) of GA₃-AM. 24 h after transfection, the cell culture medium was exchanged with fresh medium, supplemented with different concentrations of GA₃-AM solved in DMSO, per well. (A) and (B) After four hours of incubation and subsequent fixation of the cells, potential protein-protein-interactions between GID1b- and GAI-constructs were measured by bleaching the fluorescence signal of the acceptor-fluorophore mCherry and monitoring a potential increase in fluorescence emission of the donor fluorophore EGFP (FRET-APB). *n* = 10, error bars represent one standard error of the mean (SEM).



783
784
785
786
787
788
789
790
791
792
793

Figure 8: Visualization of apparent FRET efficiencies of FRET-APB measurements and visualization of fluorescence lifetime of fluorescently tagged GID1 fusion proteins in different experimental conditions in mammalian HEK-293T cells. mEGFP-GID1a, b or c were co-transfected with NLS-mCherry-GAI fusion proteins. Single transfection of EGFP-GID1b served as a negative control, while fusion of GID1b to EGFP and mCherry functioned as positive control for intramolecular energy transfer. 24 h after transfection, the cell culture medium was exchanged with fresh medium (A) or live cell imaging solution (B), supplemented with 0.5 μ L DMSO or 10 μ M of GA₃-AM solved in DMSO, per well. Four hours later, cells were fixed for FRET-APB measurements (A) or kept alive for analysis of potential shifts in fluorescence lifetime of mEGFP-GID1 constructs, caused by interaction with the NLS-mCherry-GAI fusion protein (B). $n = 10$, error bars represent one standard error of the mean (SEM). Significance in A was calculated with a paired students t-test (* $P < 0.05$; ** $P < 0.01$; *** $P < 0.001$).

1 **Mammalian cell-based platform for quantitative**
2 **reconstruction of plant signaling pathways**

3

4 Tim Blomeier^{1,#}, Jennifer Andres^{1,#}, Julia Kapr¹, Lisa Schmunk², Sophia L. Samodelov³, Miguel
5 A. Blazquez⁴, Matias D. Zurbriggen^{1,*}

6

7 ¹Institute of Synthetic Biology, University of Düsseldorf and CEPLAS, Düsseldorf, Germany

8 ²Cardiovascular Strategic Research Initiative, University of Cambridge

9 ³Department of Clinical Pharmacology and Toxicology, University Hospital Zurich, Zurich, Switzerland

10 ⁴Instituto de Biología Molecular y Celular de Plantas (IBMCP), CSIC-Universidad Politécnica de Valencia, Campus UPV CPI 8E,
11 Valencia, Spain

12

13 [#]These authors contributed equally to this work

14 ^{*}Corresponding author: Email: matias.zurbriggen@uni-duesseldorf.de

15

16

17 **Supplementary Information**

18

19 Figure S1: Comparison of mammalian-2 and 3-hybrid experiments analyzing the interaction of SLY1
20 with GID1-receptors in Human embryonic kidney cells (HEK-293T).

21

22 Figure S2: Comparison of mammalian-2 and 3-hybrid experiments analyzing interactions of DELLA
23 proteins and SLY1 of *A. thaliana* in Human embryonic kidney cells (HEK-293T).

24

25 Figure S3: FRET-4-hybrid measurements of fluorescently-tagged GAI, GID1b and SLY1 protein
26 constructs in mammalian HEK-293T cells.

27

28 Table S1: Average fluorescence lifetime of fluorescently tagged GID1 fusion proteins in different
29 experimental conditions in mammalian HEK-293T cells.

30

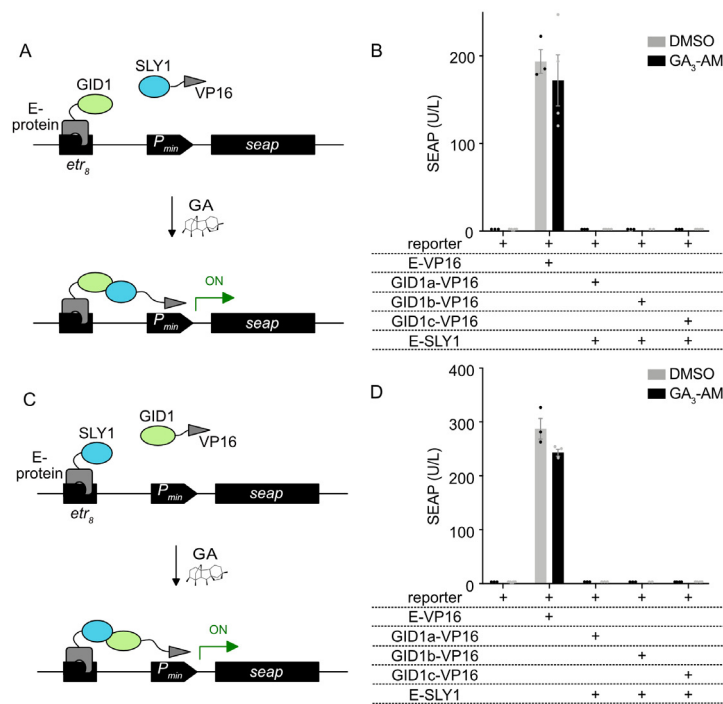
31 Table S2: Construction and description of plasmids used in this work.

32

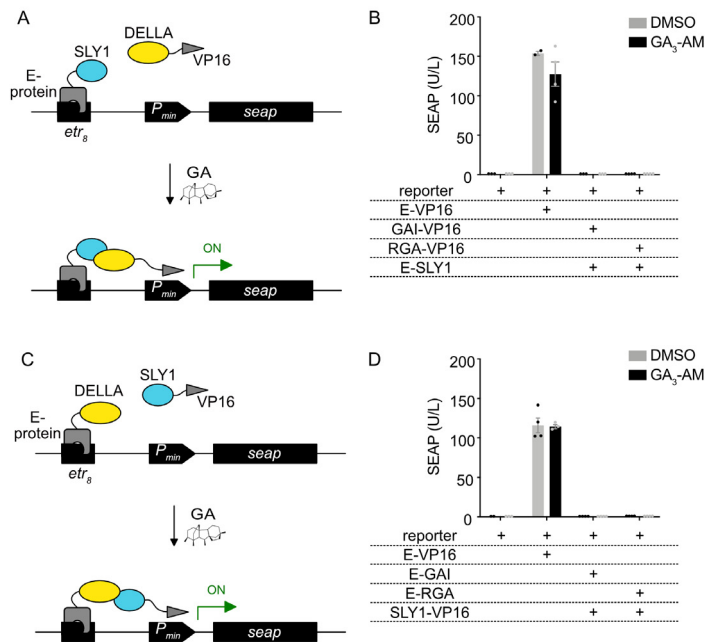
33 Table S3: Oligonucleotides used for construction of plasmids used in this work

34

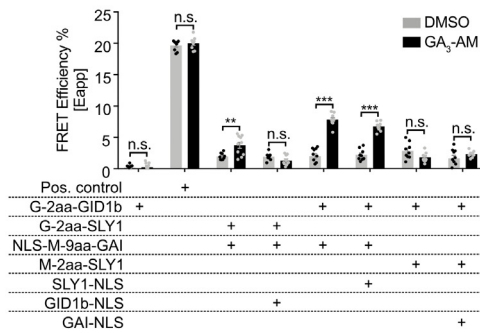
35



36
 37 **Figure S1: Comparison of mammalian-2 and 3-hybrid experiments analyzing the interaction of SLY1 with GID1-receptors in human**
 38 **embryonic kidney cells (HEK293T).** (A) and (C) Scheme of the mammalian-hybrid detection system, investigating the possible interaction of
 39 GID1-receptors and SLY1, in the presence (M3H) or absence (M2H) of gibberellic acid (GA₃-AM). GID1a, b or c (A) or SLY1 (C) were N-terminally
 40 fused to the DNA-binding macrolide repressor (E-protein), tethering it to the *etr₈* operator site on the reporter plasmid. Recruitment of SLY1
 41 (A) or GID1a, b or c (C), C-terminally fused to the VP16 transactivation domain, recruits the transcriptional activation machinery to the
 42 cytomegalovirus minimal promoter (*P_{CMVmin}*) and induces the expression of the secreted alkaline phosphatase reporter gene. (B) and (D)
 43 Macrolide repressor-based split-transcription factor system for analysis of GA-dependent interactions between E-GID1 and SLY1-VP16 (B) or
 44 E-SLY1 and GID1-VP16 (D). 50,000 HEK-293T cells were seeded in 24-well plates and transfected 24 hours later with a reporter plasmid,
 45 containing the human secreted alkaline phosphatase (SEAP) under control of the human cytomegalovirus minimal promoter, positioned
 46 downstream of repetitions of an operator sequence for E (*etr₈*). A constitutively expressed fusion of both, the DNA-binding domain (E) and
 47 the Herpes simplex-derived transactivation domain (VP16) acted as positive control for gene expression, while single transfection of the
 48 reporter was used as negative control for controlling leakiness of the system in the different conditions. For quantitative analysis of GA-
 49 dependent interactions, a bicistronic vector containing the mentioned protein combinations, was co-transfected. 24 hours post transfection,
 50 the medium was exchanged by fresh medium containing either 10 μM GA₃-AM, dissolved in DMSO, or DMSO as a control. Another 24 hours
 51 SEAP-production was quantified using a colorimetric assay. *n* = 4, error bars represent one standard error of the mean (SEM).
 52



53
 54
 55 **Figure S2 Comparison of mammalian-2 and 3-hybrid experiments analyzing interactions of DELLA proteins and SLY1 of *A. thaliana* in**
 56 **human embryonic kidney cells (HEK293T). (A) and (C) Scheme of the mammalian-hybrid detection system, investigating the possible**
 57 **interaction of SLY1 and DELLA proteins in the presence (M3H) or absence (M2H) of gibberellic acid (GA₃-AM). SLY1 (A) or DELLA proteins GAI**
 58 **or RGA (C) were N-terminally fused to the DNA-binding macrolide repressor (E), tethering it to the *etr₈* operator site on the reporter plasmid.**
 59 **Recruitment of GAI or RGA (A) or SLY1 (C), C-terminally fused to the VP16 transactivation domain, recruits the transcriptional activation**
 60 **machinery to the cytomegalovirus minimal promoter (*P_{CMVmin}*) and induces the expression of the secreted alkaline phosphatase reporter**
 61 **gene. (B) and (D) Macrolide repressor-based split-transcription factor system for analysis of GA-dependent interactions between E-SLY1 and**
 62 **DELLA-VP16 (B) or E-DELLA and SLY1-VP16 (D). 50,000 HEK-293T cells were seeded in 24-well plates and transfected 24 hours later with a**
 63 **reporter plasmid, containing the human secreted alkaline phosphatase (SEAP) under control of the human cytomegalovirus minimal**
 64 **promoter, positioned downstream of repetitions of an operator sequence for E (*etr₈*). A constitutively expressed fusion of both, the DNA-**
 65 **binding domain (E) and the herpes simplex-derived transactivation domain (VP16) acted as positive control for gene expression, while single**
 66 **transfection of the reporter was used as negative control for controlling leakiness of the system in the different conditions. For quantitative**
 67 **analysis of GA-dependent interactions, a bicistronic vector containing the mentioned protein combinations, was co-transfected. 24 hours**
 68 **post transfection, the medium was exchanged by fresh medium containing either 10 μM GA₃-AM, dissolved in DMSO, or DMSO as a control.**
 69 **Another 24 hours SEAP-production was quantified using a colorimetric assay. *n* = 4, error bars represent one standard error of the mean**
 70 **(SEM).**
 71
 72
 73
 74
 75



76
77
78
79
80
81
82
83
84
85
86
87
88
89
90
91
92
93

Figure S3: FRET-4-hybrid measurements of fluorescently-tagged GAI, GID1b and SLY1 protein constructs in mammalian HEK-293T cells. FRET-APB measurements of different combinations of mEGFP-tagged GID1b, nuclear localized N-terminally mCherry fused GAI and N-terminally EGFP or mCherry fused SLY1. Further co-transfection of a nuclear localized, non-fluorescent variant of respective third component was performed after supplementation of DMSO (grey bars) or GA₃-AM (black bars). 24 h after transfection, the cell culture medium was exchanged with fresh medium, supplemented with 0.5 μL DMSO or 10 μM of GA₃-AM solved in DMSO, per well. After four hours of incubation and subsequent fixation of the cells, potential protein-protein-interactions between the transfected proteins were measured by bleaching the fluorescence signal of the acceptor-fluorophore mCherry and monitoring a potential increase in fluorescence emission of the donor fluorophore EGFP (FRET-APB). Intramolecular fusion of EGFP and mCherry to GID1b served as positive control for FRET, while the single transfection of EGFP-GID1b was used as negative control. *n* = 10, error bars represent one standard error of the mean (SEM). Significance was calculated with a paired students t-test (**P* < 0.05; ***P* < 0.01; ****P* < 0.001).

Table S1: Average fluorescence lifetime of fluorescently tagged GID1 fusion proteins in different experimental conditions in mammalian HEK293T cells.

	Average fluorescence lifetime [ns]	
	DMSO	GA ₃ -AM
mEGFP-GID1b	2.49	2.48
GID1b-mEGFP-mCherry	2.13	2.10
mEGFP-GID1a + NLS-mCherry-GAI	2.48	2.44
mEGFP-GID1b + NLS-mCherry-GAI	2.47	2.34
mEGFP-GID1c + NLS-mCherry-GAI	2.46	2.39

94
95
96
97
98
99
100
101
102
103
104
105
106
107

108
109
110**Table S2: Construction and description of plasmids used in this work. (All plasmids were constructed using AQUA and Gibson assembly cloning methods.)**

Plasmid	Description	Reference
pHB090	P_{SV40}-PIF1-mEGFP-pA P _{SV40} -driven mammalian expression vector encoding <i>A. thaliana</i> PIF1 fused to the fluorescent protein mEGFP.	unpublished
pKM081	etr_F-P_{CMVmin}-SEAP-pA Vector encoding SEAP under control of a modified P _{ETR} .	(Müller et al., 2013)
pKM195	(pifO)₄-P_{hCMVmin}-SEAP-pA Vector encoding SEAP under control of a pif operator-CMVmin promoter.	unpublished
pRSET	PT7-driven bacterial expression vector	Novagen
pSJ050	P_{SV40}-phyC-mCherry-pA P _{SV40} -driven mammalian expression vector encoding <i>A. thaliana</i> phytochrome C fused to the fluorescent protein mCherry.	unpublished
pSLS404	P_{CaMV35S}-Renilla-2A-GAI-Firefly-myc-pA Ratiometric gibberellin sensor plasmid with <i>A. thaliana</i> DELLA protein GAI as SM for use in plant cells.	unpublished
pSLS405	P_{CaMV35S}-Renilla-2A-RGA-Firefly-myc-pA Ratiometric gibberellin sensor plasmid with the <i>A. thaliana</i> DELLA protein RGA as SM for use in plant cells.	unpublished
pSLS411	P_{SV40}-GID1a-pA Expression vector encoding the <i>A. thaliana</i> gibberellin receptor GID1a under control of P _{SV40} .	unpublished
pSLS412	P_{SV40}-GID1b-pA Expression vector encoding the <i>A. thaliana</i> gibberellin receptor GID1b under control of P _{SV40} .	unpublished
pSLS413	P_{SV40}-GID1c-pA Expression vector encoding the <i>A. thaliana</i> gibberellin receptor GID1c under control of P _{SV40} .	unpublished
pSLS414	P_{SV40}-SLY1-pA Expression vector encoding <i>A. thaliana</i> F-Box protein SLY1 under control of P _{SV40} .	unpublished
pSLS433	P_{SV40}-GID1a-NLS-HA-pA The <i>A. thaliana</i> gibberellin receptor GID1a was amplified from pSLS411 with oSLS414/oSLS438. pMZ333 was amplified with oSLS436/oSLS442. Both fragments were assembled using Gibson cloning.	This work

Appendix

pSLS434	P_{SV40}-GID1b-NLS-HA-pA The <i>A.thaliana</i> gibberellin receptor GID1b was amplified from pSLS412 with oSLS416/oSLS439. pMZ333 was amplified with oSLS436/oSLS442. Both fragments were assembled using Gibson cloning.	This work
pSLS435	P_{SV40}-GID1c-NLS-HA-pA The <i>A.thaliana</i> gibberellin receptor GID1c was amplified from pSLS413 with oSLS418/oSLS440. pMZ333 was amplified with oSLS436/oSLS442. Both fragments were assembled using Gibson cloning.	This work
pSLS436	P_{SV40}-SLY1-NLS-HA-pA The <i>A.thaliana</i> F-Box protein SLY1 was amplified from pSLS414 with oSLS420/oSLS441. pMZ333 was amplified with oSLS436/oSLS442. Both fragments were assembled using Gibson cloning.	This work
pSLS437	P_{SV40}-GAI-NLS-FLAG-pA The <i>A.thaliana</i> DELLA protein GAI was amplified from a GAI containing plasmid (ABRC) with oSLS444/oSLS445. pMZ333 was amplified with oSLS448/oSLS442. Both fragments were assembled using Gibson cloning.	This work
pSLS438	P_{SV40}-RGA-NLS-FLAG-pA The <i>A.thaliana</i> DELLA protein RGA was amplified from a RGA containing plasmid (ABRC) with oSLS446/oSLS447. pMZ333 was amplified with oSLS448/oSLS442. Both fragments were assembled using Gibson cloning.	This work
pSLS443	P_{SV40}-ARR1DDDK-NLS-HA-pA ARR1DDDK-NLS-HA was amplified from a plasmid received from the Alabadi/Blázquez lab, IBMCP Valencia and amplified with oSLS454/455. pMZ333 was amplified with oSLS436/oSLS442. Both fragments were assembled using Gibson cloning.	This work
pSLS446	P_{SV40}-ARR1DDDK-VP16-NLS-HA-pA ARR1DDDK-NLS-HA was amplified from a plasmid received from the Alabadi/Blázquez lab, IBMCP Valencia and amplified with oSLS454/463. VP16-NLS-HA was amplified from pKM018 with oSLS443/oSLS466. pMZ333 was amplified with oSLS436/oSLS442. All fragments were assembled using Gibson cloning.	This work
pSLS454	TCS-P_{hCMVmin}-SEAP-pA The repetitive TCS motif was amplified from a plasmid received from the Alabadi/Blázquez lab, IBMCP Valencia and amplified with oSLS470/oSLS471. pKM195 was linearized with NruI/EcoRV. Both fragments were assembled using Gibson cloning.	This work
pSLS470	P_{CaMV35S}-Renilla-2A-RGAΔ17-Firefly-myc-pA	unpublished
pWW035	P_{SV40}-E-VP16-pA	(Weber et al., 2002)
pJATB001	P_{SV40}-GAI-VP16-IRES-TetR-PIF6(1-100)-pA GAI was PCR amplified from pSLS404 with oJATB001/oJATB002. pPF001 was linearized with SpeI/EcoRV. Both fragments were assembled using AQUA cloning.	This work

Appendix

pJATB002	P_{SV40}-RGA-VP16-IRES-TetR-PIF6(1-100)-pA RGA was PCR amplified from pSLS405 with oJATB003/oJATB004. pPF001 was linearized with SpeI/EcoRV. Both fragments were assembled using AQUA cloning.	This work
pJATB003	P_{SV40}-GAI-VP16-IRES-TetR-Gid1a-pA GID1a was PCR amplified from pSLS411 with oJATB005/oJATB006. pJATB001 was linearized with BsrGI/AscI. Both fragments were assembled using AQUA cloning.	This work
pJATB004	P_{SV40}-GAI-VP16-IRES-TetR-Gid1b-pA GID1b was PCR amplified from pSLS412 with oJATB007/oJATB008. pJATB001 was linearized with BsrGI/AscI. Both fragments were assembled using AQUA cloning.	This work
pJATB005	P_{SV40}-GAI-VP16-IRES-TetR-Gid1c-pA GID1c was PCR amplified from pSLS413 with oJATB009/oJATB010. pJATB001 was linearized with BsrGI/AscI. Both fragments were assembled using AQUA cloning.	This work
pJATB006	P_{SV40}-RGA-VP16-IRES-TetR-Gid1a-pA GID1a was PCR amplified from pSLS411 with oJATB005/oJATB006. pJATB002 was linearized with BsrGI/AscI. Both fragments were assembled using AQUA cloning.	This work
pJATB007	P_{SV40}-RGA-VP16-IRES-TetR-Gid1b-pA GID1b was PCR amplified from pSLS412 with oJATB007/oJATB008. pJATB002 was linearized with BsrGI/AscI. Both fragments were assembled using AQUA cloning.	This work
pJATB008	P_{SV40}-RGA-VP16-IRES-TetR-Gid1c-pA GID1c was PCR amplified from pSLS413 with oJATB009/oJATB010. pJATB002 was linearized with BsrGI/AscI. Both fragments were assembled using AQUA cloning.	This work
pJATB023	P_{SV40}-GAI-VP16-IRES-TetR-SLY1-pA SLY1 was PCR amplified from pSLS414 with oJATB029/oJATB030. pJATB001 was linearized with BsrGI/AscI. Both fragments were assembled using AQUA cloning.	This work
pJATB024	P_{SV40}-RGA-VP16-IRES-TetR-SLY1-pA SLY1 was PCR amplified from pSLS414 with oJATB029/oJATB030. pJATB002 was linearized with BsrGI/AscI. Both fragments were assembled using AQUA cloning.	This work
pJATB025	P_{SV40}-SLY1-VP16-IRES-TetR-Gid1a-pA SLY1 was PCR amplified from pSLS414 with oJATB031/oJATB032. pJATB003 was linearized with SpeI/EcoRV. Both fragments were assembled using AQUA cloning.	This work
pJATB026	P_{SV40}-SLY1-VP16-IRES-TetR-Gid1b-pA SLY1 was PCR amplified from pSLS414 with oJATB031/oJATB032. pJATB004 was linearized with SpeI/EcoRV. Both fragments were assembled using AQUA cloning.	This work

Appendix

pJATB027	P_{SV40}-SLY1-VP16-IRES-TetR-Gid1c-pA SLY1 was PCR amplified from pSLS414 with oJATB031/oJATB032. pJATB005 was linearized with SpeI/EcoRV. Both fragments were assembled using AQUA cloning.	This work
pJATB028	P_{SV40}-GAI-VP16-IRES-TetR-RGA-pA RGA was PCR amplified from pSLS405 with oJATB033/oJATB034. pJATB001 was linearized with BsrGI/AscI. Both fragments were assembled using AQUA cloning.	This work
pJATB029	P_{SV40}-RGA-VP16-IRES-TetR-GAI-pA GAI was PCR amplified from pSLS404 with oJATB035/oJATB036. pJATB002 was linearized with BsrGI/AscI. Both fragments were assembled using AQUA cloning.	This work
pJATB030	P_{SV40}-Gid1a-VP16-IRES-TetR-GAI-pA GID1a was PCR amplified from pSLS411 with oJATB037/oJATB038. pJATB029 was linearized with SpeI/EcoRV. Both fragments were assembled using AQUA cloning.	This work
pJATB031	P_{SV40}-Gid1b-VP16-IRES-TetR-GAI-pA GID1b was PCR amplified from pSLS412 with oJATB039/oJATB040. pJATB029 was linearized with SpeI/EcoRV. Both fragments were assembled using AQUA cloning.	This work
pJATB032	P_{SV40}-Gid1c-VP16-IRES-TetR-GAI-pA GID1c was PCR amplified from pSLS413 with oJATB041/oJATB042. pJATB029 was linearized with SpeI/EcoRV. Both fragments were assembled using AQUA cloning.	This work
pJATB033	P_{SV40}-Gid1a-VP16-IRES-TetR-RGA-pA GID1a was PCR amplified from pSLS411 with oJATB037/oJATB038. pJATB028 was linearized with SpeI/EcoRV. Both fragments were assembled using AQUA cloning.	This work
pJATB034	P_{SV40}-Gid1b-VP16-IRES-TetR-RGA-pA GID1b was PCR amplified from pSLS412 with oJATB039/oJATB040. pJATB028 was linearized with SpeI/EcoRV. Both fragments were assembled using AQUA cloning.	This work
pJATB035	P_{SV40}-Gid1c-VP16-IRES-TetR-RGA-pA GID1c was PCR amplified from pSLS413 with oJATB041/oJATB042. pJATB028 was linearized with SpeI/EcoRV. Both fragments were assembled using AQUA cloning.	This work
pJATB057	P_{SV40}-SLY1-VP16-IRES-TetR-GAI-pA GAI was PCR amplified from pSLS404 with oJATB035/oJATB036. pJATB025 was linearized with BsrGI/AscI. Both fragments were assembled by AQUA cloning.	This work
pJATB058	P_{SV40}-SLY1-VP16-IRES-TetR-RGA-pA RGA was PCR amplified from pSLS405 with oJATB033/oJATB034. pJATB025 was linearized with BsrGI/AscI. Both fragments were assembled by AQUA cloning.	This work
pJATB059	P_{SV40}-GID1a-VP16-IRES-TetR-SLY1-pA GID1a was PCR amplified from pSLS411 with oJATB037/oJATB038. pJATB023 was linearized with SpeI/EcoRV. Both fragments were assembled using AQUA cloning.	This work

Appendix

pJATB060	P_{SV40}-GID1b-VP16-IRES-TetR-SLY1-pA GID1b was PCR amplified from pSLS412 with oJATB039/oJATB040. pJATB023 was linearized with SpeI/EcoRV. Both fragments were assembled using AQUA cloning.	This work
pJATB061	P_{SV40}-GID1c-VP16-IRES-TetR-SLY1-pA GID1c was PCR amplified from pSLS413 with oJATB041/oJATB042. pJATB023 was linearized with SpeI/EcoRV. Both fragments were assembled using AQUA cloning.	This work
pJATB066	P_{SV40}-GAI-VP16-IRES-E-GID1a-pA E-Protein was PCR-amplified from pWW035 with oJATB074/075. pJATB003 was linearized with NotI/BsrGI. Both fragments were assembled using AQUA cloning.	This work
pJATB067	P_{SV40}-GAI-VP16-IRES-E-GID1b-pA E-Protein was PCR-amplified from pWW035 with oJATB074/076. pJATB004 was linearized with NotI/BsrGI. Both fragments were assembled using AQUA cloning.	This work
pJATB068	P_{SV40}-GAI-VP16-IRES-E-GID1c-pA E-Protein was PCR-amplified from pWW035 with oJATB074/077. pJATB005 was linearized with NotI/BsrGI. Both fragments were assembled using AQUA cloning.	This work
pJATB069	P_{SV40}-RGA-VP16-IRES-E-GID1a-pA E-Protein was PCR-amplified from pWW035 with oJATB074/075. pJATB006 was linearized with NotI/BsrGI. Both fragments were assembled using AQUA cloning.	This work
pJATB070	P_{SV40}-RGA-VP16-IRES-E-GID1b-pA E-Protein was PCR-amplified from pWW035 with oJATB074/076. pJATB007 was linearized with NotI/BsrGI. Both fragments were assembled using AQUA cloning.	This work
pJATB071	P_{SV40}-RGA-VP16-IRES-E-GID1c-pA E-Protein was PCR-amplified from pWW035 with oJATB074/077. pJATB008 was linearized with NotI/BsrGI. Both fragments were assembled using AQUA cloning.	This work
pJATB072	P_{SV40}-GID1a-VP16-IRES-E-GAI-pA E-Protein was PCR-amplified from pWW035 with oJATB074/078. pJATB030 was linearized with NotI/BsrGI. Both fragments were assembled using AQUA cloning.	This work
pJATB073	P_{SV40}-GID1b-VP16-IRES-E-GAI-pA E-Protein was PCR-amplified from pWW035 with oJATB074/078. pJATB031 was linearized with NotI/BsrGI. Both fragments were assembled using AQUA cloning.	This work
pJATB074	P_{SV40}-GID1c-VP16-IRES-E-GAI-pA E-Protein was PCR-amplified from pWW035 with oJATB074/078. pJATB032 was linearized with NotI/BsrGI. Both fragments were assembled using AQUA cloning.	This work
pJATB075	P_{SV40}-GID1a-VP16-IRES-E-RGA-pA E-Protein was PCR-amplified from pWW035 with oJATB074/079. pJATB033 was linearized with NotI/BsrGI. Both fragments were assembled using AQUA cloning.	This work

Appendix

pJATB076	P_{SV40}-GID1b-VP16-IRES-E-RGA-pA E-Protein was PCR-amplified from pWW035 with oJATB074/079. pJATB034 was linearized with NotI/BsrGI. Both fragments were assembled using AQUA cloning.	This work
pJATB077	P_{SV40}-GID1c-VP16-IRES-E-RGA-pA E-Protein was PCR-amplified from pWW035 with oJATB074/079. pJATB035 was linearized with NotI/BsrGI. Both fragments were assembled using AQUA cloning.	This work
pJATB078	P_{SV40}-SLY1-VP16-IRES-E-GID1a-pA E-Protein was PCR-amplified from pWW035 with oJATB074/075. pJATB025 was linearized with NotI/BsrGI. Both fragments were assembled using AQUA cloning.	This work
pJATB079	P_{SV40}-SLY1-VP16-IRES-E-GID1b-pA E-Protein was PCR-amplified from pWW035 with oJATB074/076. pJATB026 was linearized with NotI/BsrGI. Both fragments were assembled using AQUA cloning.	This work
pJATB080	P_{SV40}-SLY1-VP16-IRES-E-GID1c-pA E-Protein was PCR-amplified from pWW035 with oJATB074/077. pJATB027 was linearized with NotI/BsrGI. Both fragments were assembled using AQUA cloning.	This work
pJATB081	P_{SV40}-SLY1-VP16-IRES-E-GAI-pA E-Protein was PCR-amplified from pWW035 with oJATB074/078. pJATB057 was linearized with NotI/BsrGI. Both fragments were assembled using AQUA cloning.	This work
pJATB082	P_{SV40}-SLY1-VP16-IRES-E-RGA-pA E-Protein was PCR-amplified from pWW035 with oJATB074/079. pJATB058 was linearized with NotI/BsrGI. Both fragments were assembled using AQUA cloning.	This work
pJATB083	P_{SV40}-GID1a-VP16-IRES-E-SLY1-pA E-Protein was PCR-amplified from pWW035 with oJATB074/080. pJATB059 was linearized with NotI/BsrGI. Both fragments were assembled using AQUA cloning.	This work
pJATB084	P_{SV40}-GID1b-VP16-IRES-E-SLY1-pA E-Protein was PCR-amplified from pWW035 with oJATB074/080. pJATB060 was linearized with NotI/BsrGI. Both fragments were assembled using AQUA cloning.	This work
pJATB085	P_{SV40}-GID1c-VP16-IRES-E-SLY1-pA E-Protein was PCR-amplified from pWW035 with oJATB074/080. pJATB061 was linearized with NotI/BsrGI. Both fragments were assembled using AQUA cloning.	This work
pJATB086	P_{SV40}-GAI-VP16-IRES-E-SLY1-pA E-Protein was PCR-amplified from pWW035 with oJATB074/080. pJATB023 was linearized with NotI/BsrGI. Both fragments were assembled using AQUA cloning.	This work
pJATB087	P_{SV40}-RGA-VP16-IRES-E-SLY1-pA E-Protein was PCR-amplified from pWW035 with oJATB074/080. pJATB024 was linearized with NotI/BsrGI. Both fragments were assembled using AQUA cloning.	This work

Appendix

pTB053	P_{SV40}-PIF3-9AA-Linker-mEGFP-pA Expression vector encoding the <i>A.thaliana</i> PIF fused to the fluorescent protein mEGFP under control of P _{SV40} .	unpublished
pTB200	P_{SV40}-GAI-mCherry-pA GAI was amplified from pSLS405 with oligos oTB064/065. mCherry was amplified from pSJ050 with oligos oTB066/067. pMZ333 was linearized by NotI/XbaI. Fragments were assembled using AQUA cloning.	This work
pTB204	P_{SV40}-GID1b-EGFP-pA GID1b was amplified from pSLS412 with oligos oTB077/083. mEGFP was amplified from pHB090 with oligos oTB085/061. pMZ333 was linearized by NotI/XbaI. Fragments were assembled using AQUA cloning.	This work
pTB210	P_{SV40}-ARR1ΔDKK-mEGFP-pA ARR1ΔDKK was amplified from pSLS443 with oligos oTB099/100. mEGFP was amplified from pTB204 with oligos oTB101/102. pMZ333 was linearized by NotI/XbaI. Fragments were assembled using AQUA cloning.	This work
pTB227	P_{SV40}-GID1b-9AA-Linker-mEGFP-pA GID1b was PCR-amplified from pSLS434 with oTB203/204. pTB053 was linearized by NotI/AfeI. Both fragments were assembled using AQUA cloning.	This work
pTB228	P_{SV40}-GID1b-9AA-Linker-mEGFP-9AA-Linker-mCherry-pA mCherry was amplified from pTB200 with oTB255/256. pTB227 was PCR-amplified with oTB212/254. Both fragments were assembled using AQUA cloning.	This work
pTB233	P_{SV40}-GAI-9AA-Linker-mCherry-CAAX(unphosphorylatable)-pA GAI was PCR-amplified from pTB200 with oTB064/244. pTB216 was PCR-amplified with oTB210/246. Both fragments were assembled using AQUA cloning.	This work
pTB235	P_{SV40}-mEGFP-GID1b-pA GID1b was PCR-amplified from pTB204 with oTB248/249. pTB400 was PCR-amplified with oTB212/247. Both fragments were assembled using AQUA cloning.	This work
pTB239	P_{SV40}-GAI-9AA-Linker-mCherry-NLS-pA GAI-9AA-Linker-mCherry was PCR-amplified from pTB233 with oTB064/257. pMZ333 was linearized by NotI/XbaI. Both fragments were assembled using AQUA cloning.	This work
pTB240	P_{SV40}-GAI-9AA-Linker-mCherry-NES-pA GAI-9AA-Linker-mCherry was PCR-amplified from pTB233 with oTB064/258. pMZ333 was linearized by NotI/XbaI. Both fragments were assembled using AQUA cloning.	This work
pTB243	P_{SV40}-GAI-9AA-Linker-mCherry-pA GAI-9AA-Linker-mCherry was PCR-amplified from pTB233 with oTB064/261. pMZ333 was linearized by NotI/XbaI. Both fragments were assembled using AQUA cloning.	This work

Appendix

pTB245	P_{SV40}-mCherry-9AA-Linker-GAI-pA mCherry was PCR-amplified from pTB200 with oTB263/264. GAI was PCR-amplified from pTB216 with oTB265/266. pMZ333 was linearized by NotI/XbaI. Fragments were assembled using AQUA cloning.	This work
pTB258	P_{SV40}-NLS-mCherry-5AA-Linker-GAI-pA GAI was PCR-amplified from pTB200 with oTB296/266. pTB262 was PCR-amplified with oTB212/247. Both fragments were assembled using AQUA cloning.	This work
pTB259	P_{SV40}-NLS-mCherry-7AA-Linker-GAI-pA GAI was PCR-amplified from pTB200 with oTB297/266. pTB262 was PCR-amplified with oTB212/247. Both fragments were assembled using AQUA cloning.	This work
pTB262	P_{SV40}-NLS-mCherry-9AA-Linker-GAI-pA mCherry-GAI was PCR-amplified from pTB245 with oTB291/266. pMZ333 was linearized by NotI/XbaI. Both fragments were assembled using AQUA cloning.	This work
pTB263	P_{SV40}-mCherry-GID1b-pA GID1b was PCR-amplified from pTB204 with oTB249/292. pTB245 was PCR-amplified with oTB212/247. Both fragments were assembled using AQUA cloning.	This work
pTB264	P_{SV40}-NLS-mEGFP-9AA-Linker-GAI-pA mEGFP was PCR-amplified from pTB210 with oTB291/264. pTB262 was PCR-amplified with oTB265/293. Both fragments were assembled using AQUA cloning.	This work
pTB265	P_{SV40}-mEGFP-NLS-pA mEGFP was PCR-amplified from pTB210 with oTB299/300. pMZ333 was linearized by NotI/XbaI. Both fragments were assembled using AQUA cloning.	This work
pTB267	P_{SV40}-mEGFP-GID1a-pA GID1a was PCR-amplified from pJATB006 with oTB301/302. pTB400 was PCR-amplified with oTB212/247. Both fragments were assembled using AQUA cloning.	This work
pTB268	P_{SV40}-mEGFP-GID1c-pA GID1c was PCR-amplified from pJATB008 with oTB303/304. pTB400 was PCR-amplified with oTB212/247. Both fragments were assembled using AQUA cloning.	This work
pTB271	P_{SV40}-mCherry-SLY1-pA SLY1 was PCR-amplified from pJATB023 with oTB318/320. pTB263 was PCR-amplified with oTB212/247. Both fragments were assembled using AQUA cloning.	This work
pTB272	P_{SV40}-mEGFP-SLY1-pA SLY1 was PCR-amplified from pJATB023 with oTB319/320. pTB400 was PCR-amplified with oTB212/247. Both fragments were assembled using AQUA cloning.	This work
pTB400	P_{SV40}-mEGFP-PAS-LOV_{wr}-pA Expression vector encoding the PASLOV fused to the fluorescent protein mEGFP under control of P _{SV40} .	unpublished

112
113
114

Table S3: Oligonucleotides used for cloning in this work.

Oligonucleotide	Sequence (5' → 3')
oJATB001	GTCTTTTATTTTCAGGTCCCAGGATCGGAATTGACTAGTCCACCATGAAGAGAGATCAT
oJATB002	CTACCAGCACTACCAGCACTATCGAATTCGATATCATTGGTGGAGAGTTTCCAAG
oJATB003	GTCTTTTATTTTCAGGTCCCAGGATCGGAATTGACTAGTCCACCATGAAGAGAGATCATCACC AATTCC
oJATB004	CTACCAGCACTACCAGCACTATCGAATTCGATATCGTACGCCGCCGTCGA
oJATB005	AGGCGGTGGAAGTGGTGGCGGAGGTAGCGATTGTACAATGGCTGCGAGCGAT
oJATB006	TATCTTATCATGTCTGGATCGAAGCTTTTAGGCGCGCCTTAACATCCGCGTTTACAAACG
oJATB007	AGGCGGTGGAAGTGGTGGCGGAGGTAGCGATTGTACAATGGCTGGTGGTAACGA
oJATB008	TATCTTATCATGTCTGGATCGAAGCTTTTAGGCGCGCCCTAAGGAGTAAGAAGCACAGGA
oJATB009	GAGGCGGTGGAAGTGGTGGCGGAGGTAGCGATTGTACAATGGCTGGAAGTGAAGAAG
oJATB010	TATCTTATCATGTCTGGATCGAAGCTTTTAGGCGCGCCTATTGGCATTCTGCGTTTA
oJATB029	GGCGGTGGAAGTGGTGGCGGAGGTAGCGATTGTACAATGAAGCGCAGTACTACC
oJATB030	TATCTTATCATGTCTGGATCGAAGCTTTTAGGCGCGCCTATTGGATTCTGGAAGAGGTC
oJATB031	TCTTTTATTTTCAGGTCCCAGGATCGGAATTGACTAGTCCACCATGAAGCGCAGT
oJATB032	ACTACCAGCACTACCAGCACTATCGAATTCGATATCTTTGGATTCTGGAAGAGGTCTCTTA
oJATB033	GGCGGTGGAAGTGGTGGCGGAGGTAGCGATTGTACAATGAAGAGAGATCATCACC AATT CCAAGG
oJATB034	TATCTTATCATGTCTGGATCGAAGCTTTTAGGCGCGCCCTAGTACGCCGCCGTCGA
oJATB035	GGCGGTGGAAGTGGTGGCGGAGGTAGCGATTGTACAATGAAGAGAGATCATCATCATCA TC
oJATB036	TATCTTATCATGTCTGGATCGAAGCTTTTAGGCGCGCCCTAATTGGTGGAGAGTTTCCAAG
oJATB037	ACTACCAGCACTACCAGCACTATCGAATTCGATATCACATTCGCGTTTACAAACGC
oJATB038	CTTTTATTTTCAGGTCCCAGGATCGGAATTGACTAGTCCACCATGGCTGCGAGCGAT
oJATB039	ACTACCAGCACTACCAGCACTATCGAATTCGATATCAGGAGTAAGAAGCACAGGACTTG
oJATB040	CTTTTATTTTCAGGTCCCAGGATCGGAATTGACTAGTCCACCATGGCTGGTGG
oJATB041	CTTTTATTTTCAGGTCCCAGGATCGGAATTGACTAGTCCACCATGGCTGGAAG
oJATB042	ACTACCAGCACTACCAGCACTATCGAATTCGATATCTTGGCATTCTGCGTTTACAAATG
oJATB074	ACAGATTGTTATCATAAAGCGAATTGGATTGCGGCCGCGAATTCATATGCCCCGCCCAA G
oJATB075	AATAAGATTAACCTTCATCGCTCGCAGCCATTCTGCGGAACCAGCACTGCCGGCGCTGTT ATGTACAATTAAGCTGTACGCGGACG
oJATB076	GTTAAGGTTGACTTCGTTACCACCGCCATTCTGCGGAACCAGCACTGCCGGCGCTGTT ATGTACAATTAAGCTGTACGCGGACG
oJATB077	AATAAGATTAACCTTCATCGCTCGCAGCCATTCTGCGGAACCAGCACTGCCGGCGCTGTT TGTACAATTAAGCTGTACGCGGACG
oJATB078	ATGATGATGATGATGATGATCTCTTTCATACCAGCACTACCAGCACTACCAGCACTGTTA TGTACAATTAAGCTGTACGCGGACG
oJATB079	CGTCCGCGTACAGCTTAATTGTACATAACAGTGTGGTAGTGTGGTAGTGTGGTATGA AGAGAGATCATCACC AATTCCAAGG
oJATB080	CAAAATCAGAGTCGGTAGTACTGCGCTTATTCTGCGGAACCAGCACTGCCGGCGCTGTT ATGTACAATTAAGCTGTACGCGGACG
oSLS414	CAGGTCCCAGGATCGAATTGCGGCCGAGGAGGCCACCATTGGCTGCGAGCGATGAAG TTAATCTTATTG
oSLS416	CAGGTCCCAGGATCGAATTGCGGCCGAGGAGGCCACCATTGGCTGGTGGTAACGAAG TCAACC
oSLS418	CAGGTCCCAGGATCGAATTGCGGCCGAGGAGGCCACCATTGGCTGGAAGTGAAGAAG TTAATCTTATTGAG
oSLS420	CAGGTCCCAGGATCGAATTGCGGCCGAGGAGGCCACCATTGGCTGGAAGTGAAGAAG CTCTG
oSLS436	TACCCATACGATGTTCCAGATTACGCTTAGTCTAGAGTCGACCTGCAGCCCAAG
oSLS438	AGCGTAATCTGGAACATCGTATGGGTACACCTTCGCTTTTTCTTGGGACATTCGCGGTT ACAAACGCCGAAATC
oSLS439	AGCGTAATCTGGAACATCGTATGGGTACACCTTCGCTTTTTCTTGGGAGGAGTAAGAAG CACAGGACTTGACTTG
oSLS440	AGCGTAATCTGGAACATCGTATGGGTACACCTTCGCTTTTTCTTGGGTTGGCATTCTGCG TTTACAAATGCAGCTATC
oSLS441	AGCGTAATCTGGAACATCGTATGGGTACACCTTCGCTTTTTCTTGGGTTGGATTCTGGA AGAGGTCTCTTAGTG

Appendix

oSLS442 CCGCAATTCGATCCGGGACCTG
oSLS443 GAATTCGATAGTCTGGTAGTCTGGTAG
oSLS444 CAGGTCCCGGATCGAATTGCGGCCGAGGAGGCCACCATGAAGAGAGATCATCATCA
TCATCATCATCAAGATAAG
oSLS445 CTACTTGTATCGTCTGCTTGTAGTCCACCTTCCGCTTTTTCTTGGGATTGGTGGAGAGT
TTCCAAGCCGAG
oSLS446 CAGGTCCCGGATCGAATTGCGGCCGAGGAGGCCACCATGAAGAGAGATCATCACCA
ATTCCAAGGTC
oSLS447 CTACTTGTATCGTCTGCTTGTAGTCCACCTTCCGCTTTTTCTTGGGGTACGCCGCCGTC
GAGAGTTTC
oSLS448 GACTACAAGGACGACGATGACAAGTAGTCTAGAGTCGACCTGCAGCCCAAG
oSLS454 CAGGTCCCGGATCGAATTGCGGCCGAGGAGGCCACCATGTACCGAAGAGGAAAG
ACGAGG
oSLS455 AGCGTAATCTGGAACATCGTATGGGTACACCTTCCGCTTTTTCTTGGGAACCGGAATGTTA
TCGATGGAGTATGCG
oSLS463 CTACCAGCACTACCAGCACTATCGAATTCAACCGGAATGTTATCGATGGAGTATGCG
oSLS466 AGCGTAATCTGGAACATCGTATGGGTACACCTTCCGCTTTTTCTTGGGCC
oSLS470 GAAAAGTGCCACCTGACGTCGTCGACGATATCGGCCAGTGCCAAGCTTATGCTAGC
oSLS471 ACGAGCTCTGCTTATATAGGGCTAGCTCGCGAGAGGAAGGGCTTGGCTAGAAAAATCC
oTB061 CTGGATCGAAGCTTGGGCTGCAGGTCGACTGATATCTTACTTGTACAGCTCGTCCATGC
oTB064 TCTTTTATTTAGGTCCCGGATCGAATTGCGCGGCCGCCACCATGAAGAGAGATCAT
oTB065 ATCCTCCTCGCCCTTGTCTACCATGCTGAATTGGTGGAGAGTTTCCAA
oTB066 GCCACCTCGGCTTGGAACTCTCCACCAATTCAGCAATGGTGGAGCAAGGG
oTB067 CTGGATCGAAGCTTGGGCTGCAGGTCGACTTCTAGACTACTTGTACAGCTCGTCCATGC
oTB077 TCTTTTATTTAGGTCCCGGATCGAATTGCACCGGTCCACCATGGCTGGTGG
oTB083 CAGCTCCTCGCCCTTGTCTACCATGCTGCCAGGAGTAAGAAGCACAGGACTTG
oTB085 AGCAAGTCAAGTCTGTGCTTCTACTCCTGGCAGCATGGTGGAGCAAG
oTB099 TCTTTTATTTAGGTCCCGGATCGAATTGCGCGGCCGCCACCATGTACCGAA
oTB100 CAGCTCCTCGCCCTTGTCTACCATGCTGCCAACCAGGAATGTTATCGATGG
oTB101 GACGCATACTCCATCGATAACATTCCGGTTGGCAGCATGGTGGAGCAAG
oTB102 GATCGAAGCTTGGGCTGCAGGTCGACTCTAAGCGCTTTACTTGTACAGCTCGTCCATGC
oTB203 TCTTTTATTTAGGTCCCGGATCGAATTGCGCGGCCGCCACCATGGCTGGTGG
oTB204 CTTGCTACCATGCCGCTGGCGCTGCCAGCGCTGGCGCCAGGAGTAAGAAGCACAGGAC
TTGA
oTB210 GCAATTCGATCCGGGACCT
oTB212 AGTCGACCTGCAGCCC
oTB244 CATGTTATCCTCCTCGCCCTTGTCTACCATGCCGCTGGCGCTGCCAGCGCTGGCGCCATT
GGTGGAGAGTTTCCAA
oTB246 ATGGTGAGCAAGGGCGAG
oTB247 CTTGTACAGCTCGTCCATGCC
oTB248 ATCACTCTGGCATGGACGAGCTGTACAAGGGCAGCATGGCTGGTGGTAACGAAGT
oTB249 CTGGATCGAAGCTTGGGCTGCAGGTCGACTGCGATCGCCTAAGGAGTAAGAAGCACAGG
ACTT
oTB254 GCGCGCCGCTGCCGGCCTGCCGCTGGCCTTGTACAGCTCGTCCATGCC
oTB255 GCCAGCGCAGCGCCGGCAGCGGCCCATGGTGGAGCAAGGGCGA
oTB256 CTGGATCGAAGCTTGGGCTGCAGGTCGACTGCGATCGCCTACTTGTACAGCTCGTCCATG
C
oTB257 CTGGATCGAAGCTTGGGCTGCAGGTCGACTGATATCCTACACCTTCTCTTCTTTGGC
TTGTACAGCTCGTCCAT
oTB258 CTGGATCGAAGCTTGGGCTGCAGGTCGACTGATATCCTAGATGGTGGGTCGCCAAGCTT
CTTGGTATCTTGTACAGCTCGTCCAT
oTB261 CTGGATCGAAGCTTGGGCTGCAGGTCGACTGATATCCTACTTGTACAGCTCGTCCAT
oTB263 TCTTTTATTTAGGTCCCGGATCGAATTGCGCGGCCGCCACCATGGTGGAGCAAGGGCG
A
oTB264 GCCGCTGGCGCTGCCAGCGCTGGCGCCCTTGTACAGCTCGTCCATGC
oTB265 GGCGCCAGCGCTGGCAGCGCCAGCGGCATGAAGAGAGATCATCATCATCATC
oTB266 CTGGATCGAAGCTTGGGCTGCAGGTCGACTGCGATCGCCTAATGGTGGAGAGTTTCCAA
oTB291 TCTTTTATTTAGGTCCCGGATCGAATTGCGCGGCCGCCACCATGCCAAAGAAGAAGAG
GAAGGTGATGGTGGAGCAAGGGCG

Appendix

oTB292 TCCACCGCGGCATGGACGAGCTGTACAAGGGCAGCATGGCTGGTGGTAACGAAGT
oTB293 GCAATTCGATCCGGGA
oTB296 CCACCGCGGCATGGACGAGCTGTACAAGGGCGCCAGCGCTGGCATGAAGAGAGATCA
TCATCATCATC
oTB297 CCACCGCGGCATGGACGAGCTGTACAAGGGCGCCAGCGCTGGCAGCGCCATGAAGAG
AGATCATCATCATC
oTB299 TCTTTTATTTAGGTCCCAGGATCGAATTGCGCGGCCGCCACCATTGGTGAGCAAGGGCG
A
oTB300 CTGGATCGAAGCTTGGGCTGCAGGTCGACTGATATCCTACACCTTCCTCTTCTTTGGC
TTGTACAGCTCGTCCATGC
oTB301 ATCACTCTCGGCATGGACGAGCTGTACAAGGGCAGCATGGCTGCGAGCGATG
oTB302 CTGGATCGAAGCTTGGGCTGCAGGTCGACTGCGATCGCTTAACATTCCGCGTTTACAAAC
GC
oTB303 ATCACTCTCGGCATGGACGAGCTGTACAAGGGCAGCATGGCTGGAAGTGAAGAAG
oTB304 CTGGATCGAAGCTTGGGCTGCAGGTCGACTGCGATCGCTCATTGGCATTCTGCGTTTA
oTB318 TCCACCGCGGCATGGACGAGCTGTACAAGGGCAGCATGAAGCGCAGTACTACC
oTB319 ATCACTCTCGGCATGGACGAGCTGTACAAGGGCAGCATGAAGCGCAGTACTACC
oTB320 CTGGATCGAAGCTTGGGCTGCAGGTCGACTGCGATCGCTTATTGGATTCTGGAAGAGGT
oTB331 GGCGGTGGAAGTGGTGGCGAGGTAGCGATGCGATCGCTATGGAAGCAAAACCTTAGC

115

116

117 References

118

119 **Müller K, Engesser R, Schulz S, Steinberg T, Tomakidi P, Weber CC, Ulm R, Timmer J,**

120 **Zurbriggen MD, Weber W** (2013) Multi-chromatic control of mammalian gene

121 expression and signaling. *Nucleic Acids Res* **41**: e124–e124

122 **Weber W, Fux C, Daoud-El Baba M, Keller B, Weber CC, Kramer BP, Heinzen C, Aubel D,**

123 **Bailey JE, Fussenegger M** (2002) Macrolide-based transgene control in mammalian cells

124 and mice. doi: 10.1038/nbt731

125

7.1.2 Blue Light-Operated CRISPR/Cas13b-Mediated mRNA Knockdown (Lockdown)

COMMUNICATION

**ADVANCED
BIOLOGY**
www.advanced-bio.com

Blue Light-Operated CRISPR/Cas13b-Mediated mRNA Knockdown (Lockdown)

Tim Blomeier, Patrick Fischbach, Leonie-Alexa Koch, Jennifer Andres, Miguel Miñambres, Hannes Michael Beyer, and Matias Daniel Zurbriggen*

The introduction of optogenetics into cell biology has furnished systems to control gene expression at the transcriptional and protein stability level, with a high degree of spatial, temporal, and dynamic light-regulation capabilities. Strategies to downregulate RNA currently rely on RNA interference and CRISPR/Cas-related methods. However, these approaches lack the key characteristics and advantages provided by optical control. “Lockdown” introduces optical control of RNA levels utilizing a blue light-dependent switch to induce expression of CRISPR/Cas13b, which mediates sequence-specific mRNA knockdown. Combining Lockdown with optogenetic tools to repress gene-expression and induce protein destabilization with blue light yields efficient triple-controlled downregulation of target proteins. Implementing Lockdown to degrade endogenous mRNA levels of the cyclin-dependent kinase 1 (hCdk1) leads to blue light-induced G2/M cell cycle arrest and inhibition of cell growth in mammalian cells.

The integration of optogenetic switches into a broad range of molecular tools has recently revolutionized biological studies by opening the possibility to control cellular processes with unmatched spatiotemporal precision. A myriad of optoswitches has been engineered and applied in prokaryotic and eukaryotic cells to regulate gene expression, subcellular protein localization, enzyme activity, and even to develop light-controllable biohybrid materials among other processes and systems (see www.optobase.com).^[1]

The late explosion of enabling technologies to modulate the flow of genetic information, made possible through methods

T. Blomeier, Dr. P. Fischbach, L.-A. Koch, Dr. J. Andres, Dr. M. Miñambres, Dr. H. M. Beyer, Prof. M. D. Zurbriggen
Institute of Synthetic Biology and CEPLAS
University of Düsseldorf
Düsseldorf 40225, Germany
E-mail: matias.zurbriggen@uni-duesseldorf.de
Dr. M. Miñambres
Institute of Plant Biochemistry and CEPLAS
University of Düsseldorf
Düsseldorf 40225, Germany

 The ORCID identification number(s) for the author(s) of this article can be found under <https://doi.org/10.1002/adbi.202000307>.

© 2021 The Authors. Advanced Biology published by Wiley-VCH GmbH. This is an open access article under the terms of the Creative Commons Attribution-NonCommercial-NoDerivs License, which permits use and distribution in any medium, provided the original work is properly cited, the use is non-commercial and no modifications or adaptations are made.

DOI: 10.1002/adbi.202000307

Adv. Biology 2021, 2000307

2000307 (1 of 7)

that derive from clustered regularly interspaced short palindromic repeats (CRISPR)-based techniques, currently positively reshapes biological studies.^[2] Key applications of the specific DNA-recognizing CRISPR/Cas9 systems encompass for example genome editing and transcriptional regulation with high sequence specificity.^[2–6] In recent years, these technologies led to major advances in synthetic biology, gene therapy, and gene modification in almost every model organism. Various Cas-variants were subsequently derived from different microorganisms and utilized to overcome some of the limitations restricting in vivo applications, or enabled the recognition of RNA instead of DNA.^[2,7–9] Among those, the discovery of the RNA-targeting Cas13 proteins yielded in powerful RNA-editing tools.^[9,10] Cas13 belongs to type VI CRISPR effectors and has been utilized for specific knockdown of endogenous RNAs in human cells and manipulation of alternative RNA splicing.^[9,11] While the DNA-targeting CRISPR/Cas9 systems require the presence of a short protospacer adjacent motif (PAM) sequence at the editing site, Cas13 is PAM-independent.^[9,10]

Recent engineering efforts of CRISPR/Cas tools for optogenetic regulation expanded their capabilities including high spatial and temporal control precision,^[12–19] however, these systems exclusively target DNA. Only few light-regulated RNA modification tools currently exist, mostly based on RNA interference or short regulatory RNAs, which are CRISPR-independent.^[20–23]

We devised here an optogenetic tool to destabilize cellular mRNA by enabling optical control of RNA-targeting CRISPR/Cas13 systems. For this, we combined a blue light-inducible gene expression switch^[24] with the *Prevotella* sp.-derived Cas13b effector (*PspCas13b*),^[9] resulting in a system termed Lockdown (blue light-operated CRISPR/Cas13b-mediated mRNA knockdown). Blue light activates the gene switch to induce the expression of *PspCas13b* which, in the presence of a gRNA targeting the mRNA of interest, leads to downregulation of said RNA. Our results demonstrate how Lockdown can be used to regulate cellular processes with blue light through specific mRNA degradation. In our tests, these induced G2 cell cycle arrest and inhibition of cell growth under blue light.^[25,26] We further combined Lockdown with the recently published “Blue-OFF” system for synergistic triple-targeted downregulation of proteins.^[27,28]

To engineer the Lockdown system, we used a split transcription factor based on a modified light-oxygen-voltage domain

© 2021 The Authors. Advanced Biology published by Wiley-VCH GmbH

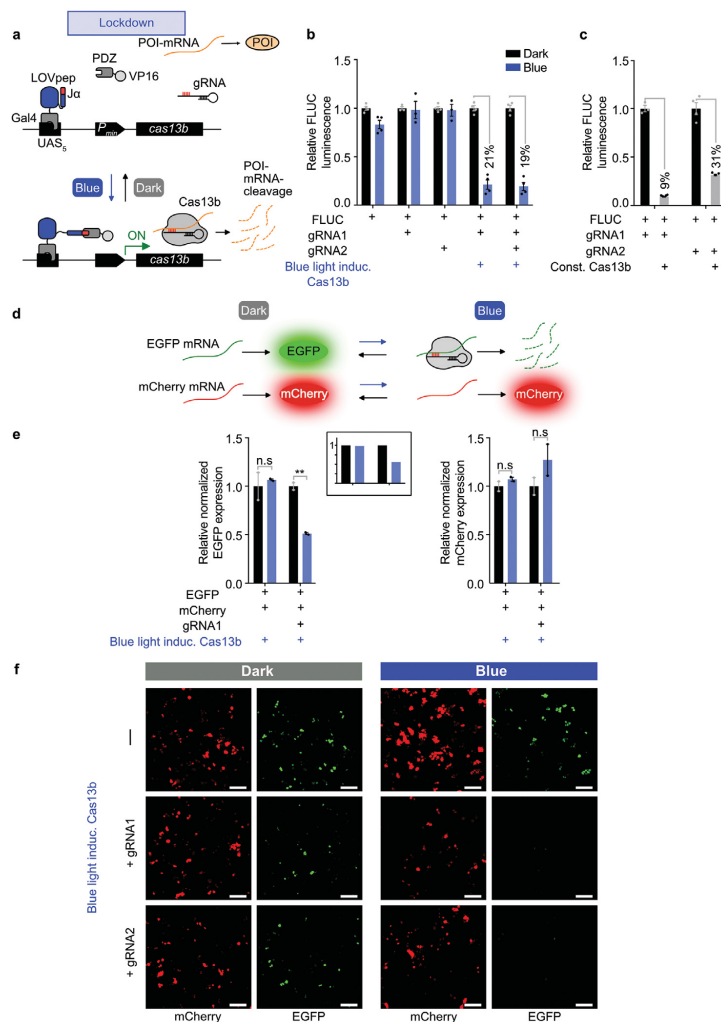


Figure 1. Design and characterization of the Lockdown system. a) Lockdown architecture. The blue light-responsive split transcription factor, bound to DNA via Gal4, activates expression of the gene encoding Cas13b upon illumination. Light recruits the transcriptional activator VP16 via exposure of a PDZ-interacting epitope embedded in the J α helix. A specific gRNA guides Cas13b to cleave a target mRNA encoding a protein of interest (POI). b) Co-expression of FLUC-specific gRNA1 (pTBPF003) or gRNA2 (pTBPF004) causes reduction of FLUC (pTBPF015) levels in HEK-293T cells using Lockdown to control the expression of Cas13b. The cells were either illuminated with 460 nm light for 24 h (blue bars) or kept in the dark (black bars). Values from illuminated samples were normalized to the corresponding sample kept in the dark. c) Experiment as in (b), but with co-expression of constitutive Cas13b (pC0046). Data were normalized to the conditions lacking the Cas13b expression plasmid. (b,c) $n = 4$; error bars represent one standard error of the mean (SEM). Significance was calculated with a paired students t -test ($*P < 0.05$; $**P < 0.01$; $***P < 0.001$). Inlet figure (center) shows the quantification of normalized intensities of an α -EGFP western blot analysis of the same experiment (see Figure S5, Supporting Information). d) Schematic of the blue light-induced knockdown of EGFP mRNA. Under blue light, Lockdown specifically degrades mRNA encoding EGFP while leaving mCherry unaffected. e) Quantification of EGFP (left) and mCherry (right) expression via qRT-PCR. HEK-293T cells were co-transfected with the blue light switch, P_{PCIK}-EGFP, and P_{SV40}-mCherry. An EGFP-specific gRNA was included (gRNA1, pTBPF005). Illumination for 48 h was started 4 h post transfection, or cells were kept in the dark. $n = 2$; error bars represent one standard error of the mean (SEM). Significance was calculated with a paired students t -test ($*P < 0.05$; $**P < 0.01$; $***P < 0.001$). Inlet figure (center) shows the quantification of normalized intensities of an α -EGFP western blot analysis of the same experiment (see Figure S5, Supporting Information). f) Microscopic analysis of EGFP and mCherry expression. HEK-293T cells were co-transfected with Lockdown and EGFP-specific gRNAs (-, none; gRNA1, pTBPF005; gRNA2, pTBPF006). Illumination conditions as in (e). Pictures were acquired by confocal imaging of EGFP and mCherry. Scale bar, 100 μ m.

from phototropin 1 of *Avena sativa* (AsLOV2) to express an engineered variant of PspCas13b (Figure 1a).^[19,24,29] We placed the gene encoding PspCas13b downstream of a minimal human cytomegalovirus promoter harboring five adjacent repeats of the Gal4 upstream activating sequence (UAS₅). Bound to DNA via fusion to the Gal4 DNA-binding domain, AsLOV2 exposes a C-terminal epitope tag through relaxation of the J α -helix under blue light. Tag exposure recruits the transcriptional activation domain VP16, which is fused to the tag-interacting ePDZ domain and leads to initiation of PspCas13b gene transcription and subsequent translation. Constitutive co-expression of a sequence-specific gRNA *in trans*, guides PspCas13b to cleave target RNAs. Due to the half life time of the AsLOV2 domain in the excited state of 17 s,^[29] the transcriptional activation complex rapidly dissociates in the darkness stopping further transcription of PspCas13b.^[24]

We first tested whether Lockdown would specifically downregulate mRNA under blue light (Figure 1b,c). We designed two gRNAs targeting Firefly luciferase (FLUC) mRNA and co-expressed them with FLUC in Human embryonic kidney cells (HEK-293T). As expected, only the presence of a suitable gRNA and blue light illumination (10 $\mu\text{mol m}^{-2} \text{s}^{-1}$ at 460 nm for 24 h) reduced FLUC-levels down to about 20% compared to levels obtained from cells kept in the dark (Figure 1b). The repression levels under blue light matched the levels obtained upon constitutive PspCas13b expression (Figure 1c).^[9]

In order to assess the functionality of the system in a different experimental setup, and in particular for future mid-throughput applications, we illuminated Chinese hamster ovary cells (CHO-K1) in 96-well glass bottom plates with different blue light intensities using an optoPlate-96 illumination device (Figure S1, Supporting Information).^[30,31] In this multi-well plate format, the downregulation of FLUC levels under blue light compared well with the results in HEK-293T cells (Figure 1b), even at lower light intensities.

We next set to complete the evaluation of the functionality of the system, by performing an experiment to analyze the effects of Lockdown as reflected at the mRNA and protein levels using three different methods (Figure 1d–f). For this, we designed two EGFP-specific gRNAs and expressed EGFP from a constitutive PGK promoter. Co-expression of mCherry served as control to validate that loss of EGFP abundance under blue light occurs specifically and not as a result of an artifact. Quantitative real-time PCR (qRT-PCR) experiments showed a clear reduction in mRNA levels for EGFP while those of mCherry remained comparable between samples that were either illuminated with blue light or kept in the dark (Figure 1e). The mRNA degradation effects also showed the expected dependence on the presence of a corresponding selective gRNA. In a microscopic analysis at the whole cell level, EGFP fluorescence remained unaffected in the absence of the Lockdown components with the matching gRNA, regardless of the illumination condition (Figure 1f, upper panel and Figure S2, Supporting Information). In contrast, the Lockdown system including either gRNA strongly reduced the EGFP signal in blue light conditions, while mCherry remained comparable in all conditions (Figure 1f, lower panels and Figure S2, Supporting Information). We further confirmed the microscopically-observed reduction in EGFP

signal under blue light using western blot analysis (Figure 1e (center) and Figure S5, Supporting Information).

Methods for downregulation of protein abundance usually target only one step of the gene expression process, which spans from the regulation of transcriptional initiation of a specific gene up to ribosomal translation into the final protein and the stability thereof.^[7,32] However, these methods are often insufficient to entirely block and/or reduce the abundance of a specific protein. A recently published optogenetic system for downregulation of protein levels (Blue-OFF) demonstrated the effect of a synergistic regulation on different levels.^[27] The system consists of two components, B-LID (blue light-inducible degradation domain), a blue light-activated protein degradation module fused to the protein of interest, and the light-responsive KRAB-EL222 repressor protein. Combined light-induced repression of transcription using KRAB-EL222 and protein stability with B-LID decreased the abundance of given cellular target proteins substantially.^[27] The remaining protein levels present after induction of transcriptional repression and protein degradation likely result from mRNA transcribed before the repression was exerted. Hence, we hypothesize that by degrading the remaining mRNA, Lockdown could contribute to a quantitative loss of the protein. We therefore combined the Blue-OFF system with Lockdown to simultaneously repress the abundance of FLUC on three regulation levels: transcriptional repression, mRNA degradation, and protein degradation (Figure 2a,b). First, we transfected HEK-293T cells with the different components of the Blue-OFF system achieving a reduction of the relative protein abundance down to 3.3% after induction with blue light in comparison to darkness (Figure 2b and Figure S3, Supporting Information). The combination of Lockdown utilizing any of the gRNAs (see Figure 1b,c) with the Blue-OFF system led to a reduction of around 99% of FLUC under blue light, demonstrating the advantages of integrating the different systems for the quantitative depletion of a protein of interest.

To demonstrate the ability of Lockdown to regulate cellular processes, we aimed at knocking down endogenous genes in mammalian cells. Since this approach does not require further protein engineering, one can in principle easily adapt the strategy to any endogenous RNA by expressing an ad hoc designed gRNA. The human cyclin-dependent kinase 1 (Cdk1)-family of kinases constitutes one of the main regulators integrating external and internal stimuli that influence cell cycle control and cell division.^[25,33–36] Cdk1 plays an essential role at the checkpoint coordinating the G2/M phase transition.^[25,26,37,38] Inhibition of Cdk1 in human cells stalls the cell cycle through a G2/M arrest, and dysregulation of factors associated with the control of Cdks frequently engage in tumor development.^[34] We designed two gRNAs targeting endogenously produced human CDK1 mRNA and tested the effects caused by blue light-induced degradation in HEK-293T cells (Figure 3a,b). Lockdown including either of the gRNA led to a significant reduction in the total cell count when cells were illuminated with blue light (Figure 3b and Figure S4, Supporting Information). The observations demonstrate the feasibility of a generalized use and the applicability of Lockdown for the blue light-dependent downregulation of endogenous mRNAs.

Use of RNA interference approaches and riboswitches have significantly contributed to groundbreaking advances in life

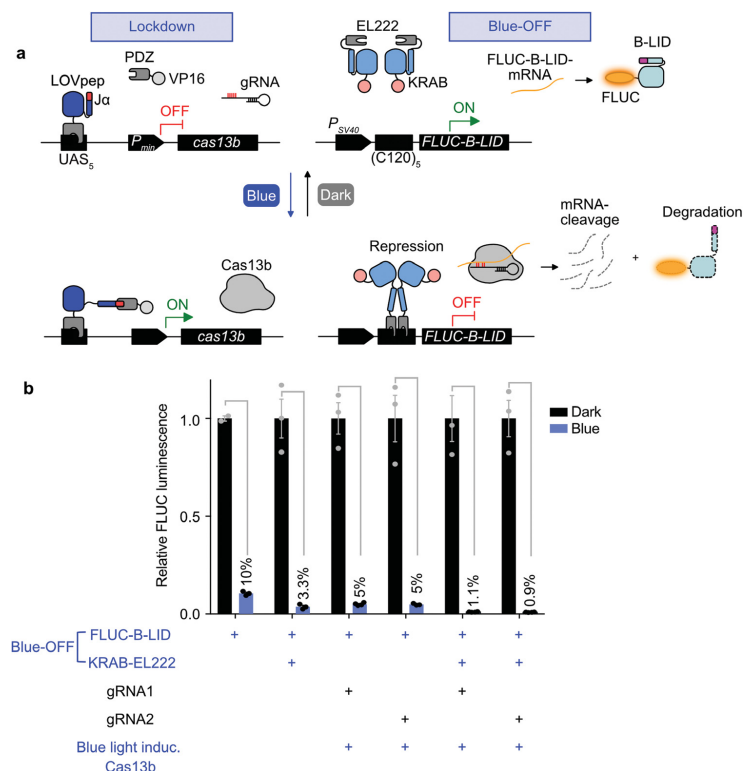


Figure 2. Combined repression of protein levels using Lockdown and Blue-OFF. a) Schematic description of the Lockdown and Blue-OFF combination setup. In the dark, Lockdown and Blue-OFF are inactive, leading to usual expression levels of target proteins (FLUC). Under blue light, Cas13b (Lockdown) cleaves the target mRNA, whereas the KRAB-EL222 repressor protein and the B-LID degen (Blue-OFF) repress FLUC production on the transcriptional and post-translational level, respectively. Under blue light, the Blue-OFF system acts by recruiting the KRAB repressor to the promoter by binding of EL222 to 5 repeats of the C120 sequence. B-LID is fused to the FLUC target protein and exposes a RRRG-degen sequence upon illumination, leading to proteasomal degradation. b) Combinatorial analysis of the Lockdown and Blue-OFF components shown in (a). FLUC bioluminescence was determined from lysates of HEK-293T cells expressing the indicated components. The gRNAs from Figure 1b,c were used. Cells were illuminated with 460 nm light for 24 h, or kept in the dark. Values were normalized to the corresponding dark sample. $n = 4$, error bars indicate one standard error of the mean (SEM).

sciences.^[39–42] These RNA tools have for example successfully been used to study signaling pathways, cancer therapeutics, and cell cycle regulation.^[42,43] However, only a few optogenetic tools for the control of mRNA exist.^[20–23] The here-described Lockdown system combines optogenetic regulation of transcription with RNA-guided RNA processing by the *PspCas13b* ribonucleoprotein to generate optogenetic control of RNA degradation. Lockdown is compatible and synergistically active with the Blue-OFF system, achieving nearly complete depletion of a protein through combined blue light-triple-induction of transcriptional repression, and mRNA and protein degradation.^[27] Lockdown synergistically combines recent independent developments in synthetic biology: One is the optogenetic switch that controls the temporal and spatial resolution of the system as well as *PspCas13b* levels depending on blue light intensity.^[24,29]

The other development is *PspCas13b*, which mainly contributes to the knockdown specificity of the system what indirectly influences also the overall efficacy. The *PspCas13b* component itself combined with Lockdown remains unchanged from earlier reports and therefore one can assume that previous characterizations of the system indicating a high specificity are valid.^[9] The LOV2-based blue light photoswitch has short dark reversion kinetics, therefore the use as gene-expression system requires a near constant illumination over the desired induction time and high light intensities when used in deep tissues due to the low penetration depth of said short wavelengths. However, it benefits from the readily bioavailable FMN cofactor in contrast to red and green optogenetic switches.

The last decade has witnessed hundreds of applications where optoswitches targeted diverse cellular processes.^[1] This

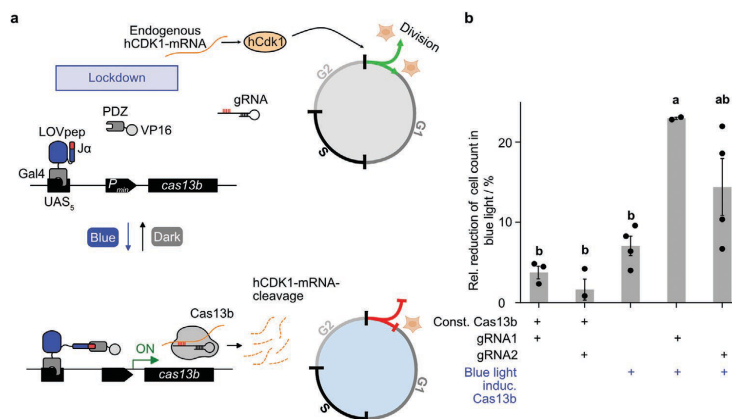


Figure 3. Cell cycle control using Lockdown. a) Human Cdk1 controls cell cycle G2/M transition. Blue light illumination activates Lockdown (see Figure 1a) to degrade endogenous hCdk1 mRNA, leading to G2 cell cycle arrest and inhibition of cell division. Constitutively expressed gRNA determines the specificity of the hCdk1 mRNA. b) The total cell count was determined from HEK-293T cells expressing the indicated components. The cell count reduction in response to 24 h of blue light illumination is shown. Illumination was started 4 h post transfection. For total cell numbers see Figure S4, Supporting Information. gRNA1 and gRNA2 were expressed from plasmids pTBPF021 and pTBPF020, respectively. $n = 4$, error bars indicate one standard error of the mean (SEM). The statistical significance was determined using a one-way ANOVA analysis ($P < 0.01$) and is indicated with bold letters.

work illustrates the potential of combining optogenetic tools for the simultaneous and orthogonal control of molecular processes. We show the wide applicability by precisely targeting different exo- and endogenous mRNAs, what solely requires the ad hoc design of a specific Cas13 gRNA. Lockdown advances the precise study of physiological effects, such as modulation of the cell cycle, and holds the future potential to assist in the investigation of unknown cellular processes.

Experimental Section

All used and designed plasmids and oligonucleotides are described in Tables S1 and S2, Supporting Information. Oligonucleotides used for quantitative real-time PCR are described in Table S3, Supporting Information. All gRNAs used in this study were designed as described elsewhere and inserted into an U6 promoter-driven mammalian expression vector.^[9] All gRNA sequences are described in Table S4 (Supporting Information). All experiments are based on transient plasmid transfection of the respective mammalian cells.

Human embryonic kidney cells (HEK-293T; DSMZ, Braunschweig, Germany) and Chinese hamster ovary cells (CHO-K1; DSMZ) were cultivated and seeded as described elsewhere.^[44] Cells were transfected in 24-well (5×10^4 cells) or 96-well (8×10^3 cells) plates using polyethyleneimine (PEI; Polysciences Inc. Europe, Hirschberg, Germany; no. 23966-1) as described.^[44] If not indicated otherwise, all plasmids were transfected with the Lockdown system consisting of the AsLOV2-based blue light system (plasmid pKM516),^[24] the inducible PspCas13b (pTBPF001), and a sequence-specific gRNA plasmid (Table S4, Supporting Information) in equal amounts w/w. 24 h post transfection, cells were illuminated with 460 nm light for the indicated periods of time with a light intensity of $10 \mu\text{mol m}^{-2} \text{s}^{-1}$ or kept in darkness (typically for 24 h, unless indicated otherwise). Samples were illuminated using custom built LED light boxes housing 460 nm light-emitting LEDs.^[45] In Figure S1, Supporting Information, illumination was done in

optoPlate-96 illumination devices.^[30,31] Cell culture work was performed using safe light (522 nm) to prevent unintended activation of the light-sensitive systems.

To quantify luciferase bioluminescence, cells were lysed and incubated as previously described.^[27] For cells grown in 96-well plates, the supernatant was removed and the substrate was directly added to the cells without prior cell lysis. Luminescence was monitored using a Centro XS³ LB960 Microplate Luminometer (Berthold Technologies, Bad Wildbad, Germany). Confocal imaging was performed with an Eclipse Ti microscope (Nikon, Tokyo, Japan) equipped with a C2plus confocal laser scanner and a 20x air objective, NA = 0.45. Cells were seeded on glass coverslips and fixed with paraformaldehyde as described.^[46] EGFP and mCherry fluorescence were visualized using an excitation laser of 488 and 561 nm and emission filters of 505–545 and 570–620 nm, respectively.

For qRT-PCR experiments, RNA was isolated using the NucleoSpin RNA Plus Kit (Macherey Nagel, Düren, Germany). The yielded RNA was further converted into cDNA utilizing the LunaScript RT SuperMix Kit (NEB, Ipswich, MA, USA). qRT-PCR experiments were conducted using a OneStepPlus Real-Time PCR system Thermal Cycling Block (Applied Biosystems, Foster City, CA, USA) and a Luna Universal Probe qPCR Master Mix (NEB) with 10 ng of cDNA per sample in triplicate reactions. Cycling conditions were set according to the master mix manufacturer's protocol.

For western blot experiments, HEK-293T cells were lysed in radioimmunoprecipitation buffer ($150 \times 10^{-3} \text{ M NaCl}$, $20 \times 10^{-3} \text{ M Tris-HCl}$, pH 7.5, 0.1% NP40, $5 \times 10^{-3} \text{ M EDTA}$) containing cComplete Mini protease inhibitor (Roche, Basel, Switzerland). The lysates were centrifuged at 13000 g for 10 min at 4 °C and the supernatants were transferred into new reaction tubes. The samples were mixed with 4x SDS buffer (Sigma Aldrich, St. Louis, MO, USA) (4:1) and incubated at 95 °C for 10 min. 10 μL of each sample were separated by SDS-PAGE on a 15% polyacrylamide gel and subsequently transferred onto a polyvinylidene fluoride membrane (Bio-Rad Laboratories, Hercules, CA, USA). The membranes were treated with the anti-GFP (Torrey Pines Biolabs, Secaucus, NJ, USA; TP-401) or anti-Actin (Sigma-Aldrich; A2066) primary antibodies. Protein detection was performed using an

anti-rabbit secondary antibody conjugated to horseradish peroxidase (Cell Signaling, Danvers, MA, USA; 70745) and the ECL detection kit (GE Healthcare, Chicago, IL, USA). Chemiluminescence was visualized using a Universal Hood III imaging system (Bio-Rad Laboratories). Band intensities were measured using ImageJ (National Institutes of Health, Bethesda, MD, USA) and normalized to the respective loading control.

For cell proliferation assays, HEK-293T cells (30×10^4 cells) were seeded in 24-well cell culture dishes and transfected as described above. Illumination was started 4 h post transfection as described before. The next day, cells were trypsinized (250 μ L, Trypsin/EDTA, PAN Biotech, Aidenbach, Germany; P10-0233500) for 4 min at 37 °C and resuspended. DMEM complete medium (1 mL) was added and cell suspension (200 μ L) was added to CASYton buffer (10 mL, OMNI Life Science, Bremen, Germany; 5651808) inside a CASYcup (OMNI Life Science) before the cell concentration was determined by electronic current exclusion (ECE) technology with a Cell counter CASY (OMNI Life Science).

Data analysis, calculation of corresponding *P*-values, and generation of graphs were done using GraphPad Prism 7 (GraphPad Software, Inc.). Data from illuminated samples shown in Figures 1b,e and 2b and Figures S1, S3 and S4 (Supporting Information) were normalized to the corresponding sample kept in the dark. In Figure 1c, data were normalized to the conditions lacking the Cas13b expression plasmid. Significance of equally treated samples of the respective light conditions in Figure 1e was calculated using a paired two-sided student's *t*-test. The statistical significance of reduction in total cell numbers in Figure 3b was determined using a one-way ANOVA analysis ($P < 0.01$) and is indicated with bold letters. Statistical outliers were determined and excluded as described elsewhere.^[47]

Supporting Information

Supporting Information is available from the Wiley Online Library or from the author.

Acknowledgements

T.B. and P.F. contributed equally to this work. The authors thank R. Wurm, M. Gerads, and S. Kuschel for valuable technical assistance; the group of Prof. Andreas Weber for help with the qRT-PCR experiments; and J. Schmidt (University of Freiburg, Germany) for designing and constructing the light boxes. The authors thank M. Hörner for optoPlate-96 programming support. This work was supported in part by the Deutsche Forschungsgemeinschaft (DFG, German Research Foundation) under Germany's Excellence Strategies CEPLAS – EXC-1028 project no. 194465578 and EXC-2048/1 – Project no. 390686111, the iGRAD Plant (IRTG 1525), Grant ZU259/2-1, and the Collaborative Research Center SFB1208 (project no. 267205415) to MDZ; the European Commission – Research Executive Agency (H2020 Future and Emerging Technologies FET-Open project no. 801041 CyGenTig to MDZ; and the Human Frontiers Scientific Program Porject no. RGY0063 to MDZ. TB was supported for this research through the International Max Planck Research School (IMPRS) on Understanding Complex Plant Traits using Computational and Evolutionary Approaches at the Max Planck Institute for Plant Breeding Research and the Universities of Düsseldorf and Cologne.

Open access funding enabled and organized by Projekt DEAL.

Conflict of Interest

The authors declare no conflict of interest.

Data Availability Statement

Data and materials are available on request.

Keywords

blue light-gene expression control, CRISPR/Cas13b, mammalian synthetic biology, optogenetics, RNA downregulation

Received: September 27, 2020

Revised: January 14, 2021

Published online:

- [1] K. Kolar, C. Knobloch, H. Stork, M. Žnidarič, W. Weber, *ACS Synth. Biol.* **2018**, *7*, 1825.
- [2] A. Pickar-Oliver, C. A. Gersbach, *Nat. Rev. Mol. Cell Biol.* **2019**, *20*, 490.
- [3] M. Tabebordbar, K. Zhu, J. K. W. Cheng, W. L. Chew, J. J. Widrick, W. X. Yan, C. Maesner, E. Y. Wu, R. Xiao, F. A. Ran, L. Cong, F. Zhang, L. H. Vandenbergh, G. M. Church, A. J. Wagers, *Science* **2016**, *351*, 407.
- [4] D. G. Ousterout, A. M. Kabadi, P. I. Thakore, W. H. Majoros, T. E. Reddy, C. A. Gersbach, *Nat. Commun.* **2015**, *6*, 6244.
- [5] P. D. Hsu, E. S. Lander, F. Zhang, *Cell* **2014**, *157*, 1262.
- [6] A. V. Anzalone, P. B. Randolph, J. R. Davis, A. A. Sousa, L. W. Koblan, J. M. Levy, P. J. Chen, C. Wilson, G. A. Newby, A. Raguram, D. R. Liu, *Nature* **2019**, *576*, 149.
- [7] C. Fellmann, B. G. Gowen, P.-C. Lin, J. A. Doudna, J. E. Corn, *Nat. Rev. Drug Discovery* **2017**, *16*, 89.
- [8] S. C. Strutt, R. M. Torrez, E. Kaya, O. A. Negrete, J. A. Doudna, *Elife* **2018**, *7*, 32724.
- [9] D. B. T. Cox, J. S. Gootenberg, O. O. Abudayyeh, B. Franklin, M. J. Kellner, J. Joung, F. Zhang, *Science* **2017**, *358*, 1019.
- [10] A. K. Brooks, T. Caj, *Curr. Opin. Biotechnol.* **2018**, *52*, 95.
- [11] S. Konermann, P. Lotfy, N. J. Brideau, J. Oki, M. N. Shokhirev, P. D. Hsu, *Cell* **2018**, *173*, 665.
- [12] L. R. Polstein, C. A. Gersbach, *Nat. Chem. Biol.* **2015**, *11*, 198.
- [13] Y. Nihongaki, F. Kawano, T. Nakajima, M. Sato, *Nat. Biotechnol.* **2015**, *33*, 755.
- [14] F. Bubeck, M. D. Hoffmann, Z. Harteveid, S. Aschenbrenner, A. Bietz, M. C. Waldhauer, K. Börner, J. Fakhiri, C. Schmelas, L. Dietz, D. Grimm, B. E. Correia, R. Eils, D. Niopek, *Nat. Methods* **2018**, *15*, 924.
- [15] Y. Nihongaki, Y. Furuhashi, T. Otobe, S. Hasegawa, K. Yoshimoto, M. Sato, *Nat. Methods* **2017**, *14*, 963.
- [16] Y. Yu, X. Wu, N. Guan, J. Shao, H. Li, Y. Chen, Y. Ping, D. Li, H. Ye, *Sci. Adv.* **2020**, *6*, eabb1777.
- [17] X. X. Zhou, X. Zou, H. K. Chung, Y. Gao, Y. Liu, L. S. Qi, M. Z. Lin, *ACS Chem. Biol.* **2018**, *13*, 443.
- [18] Y. Chen, X. Yan, Y. Ping, *ACS Mater. Lett.* **2020**, *2*, 644.
- [19] X. Chen, Y. Chen, H. Xin, T. Wan, Y. Ping, *Proc. Natl. Acad. Sci. USA* **2020**, *117*, 2395.
- [20] P. Vogel, A. Hanswillemenke, T. Stafforst, *ACS Synth. Biol.* **2017**, *6*, 1642.
- [21] N. Y. Kim, S. Lee, J. Yu, N. Kim, S. S. Won, H. Park, W. D. o Heo, *Nat. Cell Biol.* **2020**, *22*, 341.
- [22] A. M. Weber, J. Kaiser, T. Ziegler, S. Pils, C. Renzl, L. Sixt, G. Pietruschka, S. Moniot, A. Kakoti, M. Juraschitz, S. Schrottke, L. Lledo Bryant, C. Steegborn, R. Bittl, G. Mayer, A. Möglich, *Nat. Chem. Biol.* **2019**, *15*, 1085.
- [23] S. Pils, C. Morgan, M. Choukeife, A. Möglich, G. Mayer, *Nat. Commun.* **2020**, *11*, 4825.

- [24] K. Müller, R. Engesser, J. Timmer, M. D. Zurbriggen, W. Weber, *ACS Synth. Biol.* **2014**, *3*, 796.
- [25] M. Malumbres, *Genome Biol.* **2014**, *15*, 122.
- [26] R. Prevo, G. Pirovano, R. Puliyadi, K. J. Herbert, G. Rodriguez-Berriguete, A. O'Docherty, W. Greaves, W. G. McKenna, G. S. Higgins, *Cell Cycle* **2018**, *17*, 1513.
- [27] J. Baaske, P. Gonschorek, R. Engesser, A. Dominguez-Monedero, K. Raute, P. Fischbach, K. Müller, E. Cachat, W. W. A. Schamel, S. Minguet, J. A. Davies, J. Timmer, W. Weber, M. D. Zurbriggen, *Sci. Rep.* **2018**, *8*, 15024.
- [28] P. Fischbach, P. Gonschorek, J. Baaske, J. A. Davies, W. Weber, M. D. Zurbriggen, *Methods Mol. Biol.* **2020**, 2173, 159.
- [29] D. Strickland, Y. Lin, E. Wagner, C. M. Hope, J. Zayner, C. Antoniou, T. R. Sosnick, E. L. Weiss, M. Glotzer, *Nat. Methods* **2012**, *9*, 379.
- [30] L. J. Bugaj, W. A. Lim, *Nat. Protoc.* **2019**, *14*, 2205.
- [31] O. S. Thomas, M. Hörner, W. Weber, *Nat. Protoc.* **2020**, *15*, 2785.
- [32] F. Crick, *Nature* **1970**, 227, 561.
- [33] A. V. Leopold, K. G. Chernov, V. V. Verkhusha, *Chem. Soc. Rev.* **2018**, *47*, 2454.
- [34] M. Malumbres, A. Carnero, *Prog. Cell Cycle Res.* **2003**, *5*, 5.
- [35] D. O. Morgan, *Annu. Rev. Cell Dev. Biol.* **1997**, *13*, 261.
- [36] S. Lim, P. Kaldis, *Development* **2013**, *140*, 3079.
- [37] M. C. de Gooijer, A. van den Top, I. Bockaj, J. H. Beijnen, T. Würdinger, O. van Tellingen, *FEBS Open Bio* **2017**, *7*, 439.
- [38] M. Malumbres, M. Barbacid, *Nat. Rev. Cancer* **2009**, *9*, 153.
- [39] M. Vogel, J. E. Weigand, B. Kluge, M. Grez, B. Suess, *Nucleic Acids Res.* **2018**, *46*, 48.
- [40] K. J. Dery, V. Gusti, S. Gaur, J. E. Shively, Y. Yen, R. K. Gaur, *Methods Mol. Biol.* **2009**, 555, 127.
- [41] A. M. Celotto, B. R. Graveley, *RNA* **2002**, *8*, 718.
- [42] C. P. Dillon, P. Sandy, A. Nencioni, S. Kissler, D. A. Rubinson, L. Van Parijs, *Annu. Rev. Physiol.* **2005**, *67*, 147.
- [43] M. Sierant, D. Piotrkowska, B. Nawrot, *Acta Neurobiol. Exp.* **2015**, *75*, 36.
- [44] K. Müller, R. Engesser, S. Schulz, T. Steinberg, P. Tomakidi, C. C. Weber, R. Ulm, J. Timmer, M. D. Zurbriggen, W. Weber, *Nucleic Acids Res.* **2013**, *41*, 124.
- [45] K. Müller, R. Engesser, S. Metzger, S. Schulz, M. M. Kämpf, M. Busacker, T. Steinberg, P. Tomakidi, M. Ehrbar, F. Nagy, J. Timmer, M. D. Zurbriggen, W. Weber, *Nucleic Acids Res.* **2013**, *41*, 77.
- [46] H. M. Beyer, S. Juillot, K. Herbst, S. L. Samodelov, K. Müller, W. W. Schamel, W. Römer, E. Schäfer, F. Nagy, U. Strähle, W. Weber, M. D. Zurbriggen, *ACS Synth. Biol.* **2015**, *4*, 951.
- [47] J. L. Jacobs, J. D. Dinman, *Nucleic Acids Res.* **2004**, *32*, 160.

© 2021 Wiley-VCH GmbH

ADVANCED BIOLOGY

Supporting Information

for *Adv. Biology*, DOI: 10.1002/adbi.202000307

**Blue Light-Operated CRISPR/Cas13b-Mediated mRNA
Knockdown (Lockdown)**

*Tim Blomeier, Patrick Fischbach, Leonie-Alexa Koch,
Jennifer Andres, Miguel Miñambres, Hannes Michael Beyer,
and Matias Daniel Zurbriggen**

Copyright WILEY-VCH Verlag GmbH & Co. KGaA, 69469 Weinheim, Germany, 2018.

Supporting Information

Blue Light-Operated CRISPR/Cas13b-mediated mRNA Knockdown (Lockdown)

*Tim Blomeier, Patrick Fischbach, Leonie-Alexa Koch, Jennifer Andres, Miguel Miñambres, Hannes Michael Beyer, Matias Daniel Zurbriggen**

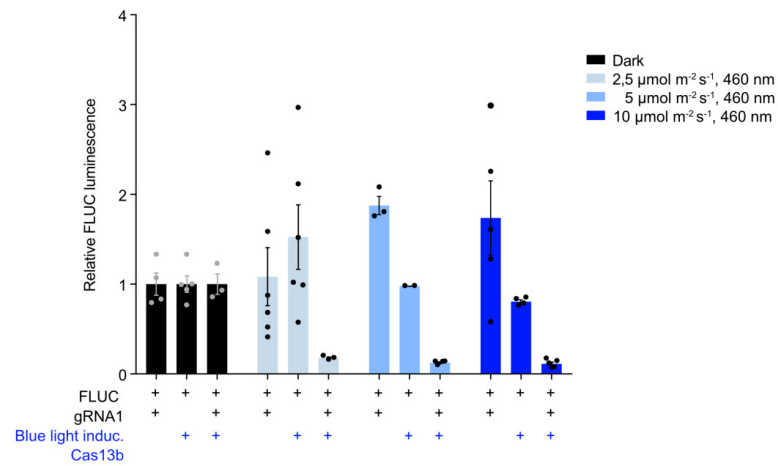


Figure S1. Light-dose response of Lockdown in CHO-K1 cells using an optoPlate-96 setup.

CHO-K1 cells were transfected with constructs for constitutive expression of FLUC (pTBPF015), the Lockdown system (pTBPF001, pKM516) and gRNA1 (pTBPF003). Control cells were transfected without Lockdown or without the gRNA. 4 h post transfection, the cells were illuminated with 2.5, 5, or 10 $\mu\text{mol m}^{-2} \text{s}^{-1}$ of 460 nm light using an optoPlate-96 illumination device^[1,2] (blue bars) or kept in the dark (black bars) for 24 h. FLUC luminescence was determined and normalized to the corresponding dark samples (black bars). $n = 6$, error bars indicate one standard error of the mean (SEM).

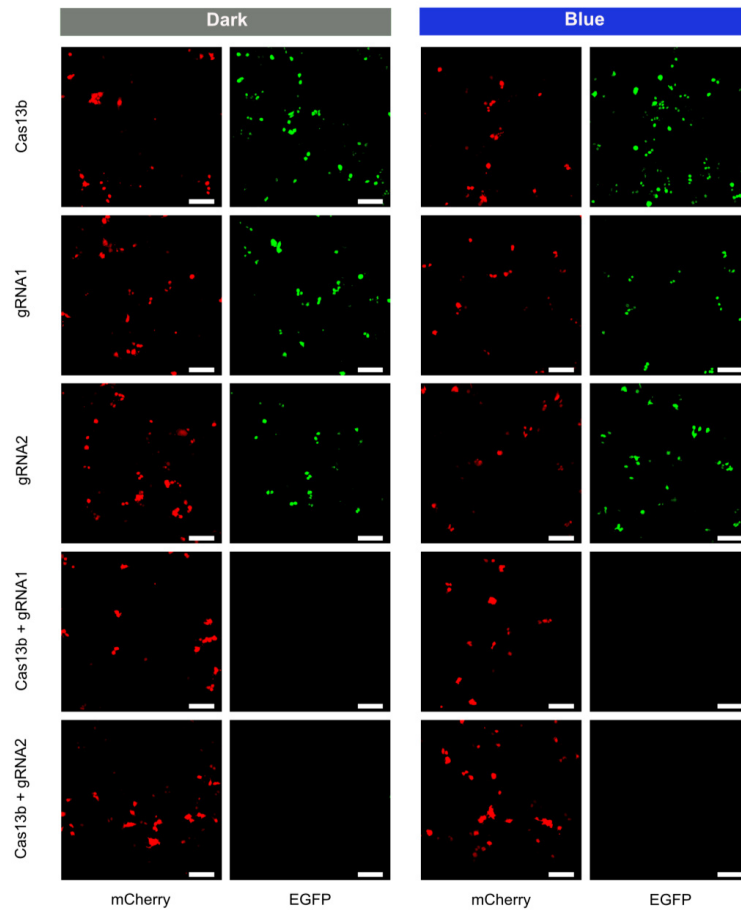


Figure S2. Confocal fluorescence microscopy of the Cas13b-mediated down-regulation of EGFP mRNA. HEK-293T cells were co-transfected with plasmids encoding PGK-driven EGFP (pTBPF018), SV40-driven mCherry (pTBPF014) and constitutively expressed Cas13b (pC0046), an EGFP-specific gRNA (gRNA1, pTBPF005; gRNA2, pTBPF006) or combinations of Cas13b and either of the gRNAs. 4 h post transfection, cells were either illuminated with $10 \mu\text{mol m}^{-2} \text{s}^{-1}$ of blue light (460 nm) or kept in the dark for 48 h. Cells were subsequently fixed and imaged by confocal microscopy.

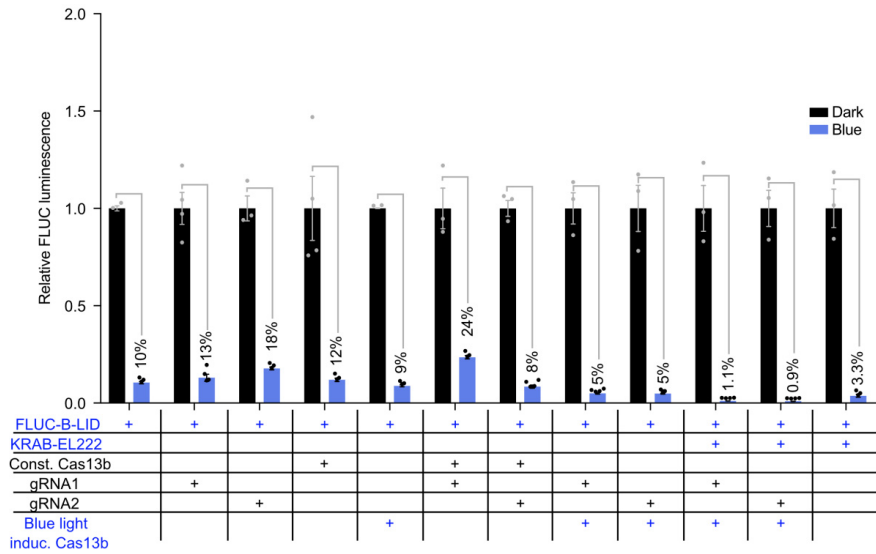


Figure S3. Combined repression of protein levels using the Lockdown and Blue-OFF optogenetic systems.

Representation of all tested combinations of the experiment in Figure 2. HEK-293T cells were transfected with FLUC fused to the blue light-inducible degron (FLUC-B-LID; pMZ1203). Cotransfection with a plasmid encoding KRAB-EL222 (pKM565) constitutes the entire Blue-OFF system. In order to combine the different blue light inducible modules, the Lockdown system (pTBPF001, pKM516) and one of the gRNAs (gRNA1, pTBPF003; gRNA2, pTBPF004) was combined with FLUC-B-LID or the complete Blue-OFF system. Additionally, combinations with constitutively expressed Cas13b (pC0046) and the indicated gRNAs were tested. Cells were kept in dark for 24 h followed by irradiation with $10 \mu\text{mol m}^{-2} \text{s}^{-1}$ of 460 nm light for 24 h (blue bars) or continuously kept in the dark (black bars). FLUC luminescence levels were normalized to their corresponding dark control. $n = 4$, error bars indicate one standard error of the mean (SEM).

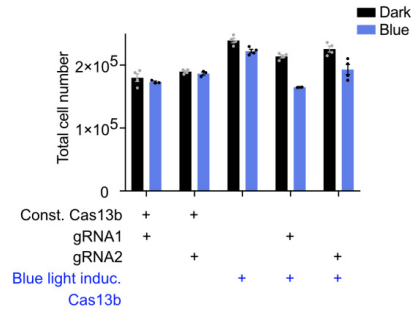


Figure S4. Cell cycle control using Lockdown. Representation of the total cell number count of the experiment shown in Figure 3. $n = 4$, the error bars indicate one standard error of the mean (SEM).

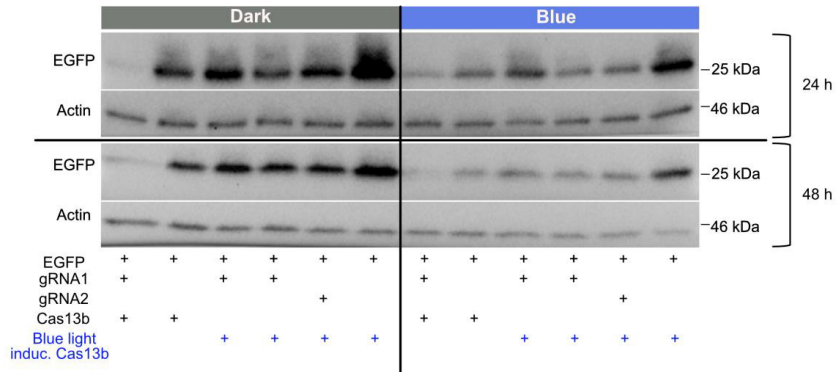


Figure S5. Analysis of protein expression levels via western blot. Representative western blot image showing the protein expression of EGFP and actin (loading control) in HEK-293T cells illuminated for 24 h (upper panels) or 48 h with blue light or kept in the dark. Transfected components are listed below the image. (Quantified intensities are shown in Figure 1e, results after 48 h were used).

Supplementary Table S1. Plasmids used and designed in this study.

Plasmid	Description	Reference
pTBPF001	UAS₅-PspCas13b-NES-HA-pA Plasmid pKM083 was PCR-amplified with oTBPF003 and oTBPF004. <i>PspCas13b</i> was amplified from pC0046 with oTBPF001 and oTBPF002. Both fragments were assembled using AQUA cloning.	This work
pTBPF003	P_{U6}-FLUC gRNA1-PspCas13bDR-pA pC0043 was linearized by digestion with <i>BbsI</i> and assembled with oTBPF009 using AQUA cloning.	This work
pTBPF004	P_{U6}-FLUC gRNA2-PspCas13bDR-pA Plasmid pC0043 was linearized by digestion with <i>BbsI</i> and assembled with oTBPF010 using AQUA cloning.	This work
pTBPF005	P_{U6}-EGFP gRNA1-PspCas13bDR-pA Plasmid pC0043 was linearized by digestion with <i>BbsI</i> and assembled with oTBPF011 using AQUA cloning.	This work
pTBPF006	P_{U6}-EGFP gRNA2-PspCas13bDR-pA Plasmid pC0043 was linearized by digestion with <i>BbsI</i> -HF and assembled with oTBPF012 using AQUA cloning.	This work
pTBPF014	P_{SV40}-mCherry-pA Plasmid pJA086 was linearized with <i>NotI</i> and <i>XbaI</i> , mCherry was PCR-amplified from pSJ025 with oTBPF034 and oTB035. Both fragments were assembled using AQUA cloning.	This work
pTBPF015	P_{SV40}-FLUC-pA Plasmid pLKPTBPF001 was linearized with <i>XhoI</i> and <i>BamHI</i> , the P _{SV40} promoter was PCR-amplified from pMZ1203 with oTBPF036 and oTBPF037. Both fragments were assembled by AQUA cloning.	This work
pTBPF018	P_{PGK}-EGFP-pA Plasmid pJA086 was linearized with <i>NheI</i> and <i>XhoI</i> , P _{PGK} was PCR-amplified from pLJM1-GFP with oTBPF041 and oTBPF042. Both fragments were assembled using AQUA cloning.	This work

Appendix

pTBPF020	P_{U6}-hCDK1 gRNA2-<i>Psp</i>Cas13bDR-pA Plasmid pC0043 was linearized with <i>Bbs</i> I and assembled with oTBPF0047 using Gibson cloning.	This work
pTBPF021	P_{U6}-hCDK1 gRNA1-<i>Psp</i>Cas13bDR-pA Plasmid pC0043 was linearized with <i>Bbs</i> I and assembled with oTBPF048 using Gibson cloning.	This work
pJA086	P_{SV40}-EGFP-pA P _{SV40} driven mammalian expression vector encoding the fluorescent protein EGFP.	Unpublished
pLKTBPFO01	P_{CMV}-FLUC-pA P _{CMV} -driven mammalian expression vector encoding the firefly luciferase.	Unpublished
pMZ333	P_{SV40} driven mammalian expression vector derived from <i>Xba</i>I/<i>Not</i>I digested pSAM200. ^[3]	[4]
pKM083	UAS₅-TATA-GLUC-pA Vector encoding <i>Gussia</i> luciferase (GLUC) under control of P _{Gal4} .	[5]
pKM516	P_{SV40}-Gal4BD-LOVpep[T406A,T407A,I532A]-IRESPV-ePDZb-VP16-NLS-pA P _{SV40} -driven bicistronic mammalian vector encoding Gal4BD-LOVpep[T406A,T407A,I532A] and ePDZb-VP16-NLS.	[5]
pKM565	P_{SV40}-KRAB-EL222-pA P _{SV40} -driven mammalian expression vector encoding the light-responsive repressor KRAB-EL222.	[6]
pMZ1203	P_{SV40}-(C120)₅-FLUC-B-LID-pA P _{SV40} -driven mammalian expression vector encoding the firefly luciferase fused to a blue light-inducible degron (B-LID), containing the EL222-DNA-binding site (C120) ₅ .	[6]
pSJ025	P_{SV40}-<i>At</i>PHYB-mCherry-pA P _{SV40} -driven mammalian expression vector encoding <i>A. thaliana</i>	[4]

Appendix

	phytochrome B fused to the fluorescent protein mCherry.	
pC0043	P_{U6}-PspCas13b DR-BbsI-BbsI-pA P _{U6} -driven mammalian expression vector for cloning of guide RNAs compatible with <i>PspCas13b</i> .	pC0043- <i>PspCas13b</i> crRNA was a gift from Feng Zhang (Addgene #103854) ^[7]
pC0046	P_{EF1α}-PspCas13b-NES-HIV P _{EF1α} driven mammalian expression vector for expression of <i>PspCas13b</i> for knockdown of target RNAs in combination with compatible gRNAs.	pC0046-EF1α- <i>PspCas13b</i> -NES-HIV was a gift from Feng Zhang (Addgene #103862) ^[7]
pLJM1-GFP	5'LTR-RRE-P_{CMV}-EGFP-P_{PGK}-Puro^r-3'LTR 3 rd generation lentiviral vector for EGFP fusion; PGK-driven puromycin resistance.	pLJM1-EGFP was a gift from David Sabatini (Addgene #19319) ^[8]

Supplementary Table S2. Oligonucleotides used in this study.

Oligonucleotide	Sequence (5' → 3')
oTBPF001	CGTTCGAGATCTGCGATCTAAGTAAGCTTGCCACCATGAACATCCCC GCTCTGGTGGAAAAC
oTBPF002	CTCCATTCATAAGTTCATAGGATGGGCGGCCGCTTAGGCATAGTCG GGGACATCATATGG
oTBPF003	GCGGCCGCCCATCCTATGG
oTBPF004	GGTGGCCAAGCTTACTTAGATCGCAG
oTBPF009	ATAGCCCTCAAACTGGACCTTCCACAACGAGGTGGACATTACCTAC GCCGAGTACTTCGGTGTTTCGTCCTTCCACAAGATATATAA
oTBPF010	ATAGCCCTCAAACTGGACCTTCCACAACCCAGGTAACCATGAC CGAGAAGGAGATCGGTGTTTCGTCCTTCCA
oTBPF011	ATAGCCCTCAAACTGGACCTTCCACAACCTGGACGGCGACGTAAC CGCCACAAGTTCGGTGTTTCGTCCTTCCACAAGA
oTBPF012	ATAGCCCTCAAACTGGACCTTCCACAACCCAGTCCAAGCTGAGC AAAGACCCCAACCGGTGTTTCGTCCTTCCACAAGATATATA
oTBPF034	TTTTGTCTTTATTTTCAGGTCCCGGATCGAATTGCGGCCGCATGGTGAG CAAGGGCGAGGAGG

Appendix

oTBPF035	CTGGATCGAAGCTTGGGCTGCAGGTCGACTTCTAGACTACTTGTACAGCTCGTCCATGCCG
oTBPF036	CATGTTTGACAGCTTATCATCGATAAGCTAGCTTGGATCCCTGTGGAA TGTGTGTCAGTTAGGGTG
oTBPF037	TTACCAGTTAACTTTCTGGTTTTCCAGTTCCTCGAGAGCTTTTGGAAA AGCCTAGGCCTCC
oTBPF041	TTTCATGTTTGACAGCTTATCATCGATAAGCTAGCTTGGGGTTGCGC CTTTTCCAAGGC
oTBPF042	TTACCAGTTAACTTTCTGGTTTTCCAGTTCCTCGAGCTGGGGAGAGAG GTCGGTGATTG
oTBPF047	ATAGCCCCTCAAACTGGACCTTCCACAACGCCAGAGCTTTTGGAAATA CCTATCAGAGTAGGTGTTTCGTCCTTCCACAAGATATATAA
oTBPF048	ATAGCCCCTCAAACTGGACCTTCCACAACGGGCACTCCCAATAATGA AGTGTGGCCAGAGGTGTTTCGTCCTTCCACAAGATATATAA

Supplementary Table S3: Oligonucleotides designed and used for RT-qPCR experiments in this study.

Oligonucleotide	Sequence (5' → 3')
oTB351 GAPDH Fwd	GTCTCCTCTGACTTCAACAGCG
oTB352 GAPDH Rev	ACCACCCTGTTGCTGTAGCCAA
oTB359 EGFP Fwd	GGGCACAAGCTGGAGTACAA
oTB360 EGFP Rev	GTCCTCGATGTTGTGGCG
oTB361 mCherry Fwd	AAGCAGAGGCTGAAGCTGAAGG
oTB362 mCherry rev	GCGTTCGTA CTGTTCCACGATG

Supplementary Table S4: Guide RNAs designed and used in this study.

gRNA	Sequence (5' → 3')
Firefly 1	GAGGTGGACATTACCTACGCCGAGTACTTC
Firefly 2	CACGGTAAAACCATGACCGAGAAGGAGATC
EGFP 1	CTGGACGGCGACGTAAACGGCCACAAGTTC
EGFP 2	ACCCAGTCCAAGCTGAGCAAAGACCCCAAC
hCDK1 1	GGGCACTCCCAATAATGAAGTGTGGCCAGA

Appendix

hCDK1 2	GCCAGAGCTTTTGAATACCTATCAGAGTA
---------	-------------------------------

Supporting References

- [1] L. J. Bugaj, W. A. Lim, *Nat. Protoc.* **2019**, *14*, 2205.
- [2] O. S. Thomas, M. Hörner, W. Weber, *Nat. Protoc.* **2020**, *15*, 2785.
- [3] M. Fussenegger, S. Moser, X. Mazur, J. E. Bailey, *Biotechnol. Prog.* **1997**, *13*, 733.
- [4] H. M. Beyer, S. Juillot, K. Herbst, S. L. Samodelov, K. Müller, W. W. Schamel, W. Römer, E. Schäfer, F. Nagy, U. Strähle, W. Weber, M. D. Zurbriggen, *ACS Synth. Biol.* **2015**, *4*, 951.
- [5] R. Engesser, J. Timmer, M. D. Zurbriggen, W. Weber, **2014**.
- [6] J. Baaske, P. Gonschorek, R. Engesser, A. Dominguez-Monedero, K. Raute, P. Fischbach, K. Müller, E. Cachat, W. W. A. Schamel, S. Minguet, J. A. Davies, J. Timmer, W. Weber, M. D. Zurbriggen, *Sci. Rep.* **2018**, *8*, 15024.
- [7] D. B. T. Cox, J. S. Gootenberg, O. O. Abudayyeh, B. Franklin, M. J. Kellner, J. Joung, F. Zhang, *Science* **2017**, *358*, 1019.
- [8] Y. Sancak, T. R. Peterson, Y. D. Shaul, R. A. Lindquist, C. C. Thoreen, L. Bar-Peled, D. M. Sabatini, *Science* **2008**, *320*, 1496.

7.1.3 UV-B light-inducible system for the transcriptional control of gene expression in *A. thaliana* mesophyll protoplasts

1 UV-B light-inducible system for the transcriptional control 2 of gene expression in *A. thaliana* mesophyll protoplasts

3
4 Tim Blomeier¹, Uriel Urquiza-Garcia¹, Giovanni Giuriani¹, Matias D. Zurbriggen^{1,*}

5
6 ¹Institute of Synthetic Biology, University of Düsseldorf and CEPLAS, Düsseldorf, Germany

7
8 *Corresponding author: Email: matias.zurbriggen@uni-duesseldorf.de

9

10 11 **ABSTRACT**

12
13 **Compared to chemically inducible systems, light as an elicitor offers non-invasive,**
14 **reversible and quantitative adjustable control of molecular processes with superior**
15 **spatiotemporal resolution. However, the indispensable need for light impedes the**
16 **implementation of optogenetic tool in plants. In order to overcome this obstacle, we**
17 **engineered the UV-B_{ON} system, an optogenetic switch based on the UV-B induced**
18 **interaction of the endogenous plant components COP1 and UVR8 for controlling gene**
19 **expression in plant systems, previously characterized in mammalian cells. Here, we**
20 **present the design, implementation and characterization of the UV-B_{ON} switch in *A.***
21 ***thaliana* mesophyll protoplasts, expanding the toolbox of optogenetic tools for plant**
22 **systems.**

23 24 **INTRODUCTION**

25
26 Synthetic light-controlled gene switches outperform their chemically inducible counterparts
27 with their key characteristics like tight quantitative control, minimized invasiveness and highly
28 precise and reversible control of the spatiotemporal induction (Müller et al., 2015; Andres et
29 al., 2019). Hence, development of genetically encoded, light-regulated proteins and switches
30 not only revolutionized neuroscience in the beginning of the century but also generated a large
31 toolbox of optogenetically controlled gene switches and proteins for application in animal,
32 bacterial, fungi and plant systems (Beyer et al., 2015; Fan and Lin, 2015; Müller et al., 2015;
33 Kolar and Weber, 2017; Salinas et al., 2017; Kolar et al., 2018; Liu et al., 2018; Krueger et al.,
34 2019). Since the life cycle of plants indispensably depends on the exposure to ambient light,
35 optogenetic tools cannot easily be adapted for application in plants.

36 Nevertheless, sophisticated engineering led to generation of switches bypassing activation by
37 ambient light and avoiding interference with the endogenous photosynthetic circuitry or other
38 light-triggered signaling events (Andres et al., 2019; Christie and Zurbriggen, 2020). One
39 technique of overcoming the mentioned obstacles is the induction of system by a small range
40 of wavelength, while light from other regions of the spectrum or the exposure to ambient light
41 deactivates the system. The recently described PULSE system combines a previously
42 described switch with reversible activation and deactivation by red and far red light (R_{ON})

43 (Müller et al., 2014; Ochoa-Fernandez et al., 2016) with repression under blue light (B_{OFF}),
44 providing activation only with monochromatic red light (Ochoa-Fernandez et al., 2020). Another
45 approach used a system only active in the dark, while green light, with minimal interference to
46 the plants endogenous photoreceptors, deactivates the induction (Chatelle et al., 2018).
47 However, this system requires the addition of vitamin B12 which is not naturally produced in
48 plants.

49 For the purpose of expanding the toolbox of plant usable, light-responsive switches, we
50 prototyped a UV-B optogenetic system based on previous studies on multichromatic
51 optogenetics in mammalian cells (Müller et al., 2013b). Therefore, we used protoplast as a
52 rapid prototyping platform, which has recently been adopted extensively for plant synthetic
53 biology (Schaumberg et al., 2016; Lin et al., 2020; Ochoa-Fernandez et al., 2020; Lin et al.,
54 2021).

55 We adapted the UV-B responsive split transcription factor system based on the core domain
56 of *A. thaliana* UV-B photoreceptor UV RESISTANCE LOCUS 8 (UVR8) (residues 12-381) and
57 the WD40 domain of CONSTITUTIVELY PHOTOMORPHOGENIC 1 (COP1). UV-B signaling
58 has been reviewed comprehensively recently (Podolec et al., 2021). However, in a nutshell, in
59 the absence of UV-B, UV RESISTANCE LOCUS 8 (UVR8) homodimerizes, while exposure to
60 UV-B disrupts the dimerization (Rizzini et al., 2011). The now monomeric UVR8 is the active
61 conformer and enables interaction with the E3-ubiquitin ligase COP1. Point of the interaction
62 is the conserved WD40 domain (residues 336-674) of COP1 (Favory et al., 2009). Mediated
63 by direct interaction with REPRESSOR OF UV-B PHOTOMORPHOGENESIS 1 (RUP1) and
64 RUP2, UVR8 homodimerizes again in the dark, inhibiting the interaction with COP1 (Gruber et
65 al., 2010; Heijde and Ulm, 2013).

66 Hence, we used the described UV-B dependent interaction of UVR8 and COP1 as core of our
67 optogenetic switch. As previously demonstrated in mammalian cells, the system is based on
68 the truncated version of UVR8 with removed N- and C-terminal tails, in order to avoid any
69 interaction with endogenous pathways, and the WD40 domain of COP1, necessary and
70 sufficient for interaction with UVR8 (Rizzini et al., 2011), were used for our switch.

71 We demonstrate that the described UV- B_{ON} optogenetic system is not activated by light of
72 other wavelengths than UV-B. Our system effectively incorporates a new wavelength for
73 optogenetic applications for photoautotrophic organisms like plants.

74

75 RESULTS

76

77 Design, adaptation and test of the UV- B_{ON} system for use in plant cells.

78 In order to create a UV-B light inducible split transcription factor system, COP was N-terminally
79 fused to a transactivation domain (VP16), while UVR8 was bound to the DNA-binding
80 macrolide repressor (E) on its N-terminal. E is bound to a specific DNA-motif (erythromycin

81 resistance operator; etr_B) on the reporter plasmid, containing the reporter gene under control
82 of a minimal human cytomegalovirus immediate early promoter ($P_{hCMVmin}$). Since activation of
83 gene expression of this synthetic inducible promoter (etr_B-P_{CMVmin}) composition in plants cells
84 was shown before for the Red_{ON} system (Müller et al., 2014; Ochoa-Fernandez et al., 2016;
85 Ochoa-Fernandez et al., 2020), the reporter plasmid design was adapted from this previous
86 studies. Here, we are effectively utilizing the capacity of this systems in reporting the
87 heterodimerization of E-UVR8 and COP1(WD40)-VP16 upon illumination with UV-B light,
88 consequently resulting in an optogenetic system capable of inducing the expression of a gene
89 of interest (GOI). In the dark, UVR8 homodimerizes without activating gene expression. Upon
90 illumination with light of the UV-B range of wavelengths, UVR8 monomerizes and is able to
91 interact with COP1, generating close proximity of VP16 to the minimal promoter. Subsequent,
92 the transcriptional machinery is recruited, inducing expression of the GOI. Reconversion of
93 UVR8 to the homodimerized state in the absence of UV-B terminates gene expression.

94 For the purpose of adapting the switch designed for usage in mammalian cells, E-UVR8 and
95 COP1-VP16 were expressed under control of the plant specific CaMV35S promoter,
96 functioning in *A. thaliana*. Further, the SEAP reporter gene was exchanged by the highly
97 sensitive firefly luciferase (FLUC) (Figure 1 A). To avoid influence of light from other
98 wavelength than UV-B, a glass filter in the band of 260 – 390 nm was placed between the light
99 source and the protoplasts. *A. thaliana* mesophyll protoplasts were isolated and transformed
100 as described (Ochoa-Fernandez et al., 2016). This protocol allowed the simultaneous
101 transformation of plasmids carrying individual components. Therefore, allowing rapid
102 evaluation on different versions of the systems constituents. Transformation with the indicated
103 components was followed by four hours of incubation in the dark and another 18 hours of
104 illumination with light of 311 nm ($7 \mu\text{mol m}^{-2} \text{s}^{-1}$) or incubation in the dark. While a fusion of E-
105 VP16 acted as positive control of the E-based system, single transformation of the reporter
106 plasmid was used for determining the background activation of the synthetic promoter. Further,
107 we utilized a constitutively expressed renilla luciferase (RLUC) as normalizing element.

108 After exposure to the described light conditions, luciferase activity was determined by
109 calculating the FLUC/RLUC ratio. In our positive control we observed a subtle reduction of
110 FLUC/RLUC ratio between darkness and UV-B ($7 \mu\text{mol m}^{-2} \text{s}^{-1}$ of 311 nm), while the synthetic
111 promoter on its own did not show any mentionable background activity. The results of these
112 controls suggested a reliable operation of the system in darkness and upon UV-B treatment
113 (Figure 1 B). In combination with our reporter construct and the normalization element, we
114 tested several versions of E-UVR8 and COP1-VP16, evaluating FLUC/RLUC in both darkness
115 and UV-B conditions (Figure 1B). At first, the original switch, with the required changes for
116 application in plant cells was tested. Further, both proteins were fused to a nuclear localization,
117 guaranteeing the nuclear abundance of all needed components, to compare their function.

118 Nuclear localization of UVR8 reduced leakiness in combination with both variants of COP1,
119 but also decreased the activity of the system in UV-B illumination. Both combinations
120 possessed a comparable dynamic range between protoplasts kept in the dark and UV-B
121 exposed counterparts of 16- and 13-fold, respectively. The UVR8 variant without NLS showed
122 stronger activation in co-transformation with the non-tagged COP1, with a comparable
123 induction fold of 13x. Co-expression of COP1-VP16-NLS led to a weaker activation of the
124 system in UV-B with the lowest measured induction fold of 8. Since the non-tagged variant of
125 UVR8(12-381) displayed the strongest UV-B induced activation, a full-length version of UVR8
126 was further compared to the truncated version. In relation to the previously described
127 combinations, co-transformation of the complete UVR8 protein and both COP1 version, led to
128 a much stronger activation of the system with induction folds of 38 (COP1-VP16) and 28
129 (COP1-VP16-NLS) (Figure 1 B).

130

131 **RUP1/2 have a minimal impact on optogenetic applicability**

132 We also compared the systems' functionality between protoplast isolated from wild type (Col-
133 0) plants to *rup1/rup2* double mutant protoplasts. Based on the reported role of RUP1 and
134 RUP2 in promoting UVR8 homodimerization in darkness (Gruber et al., 2010; Heijde and Ulm,
135 2013), we performed the same experiment as above described for wild type protoplasts.
136 Interestingly, we observed an increase in FLUC/RLUC ration and enhanced response for the
137 combinations of the full-length E-UVR8 and COP1(WD40)-VP16. The latter suggests a
138 possible role of RUP1 and RUP2 regulation of UVR8-COP1 interaction in the UV-B illumination
139 conditions we tested (Figure 1 C). However, regarding the optogenetic applicability, we do not
140 have experimental support for critical differences between Col-0 and the *rup1/rup2* double
141 mutant. Therefore, we focused our efforts only in the Col-0 wild type.

142

143 **Kinetic experiments suggest tight control of UV-B inducibility**

144 One aim in optogenetic control is the possibility of high temporal resolution regarding the
145 inducibility of the system. Therefore, we performed a time series experiment for evaluating the
146 dynamics of the system (Figure 2). Here, the UVR8-COP1 combination with the broadest
147 dynamic range, composed of the full length UVR8 and COP1-VP16, was transformed. While
148 three hours after exposure to UV-B light of 311 nm ($7 \mu\text{mol m}^{-2} \text{s}^{-1}$) no activation of the system
149 was measured, three hours later an induction of six-fold in UV-B was detected. Expression of
150 FLUC further increases, while only a small increase in activity was measured between nine
151 and 18 hours of illumination. The induction fold only rose from 14.8 after nine hours of
152 illumination to 15.0 after 18 hours. Subsequent, the induction of the system decreased to 10.2-
153 fold after 24 hours. The data then suggest that the system reaches steady state expression
154 after 18 hours. Longer exposure times to pure UV-B light might have an impact on the

155 protoplast viability. However, further research in this direction needs to be conducted for such
156 prolonged periods of time. The kinetic experiment also offered the possibility of testing a
157 quantitative representation of the system. Therefore, we captured the interactions described
158 before in an ordinary differential equations (ODE) model (Figure S1). After fitting the model to
159 the data, we observed large correlations in model parameters, suggesting that a simpler model
160 parametrization could capture the experimental observations. After significantly reducing the
161 number of parameters in a new parametrization, we were able to constrain the model
162 parameters. Interestingly, we were not able to capture the systems dynamics from the start of
163 the experiment, suggesting two alternative hypotheses: One explanation could be the low
164 sensitivity, impeding the detection of signal in early stages. The alternative hypothesis we
165 propose is possibility of inhibition of our synthetic system by elements of the endogenous
166 phototransduction pathway in darkness. We hypothesize that the endogenous COP1 could
167 potentially inhibit the interaction between E-UVR8 and COP1(WD40)-VP16.

168

169 **Incubation in ambient light conditions improves the induction of the UV-B_{ON} system**

170 Given that we had all the components at hand, we tested the second hypothesis. Therefore,
171 we incubated the plant protoplasts in the presence of white light for four hours, aiming to reduce
172 this inhibitory effect by relocating COP1 from the nucleus into the cytosol (von Arnim and Deng,
173 1994; Lau and Deng, 2012; Pacin et al., 2014; Yin et al., 2016). Here the previously applied
174 incubation in darkness was compared with incubation under ambient light conditions in a
175 growth chamber. Surprisingly we observed an increase on the FF/REN ratio to 22-fold after
176 treatment with artificial white light, compared to 15-fold after incubation in darkness (Figure 3).
177 These results supported our first hypothesis and showed the importance of mathematical
178 modelling of the synthetic system to characterize the impact of endogenous components in a
179 non-orthogonal chassis.

180

181 **Activation of UV-B_{ON} system only in the presence of UV-B**

182 In a following experiment, the influence of light from other wavelength on the induction of the
183 described was evaluated (Figure 4). Therefore, the protoplasts were not only exposed to light
184 of 311 nm, but additionally to white ($10 \mu\text{mol m}^{-2}\text{s}^{-1}$ for the following wavelength ranges: blue
185 420–490 nm, red 620–680 nm, and far-red 700–750 nm; see (Ochoa-Fernandez et al., 2020)),
186 red (660 nm; $5 \mu\text{mol m}^{-2}\text{s}^{-1}$) and blue light (460 nm; $5 \mu\text{mol m}^{-2}\text{s}^{-1}$). The duration of illumination
187 was, as before, 18 hours, after 4 hours of incubation in the dark. Since the protoplasts are from
188 the same round of transformation as in the experiment diagrammed in Figure 3, the same
189 values of protoplasts incubated in darkness are the same as in Figure 3. Even though all light
190 conditions had an effect on the fitness of the protoplast In the described experiment, since the
191 E-VP16 held a lower FLUC/RLUC ratio than protoplast kept in the dark, illumination with UV-

192 B led to an induction in FLUC/RLUC ratio of 15-fold for the UVR8-COP1 switch, compared to
193 protoplasts kept in darkness. The three other light conditions led to no induction of the system
194 greater than in protoplasts of the control group kept in the dark, while the reporter only negative
195 control did not indicate any changes in FLUC/RLUC ratio in all tested light conditions. In
196 summary, our system only showed activation in UV-B while white, red and blue light did not
197 induce any production of FLUC.

198

199 **DISCUSSION**

200 Chemically inducible systems for the control of gene expression or other cellular processes
201 have highly contributed to improve or understanding of cellular processes in plants (Zuo and
202 Chua, 2000; Moore et al., 2006; Andres et al., 2019). However, these switches have critical
203 limitations regarding the spatiotemporal regulation, as well as the toxicity effects (Andres et
204 al., 2019). Optogenetically controlled systems for gene expression overcome these obstacles
205 by using light as non-toxic inducer with precisely controllable spatiotemporal resolution and
206 quantitative regulation. While optogenetic tools were extensively implemented for the
207 application in animal, bacterial or yeast systems (Beyer et al., 2015; Fan and Lin, 2015; Müller
208 et al., 2015; Kolar and Weber, 2017; Salinas et al., 2017; Kolar et al., 2018; Liu et al., 2018;
209 Krueger et al., 2019), the transfer to plant system lags behind. The essential need of light for
210 the plants' lifecycle and growth, demands more sophisticated approaches for circumventing
211 the activation of the endogenous light-induced signaling events.

212 With the development of the UV-B responsive optogenetic UV-B_{ON} switch we expand the short
213 list of light-inducible tools for the manipulation of gene expression in plants. The UV-B_{ON}
214 system displayed a strong induction of gene expression after the exposure to light of the UV-
215 B range of wavelengths, while light from other ranges did not activate the system at all.

216 It does not depend on an "OFF-module" for deactivation of the gene expression under other
217 light conditions than UV-B and the thereby simpler organization and smaller size of the system,
218 could be a benefit compared to other systems like PULSE (Ochoa-Fernandez et al., 2020). In
219 addition, combination of UVR8_{ON} with other light-responsive modules like the Red_{ON} or the
220 BLUE_{OFF} switches (Müller et al., 2014; Ochoa-Fernandez et al., 2016; Ochoa-Fernandez et al.,
221 2020) could expand the range of applications for multichromatic control of gene expression in
222 plant systems. Since the general buildup of the switch is very similar to the Red_{ON}-switch and
223 both systems use the macrolide repressor E protein for DNA-binding, UV-B_{ON} is fully functional
224 with the P_{Opto}-reporter of PULSE without the need of any modification. Further, the attempt of
225 incubating the protoplasts in ambient light, emerging from fitting an ordinary differential
226 equations (ODE) model to our obtained kinetics data of the system, ultimately indicated
227 beneficial effects on induction-fold of the system, while it seemed to be beneficial for protoplast
228 fitness after transformation. This leads to the hypothesis that simple filtration of light of the UV

229 range of wavelength might allow the expression of the system in full plants, growing under
230 ambient light conditions without activation. Nevertheless, subsequent experiments of the
231 functionality of the system in ambient light conditions with supplemented UV-B irradiation need
232 to be performed to proof this hypothesis. However, the transfer of the system into stable plant
233 lines expressing the switch will be needed to test if the indicated characteristics of the systems
234 can be transferred from protoplasts to full plants.

235

236 MATERIALS AND METHODS

237

238 Protoplast isolation and transformation

239

240 Preparation of seedlings, plant growth conditions, protoplast isolation and transformation was
241 performed as described by Ochoa-Fernandez et al., 2016. A total of 40 µg of DNA was
242 transformed with ratios of 15 µg for COP1 and UVR8 containing plasmids, respectively and
243 7.5 µg of the etr_8 - $P_{hCMVmin}$ -FLUC reporter, as well as 2.5 µg of the RLUC containing plasmid for
244 normalization of FLUC luminescence.

245

246 UV-Light experiments in protoplasts

247

248 After transformation, 800 µL of each transformation set-up was transferred to a 24 well plate,
249 followed by 4 hours of incubation under the respective conditions (in the dark or exposed to
250 white light of the plant growth chamber). Subsequent to incubation, protoplasts were
251 illuminated with light of 311 nm (UV-B) or kept in darkness (typically for 18 h, unless indicated
252 otherwise).

253

254 Luminescence analysis of protoplast experiments

255

256 4 replicates of 80 µL of each sample were into two separate white 96-well assay plates for
257 parallel measurement of firefly luciferase (FLUC) and renilla luciferase (RLUC) in two separate
258 microplate readers. Before the measurement, 20 µl of firefly substrate [0.47 mM D-luciferin
259 (Biosynth AG, Staad, Switzerland), 20 mM tricine, 2.67 mM $MgSO_4 \cdot 7H_2O$, 0.1 mM
260 $EDTA \cdot 2H_2O$, 33.3 mM dithiothreitol, 0.52 mM adenosine 5'-triphosphate, 0.27 mM acetyl-
261 coenzyme A, 5 mM NaOH, 0.26 mM $MgCO_3 \cdot 5H_2O$, in H_2O] were added to each well for firefly
262 measurement, while coelenterazine (472 mM coelenterazine stock solution in methanol,
263 diluted directly before use 1:15 in phosphate-buffered saline) were added to each well of the
264 renilla measurement plate. Firefly and renilla luminescence were measured in a Centro XS3
265 LB960 Microplate Luminometer (Berthold Technologies, Bad Wildbad, Germany).

266

267

268

269

270 Light source and illumination conditions
271

272 UV-B illumination of protoplast samples was performed with a UVB narrowband lamp (Philips,
273 prod. no. PL-S 9W/01) covered by an ultraviolet transmitting, visible light absorbing filter (U340,
274 Hoya, Tokyo, Japan), to eliminate non-UV-B wavelengths. Light intensity was adjusted by
275 changing the distance from light source to the sample to $7 \mu\text{mol m}^{-2} \text{s}^{-1}$ of 311 nm UV-B light,
276 if not indicated otherwise. Illumination with white, red or blue light was performed with custom-
277 made LED light boxes, as previously described (Müller et al., 2013a; Ochoa-Fernandez et al.,
278 2016; Ochoa-Fernandez et al., 2020)

279
280 **SUPPLEMENTARY INFORMATION**

281
282 Supplementary information are available on request.

283
284 **ACKNOWLEDGEMENTS**

285
286 The authors thank R. Wurm, M. Gerads and S. Kuschel for valuable technical assistance;
287 Jennifer Andres and Leonie-Alexa Koch for helpful comments on the manuscript. This work
288 was supported in part by the Deutsche Forschungsgemeinschaft (DFG, German Research
289 Foundation) under Germany's Excellence Strategies CEPLAS – EXC-1028 project no.
290 194465578 and EXC-2048/1 – Project no. 390686111, the iGRAD Plant (IRTG 1525), Grant
291 ZU259/2-1, and the Collaborative Research Center SFB1208 (project no. 267205415) to MDZ;
292 the European Commission – Research Executive Agency (H2020 Future and Emerging
293 Technologies FET-Open project no. 801041 CyGenTig to MDZ; and the Human Frontiers
294 Scientific Program Project no. RGY0063 to MDZ. TB was supported for this research through
295 the International Max Planck Research School (IMPRS) on Understanding Complex Plant
296 Traits using Computational and Evolutionary Approaches at the Max Planck Institute for Plant
297 Breeding Research and the Universities of Düsseldorf and Cologne.

298
299 **COMPETING OF INTERESTS**

300
301 The authors declare no conflict of interest.

302
303 **AUTHOR CONTRIBUTION**

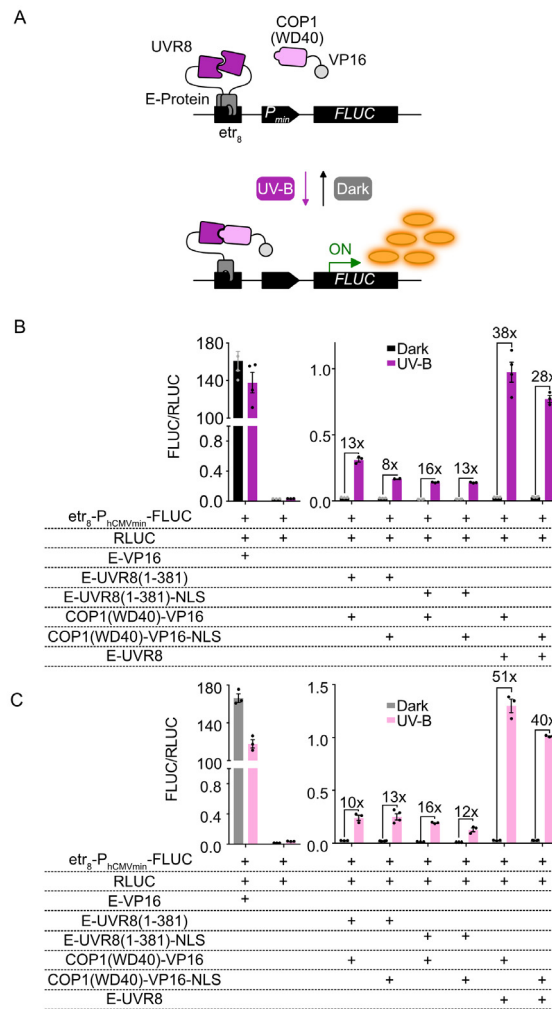
304
305 TB designed and performed the experiments, analyzed the data and wrote the manuscript. UU
306 performed the mathematical modelling, analyzed the experiments and wrote the manuscript.
307 GG performed the experiment diagrammed in Figure 1 A and B. MDZ designed the
308 experiments, analyzed the data and wrote the manuscript.

309
310
311
312
313

314 REFERENCES

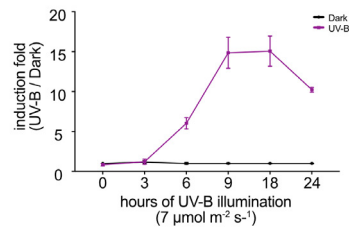
- 315
- 316 **Andres J, Blomeier T, Zurbriggen MD** (2019) Synthetic Switches and Regulatory Circuits in
317 Plants. *Plant Physiol* **179**: 862–884
- 318 **von Arnim AG, Deng X-W** (1994) Light inactivation of arabidopsis photomorphogenic
319 repressor COP1 involves a cell-specific regulation of its nucleocytoplasmic partitioning.
320 *Cell* **79**: 1035–1045
- 321 **Beyer HM, Naumann S, Weber W, Radziwill G** (2015) Optogenetic control of signaling in
322 mammalian cells. *Biotechnol J* **10**: 273–283
- 323 **Chatelle C, Ochoa-Fernandez R, Engesser R, Schneider N, Beyer HM, Jones AR, Timmer**
324 **J, Zurbriggen MD, Weber W** (2018) A Green-Light-Responsive System for the Control
325 of Transgene Expression in Mammalian and Plant Cells. *ACS Synth Biol* **7**: 1349–1358
- 326 **Christie JM, Zurbriggen MD** (2020) Optogenetics in plants. *New Phytol* nph.17008
- 327 **Fan LZ, Lin MZ** (2015) Optical control of biological processes by light-switchable proteins.
328 *Wiley Interdiscip Rev Dev Biol* **4**: 545–54
- 329 **Favory J-J, Stec A, Gruber H, Rizzini L, Oravec A, Funk M, Albert A, Cloix C, Jenkins**
330 **GI, Oakeley EJ, et al** (2009) Interaction of COP1 and UVR8 regulates UV-B-induced
331 photomorphogenesis and stress acclimation in Arabidopsis. *EMBO J* **28**: 591–601
- 332 **Gruber H, Heijde M, Heller W, Albert A, Seidlitz HK, Ulm R** (2010) Negative feedback
333 regulation of UV-B-induced photomorphogenesis and stress acclimation in Arabidopsis.
334 *Proc Natl Acad Sci U S A* **107**: 20132–7
- 335 **Heijde M, Ulm R** (2013) Reversion of the Arabidopsis UV-B photoreceptor UVR8 to the
336 homodimeric ground state. *Proc Natl Acad Sci U S A* **110**: 1113–8
- 337 **Kolar K, Knobloch C, Stork H, Žnidarič M, Weber W** (2018) OptoBase: A Web Platform for
338 Molecular Optogenetics. *ACS Synth Biol* **7**: 1825–1828
- 339 **Kolar K, Weber W** (2017) Synthetic biological approaches to optogenetically control cell
340 signaling. *Curr Opin Biotechnol* **47**: 112–119
- 341 **Krueger D, Izquierdo E, Viswanathan R, Hartmann J, Pallares Cartes C, De Renzis S**
342 (2019) Principles and applications of optogenetics in developmental biology.
343 *Development*. doi: 10.1242/dev.175067
- 344 **Lau OS, Deng XW** (2012) The photomorphogenic repressors COP1 and DET1: 20 years later.
345 *Trends Plant Sci* **17**: 584–93
- 346 **Lin Q, Jin S, Zong Y, Yu H, Zhu Z, Liu G, Kou L, Wang Y, Qiu J-L, Li J, et al** (2021) High-
347 efficiency prime editing with optimized, paired pegRNAs in plants. *Nat Biotechnol* **1**–5
- 348 **Lin Q, Zong Y, Xue C, Wang S, Jin S, Zhu Z, Wang Y, Anzalone A V., Raguram A, Doman**
349 **JL, et al** (2020) Prime genome editing in rice and wheat. *Nat Biotechnol* **38**: 582–585
- 350 **Liu Z, Zhang J, Jin J, Geng Z, Qi Q, Liang Q** (2018) Programming Bacteria With Light-
351 Sensors and Applications in Synthetic Biology. *Front Microbiol* **9**: 2692
- 352 **Moore I, Samalova M, Kurup S** (2006) Transactivated and chemically inducible gene
353 expression in plants. *Plant J* **45**: 651–683
- 354 **Müller K, Engesser R, Metzger S, Schulz S, Kämpf MM, Busacker M, Steinberg T,**
355 **Tomakidi P, Ehrbar M, Nagy F, et al** (2013a) A red/far-red light-responsive bi-stable
356 toggle switch to control gene expression in mammalian cells. *Nucleic Acids Res* **41**: e77–
357 e77
- 358 **Müller K, Engesser R, Schulz S, Steinberg T, Tomakidi P, Weber CC, Ulm R, Timmer J,**
359 **Zurbriggen MD, Weber W** (2013b) Multi-chromatic control of mammalian gene
360 expression and signaling. *Nucleic Acids Res* **41**: e124–e124
- 361 **Müller K, Naumann S, Weber W, Zurbriggen MD** (2015) Optogenetics for gene expression
362 in mammalian cells. *Biol Chem* **396**: 145–152
- 363 **Müller K, Siegel D, Jahnke FR, Gerrer K, Wend S, Decker EL, Reski R, Weber Abce W,**
364 **Zurbriggen MD** (2014) A red light-controlled synthetic gene expression switch for plant
365 systems †. *Mol BioSyst* **10**: 1679
- 366 **Ochoa-Fernandez R, Abel NB, Wieland F-G, Schlegel J, Koch L-A, Miller JB, Engesser**
367 **R, Giuriani G, Brandl SM, Timmer J, et al** (2020) Optogenetic control of gene
368 expression in plants in the presence of ambient white light. *Nat Methods* **17**: 717–725
- 369 **Ochoa-Fernandez R, Samodelov SL, Brandl SM, Wehinger E, Müller K, Weber W,**

- 370 **Zurbriggen MD** (2016) Optogenetics in Plants: Red/Far-Red Light Control of Gene
 371 Expression. *Methods Mol. Biol.* pp 125–139
- 372 **Pacín M, Legris M, Casal JJ** (2014) Rapid decline in nuclear constitutive
 373 photomorphogenesis1 abundance anticipates the stabilization of its target elongated
 374 hypocotyl5 in the light. *Plant Physiol* **164**: 1134–8
- 375 **Podolec R, Demarsy E, Ulm R** (2021) Perception and Signaling of Ultraviolet-B Radiation in
 376 Plants. *Annu Rev Plant Biol* **72**: annurev-arplant-050718-095946
- 377 **Rizzini L, Favory J-J, Cloix C, Faggionato D, O'Hara A, Kaiserli E, Baumeister R, Schafer
 378 E, Nagy F, Jenkins GI, et al** (2011) Perception of UV-B by the Arabidopsis UVR8 Protein.
 379 *Science* (80-) **332**: 103–106
- 380 **Salinas F, Rojas V, Delgado V, Agosin E, Larrondo LF** (2017) Optogenetic switches for
 381 light-controlled gene expression in yeast. *Appl Microbiol Biotechnol* **101**: 2629–2640
- 382 **Schaumberg KA, Antunes MS, Kassaw TK, Xu W, Zalewski CS, Medford JI, Prasad A**
 383 (2016) Quantitative characterization of genetic parts and circuits for plant synthetic
 384 biology. *Nat Methods* **13**: 94–100
- 385 **Yin R, Skvortsova MY, Loubéry S, Ulm R** (2016) COP1 is required for UV-B-induced nuclear
 386 accumulation of the UVR8 photoreceptor. *Proc Natl Acad Sci U S A* **113**: E4415-22
- 387 **Zuo J, Chua N-H** (2000) Chemical-inducible systems for regulated expression of plant genes.
 388 *Curr Opin Biotechnol* **11**: 146–151
- 389



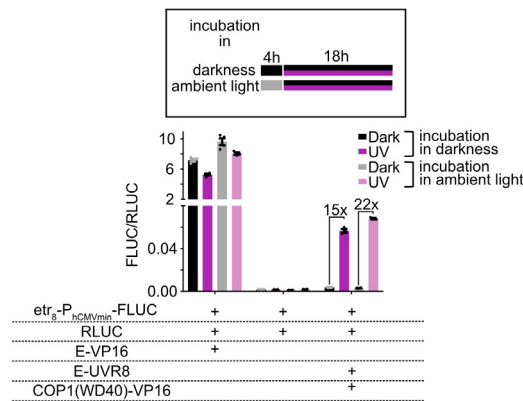
390
391
392
393
394
395
396
397
398
399
400
401
402
403

Figure 1: Mode of function and characterization of the UV-B light-induced gene expression system (UV-B_{ON}) for application in *A. thaliana* protoplasts. (A) Mode of function. Under dark conditions, UVR8 dimers fused to the macrolide repressor E, are bound to the octameric *etr₈* operator sequence on the reporter plasmid without activating gene expression. Upon illumination with UV-B light (311 nm) dimerization of UVR8 is disrupted by conformational change of UVR8 to its open state. The open, non-dimerized state is able to bind to COP1(WD40) and recruits it to the reporter plasmid. COP1(WD40) is fused to the VP16 transactivation domain, now in close proximity to the minimal promoter, initiating gene expression of the firefly luciferase (FLUC) reporter gene. In absence of UV-B illumination, UVR8 spontaneously reverts back to the closed state, terminating the gene expression (adapted from Müller et al., 2013b). Characterization of the UV-B inducible gene expression system in wild type (B) or *rup1/rup2* double mutant (C) protoplasts of *A. thaliana*. Protoplasts were isolated and transformed with the indicated components. After transformation and four hours of incubation in the dark, protoplasts were exposed to light of 311 nm ($7 \mu\text{mol m}^{-2} \text{s}^{-1}$) for 18 hours (purple bars) of kept in the dark (black/grey bars) before the FLUC expression, normalized to constitutively expressed renilla luciferase (RLUC), was determined. $n = 4$, error bars indicate one standard error of the mean (SEM).



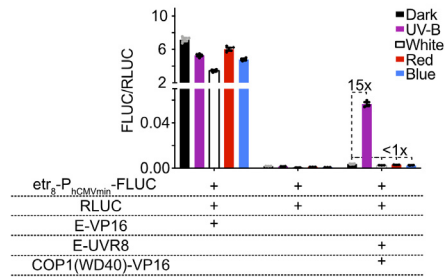
404
405
406
407
408
409
410
411
412

Figure 2: Kinetics of the UV-B inducible gene expression system (UV-B_{ON}) in wild type protoplasts of *A. thaliana*. Protoplasts were isolated and transformed with E-UVR8 and COP1(WD40)-VP16 and the reporter plasmid (etr_B-P_{CMVmin}-FLUC). After transformation and four hours of incubation in the dark, protoplasts were exposed to light of 311 nm (7 μmol m⁻² s⁻¹) or kept in the dark for the indicated time intervals before the FLUC expression, normalized to constitutively expressed renilla luciferase (RLUC), was determined. Values were normalized to the corresponding dark sample. *n* = 4, error bars indicate one standard error of the mean (SEM).



413
414
415
416
417
418
419
420
421

Figure 3: Characterization of the UV-B light-induced gene expression system (UV-B_{ON}) for application in *A. thaliana* protoplasts after different incubation conditions. Protoplasts were isolated and transformed with the indicated components. After transformation and four hours of incubation in the dark or under ambient light, protoplasts were exposed to light of 311 nm (7 μmol m⁻² s⁻¹; purple/rose bars) for 18 hours or kept in the dark (black/grey bars) before the FLUC expression, normalized to constitutively expressed renilla luciferase (RLUC), was determined. *n* = 4, error bars indicate one standard error of the mean (SEM).



422

423

424

425

426

427

428

429

430

Figure 4: Characterization of the UV-B light-induced gene expression system (UV-B_{ON}) for application in *A. thaliana* protoplasts in different light conditions. Protoplasts were isolated and transformed with the indicated components. After transformation and four hours of incubation in the dark, protoplasts were exposed to light of 311 nm ($7 \mu\text{mol m}^{-2} \text{s}^{-1}$; purple bars), white light ($10 \mu\text{mol m}^{-2} \text{s}^{-1}$ for the following wavelength ranges: blue 420–490 nm, red 620–680 nm, and far-red 700–750 nm; white bars), blue light of 460 nm ($5 \mu\text{mol m}^{-2} \text{s}^{-1}$; blue bars), red light of 660 nm ($5 \mu\text{mol m}^{-2} \text{s}^{-1}$, red bars) for 18 hours or kept in the dark (black bars) before the FLUC expression, normalized to constitutively expressed renilla luciferase (RLUC), was determined. $n = 4$, error bars indicate one standard error of the mean (SEM).

1 UV-B light-inducible system for the control of gene
2 expression in *A. thaliana* mesophyll protoplasts

3

4 Tim Blomeier¹, Uriel Urquiza-Garcia¹, Giovanni Giuriani¹, Matias D. Zurbriggen^{1,*}

5

6 ¹Institute of Synthetic Biology, University of Düsseldorf and CEPLAS, Düsseldorf, Germany

7

8 *Corresponding author: Email: matias.zurbriggen@uni-duesseldorf.de

9

10

11 SUPPLEMENTARTY INFORMATION

12

13 Figure S1: Graph diagramming the ordinary differential equations (ODE) model fitted to the
14 kinetic experiment of the UV-B_{ON} system described in Figure 2.

15

16 Table S1: Construction and description of plasmids used in this work.

17

18 Table S2: Oligonucleotides used for cloning in this work.

19

20

21 Description of the mathematical modeling approach:

22

23 1. Reproducibility

24 In order to ensure reproducible computational results, we implemented a docker container
25 (similar to Urquiza-García and Millar, 2021). The docker container can be obtained by typing
26 `docker pull uurquiza/uv_modelling:latest`. Nonetheless the docker file can be found in the
27 supplementary data. The system built using:

28 `docker built -t uurquiza/uv_modelling:latest .`

29 In order to start the container, navigate to the folder enclosing the script files and type:

30 `sh start.sh`

31 Once inside the docker image type

32 `jn`

33 this will start jupyterlab which is accessible on the local computer web-browser by typing

34 `localhost:8888/`

35

36 2. Modelling the UV optogenetic system

37 In order to test if the system behaves to our expectation, we created a mathematical model
38 based on Ordinary Differential Equations (ODEs) that integrates our basic assumptions of how
39 the optogenetic system operates. The time scale of the system is in hours while the mass scale
40 currently presents arbitrary units. The trailing *c* denotes concentration.

41

$$42 \quad \frac{dcU8}{dt} = n_1 + Lk_1cU8_d - k_2cU8^2 - k_3cC16cU8 + k_4cCU - m_1cU8$$

$$43 \quad \frac{dcC16}{dt} = n_2 + k_4cCU - k_3cC16cU8 - m_3cC16$$

$$44 \quad \frac{cU8_d}{dt} = k_2cU8^2 - Lk_1cU8_d - m_2cU8_d$$

$$45 \quad \frac{dCU}{dt} = k_3cC16cU8 - k_4cCU - m_4cCU$$

$$46 \quad \frac{cLUC}{dt} = n_3 \frac{cCU}{g1 + cCU} - m_5cLUC$$

47

48 The most important assumption is the system operates without interference from the
 49 endogenous light phototransduction pathways. Now in particular, we assume a constitutive net
 50 production of E-UVR8 ($cU8$) and COP(WD40)-VP16 ($cC16$) represented by parameters n_1 and
 51 n_2 . We assumed constant degradation across the experiment represented by m_1 and m_3 . We
 52 also assume that upon production E-UVR8 and COP1(WD40)-VP16 are instantaneously
 53 transported into the nucleus. In darkness we assume dimerization of E-UVR8 with rate
 54 constant k_2 . Under UV-B illumination represented by L monomerization of E-UVR8 dimers
 55 takes place with rate constant k_1 . L has units of $\mu\text{mol}/\text{m}^2\text{s}$. E-UVR8 monomers can
 56 interact with COP1-VP16 with rate constant k_3 which results in the formation of the E-
 57 UVR8:COP1(WD40)-VP16 (cCU). The complex can dissociate with a rate constant k_4 . The
 58 cCU complex can then activate the expression of a firefly luciferase reporter gene ($cLUC$). We
 59 assume hill type kinetics without cooperativity. The latter functional form modulates LUC's net
 60 production rate n_3 . LUC degrades with decay constant m_5 with value of 0.15 h^{-1} .

61

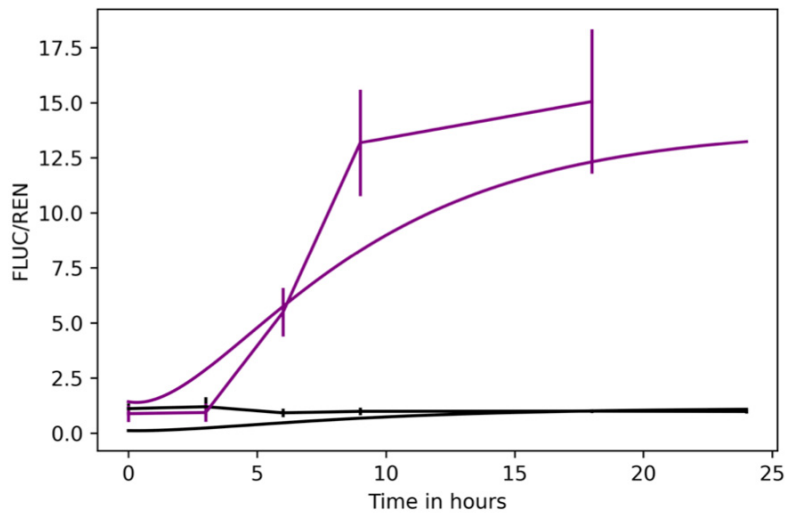
62 3. Model Fitting to time series of LUC activity in protoplast

63 Using this model, we tested if we could explain the dynamic for the observable variable LUC.
 64 We performed computational fitting of the model using Tellurium and Lmfit in python. We
 65 obtained scaling factors automatically as described by Brown and Sethna, 2003. The number
 66 of data points is lower than the number of parameters therefore we artificially fixed some of
 67 them for example the LUC decay constant m_5 (assuming, same reporter characteristics as the
 68 one described by Urquiza-García and Millar, 2019). Furthermore, we fixed the net production
 69 rates of E-UVR8 and COP1(WD40)-VP16. These parameters effectively determine the mass
 70 scale however we can set them to nominal values (e.g. 1). We are currently mainly interested

71 in explaining the time series shape rather than the mass-scale of the system. Therefore, the
 72 model has absolute time units, however remains with arbitrary mass units.
 73

$$\begin{aligned} \frac{d([cC16] \cdot V_{cell})}{dt} &= +V_{cell} \cdot (n2 + k4 \cdot [cCU] - k3 \cdot [cC16] \cdot [cU8] - m3 \cdot [cC16]) \\ \frac{d([cU8] \cdot V_{cell})}{dt} &= +V_{cell} \cdot (n1 + L \cdot k1 \cdot [cU8d] - k2 \cdot [cU8] \cdot [cU8] - k3 \cdot [cC16] \cdot [cU8] + k4 \cdot [cCU] - m1 \cdot [cU8]) \\ \frac{d([cU8d] \cdot V_{cell})}{dt} &= +V_{cell} \cdot (k2 \cdot [cU8] \cdot [cU8] - L \cdot k1 \cdot [cU8d] - m2 \cdot [cU8d]) \\ \frac{d([cCU] \cdot V_{cell})}{dt} &= +V_{cell} \cdot ([cC16] \cdot [cU8] - k4 \cdot [cCU] - m4 \cdot [cCU]) \end{aligned}$$

74
$$\frac{d([cLUC] \cdot V_{default_compartment})}{dt} = + \left(V_{cell} \cdot \left(\frac{n1 \cdot [cCU]}{g1 + [cCU]} - m5 \cdot [cLUC] \right) \right)$$



75
 76 Figure S1: Graph diagramming the ordinary differential equations (ODE) model fitted to the kinetic experiment of the UV-
 77 BON system described in Figure 2.
 78

79
 80 Table S1: Construction and description of plasmids used in this work. (All plasmids were constructed using AQUA and
 81 Gibson assembly cloning methods.)
 82
 83

Plasmid	Description	Reference
pGB109	P_{CaMV35S}-RLUC-pA P _{CaMV35S} -driven plant expression vector encoding the renilla luciferase.	GoldenBraid Database
pKM081	etr₈-P_{CaMVmin}-SEAP-pA	(Müller et al., 2013)

pMZ820	P_{CaMV35S}-E-UVR8(12-381)-pA P _{CaMV35S} -driven plant expression vector encoding <i>A. thaliana</i> UVR8(12-381) fused to the macrolide repressor E.	This work
pMZ821	P_{CaMV35S}-COP1(WD40)-VP16-pA P _{CaMV35S} -driven plant expression vector encoding the WD40 domain of <i>A. thaliana</i> COP1 fused to the VP16 transactivation domain.	This work
pMZ824	P_{CaMV35S}-E-VP16-NLS-pA P _{CaMV35S} -driven plant expression vector encoding the macrolide repressor E fused to the VP16 transactivation domain and a nuclear localization domain.	(Müller et al., 2014)
pMZ827	P_{CaMV35S}-E-PIF6(1-100)-NLS-pA P _{CaMV35S} -driven plant expression vector encoding nuclear-targeted E-PIF6(1-100)	(Müller et al., 2014)
pMZ836	etr₈-P_{hCMVmin}-FLUC-pA	(Müller et al., 2014)
pROF052	etr₈-P_{hCMVmin}-FLUC-pA pMZ836 and pKM081 were digested with EcoRI/SbfI. CIP was added to pMZ836 and fragments etr ₈ (pKM081) and P-CMVmin-FLUC-pA (pMZ836) were purified and ligated.	This work
pROF150	P_{CaMV35S}-E-UVR8(12-381)-NLS-pA E-UVR8 was amplified from pMZ820 with oligos oROF003/157. pMZ827 was linearized by EcoRI/NdeI. Both fragments were assembled by AQUA cloning.	This work
pROF151	P_{CaMV35S}-COP1(WD40)-VP16-NLS-pA COP1(WD40)-VP16 was amplified from pMZ821 with oligos oROF003/158. pMZ827 was linearized by EcoRI/NdeI. Both fragments were assembled by AQUA cloning.	This work
pRSET	PT7-driven bacterial expression vector	Novagen
pTB511	P_{35S}-E-UVR8-pA UVR8 was amplified from synthesized UVR8 from IDT and amplified with oTB216/217. pMZ820 was linearized by EcoRI/SgrAI. Both fragments were assembled using AQUA cloning.	This work

84
85
86
87

Table S2: Oligonucleotides used for cloning in this work.

Oligonucleotide	Sequence (5' → 3')	88
oTB216	CACATGCGTCCGCGTACAGCGGTACCGGCGGGCGCCGCATGGCGGAGGATATGGCT	
oTB217	CCGGTGGATCCAAGCTTCTCGAGCCCGGGGAATTCTCAAATTCGTACACGCTTGACA TCA	
oROF003	AGGTAAGCTTGGTACCACC	
oROF157	TGGATCCAAGCTTCTCGAGCCCGGGGAATTCCTACACCTTCTCTTCTTTGGTCCA TCGACGCTGAGT	
oROF158	TGGATCCAAGCTTCTCGAGCCCGGGGAATTCCTACACCTTCTCTTCTTTGGCCCA CCGTACTCGTCAAT	

89
90
91
92
93
94

- 95 **References**
96
97 **Brown KS, Sethna JP** (2003) Statistical mechanical approaches to models with many poorly
98 known parameters. *Phys Rev E* **68**: 021904
99 **Müller K, Engesser R, Schulz S, Steinberg T, Tomakidi P, Weber CC, Ulm R, Timmer J,**
100 **Zurbriggen MD, Weber W** (2013) Multi-chromatic control of mammalian gene expression
101 and signaling. *Nucleic Acids Res* **41**: e124–e124
102 **Müller K, Siegel D, Jahnke FR, Gerrer K, Wend S, Decker EL, Reski R, Weber Abce W,**
103 **Zurbriggen MD** (2014) A red light-controlled synthetic gene expression switch for plant
104 systems †. *Mol BioSyst* **10**: 1679
105 **Ochoa-Fernandez R, Samodelov SL, Brandl SM, Wehinger E, Müller K, Weber W,**
106 **Zurbriggen MD** (2016) Optogenetics in Plants: Red/Far-Red Light Control of Gene
107 Expression. *Methods Mol. Biol.* pp 125–139
108 **Urquiza-García U, Millar AJ** (2021) Testing the inferred transcription rates of a dynamic, gene
109 network model in absolute units. *bioRxiv* 2021.03.18.436071
110 **Urquiza-García U, Millar AJ** (2019) Expanding the bioluminescent reporter toolkit for plant
111 science with NanoLUC. *Plant Methods* **15**: 68
112

7.2 Review articles

Jennifer Andres*, **Tim Blomeier***, Matias D. Zurbriggen. Synthetic switches and regulatory circuits in plants, *Plant Physiol* **179**: 862–884, February 2019

*equal contribution

Contribution: Research, writing and preparation of all figures with Jennifer Andres.

7.2.1 Synthetic switches and regulatory circuits in plants



Update on Synthetic Switches and Regulatory Circuits

Synthetic Switches and Regulatory Circuits in Plants¹[OPEN]

Jennifer Andres,² Tim Blomeier,² and Matias D. Zurbriggen^{3,4}

Institute of Synthetic Biology and CEPLAS, University of Düsseldorf, 40225 Duesseldorf, Germany

ORCID ID: 0000-0002-3523-2907 (M.D.Z.).

Synthetic biology is an established but ever-growing interdisciplinary field of research currently revolutionizing biomedicine studies and the biotech industry. The engineering of synthetic circuitry in bacterial, yeast, and animal systems prompted considerable advances for the understanding and manipulation of genetic and metabolic networks; however, their implementation in the plant field lags behind. Here, we review theoretical-experimental approaches to the engineering of synthetic chemical- and light-regulated (optogenetic) switches for the targeted interrogation and control of cellular processes, including existing applications in the plant field. We highlight the strategies for the modular assembly of genetic parts into synthetic circuits of different complexity, ranging from Boolean logic gates and oscillatory devices up to semi- and fully synthetic open- and closed-loop molecular and cellular circuits. Finally, we explore potential applications of these approaches for the engineering of novel functionalities in plants, including understanding complex signaling networks, improving crop productivity, and the production of biopharmaceuticals.

Signaling processes are central to the organization and existence of any form of life. Exogenous and endogenous inputs are sensed and integrated by molecular networks in cells with feedback loops and Boolean logic decision making, resulting in a specific response (output). For this purpose, regulatory circuits are structured as a tightly and finely coordinated network of information with transfer and processing steps and chains, each individually fulfilling a specific task. These processes are in turn organized in time and space: within subcellular compartments (membranes, organelles, cytosol, and nuclei) and between cells and tissues. Signal mediators include proteins, nucleic acids, and small molecules (Lim, 2010). A key characteristic of biological regulatory networks is their modular architecture, in which building blocks are assembled in a combinatorial fashion. The constituent individual components perform a given distinct, particular function within the network, be it signals per se or switches (i.e. components that are able to detect an input signal and transform it into an output cue; Stein and Alexandrov, 2015).

Plants have evolved complex networks to integrate environmental, genetic (via spatial and temporal cues), developmental, and metabolic programs as well as the

current physiological status. The output is a response tailored to adjust the cell welfare and function in the context of a multicellular organism (Trewavas, 2005; Sheen, 2010). These systems are constantly active, monitoring the ever-varying conditions and executing outputs following both open- and closed-loop programming principles for optimal responses. Recent advances in molecular biology, genetics, and systems biology-associated technologies have led to the identification of a huge number of signaling components, cascades, and regulatory mechanisms thereof. The field of plant signaling is growing rapidly, as is our knowledge of the complexity of these networks (Jaeger et al., 2013; Lavedrine et al., 2015). Most signaling pathways comprise many components and exhibit redundancy of function, extensive feedback control, and cross-interaction with other networks. The fine-tuning involves different types of posttranslational modifications, as exemplified by the complex mesh integrating light and hormone signaling, the circadian clock, and developmental and growth processes (Pokhilko et al., 2013; Fogelmark and Troein, 2014). In addition, there is a lack of quantitative molecular tools to interrogate and monitor the dynamics of these systems (Liu and Stewart, 2015; Samodelov and Zurbriggen, 2017). This not only hinders a comprehensive understanding of the function, regulation, and effects of signaling circuits but also the targeted manipulation of metabolic and signaling networks and, consequently, the introduction of novel functionalities into plants. In combination with modern analytical technologies, synthetic biology approaches represent the key to overcoming these limitations, and they are currently revolutionizing fundamental bacterial, yeast, and metazoan research as well as the biotechnology and biomedicine industries (Lu et al., 2009; Lienert et al., 2014).

¹This work was supported by the Excellence Initiatives of the German Federal States Governments (DFG, EXC-1028-CEPLAS), a stipend from the Max-Planck-Gesellschaft (Max Planck Society), the University of Düsseldorf, and the University of Cologne.

²These authors contributed equally to the article.

³Author for contact: matias.zurbriggen@uni-duesseldorf.de.

⁴Senior author.

J.A., T.B., and M.D.Z. performed research and wrote the article.

[OPEN] Articles can be viewed without a subscription.

www.plantphysiol.org/cgi/doi/10.1104/pp.18.01362

ADVANCES

- Interplay of mathematical modeling and quantitatively characterized synthetic modules enabled the engineering of predictable and more complex synthetic signaling networks in a multiplicity of organisms; however, the implementation of these approaches in plants lags behind.
- Successful engineering of functional, fully synthetic, autoregulated, molecular and cellular devices is revolutionizing biomedical research and industrial applications.
- The first fully synthetic regulatory circuits in plants to be designed, provided the existing experimental limitations are overcome, will represent a breakthrough in the plant research paradigm and will be important for many biotechnological applications fostering a second green revolution.

Synthetic biology is a relatively new discipline bridging engineering with life sciences. It applies basic engineering principles for the modular, combinatorial assembly of biological parts into higher order complex signaling and metabolic structures. Key to the strategy is the implementation of mathematical modeling for the design and quantitative functional characterization of the molecular parts and for guiding the assembly, implementation, and optimization of the individual modules and networks (Ellis et al., 2009; Lim, 2010). Thus, inspired by nature, synthetic biology harnesses the modular architecture of biological systems. However, the goal is to develop novel molecular and cellular systems with desired properties and biological functionalities that are not present in nature. These properties range from gene switches and genetically encoded biosensors to fully synthetic autonomous molecular and cellular circuits and organelles as well as biohybrid smart materials and biopharmaceuticals (Brophy and Voigt, 2014; Lienert et al., 2014; Xie and Fussenegger, 2018). This field has already taken root in microbial systems as well as other higher eukaryotes. However, the generalized implementation of these approaches in the plant field lags behind.

This review is intended to serve as inspiration for plant scientists, raising interest in the field-changing potential of widely implementing synthetic biology principles. We will give an overview on the state of the technology and progress achieved with the application of synthetic biology strategies for studying, manipulating, and de novo engineering of signaling circuitry, with exemplary illustration of bacterial, yeast, and animal systems. The first implementations and future prospects in plant research will be highlighted, and the limitations and necessary technological advances for a

straightforward implementation in plants will be discussed. The article is structured in three parts, following a hierarchy of molecular and realization complexity, starting off with molecular switches. Chemical-inducible devices will be introduced. In particular, the implementation of light as a trigger will be highlighted, describing the groundbreaking experimental advances enabled by optogenetics and its applications for the control of cellular processes. The concepts of orthogonality in the design of the molecular parts and the need for hand-in-hand work with theoreticians/mathematical modeling will be discussed. Further aspects include the functional combination of simple synthetic switches into molecular devices implemented in cells to perform decision-making processes, such as oscillators and molecular Boolean logic gates. Finally, we will focus on semi- or fully synthetic molecular signaling networks with open- and closed-loop control configurations and the transition into cellular devices with ad hoc functionalities for applications. For example, these systems will facilitate personalized nutrition, the production of biopharmaceuticals, and the obtainment of higher crop yields in an ecologically sustainable manner.

SYNTHETIC GENETIC SWITCHES

The rational combination of sensing and effector modules allows the wiring of inputs and outputs that are normally not functionally linked in nature, with the goal of performing novel functions. These functions range from the targeted control of a cellular process and the quantitative monitoring of a molecule to the induction of enzymatic activity or posttranslational modifications. The molecular mechanisms behind the signal integration and transfer mostly involve conformational changes. These allosteric modifications are induced by interactions between proteins, nucleic acids, and small molecules (e.g. protein/protein, small molecule/protein, and RNA/DNA; Stein and Alexandrov, 2015). Synthetic switches are engineered in a modular fashion, integrating natural and de novo-designed molecular parts. Unfortunately, switches often do not perform as expected when introduced into living systems. As in engineering, having a complete quantitative functional characterization of the modules and a supporting mathematical model contributes to straightforward and optimal implementation. A series of functional parameters of switches to be evaluated include dynamic range (ratio between maximal and basal activation), leakiness (basal activity in the absence of an inducing signal), kinetics, and reversibility of function. This is also critical when using switches as building blocks for the assembly of higher order circuits (see next section). Finally, the use of orthogonal components helps to maximize the insulation of the system, with the objective of achieving independent function and reducing unwanted effects on the endogenous networks, which are not targets of the synthetic regulation. Next, chemical- and light-inducible switches for the control

Andres et al.

of gene expression and other cellular processes will be discussed. Protein and RNA switches used for quantitative monitoring of molecules and processes (sensors) will not be discussed in this review; for a comprehensive description, see Okumoto et al. (2012) and Walia et al. (2018).

Gene Expression Control

Transcriptional Switches

The principle of autoregulation is a key architectural element in genetic or biochemical networks, shared by prokaryotic and eukaryotic cells (Freeman, 2000). Therefore, the synthesis of proteins is essentially influenced by the genetic program and cellular environment and underlies a tight regulation through gene switches. A gene switch can be considered as any natural or synthetically designed module controlling gene expression at the level of DNA, RNA, or protein (post-translational modifications and stability; Xie and Fussenegger, 2018). Key building blocks of natural switches were first described by Jacob and Monod (1961) for the regulation of the lactose (lac) operon in *Escherichia coli*, which is regarded as the classic model for gene expression control. They characterized the promoter as the point of transcriptional initiation and identified controlling elements (repressors and inducers), which, upon binding with highly specific

affinity to the upstream-located operator motif, quantitatively enhance or repress mRNA transcription. This binding is dependent on the presence of a metabolite that changes the conformation (allosteric regulation) of the regulator protein (Dickson et al., 1975).

While prokaryotic gene expression circuits mostly utilize autoregulatory inhibition (negative feedback) to guarantee homeostasis, eukaryotic transcriptional regulation comprises more complex combinations of negative and positive regulators engaging in feedback loops and Boolean logic gate computing mechanisms (Savageau, 1974; Bateman, 1998; Thieffry et al., 1998; Becskei and Serrano, 2000; Freeman, 2000). A mechanistic and functional characterization of some of these simple prokaryotic regulatory elements (Beck et al., 1982; Berens et al., 1992) enabled the engineering of artificial, exogenously controlled systems of gene expression in prokaryotic and eukaryotic cells (Gardner et al., 2000; Ajo-Franklin et al., 2007). One of the first inducible gene switches is based on the tetracycline-regulated promoter of *E. coli* that controls the expression of the tetracycline-resistance-mediating *tetA* gene (Fig. 1A). In brief, a simple C-terminal fusion of the tetracycline repressor (TetR) to a transcriptional activation domain from the herpes simplex virus type 1 virion protein16 (VP16) converted the transcriptional repressor into a tetracycline-controlled transcriptional transactivator (tTA) in eukaryotic cells (Gossen and Bujard, 1992). In the absence of tetracycline, tTA binds

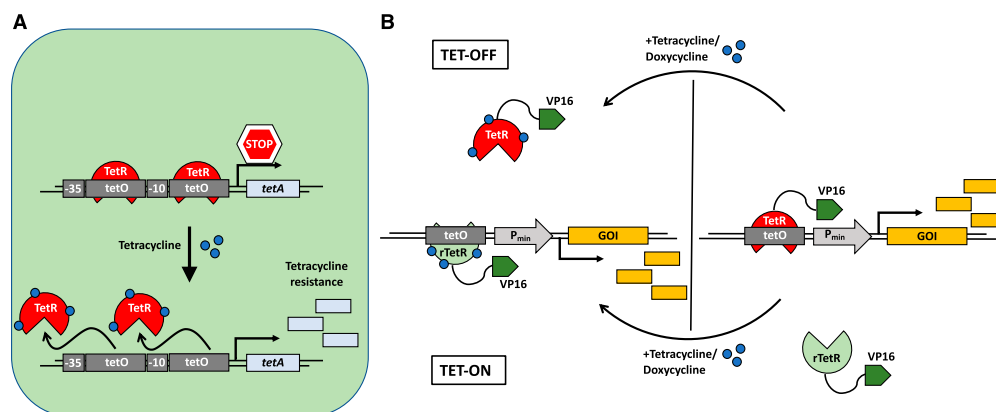


Figure 1. Illustration of the natural bacterial tetracycline resistance mechanism and synthetic tetracycline-based gene expression systems. A, In the absence of tetracycline (tet), the tet repressor (TetR) is bound to its cognate tet operator (tetO) DNA-binding motif, repressing the expression of the tet resistance-mediating *tetA* gene. Upon increasing cellular levels of tet, tet binding induces a conformational change of TetR, leading to its dissociation from the operator sequence, and expression of *tetA* ensues. B, The tet-OFF system designed for use in mammalian cells is based on a synthetic switch comprising the natural TetR fused to the activating domain of VP16 of the herpes simplex virus and a synthetic promoter with a series of repeats of the tetO motif placed upstream of a minimal promoter (e.g., human cytomegalovirus minimal promoter). The system is constitutively active and is turned OFF in the presence of the antibiotic. Implementation of a reversed TetR mutant (rTetR) generates a tet-ON system: tet induces the binding of rTetR to the target sequence, which in turn induces gene expression (tet can be replaced by other antibiotics of the tetracycline family like doxycycline). Replacement of VP16 by a transrepressor such as KRAB inverts the effect of the switch (not depicted here). GOI, Gene of interest. (Adapted from Gossen et al., 1995.)

864

Plant Physiol. Vol. 179, 2019

Downloaded on May 11, 2021. - Published by <https://plantphysiol.org>
Copyright (c) 2020 American Society of Plant Biologists. All rights reserved.

to the cognate tet-operator region on the synthetic promoter construct, activating transcription from an adjacent minimal promoter sequence. Upon addition of tetracycline, tTA is removed from the promoter and gene expression is shut off (Fig. 1B). A reversed TetR was generated by random mutagenesis (Gossen et al., 1995), which, when fused to the VP16 domain, enables tetracycline-induced transcriptional activation (Fig. 1B). Alternatively, fusion of a transrepressor instead of a transactivator to TetR or modification of the synthetic promoter region enables other positive and negative regulation configurations (Kramer et al., 2004a). Following these simple molecular engineering principles, and modifications thereof, a vast set of chemically inducible gene switches were developed for use in yeast and animal cells sensitive to antibiotics, primary and secondary metabolites, and volatiles, among other substances (for review, see Hörner and Weber, 2012).

To achieve tight and predictable control over gene expression, a quantitative characterization and mathematical modeling of the regulator/promoter-switch is needed (for the implementation of mathematical modeling into synthetic circuitry approaches, refer to the detailed works of Ellis et al. [2009] and Lim [2010]). The optimization of key parameters such as strength and kinetics of expression, leakiness, etc., can be performed subsequently by reengineering the switch components. Usual approaches include the redesign of promoter regions: introduction of multiple repeats of binding sites, point mutations to alter affinity, protein engineering, and use of different transactivators/transrepressors (Ajo-Franklin et al., 2007). The incorporation of positive and/or negative feedback loop configurations (e.g. by placing the regulator under control of its own target synthetic promoter) enables a greater dynamic range of the dose-dependent response (Gossen et al., 1995; Becskei et al., 2001). Promoters can be engineered further by combining activation and repression of gene expression in a simultaneous manner, thereby facilitating a deeper insight into gene network regulation by increasing the possible regulation conditions. Studying unregulated, repressed, activated, or simultaneously repressed/activated gene expression helped develop a model for precise prediction of the behavior of genetic networks in vivo (Guido et al., 2006). Other examples include the implementation of several chemical-, hormone-, or CRISPR/Cas-inducible or repressible switches for the control of multiregulated systems, especially for pharmacological application in mammalian cells (Weber et al., 2002; Nielsen and Voigt, 2014). Broad implementation of these gene switches in cell culture and in vivo (mouse, rat, *Drosophila* spp., zebrafish, *Caenorhabditis elegans*) represented a paradigm change in the way metabolic and signaling networks can be studied and redesigned synthetically.

In plant systems, several chemically inducible switches have been developed for a temporal and quantitative regulation of expression (Table 1). For

instance, these switches are triggered by IPTG (Wilde et al., 1992), antibiotics such as tetracycline (Gatz et al., 1992; Weinmann et al., 1994; Müller et al., 2014), macrolides and pristinamycin (Frey et al., 2001; Müller et al., 2014), copper (McKenzie et al., 1998), or ethanol (Caddick et al., 1998; Roslan et al., 2001). The most widely employed switch is a steroid-based system that allows precise temporal control over cellular processes in whole plants (Schena et al., 1991). Recently, gene switches comprising a Cas9-based repressor and regulatory modules of hormone signaling pathways (auxin, GA, and jasmonate) have been implemented in Arabidopsis (*Arabidopsis thaliana*; hormone activated Cas9-based repressor [HACRs]; Khakhar et al., 2018). The HACRs are sensitive to both exogenous hormone treatments and varying endogenous hormone levels, leading to degradation of the switch and thereby regulating target gene expression (the single guide RNA-Cas9 complex dictates the specificity). This tool can be applied to regulate hormone signaling or any other target of interest, thus allowing the manipulation of stress tolerance and yield in crop plants.

However, chemical switches have limitations concerning defined spatiotemporal activation of the system due to abundance, administration, and diffusion of the inducer molecules as well as usual toxicity effects. Recently, light-controlled genetically encoded molecular devices have been engineered and implemented in living cells to control cellular processes, giving rise to the nascent field of optogenetics (Box 1). These devices overcome the inherent restrictions of chemically regulated switches. Light-regulated switches comprise bacterial and plant photoreceptors, such as UV-B RESISTANCE8, phototropin1/EL222/CRYPTOCHROME2, CarH, PHYTOCHROME B/A, and the bacterial phytochrome BphP1, among others (for a comprehensive list, see Kolar et al., 2018). Upon absorption of light, they undergo a conformational change leading to homo/hetero-association/dissociation (Kolar and Weber, 2017). This light-dependent protein interaction relays a signal to an output module that then fulfills a cellular function. In the last decade, a multitude of optogenetic gene switches regulated by UV-B, blue, green, red, and far-red/near infrared light have been engineered and implemented for the noninvasive control of gene expression with a precise temporal and spatial resolution in prokaryotic and eukaryotic systems (Zhang and Cui, 2015; Fig. 2).

Contrary to most nonautotrophic organisms, the life cycle of plants requires exposure to sunlight, which might lead to nonintentional activation of the optogenetic systems. Therefore, the simple transfer of optogenetic tools developed in other organisms is challenging. While long-term experiments in dark conditions are harmful, exposure to a specific wavelength of light may interfere with the natural light-sensitive signaling and photosynthetic circuitry of the plant through their photoreceptors or light-sensitive pigments. These natural light-absorbing moieties might in turn interfere with the inducing light and the

Table 1. Representative synthetic switches and regulatory circuits in plants

AlcR, Promoter of the ALCR transcription factor; AlcA, alcohol dehydrogenase I from *Aspergillus nidulans*; XVE, chimeric transcription factor based on LexA-VP16-ER; OlexA, DNA-binding domain of the bacterial LexA repressor; pOp, chimeric promoter, comprising lac operators cloned upstream of a minimal cauliflower mosaic virus promoter; LhGR, transcription activator, a fusion between a high-affinity DNA-binding mutant of the lac repressor, lacIHis-17, and the transcription-activation domain II of GAL4 and the ligand-binding domain of the rat glucocorticoid receptor; TraR, autoinducer-dependent transcriptional activator from *Agrobacterium tumefaciens*; OOHl, 3-oxooctanyl-L-homoserine lactone; lacO, lac operator; LacI, lac repressor; IPTG, isopropyl β -D-thiogalactopyranoside; ACE1, promoter of the copper-binding regulatory protein; rTetR, reversed tetracycline repressor; TetR, tetracycline repressor; tetO, tetracycline operator; GAL4, Gal-responsive transcription factor GAL4; UAS, upstream activation sequence; PiP, pristinamycin repressor protein; PIR, pristinamycin I-responsive element; E, macrolide repressor protein from *E. coli*; etr8, eight MphR (A) [macrolide 2'-phosphotransferase II]-binding operators; N1, 10 N1-TATA minimal promoter; NEV, three finger protein N1-ER-VP64; HACR, hormone-activated Cas9-based repressor; dCAS9, nuclease-dead Cas9; PIF6, phytochrome-interacting factor6; CarH, light-responsive transcription factor; CarO, CarH-binding site-containing operator; TIR1, TRANSPORT INHIBITOR RESPONSE1; Aux/IAA, auxin/indole-3-acetic acid protein; Trg, transmembrane signaling protein; PhoB, phosphate regulon transcriptional regulatory protein; PhoR, phosphate regulon sensor protein; VP64, four copies of the virion protein16 domain of the herpes simplex virus type 1; ABA, abscisic acid.

Feature	System	Properties	References
Chemically inducible switches for gene expression	AlcR/AlcA	Ethanol inducible	Caddick et al. (1998) Roslan et al. (2001) Roberts et al. (2005)
	XVE/OlexA	β -Estradiol inducible	Zuo et al. (2000) Curtis and Grossniklaus (2003) Böhmndörfer et al. (2010)
	pOp/LhGR	Dexamethasone inducible	Schena et al. (1991) Aoyama and Chua (1997)
	TraR	OOHL inducible (quorum sensing system)	You et al. (2006)
	lac operator/LacI	IPTG inducible	Wilde et al. (1992)
	ACE1-based Cu-inducible promoter	Copper inducible	McKenzie et al. (1998)
	(r)TetR/tetO	Tetracycline inducible (rTet)/repressible (TetR)	Gatz et al. (1992) Weinmann et al. (1994) Müller et al. (2014)
	GAL4-UAS	Enhancer trap lines	Gardner et al. (2009) Johnson et al. (2005) Laplaze et al. (2005)
	PiP/PIR	Pristinamycin repressible	Frey et al. (2001) Müller et al. (2014)
Cas-based gene expression	E/etr8	Macrolide regulated	Müller et al. (2014)
	10xN1/NEV	4-Hydroxytamoxifen inducible	Beerli et al. (2000)
	HACR	Phytohormone inducible	Khakhar et al. (2018)
Light-regulated gene expression	dCAS9	gRNA-mediated gene-specific induction	Piatek et al. (2015) Lowder et al. (2015)
	Phytochrome B/PIF6	Red light induced/far-red light repressed	Müller et al. (2014) Ochoa-Fernandez et al. (2016)
Synthetic riboswitch	CarH/CarO	Green light repressed/dark induced	Chatelle et al. (2018)
	Synthetic theophylline riboswitch in plastids	Theophylline inducible	Verhounig et al. (2010)
MicroRNA-based gene silencing	Artificial microRNA	Gene-specific silencing	Schwab et al. (2006)
Posttranslational degradation	N-terminal degradation signal (It degron)	Temperature-controlled protein degradation	Faden et al. (2016)
Optogenetic manipulation of endogenous signaling networks	Red light-controlled up- or down-regulation of TIR1 in combination with a ratiometric auxin sensor to monitor the manipulated signaling	Red light-controlled tuning of auxin signaling	Müller et al. (2014)
Synthetic ligand detection and signal relay	TgR/PhoR fusion phosphorylates PhoB-VP64	Synthetic programmable ligand detection system	Antunes et al. (2011)
Synthetic ABA agonist	Cyanabactin: agonist of ABA IIIA receptors	Synthetic manipulation of transpiration and other physiological processes	Park et al. (2015) Vaidya et al. (2017)

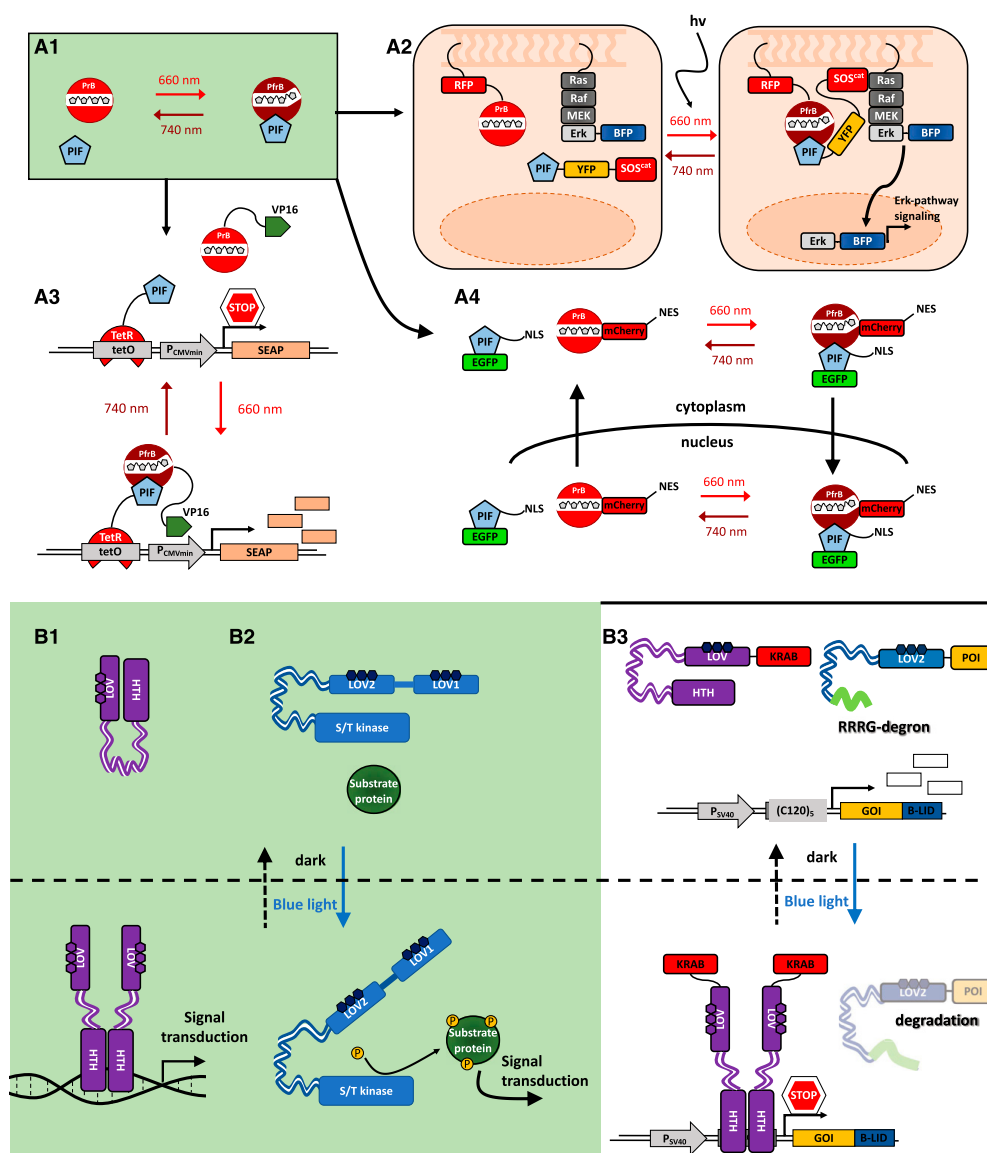


Figure 2. Optogenetic switches. Molecular principles of light-induced signaling and optogenetic tools are illustrated. A, Natural red light-inducible signaling mediated by the plant photoreceptor phytochrome B (phyB) and optogenetic tools developed based on it. A1, The red/far-red light-perceiving photoreceptor phyB remains in its inactive Pr conformation in the dark. Upon absorption of a red light photon, the photoreceptor undergoes a conformational change, converting to its active Pfr conformation. The active form can interact with several transcription factors like the bHLH transcription factors of the PHYTOCHROME INTERACTING FACTOR (PIF) family. This interaction triggers light-signaling responses. In contrast, illumination with far-red light reconverts phyB to its inactive Pr form, abolishing the interaction with PIFs (Rockwell and Lagarias, 2006). Several optogenetic approaches make use of the red light/far-red light switchable interaction of phyB and PIFs. A2, Selective activation of intracellular signaling

Andres et al.

high autofluorescence of plants, posing limitations to microscopy analysis. In addition, compared with the genetic engineering of simpler organisms, generating stable transformed plants expressing the synthetic components of the switches is a lengthy process that slows down the implementation and characterization processes.

Despite these technical and experimental constraints, the first optogenetic tools have already been successfully implemented in plants (Table 1). These include a phytochrome-based red light-inducible and a CarH-based green light-regulated expression system (Müller et al., 2014; Ochoa-Fernandez et al., 2016; Chatelle et al., 2018). The former is activated by red light and inactivated by far-red light. Simple supplementation of ambient illumination in greenhouses with low intensities of far-red light keeps the system repressed. Irradiation with red light leads to quantitatively controlled activation of gene expression (Müller et al., 2014; Chatelle et al., 2018). The second strategy comprises the engineering of a green light-inducible bacterial photoreceptor, CarH. Use of green light as a stimulus minimizes the interference with endogenous plant photoreceptors, as this region of the sunlight spectrum normally does not produce physiologically active signaling responses of relevance (Chatelle et al., 2018).

Translational and Posttranslational Switches

While transcriptional gene switches currently play a major role in customized gene expression and are used for a broad range of applications, synthetic RNA-based switches constitute a complementary approach for controlling gene expression on the translational level. The most prominent components of RNA-based tools include RNA interference (RNAi; Fire et al., 1998), microRNAs (Lagos-Quintana, 2001), aptamers, and ribozymes. While RNAi, microRNAs, and ribozymes lead to cleavage or splicing of the target mRNA (Fire et al., 1998; Warashina et al., 2000; Lagos-Quintana, 2001), aptamers bind to specific targets like metal ions, small molecules, DNA, or proteins (Xiao et al., 2008). Aptamers are structured noncoding RNAs, naturally found in riboswitches that interfere with the accessibility of the ribosomes to the mRNA, affecting translational control (Breaker, 2012; Ausländer and Fussenegger, 2017). Using the in vitro selection method SELEX (for systematic evolution of ligands by exponential enrichment; Ellington and Szostak, 1990), many aptamers for new targets have been developed, such as the synthetic tetracycline-binding aptamer (Hanson et al., 2005; Xiao et al., 2008). By integrating protein-binding aptamers, the control of translational regulation via repression or alternative splicing can be achieved (Culler et al., 2010; Endo et al., 2013). In

Figure 2. (Continued.)

pathways with light. Red light illumination induces the recruitment of the cytoplasmic fusion protein consisting of a PIF, C-terminally fused to the fluorescent protein YFP and the catalytic domain of the SOS protein (SOS^{cat}), to the membrane-bound, RFP-tagged phyB. When recruited to the membrane, SOS^{cat} is capable of activating the Ras-signaling cascade and inducing nuclear transport of BFP-Erk and subsequent Erk pathway signaling. (Adapted from Toettcher et al., 2013.) A3, Construction of a phyB-PIF-based, red light-inducible split-transcription factor system. A truncated PIF6 was N-terminally fused to the tetracycline repressor (TetR), and the synthetic protein is bound to the tetracycline operator motif tetO of a synthetic reporter construct (as in Fig. 1). In the absence of light or under far-red light illumination (740 nm), there is no expression from the minimal promoter, P_{CMVmin}. Upon illumination with red light, phyB, C-terminally fused to the VP16 transactivation domain, interacts with the PIF. The spatial proximity of the transactivator recruits the transcriptional machinery to the minimal promoter. Only in this condition is the expression of the secreted human alkaline phosphatase (SEAP) reporter gene activated. (Adapted from Müller et al., 2013a.) An adaptation of this system was engineered in Arabidopsis and tobacco (*Nicotiana tabacum*) cells and the moss *Physcomitrella patens* (Müller et al., 2014; Ochoa-Fernandez et al., 2016). A4, Reversible red light-inducible nuclear transport of phyB fusion proteins. phyB was C-terminally fused to the fluorescent protein mCherry and a nuclear export sequence (NES), while PIF3, containing an intrinsic nuclear localization sequence (NLS), was C-terminally fused to enhanced GFP (EGFP). Upon illumination with red light, the nucleocytoplasmic shuttling PIF induces nuclear transport of phyB, while far-red radiation reversed the translocation of the photoreceptor-mediated by the NES. (Adapted from Beyer et al., 2015.) B, Natural blue light-induced signal transduction mediated by the plant photoreceptor phototropin1 and the light-sensitive bacterial transcription factor EL222. A synthetic approach based on blue light-triggered conformational change of EL222 and the LOV2 domain for the dual-controlled optogenetic down-regulation of proteins in animal cells was used. B1, EL222 is a light-sensitive transcription factor from the gram-negative bacterium *Erythrobacter litoralis*. It contains a blue light-sensitive LOV domain and a helix-turn-helix (HTH)-DNA-binding domain. In the dark, the HTH domain is docked to the LOV core. Upon illumination with blue light, the interaction of LOV and the HTH domain is disrupted, enabling homodimerization of the protein via the HTH and subsequent binding to the C120-DNA motif (Nash et al., 2011). B2, Schematic illustration of light-induced signal transduction via the blue light plant photoreceptor phototropin1. In the dark, the kinase domain is bound to the LOV domain, inhibiting its phosphorylation activity. Under blue light, the kinase domain is released, inducing protein phosphorylation and downstream signal transduction. (Adapted from Kimura et al., 2006.) B3, The dual optogenetic system for targeted degradation and repression of expression of a protein of interest (POI) consists of a synthetic reporter module comprising the P_{SV40} promoter, for constitutive expression of a POI fused to the B-LID (Bonger et al., 2014) module, and the C120₂-DNA-binding motif of the EL222 protein. EL222 is fused to the trans-repressor KRAB. In the dark, the degron (peptide RRRG) is docked to the LOV domain of the B-LID, and KRAB-EL222 is not able to bind to the C120 motif on the reporter plasmid. In this case, the POI accumulates. Upon illumination with blue light, the degron is exposed, triggering proteasomal degradation of the POI-B-LID fusion protein. Simultaneously, KRAB-EL222 dimerizes binding to the C120 motif, repressing transcription of the POI-B-LID. (Adapted from Baaske et al., 2018.)

868

Plant Physiol. Vol. 179, 2019

BOX 1. Optogenetics

For chemically controlled molecular switches, drawbacks such as difficulties in removing the inducer and diffusion-rate-limited transport and availability, hamper rapid inducibility and reversibility as well as space-resolved activation. By contrast, light as an input offers unprecedented spatiotemporal resolution, tight quantitative control, and minimized invasiveness. The introduction of light-gated ion channels (opsins) into neurons (reviewed in Deisseroth and Hegemann, 2017) initiated optogenetics, a novel discipline focusing on the control of biological systems with light. Development of light-sensitive switches uses photoreceptors as the input-sensing part of the switch. A multiplicity of different optogenetic switches for the minimally invasive control of cellular processes, with precise temporal and spatial resolution, have been engineered by combining bacterial and plant photoreceptors (with absorption spectra spanning from the UV-B up to the far-red regions of the white light spectrum) with output modules (molecular function) (reviewed by Fan and Lin, 2015; Müller et al., 2015; Kolar and Weber, 2017; Salinas et al., 2017). Common applications in mammalian cells include light-controlled gene expression and genome editing using transcriptional inducers or repressors (Müller et al., 2013b; Müller et al., 2013a; Motta-Mena et al., 2014; Kaberniuk et al., 2016), two-hybrid systems for recruitment of TALE-

(Koneremann et al., 2013) and CRISPR/Cas9-based-tools (Nihongaki et al., 2015; Polstein and Gersbach, 2015), and light-induced nuclear import of transcriptional effectors (Niopek et al., 2014; Beyer et al., 2015; Niopek et al., 2016) (Figure 2). In addition, light-regulated tools for controlling subcellular localization of proteins and even whole organelles (van Bergeijk et al., 2015; Beyer et al., 2015), protein stability (Bonger et al., 2014), kinase activity, and receptor activation, among others, have been applied for precisely controlling sensitive cellular processes. We refer the reader to the webtool OptoBase, designed to guide the user in the choice of a suitable optogenetic switch for a given application (Kolar et al., 2018). Optogenetics has made key contributions of molecular tools and experimental approaches, for molecular and cell biology research, as well as biotechnological applications (Zhang and Cui, 2015). The development of optogenetic systems lags behind in plants, mostly because of the experimental constraints posed by the unavoidable exposure to environmental light. However, optogenetic approaches in plants have been reported, including phytochrome- and CarH-based, red- and green-light-inducible expression systems (Müller et al., 2014; Ochoa-Fernandez et al., 2016; Chatelle et al., 2018). This opens novel perspectives for engineering synthetic, light-triggered circuits in plants.

Box 1 Optogenetics. Citations: Koneremann et al., 2013; Müller et al., 2013a, 2013b, 2014, 2015; Bonger et al., 2014; Motta-Mena et al., 2014; Niopek et al., 2014, 2016; Beyer et al., 2015; Fan and Lin, 2015; Nihongaki et al., 2015; Polstein and Gersbach, 2015; van Bergeijk et al., 2015; Zhang and Cui, 2015; Kaberniuk et al., 2016; Ochoa-Fernandez et al., 2016; Deisseroth and Hegemann, 2017; Kolar and Weber, 2017; Salinas et al., 2017; Chatelle et al., 2018; Kolar et al., 2018.

addition, fusion of the aptamer to translational repressors or enhancers permits the up- or down-regulation of the translation rate of the target protein (Pillai et al., 2004; Van Etten et al., 2012; Paek et al., 2015). Compared with transcriptional switches, translational switches can control endogenous genes without any alteration of the genomic sequence. They are relatively small in size and therefore are amenable for use in combination with transcriptional switches when the size and number of cassettes imposes an experimental limitation (Ausländer and Fussenegger, 2017).

In plants, specific RNA-based gene silencing, using artificial antisense mRNAs or microRNAs under the control of tissue-specific or inducible promoters, has been widely used for more than 20 years. However, these approaches usually suffer from off-target effects

and provide limited exogenous and quantitative control and reduced efficiency (Schwab et al., 2006). Other examples for the translational control of gene expression in plants are limited to applications in plasmids (Verhounig et al., 2010). Recently, Faden et al. (2016) reported a posttranscriptional switch for the in planta down-regulation of protein levels based on a temperature-controlled N-terminal degradation signal. Similar to other techniques already implemented in simpler, unicellular organisms, the transfer of the system to multicellular organisms, like plants, strongly depended on the adaptation to the corresponding physiological conditions. To test the functionality of the system for reversible protein accumulation, trichome formation was manipulated after shifting the plants from a permissive to a restrictive temperature (29°C).

Andres et al.

This led to the degradation of the protein of interest, TRANSPARENT TESTA GLABRA1, thus affecting the spatiotemporal development of trichomes (Table 1).

Switches Regulating Cellular Processes

Besides transcriptional and translational switches, a plethora of chemical- and light-regulated systems have been developed for the targeted regulation of a multiplicity of cellular processes ranging from the activation/inactivation of signaling cascades (receptors, kinases, transcription factors, etc.) and membrane trafficking to the controlled movement of organelles from one pole of the cell to the other (for review, see Hörner and Weber, 2012; Kolar and Weber, 2017). Selected examples include the utilization of optogenetic tools for (1) the control of the subcellular localization of proteins (e.g. red light; Beyer et al., 2015; Fig. 2A) and blue light-induced (Niopek et al., 2014, 2016) nuclear import and export of transcriptional effectors; and (2) the light-mediated degradation/depletion of proteins (Bonger et al., 2014; Baaske et al., 2018; Fig. 2B). A comprehensive list of approaches is reviewed elsewhere (Hörner and Weber, 2012; Kolar and Weber, 2017).

SYNTHETIC GENETIC CIRCUITS

Genetic circuits combine a series of synthetic switches into networks that can perceive a signal (exogenous or endogenous, natural or synthetic), process the information, and generate an output, normally triggering gene expression (e.g. induction of a given phenotype or change in cellular morphology) and expression of a reporter to monitor a process or activation of a metabolic pathway (Lim, 2010; Xie and Fussenegger, 2018). Simple circuits perform basic functionalities and integrate few signals. Next, we will discuss toggle switches, synthetic oscillators, and Boolean logic gates, which are built up from simple combinations of a reduced number of modules. Then we will review more complex arrays of switches integrated into cell-cell communication systems, open- and closed-loop circuit control, and synthetic cellular devices and their applicability.

Simple Circuits

Since therapeutic applications are one of the driving forces for the development of functional, robust, and complex genetic circuits, many recent technical breakthroughs have been made in mammalian cell systems. First approaches included the transfer and optimization of basic synthetic circuits, previously engineered in lower organisms. An illustrative example is a simple negative feedback circuit in yeast based on the combination of two tetracycline-inducible modules, controlling the expression of EGFP and the TetR repressor (Nevozhay et al., 2009). This loop enabled a tightly

controlled, dose-dependent activation of gene expression in mammalian cells. Expression of both EGFP and TetR is regulated by the rate of influx of the inducer but subsequently restricted by the increasing level of TetR protein (Nevozhay et al., 2013).

Toggle Switches

The first combined synthetic gene switches date back to the early 2000s with the design of bistable transcriptional repression toggle switches in bacteria and mammalian cells (Ajo-Franklin et al., 2007). Here, mutual inhibition of two independent chemical- and temperature-controlled (Gardner et al., 2000) or antibiotic-inducible (Kramer et al., 2004b) promoters, each controlling the expression of the counterpart's repressor, generates two equilibrium states of induction, switchable by the respective transient induction.

Plants also employ natural toggle switches for the control of endogenous processes, such as the CLAV-ATA pathway for stem cell fate. In line with this, the implementation of synthetic toggle switches in plants could open new perspectives for the development of, for instance, a programmable path of stem cell differentiation (Medford and Prasad, 2016) or trichome development. However, the intrinsic complexity of plant signaling networks restricts the straightforward transferability of already existing synthetic systems into plants. Plants integrate a wide range of biotic and abiotic external cues like light and temperature with genetic programs in an intertwined or redundant manner. This poses experimental and theoretical constraints (resources, time, lack of thorough knowledge of regulatory mechanisms, limited genetic tools, etc.). Therefore, exhaustive design and implementation phases will be needed for engineering all the synthetic circuits discussed in this article.

Oscillators

Autonomous and self-sustained oscillating gene expression patterns, like the circadian clock or the cell cycle, are crucial to sustain pulsatile cellular activities; therefore, there is much interest in understanding their regulation and function (for review, see Schibler and Sassone-Corsi, 2002; Fig. 3A). By designing and implementing synthetic oscillators, key insights on the mechanistic principles of cellular processes can be obtained, and novel functionalities could be engineered, as described below.

After the discovery of the first gene regulation model (Jacob and Monod, 1961), theoreticians started developing mathematical models on genetic oscillatory networks, and ideas for synthetic circuits were proposed. The first prototypical oscillator, termed the Goodwin oscillator, utilizes a single protein that inhibits its own transcription; namely, it can be seen as a closed negative feedback loop (Goodwin, 1963, 1965). Several decades later, the advances in genetics and molecular and cell biology allowed engineers to implement this and other

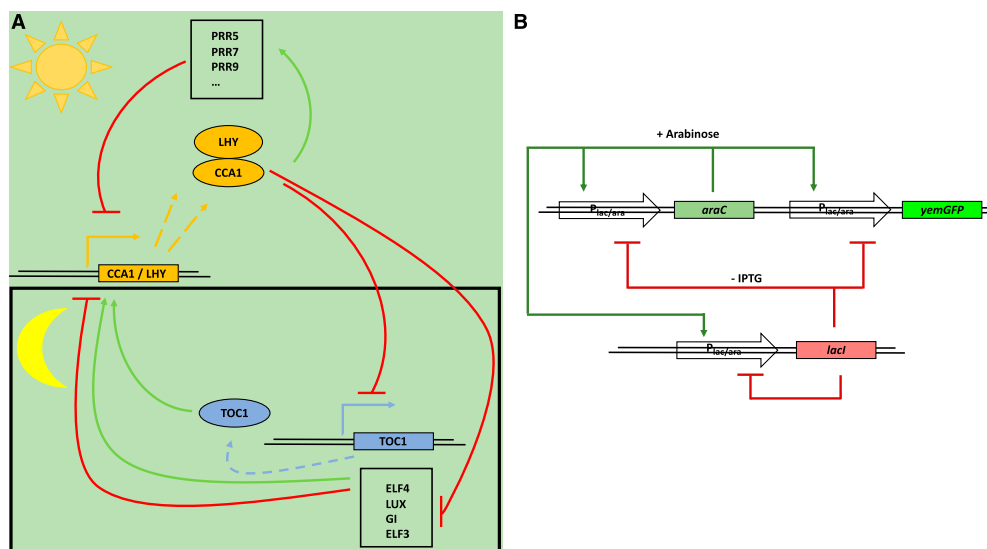


Figure 3. Molecular principle of a natural and synthetic oscillator. A, Simplified molecular model of the circadian clock in Arabidopsis (natural oscillator). The core oscillator feedback loop consists of TOC1, CCA1, and LHY. In this core oscillator, LHY and CCA1 repress the transcription of TOC1; TOC1 in turn is a positive regulator of CCA1 and LHY. In a second loop, LHY and CCA1 are also positive regulators of three TOC1 paralogs (PRR5, PRR7, and PRR9), which in turn are negative regulators of CCA1 and LHY. In a third loop, CCA1 and LHY positively regulate GI, ELF3, ELF4, and LUX; these in turn regulate CCA1 and LHY. The circadian oscillator of Arabidopsis is illustrated here in a simplified form; for clarity, several other components involved were not included. (Adapted from McClung, 2006.) B, Scheme of a synthetic oscillator engineered by Stricker et al. (2008). This synthetic oscillator comprises positive and negative feedback loops. The *araC*, *lacI*, and *yemGFP* (as a readout) genes are all under the control of the hybrid synthetic promoter $P_{lac/ara-1}$, comprising the activation operator site from the *araBAD* promoter and the repression operator site from the *lacZYA* promoter (Lutz and Bujard, 1997). In the presence of arabinose, the AraC protein activates the hybrid promoter and, thus, the gene expression of *araC*, *lacI*, and *yemGFP*, which results in two feedback loops: a positive feedback loop mediated by the produced AraC and the resulting activation of the hybrid promoter, and a negative feedback loop due to the production of the LacI protein. In the absence of IPTG, LacI negatively regulates the expression of all three genes under the control of the hybrid promoter. Both engineered feedback loops together constitute the synthetic oscillator. (Adapted from Stricker et al., 2008.)

oscillators in living cell systems (Elowitz and Leibler, 2000; Fung et al., 2005; Stricker et al., 2008; Danino et al., 2010; Ryback et al., 2013). The first of these genetic circuits implemented in *E. coli* was a synthetic oscillatory network of transcriptional regulators, known as the repressilator (Elowitz and Leibler, 2000). A repressilator is defined as a subset of genes that can repress their successor in the cycle; thus, it can be seen as an extension of the one-gene Goodwin oscillator (Müller et al., 2006; Purcell et al., 2010). The Elowitz synthetic repressilator consists of a cyclic negative feedback loop composed of three repressor proteins, which are not part of any natural biological clock/oscillator, namely, LacI (*E. coli*), TetR (Tn10 transposon), and cI (λ phage), and their corresponding cognate promoters. However, it suffered from noisy behavior, with only 40% of the *E. coli* cells showing oscillations (Elowitz and Leibler, 2000). Theoretical studies revealed that by implementing a positive feedback loop, the robustness of the

oscillations and the tunability of the amplitude and period could be improved (Hasty et al., 2002; Atkinson et al., 2003; Stricker et al., 2008; Purcell et al., 2010; Tomazou et al., 2018). Later, a dual-feedback oscillator developed by Stricker et al. (2008) achieved faster oscillatory periods, 99% oscillating cells, and decoupling from the cell cycle. The period was tuned by either IPTG, arabinose, or temperature (Fig. 3B). In most of these approaches, mathematical model-assisted design was essential for identifying the experimental parameters and molecular components (relative amounts thereof) used to tune the oscillations.

Autonomous, self-sustained, and tunable oscillatory behavior was also achieved in mammalian cells with an amplified negative feedback oscillatory mechanism (Tigges et al., 2009). The oscillator is based on an autoregulated sense-antisense transcription control circuit in the negative feedback loop leading to a delay in the repressive effect (Tigges et al., 2009; Purcell et al.,

Andres et al.

2010). An alternative approach applied in mammalian cells involved the combination of both natural and synthetic elements to create oscillatory behavior by manipulating amplitude, damping, and frequency in an independent fashion. For this purpose, the endogenous transcription factor p53, which is activated in response to cellular stress, and its negative regulator Mdm2 were utilized (Toettcher et al., 2010). This simple core negative feedback loop served as an example to define and modulate the dynamics of naturally occurring oscillatory systems in a controlled fashion. Considerable progress has been made recently to link different kinds of genetic circuits to functional synthetic self-regulated networks. This is necessary for integrating synthetic control into endogenous signaling networks, for instance, the Elowitz repressilator coupled to a modified quorum-sensing circuit of *Vibrio fischeri* and *A. tumefaciens* (Fernández-Niño et al., 2017).

Despite almost two decades of in vivo experiments and associated theoretical background on oscillators, there are still no oscillators implemented in plants. This represents a big experimental challenge. As discussed above, a major obstacle for the implementation of synthetic oscillatory networks in multicellular organisms like plants is the existence of a multiplicity of internal or external parameters, regulating metabolic and signaling pathways. A first attempt at this would be the engineering of hybrid oscillators, employing a similar approach to the one introduced by Toettcher et al. (2010). The introduction of synthetic orthogonal modules to achieve tight control over oscillatory parameters of an endogenous pathway minimizing cross talk could contribute to a broader understanding of oscillatory behavior in plant signaling and metabolic networks. In the future, fully synthetic systems could be implemented to bypass endogenous oscillators. A potential application of this would be the decoupling of endogenous metabolic pathways from the circadian clock to allow, for example, a prolonged bioproductive/anabolic daily phase, thereby increasing crop yield.

Boolean Logic Gates

Boolean logic gates utilize Boolean algebra to convert multiple input signals into truth values, meaning a true or false answer (1 or 0). In a simple way, cells use this mechanism for a plethora of decision-making processes (e.g. promoters integrate the information encoded in the combination of positive and negative transcriptional regulators bound at any given point in time, translating it into an output signal [gene expression]; Fig. 4). Following these principles, synthetic genetic circuits have been designed and successfully implemented in prokaryotes (Tamsir et al., 2011; Moon et al., 2012), yeast (Gander et al., 2017), and mammalian cells (Xie et al., 2011; Ausländer et al., 2012; Lebar et al., 2014) controlling various biological functions. They can integrate multiple molecular input signals following a set of algorithms and generate a response only if strictly

defined conditions are met (Xie and Fussenegger, 2018). For instance, an OR gate only generates an output when either input signal A or B is present, whereas both input signals have to concur for an AND gate to be true. More complex logic gates could be built in a combinatorial fashion out of these simple ones (Xie and Fussenegger, 2018). Different transcriptional regulators were used to meet these demands, including promoters functioning as input and output (Tamsir et al., 2011; Moon et al., 2012), RNAi (Xie et al., 2011), and TALE repressor (Gaber et al., 2014) and dCas9-based switches in bacteria (Nielsen and Voigt, 2014), yeast (Gander et al., 2017), and mammalian cells (Gao et al., 2016).

An illustration of such a circuit using chemically controlled transcription factors was depicted in the work of Gao et al. (2016). An efficient gene activation and repression system was designed by combining plant hormone signaling components with Sp-dCas9, which enabled the manipulation of multiple gene targets in an orthogonal mammalian cell setup. To achieve this, ABA and GA phytohormone signaling components that heterodimerize in the presence of the individual hormones (PYRABACTIN RESISTANCE1-LIKE [PYL] with ABA INSENSITIVE [ABI] for ABA and GA INSENSITIVE DWARF1 [GID1] with GIBBERELLIC ACID INSENSITIVE [GAI] for GA) were fused to either a transcriptional activator (VPR) or repressor (KRAB) or to Sp-dCas9. When the corresponding hormones are added, GID1-VPR/-KRAB and GAI-Sp-dCas9 (or PYL1-VPR/-KRAB and ABI-Sp-dCas9, respectively) heterodimerize, thereby activating or repressing gene expression from a target synthetic promoter. These switches perform very well, are robust, and show almost no leakiness. Based on these characteristics, both systems were customized and combined to construct AND, OR, NAND, and NOR Boolean logic gates. A NOT IF gate was successfully built in which expression of a gene was possible only in the presence of one inducer (e.g. ABA) while it was OFF in the presence of the second one (e.g. GA; Gao et al., 2016). This approach therefore utilized phytohormone signaling components to control multiple transcriptional outputs in an orthogonal system, namely, mammalian cells. Despite its potential applicability, to our knowledge, there has not been any synthetic Boolean logic gate implemented in plants yet.

Higher Order Genetic Circuits

The characteristics of the different levels of genetic circuits are summarized in Box 2. More complex synthetic devices connecting multiple layers of signal processing, including detection of the inducer, signal transduction, and precise (nuclear) activation of the defined output, have been implemented in prokaryotic and eukaryotic cell systems. Most of these circuits partially rely on endogenous elements, utilized for a desired purpose, in combination with the integrated synthetic, orthogonal components. Here, we describe

cell-cell communication systems and illustrate differential characteristics and applicability, currently in biomedicine, of open- and closed-loop circuit control configurations and prosthetic synthetic circuits (Box 2).

Cell-Cell Communication Systems

Unicellular and multicellular organisms rely on cell-cell communication mechanisms to regulate crucial life decisions (e.g. growth, development, organ identity, and metabolism/nutrition, among a wide range of processes). Bacteria, for instance, employ quorum sensing to assess the density of cells in their surroundings (Fig. 5A). Depending on the population density, genes responsible for key processes such as biofilm formation are up- or down-regulated (Fuqua et al., 1994; Abisado et al., 2018). Multicellular organisms

coordinate processes such as tissue development or immune cell responses employing cell-cell communication networks (Thurley et al., 2018). Different signaling molecules are used for this purpose in unicellular and multicellular organisms, including metabolites, small RNAs, peptides, and proteins. The synthetic reconstruction or de novo engineering of these communication processes can contribute to experimental strategies to both understand these processes and develop biotechnological applications (Prindle et al., 2011). In tissue engineering approaches, tight control and manipulation of cell-cell communication is needed for the establishment of edges between different populations of cells, as achieved by Kolar et al. (2015). Targeted spatiotemporally resolved induction of cell death was engineered by using bacterial quorum sensing-regulated systems (You et al., 2004). Finally,

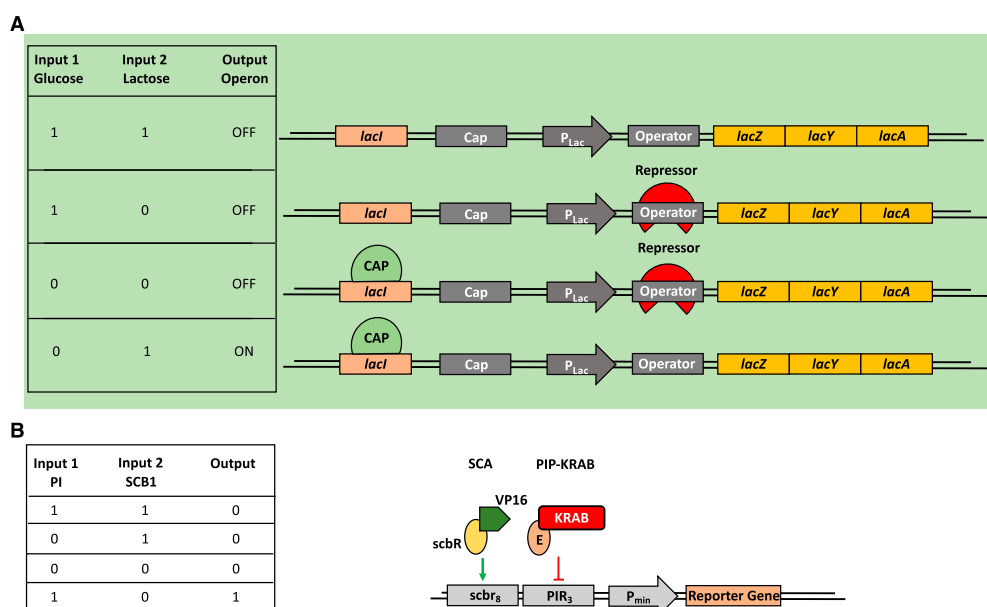


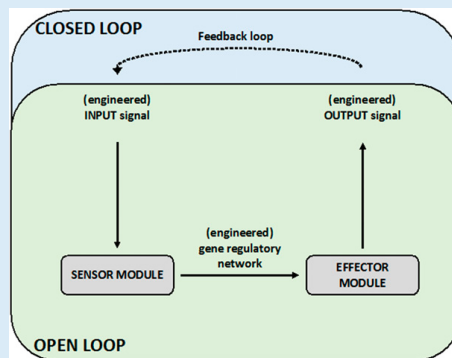
Figure 4. Natural and synthetically built AND NOT (NOT IF) Boolean logic gates. An AND NOT gate generates an output when only one specific single input signal is present, but not when there is no input signal, nor a second input, nor both signals. A, Truth table and scheme of the regulatory region of the Lac operon as an AND NOT (NOT IF) gate. This AND NOT gate only generates an output when lactose is the only single input available. If Glc and lactose are available in the cell, the lac operon is OFF because the catabolite activator protein, CAP, is not bound. The same is true when Glc, but no lactose, is available. In this case, the lac repressor is bound. In the case when there is neither Glc nor lactose, the lac operon is OFF because even though CAP is bound, the lac repressor prevents transcriptional initiation. Only when there is lactose, but no Glc, available is the lac operon ON. In the absence of Glc, CAP can bind, and because of the availability of lactose, the lac repressor is not bound. Both actions are necessary for transcriptional initiation of the lac operon. (Adapted from Phillips et al., 2009.) B, An example of an AND NOT (NOT IF) gate in synthetic biology. In this synthetic system, the transactivator SCA (transactivator of the streptogramin-responsive gene regulation system) and the transrepressor PIP-KRAB are constitutively expressed along with a reporter plasmid containing a chimeric SCA- and PIP-specific promoter. The absence of SCB1 [racemic 2-(1V-hydroxy-6-methylheptyl)-3-(hydroxymethyl)butanolide] enables the binding of the transactivator SCA to its corresponding promoter region. The presence of the transrepressor pristinamycin (PI) in turn prevents the binding of PIP-KRAB to its promoter. Thus, this engineered AND NOT gate generates an output only in the presence of pristinamycin and the absence of SCB1. (Adapted from Kramer et al., 2004a.)

Andres et al.

BOX 2. Synthetic regulatory open- and closed-loop circuits

To program novel cellular behavior, synthetic networks can be designed to respond to exogenous or endogenous biological signals in a predictable manner and yield a determined quantity of an output of choice (Kobayashi et al., 2004). Depending on the desired input and the necessity of a negative or positive feedback to fine-tune the response, open or closed genetic cellular loops can be engineered. In an open-loop system, the exogenous or endogenous biological input signal (control) is processed by a synthetic gene regulatory network that produces an output, e.g., a biological response via an effector. In this configuration, the output itself exerts no effect on the input control signal (see illustration). One typical example would be the exogenous activation of a circuit with light, as with optogenetic tools, in which the output has no effect on the input used to control the process (no feedback involved). A closed-loop system in turn implements an additional module, namely, a negative or positive feedback, directly linking the output to the input signal. These circuits are programmed to reach and maintain a target output level by continuously evaluating, comparing, and correcting the actual values, thus leading to autonomous self-regulation with improved stability, robustness, and reliability (Briat et al., 2016).

When functionally integrated into the endogenous cellular circuitry, synthetic open- and closed-loop systems offer a wide range of customized biomedical applications. Examples include designs for detecting and responding to disease-related signals or biopharmaceutical screening devices. These “prosthetic networks” are able to correct malfunctions or rectify limitations of the endogenous cellular machinery, while, compared to traditional medication, reducing the susceptibility to side effects or interference with endogenous mechanisms. Encapsulation and implantation of the system- containing “desiner cells” allows these devices to be used in vivo (reviewed by Heng et al., 2015).



Box 2 Synthetic regulatory open- and closed-loop circuits. Citations: Kobayashi et al., 2004; Heng et al., 2015; Briat et al., 2016.

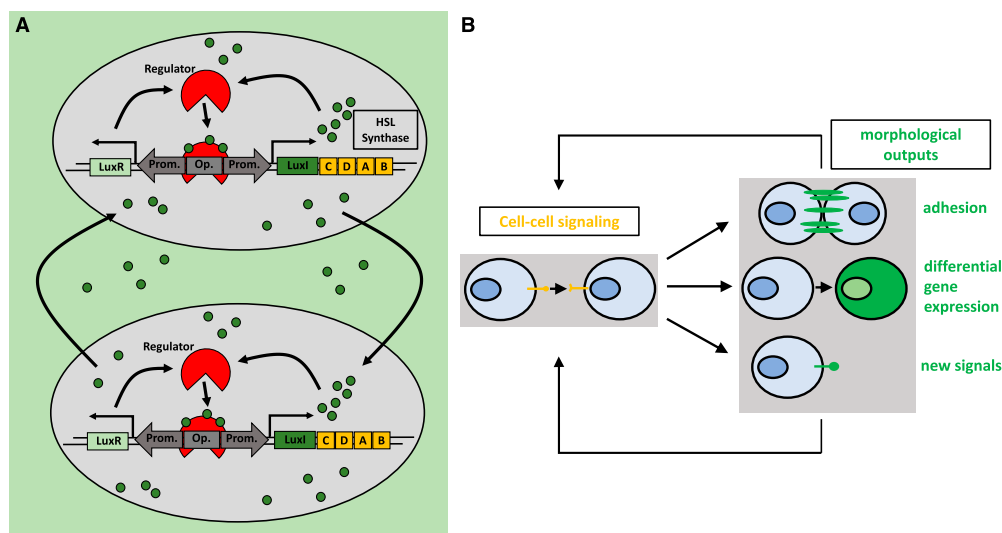


Figure 5. Cell-cell communication in bacteria and synthetic cell-cell communication networks. A, Simplified illustration of the natural homoserine lactone (HSL) quorum-sensing network in *V. fischeri*. Quorum sensing describes the ability of bacteria to assess the cell density of a population by sensing chemical signals that are produced by surrounding cells (Davis et al., 2015). HSLs, in the case of *V. fischeri* AHL, bind to the LuxR protein. LuxR then binds to its cognate operator, inducing the transcription of LuxI, which catalyzes the synthesis of AHL. AHL is able to diffuse out of the cell, accumulating in the external milieu and entering surrounding cells, thus activating the circuit in those cells. B, Engineered cell-cell communication networks in mammalian cells. Engineered cell-cell signaling via two synNotch ligand-receptor pairs was used to manipulate cell adhesion, differentiation, and the production of new cell-cell signals (Toda et al., 2018). Upon binding of the ligand to the synNotch receptor, an orthogonal transcription factor is cleaved from the cytoplasmic tail of the receptor, migrates to the nucleus, and then drives gene expression of the output proteins. These genes include fluorescent proteins as cellular markers for differentiation, several cadherins as morphological outputs, and two synNotch ligand-receptor pairs as input signals. In this way, the outputs are propagated to the next generation. (Adapted from Toda et al., 2018.)

cell adhesion through cell-cell communication was achieved by linking the synthetic notch receptor system to the expression of specific cadherin molecules and new synthetic Notch (synNotch) ligands (Toda et al., 2018; Fig. 5B). Importantly, the synNotch receptor mechanism is also utilized in potentially therapeutic engineered T-cells, which can detect given combinations of antigens (for details, see Fig. 6) instead of only one antigen (Roybal et al., 2016). These engineered combinatorial T-cells represent a breakthrough in the treatment of cancer.

In plants, cell-cell communication also plays an important role. Key regulators such as phytohormones not only control almost every aspect of plant life, like coordinating responses between tissues and organs, but also mediate interactions with symbiotic microorganisms. An example is the phytohormone strigolactone, which can act both as an endogenous phytohormone and as an exogenous signal molecule in the rhizosphere (for review, see Morffy et al., 2016). As an exogenous signal, it recruits arbuscular mycorrhizal fungi to the root to provide the plant with nutrients (i.e. phosphate) under nutrient-limiting conditions (Akiyama et al.,

2005). However, strigolactone also mediates the recognition of host roots by parasitic weeds, leading to severe yield losses (Parker, 2009). Inspired by these natural mechanisms, semi- or fully synthetic networks could be engineered to exploit novel useful symbiotic interactions under abiotic and biotic stress or to develop orthogonal signaling networks among organs. Therefore, the manipulation on command of the information flow can be used in strategies to improve crop productivity. It can also be used to abolish or reprogram detrimental or beneficial interactions between microorganisms and plants.

Open- Versus Closed-Loop Circuit Control, and Prosthetic Network Devices Two exemplary realizations of semi-hybrid open-loop control strategies are optogenetic and radio wave-inducible devices for the in vivo regulation of blood Glc levels in mice. Both devices have been developed by integrating a synthetic input module with the native Ca^{2+} -inducible NFAT-signaling pathway, activating the expression of genes involved in several developmental processes and immune responses (Crabtree and Olson, 2002; Crabtree and

Andres et al.

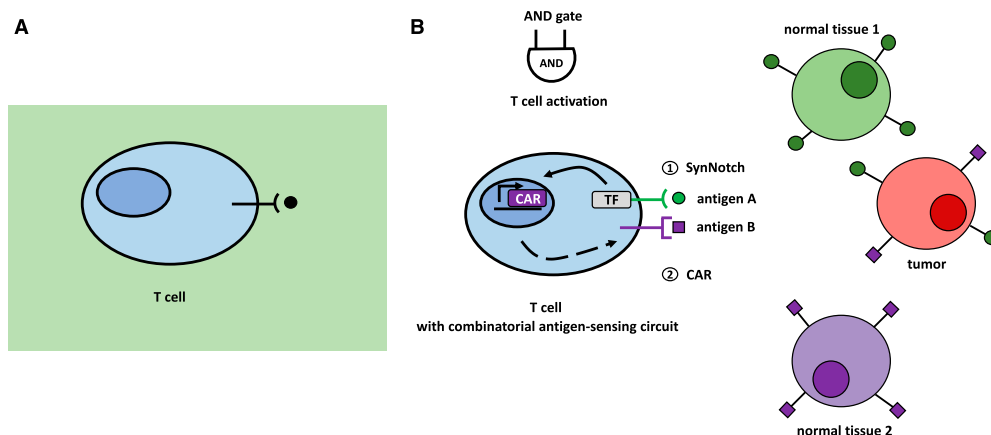


Figure 6. Natural and engineered combinatorial T-cells. A, Natural T-cell with its T-cell receptor, targeting only single antigens. This single-antigen recognition without any further control machinery can lead to off-target tissue damage. B, An engineered synthetic T-cell with new types of receptors specific for detecting given combinations of antigens. Upon binding of antigen A to the synNotch receptor, an orthogonal transcription factor is cleaved from the cytoplasmic tail of the receptor, which in turn activates CAR transcription. If a second antigen, antigen B, is recognized by the newly synthesized CAR receptor, the T-cell is activated. (Adapted from Roybal et al., 2016; Roybal and Lim, 2017.)

Schreiber, 2009). The optogenetic approach uses blue light to activate melanopsin and triggers a signaling cascade to ultimately induce a Ca^{2+} influx (Ye et al., 2011). The second circuit utilizes an engineered temperature-sensitive Ca^{2+} channel. This channel is bound by antibodies coated with ferrous oxide nanoparticles, which are heated with radio waves to trigger channel opening, leading to subsequent Ca^{2+} influx (Stanley et al., 2012).

Smole et al. (2017) reported an exemplary case of a fully synthetic network that can sense an inflammatory signal in mice and produce a response to suppress this signal (Fig. 7). They engineered a synthetic device consisting of a sensor module that, upon activation by inflammation signals, triggers the expression of a transcriptional activator, GAL4-VP16. The fusion protein not only acts as an inducer of expression of anti-inflammatory proteins by the output module but also triggers the positive feedback loop of an amplifying module, leading to enhanced levels of GAL4-VP16. A fourth module constitutively expresses GAL4 lacking the transactivation domain, competing with the GAL4-VP16 for restricting the level of activation of the system, therefore acting as a threshold device. Due to its autonomous activation by inflammatory signals, the activation of the circuit is independent of external induction. Furthermore, the system includes signal enhancement, while leakage is minimized by the thresholding module. Nevertheless, it still needs external inhibition for resetting the system to the OFF state due to the self-activating positive feedback characteristics and therefore is not strictly a closed-loop system. Ye et al. (2017) accomplished the construction

of a closed-loop, prosthetic network for the self-adjusting regulation of the insulin level in vivo, consisting of an implant of encapsulated engineered HEK cells (Fig. 8). Here, perception of insulin by the cell via its native insulin receptor leads to phosphorylation of the insulin receptor substrate 1 protein, triggering a signaling cascade that induces nuclear transport of a MAPK. In the nucleus, the MAPK phosphorylates the ELK1 domain of the synthetic fusion protein TetR-ELK1, initiating the transcriptional activity of a target gene, otherwise tightly disrupted in the absence of insulin or external supplementation of doxycycline. Programming the circuit for the production of adiponectin, a therapeutic protein involved in regulating insulin homeostasis, turns the network into a closed, self-regulating loop, increasing insulin sensitivity in different tissues. The increased sensitivity subsequently leads to reduced insulin production by pancreatic β -cells. Fulfilling a function that is missing in the cellular genetic network, synthetic regulatory circuits in mammalian systems can overcome the constraints of endogenous cellular processes. This illustrates the potential of synthetic biology for developing functional therapeutic devices and tailor-made medicine. Such complexity has not been reached yet in synthetic circuitry in plants; however, the first synthetic networks have already started to be implemented in plants, as described below.

First Attempts at Genetic Circuits in Plants Future development of complex circuitry with predictable and controllable features in plants for biotechnological applications (e.g. production of biopharmaceuticals and

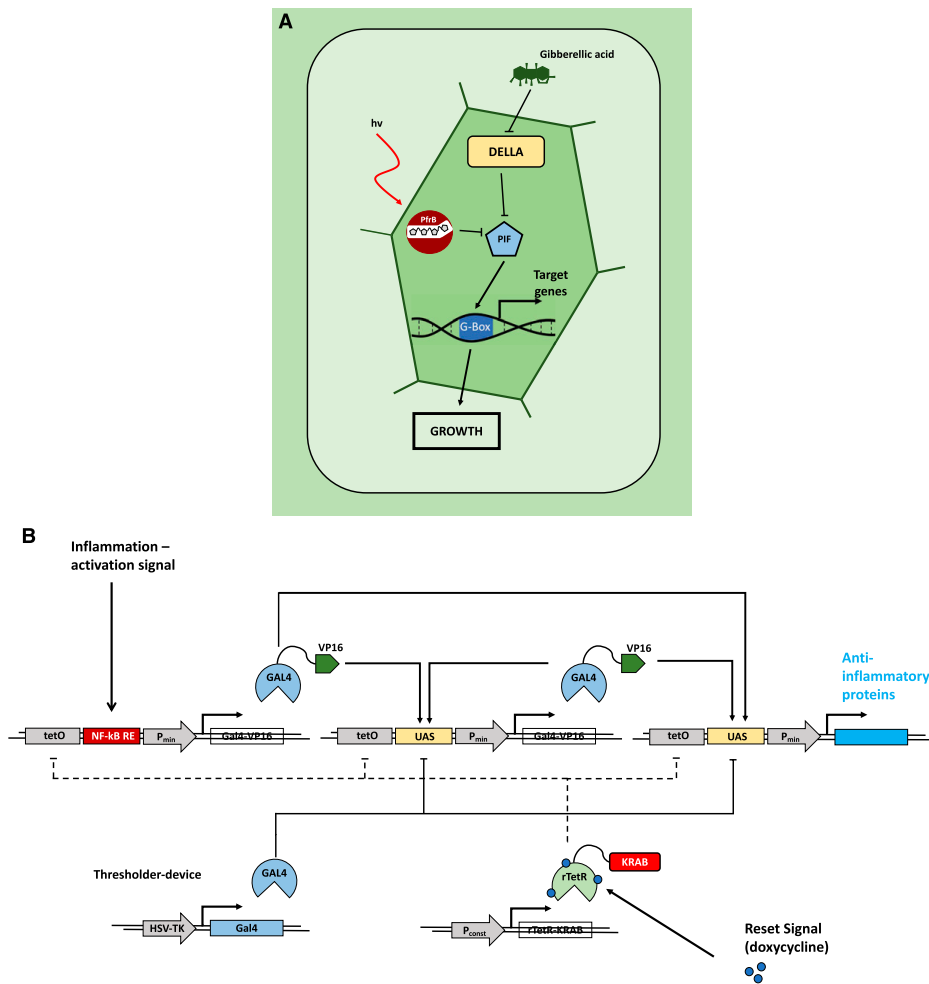


Figure 7. Natural and engineered open-loop regulatory circuits. A, GA₃-induced degradation of DELLA proteins suppresses the repression of PHYTOCHROME INTERACTING FACTORS (PIFs). The PIFs subsequently bind to G-box cis regulatory elements in the promoters of response genes, promoting growth responses. In parallel, transcription of PIFs is inhibited by the red light-induced active conformer of phytochrome B, modulating the growth promotion in response to the light conditions. (Adapted from Havko et al., 2016.) B, Schematic overview of a synthetic device for detection of inflammation signals in mammalian systems. Detection of inflammatory signals through the NF-κB-responsive element of the sensor module leads to expression of the transcriptional regulator GAL4 fused to the VP16 transactivation domain (GAL4-VP16). GAL4-VP16 subsequently binds to the UAS motif in the amplifier and effector modules, increasing the abundance of GAL4-VP16 through a self-activating positive feedback loop from the amplifier module. This triggers production of anti-inflammatory proteins via the effector module. Additionally, the system is equipped with a threshold device, constitutively expressing GAL4 lacking the transactivation domain. GAL4 competes for binding the UAS motifs with the activating GAL4-VP16, thereby restricting the initiation of the expression of the therapeutic output. A fifth module constitutively expresses the doxycycline-inducible reversed tetracycline repressor protein (rTetR) fused to the inhibitory KRAB domain. Exogenous application of doxycycline inhibits the activation of the sensor, amplifier, and effector modules by binding to their upstream tetO motifs, thus deactivating the system. (Adapted from Smole et al., 2017.)

other fine chemicals and engineering of stress-tolerant traits and enhanced nutritional content) requires one key prerequisite: namely, to have functionally well-characterized synthetic modules and switches. However, the quantitative characterization of genetic parts in plants is a time-consuming process, and the library of available parts to be used in modular assemblies is still rather limited. Moreover, the complexity of plants as multicellular organisms still remains experimentally challenging for constructing and implementing synthetic genetic circuits with a predictable outcome and robustness. A first step toward a consistent functional and quantitative categorization of molecular switches in plants was reported by Schaumberg et al. (2016); Table 1). The authors built a simple genetic circuit in plant protoplasts, comprising two genetic transcriptional switches and a dual-luciferase output. Addition of an inducer (dexamethasone or 4-hydroxytamoxifen) activates expression of a repressor protein and a firefly luciferase, which are both under the control of the same inducible promoter but on different plasmid constructs. In this case, firefly luciferase acts as a proxy for the amount of repressor. The repressor protein, on the other hand, represses Renilla luciferase expression from a second plasmid. In this way, it is possible to obtain quantitative data on the levels of a repressor protein and correlate it with its repressing activity over a target promoter (Schaumberg et al., 2016). This approach could be expanded easily to characterize, in a standardized fashion, transcriptional regulators, promoter sequences, and higher order circuitry arising from combinations of simple modules. As a note, in a recent example following the principle of bypassing endogenous pathways (in this case, a metabolic one), South et al. (2019) engineered an alternate, synthetic glycolate metabolic route. This pathway is more efficient than the endogenous photorespiratory route, increasing photosynthetic efficiency considerably (~40%), thereby leading to increased biomass production of tobacco plants. This example represents a milestone, fostering future similar strategies for other metabolic and signaling networks.

Optogenetically regulated systems have been implemented in plant cells (e.g. protoplasts) for the targeted control of signaling pathways. In a first approach, auxin regulatory networks were manipulated using a red light-inducible gene switch that allowed the quantitative control of the expression of the receptor of auxin, the F-box protein TIR1 (up-regulation and down-regulation upon expression of an antisense microRNA; Müller et al., 2014; Samodelov and Zurbriggen, 2017; Table 1). The effects of precisely tuning the sensitivity of the regulatory network to the hormone was monitored with a genetically encoded biosensor designed ad hoc (Wend et al., 2013). This open-loop system enabled inducible quantitative control and monitoring of a signaling network for the study of complex regulatory principles. This is performed in a

simple experimental platform without the need for generating mutants (Müller et al., 2014).

Another example of an open-loop system in plants is a fully synthetic signal transduction system that could potentially be used for the programmable detection of ligands (Antunes et al., 2011). In this approach, bacterial signal transduction components were adapted to eukaryotic target sequences and consequently transferred into transgenic plants. The engineered chimeric His kinase included a bacterial receptor, Tgr, fused to the His kinase PhoR. Upon binding a re-designed periplasmic binding protein in complex with the ligand of interest, this chimeric receptor phosphorylates its cognate chimeric response regulator PhoB-VP64. The response regulator in turn activates the expression of a reporter gene. Drought, in the context of climate changes, is one of the biggest challenges to food security. One promising approach to improve plant water usage is to manipulate the ABA signaling pathway, which plays a major role in drought tolerance (Helander et al., 2016). Recent advances have been made in manipulating different aspects of ABA signaling (e.g. receptor engineering and developing an ABA agonist; Park et al., 2015; Vaidya et al., 2017; Table 1). Cyanabactin is a potent, selective agonist for one distinct ABA receptor family, namely, the subfamily of IIIA receptors. These targeted approaches help bypass pleiotropic or unwanted side effects, resulting in more specific, controllable manipulation of a given signaling network. The promising case of cyanabactin could be a model for further directed design of synthetic substances and synthetic cognate receptors.

DISCUSSION AND PERSPECTIVES

In the almost 20 years since the foundational publications of synthetic devices, synthetic biology has evolved into a mature discipline that already revolutionizes fundamental research, most noticeably biomedicine, as well as the biotechnology industry. A broad range of synthetic molecular tools, regulatory and metabolic circuitry, and even synthetic organelles and genomes have been engineered and successfully applied in bacterial, yeast, and animal systems (Brophy and Voigt, 2014). As described in this article, several synthetic biosensors and switches for the control of gene expression (including a couple of optogenetic modules), genome editing, and protein stability have already been implemented in plants (for review, see Liu et al., 2013; Braguy and Zurbriggen, 2016; Walia et al., 2018). The first approaches toward combinations of switches in plant cell systems are arising, including (1) the use of an optogenetic gene switch to control hormone signaling, coupled to a genetically encoded biosensor, as a proxy of the activity of the signaling pathway (Müller et al., 2014); and (2) a semi- and a fully synthetic transduction pathway, sensing a plant hormone or a foreign metabolite, respectively, by transducing the signal into a phenotypic response (sentinel

OUTSTANDING QUESTIONS

- What technical and theoretical approaches are needed for implementing more complex genetic circuitry in plants? How can the current slow, error-prone synthetic circuitry engineering be improved for a more efficient and predictable assembly of circuits?
- Is it possible to engineer self-regulated, 'smart' pathways that have a novel function in plants with minimized interference over endogenous regulatory networks, thus avoiding negative effects on traits?
- How can the social acceptance of genetically modified plants be improved, in particular in developed countries, to contribute to solving the global question on how to feed the ever-growing world population in an ecologically sustainable manner?

approach; Antunes et al., 2006, 2009). However, engineering and implementation of more complex circuitry is not yet a reality in plant research. Plants are multicellular organisms with complex metabolism and highly regulated and intertwined signaling networks, integrating different environmental cues, like light and temperature, with the genetic program and metabolic status. Experimental constraints and slow generation times often make it cumbersome to implement and evaluate genetic circuits in the whole plant. Altogether, it is still challenging to build synthetic circuits with a predictable output and function.

In order to transition the plant synthetic biology field from a slow and error-prone engineering phase into a more automated, rational, and reliable discipline, a series of approaches have to be implemented. In this way, the development and introduction of advanced circuitry could be achieved, as is already the case for other organisms. In the first place, biosynthetic platforms for the rational design, construction, and quantitative characterization of a bigger number of variants of genetic parts need to be established. Toward this goal, adequate vectors and high-throughput DNA assembly methods are already in place (Patron, 2014; Vazquez-Vilar et al., 2018). However, experimental approaches to quantitatively and functionally describe synthetic modules, as well as hand-in-hand work with mathematical modelers to improve predictability and reliability, still lag behind. Finally, based on the experiences in yeast and animal cells, generalized incorporation of orthogonal components (sensing modules, signaling molecules, and output elements) in the designs will contribute to optimal functionality, including high control specificity, robustness of the networks, and a reduced cross-modulation of the endogenous pathways.

Given the creative and successful applications reported in other organisms, it is easy to imagine that engineering of synthetic circuits in plants will help solve many problems in the near future (see Outstanding Questions). One future goal is to achieve a quantitative increase in crop yield, a much-needed second Green Revolution, to satisfy the demands of the ever-growing world population (Wollenweber et al., 2005). Another goal is to improve plant stress tolerance to environmental hardships by manipulating phytohormone signaling pathways or introducing orthogonal networks, targeting key plant stress responses. First steps toward this were recently reported based on engineering the receptor for the phytohormone ABA and developing chemical agonists thereof to control the responses to drought (Park et al., 2015; Vaidya et al., 2017). A next step would be to design hybrid circuitry to overcome limitations and bypass endogenous regulation of plant signaling networks to improve the efficiency of existing cascades. Self-regulating, smart pathways that bypass endogenous regulation may be easier to design using fully synthetic circuits. These can be engineered to achieve a high target specificity and are orthogonal to the organism, reducing off-target effects. A further application of such smart plants could be the incorporation of synthetic circuitry to integrate information on environmental cues and the genetic program with long-distance synthetic signal transduction. For example, flowering time could be regulated upon computation of the nutrient availability (roots) and perception of environmental stress, thereby optimizing seed production. An alternative approach to increase productivity would be to decouple growth and development from regulatory elements, such as the circadian clock or other genetic programs, thereby achieving longer biosynthetic periods. It is evident that the possible applications of these approaches are endless and would completely reshape plant science. A long-term vision encompasses the implementation of synthetic cellular circuits, such as closed-loop prosthetic networks, which are capable of generating new functionalities, including immune system-like properties or optimized nutrient assimilation and production of high-value compounds. By virtue of the fast development and achievements in other higher eukaryotic systems, we will witness a paradigm change in experimental plant fundamental research and the development of green biotechnological applications in the near future.

ACKNOWLEDGMENTS

We thank Leonie-Alexa Koch for fruitful discussions and comments on the article as well as reviewer 1 for the thorough review and the valuable comments and suggestions that contributed to improve the quality of the article. We apologize to our colleagues whose work could not be cited due to space constraints.

Received November 2, 2018; accepted January 18, 2019; published January 28, 2019.

LITERATURE CITED

- Abisado RG, Benomar S, Klaus JR, Dandekar AA, Chandler JR (2018) Bacterial quorum sensing and microbial community interactions. *MBio* 9: e02331-17
- Ajo-Franklin CM, Drubin DA, Eskin JA, Gee EPS, Landgraf D, Phillips I, Silver PA (2007) Rational design of memory in eukaryotic cells. *Genes Dev* 21: 2271–2276
- Akiyama K, Matsuzaki K, Hayashi H (2005) Plant sesquiterpenes induce hyphal branching in arbuscular mycorrhizal fungi. *Nature* 435: 824–827
- Antunes MS, Ha SB, Tewari-Singh N, Morey KJ, Trofka AM, Kugrens P, Deyholos M, Medford JI (2006) A synthetic de-greening gene circuit provides a reporting system that is remotely detectable and has a re-set capacity. *Plant Biotechnol J* 4: 605–622
- Antunes MS, Morey KJ, Tewari-Singh N, Bowen TA, Smith JJ, Webb CT, Hellinga HW, Medford JI (2009) Engineering key components in a synthetic eukaryotic signal transduction pathway. *Mol Syst Biol* 5: 270
- Antunes MS, Morey KJ, Smith JJ, Albrecht KD, Bowen TA, Zdunek JK, Troupe JF, Cuneo MJ, Webb CT, Hellinga HW, et al (2011) Programmable ligand detection system in plants through a synthetic signal transduction pathway. *PLoS ONE* 6: e16292
- Aoyama T, Chua NH (1997) A glucocorticoid-mediated transcriptional induction system in transgenic plants. *Plant J* 11: 605–612
- Atkinson MR, Savageau MA, Myers JT, Ninfa AJ (2003) Development of genetic circuitry exhibiting toggle switch or oscillatory behavior in *Escherichia coli*. *Cell* 113: 597–607
- Ausländer S, Fussenegger M (2017) Synthetic RNA-based switches for mammalian gene expression control. *Curr Opin Biotechnol* 48: 54–60
- Ausländer S, Ausländer D, Müller M, Wieland M, Fussenegger M (2012) Programmable single-cell mammalian biocomputers. *Nature* 487: 123–127
- Baaske J, Gonschorek P, Engesser R, Dominguez-Monedero A, Raute K, Fischbach P, Müller K, Cachat E, Schamel WWA, Minguet S, et al (2018) Dual-controlled optogenetic system for the rapid down-regulation of protein levels in mammalian cells. *Sci Rep* 8: 15024
- Bateman E (1998) Autoregulation of eukaryotic transcription factors. *Prog Nucleic Acid Res Mol Biol* 60: 133–168
- Beck CF, Mutzel R, Barbé J, Müller W (1982) A multifunctional gene (tetR) controls Tn10-encoded tetracycline resistance. *J Bacteriol* 150: 633–642
- Beeske A, Serrano L (2000) Engineering stability in gene networks by autoregulation. *Nature* 405: 590–593
- Beeske A, Séraphin B, Serrano L (2001) Positive feedback in eukaryotic gene networks: Cell differentiation by graded to binary response conversion. *EMBO J* 20: 2528–2535
- Beerli RR, Schopfer U, Dreier B, Barbas CF III (2000) Chemically regulated zinc finger transcription factors. *J Biol Chem* 275: 32617–32627
- Berens C, Altschmied L, Hillen W (1992) The role of the N terminus in Tet repressor for tet operator binding determined by a mutational analysis. *J Biol Chem* 267: 1945–1952
- Beyer HM, Juillot S, Herbst K, Samodelov SL, Müller K, Schamel WW, Römer W, Schäfer E, Nagy F, Strähle U, et al (2015) Red light-regulated reversible nuclear localization of proteins in mammalian cells and zebrafish. *ACS Synth Biol* 4: 951–958
- Böhmdorfer G, Tramontano A, Luxa K, Bachmair A (2010) A synthetic biology approach allows inducible retrotransposition in whole plants. *Syst Synth Biol* 4: 133–138
- Bonger KM, Rakhit R, Payumo AY, Chen JK, Wandless TJ (2014) General method for regulating protein stability with light. *ACS Chem Biol* 9: 111–115
- Braguy J, Zurbriggen MD (2016) Synthetic strategies for plant signalling studies: Molecular toolbox and orthogonal platforms. *Plant J* 87: 118–138
- Breaker RR (2012) Riboswitches and the RNA world. *Cold Spring Harb Perspect Biol* 4: a003566
- Briat C, Zechner C, Khammash M (2016) Design of a synthetic integral feedback circuit: Dynamic analysis and DNA implementation. *ACS Synth Biol* 5: 1108–1116
- Brophy JAN, Voigt CA (2014) Principles of genetic circuit design. *Nat Methods* 11: 508–520
- Caddick MX, Greenland AJ, Jepson I, Krause KP, Qu N, Riddell KV, Salter MG, Schuch W, Sonnewald U, Tomsett AB (1998) An ethanol inducible gene switch for plants used to manipulate carbon metabolism. *Nat Biotechnol* 16: 177–180
- Chatelle C, Ochoa-Fernandez R, Engesser R, Schneider N, Beyer HM, Jones AR, Timmer J, Zurbriggen MD, Weber W (2018) A green-light-responsive system for the control of transgene expression in mammalian and plant cells. *ACS Synth Biol* 7: 1349–1358
- Crabtree GR, Olson EN (2002) NFAT signaling: Choreographing the social lives of cells. *Cell (Suppl)* 109: S67–S79
- Crabtree GR, Schreiber SL (2009) SnapShot: Ca²⁺-calcineurin-NFAT signaling. *Cell* 138: 210.e1
- Culler SJ, Hoff KG, Smolke CD (2010) Reprogramming cellular behavior with RNA controllers responsive to endogenous proteins. *Science* 330: 1251–1255
- Curtis MD, Grossniklaus U (2003) A Gateway cloning vector set for high-throughput functional analysis of genes in planta. *Plant Physiol* 133: 462–469
- Danino T, Mondragón-Palomino O, Tsimring L, Hasty J (2010) A synchronized quorum of genetic clocks. *Nature* 463: 326–330
- Davis RM, Muller RY, Haynes KA (2015) Can the natural diversity of quorum-sensing advance synthetic biology? *Front Bioeng Biotechnol* 3: 30
- Deisseroth K, Hegemann P (2017) The form and function of channelrhodopsin. *Science* 357: eaan5544
- Dickson RC, Abelson J, Barnes WM, Reznikoff WS (1975) Genetic regulation: The Lac control region. *Science* 187: 27–35
- Ellington AD, Szostak JW (1990) In vitro selection of RNA molecules that bind specific ligands. *Nature* 346: 818–822
- Ellis T, Wang X, Collins JJ (2009) Diversity-based, model-guided construction of synthetic gene networks with predicted functions. *Nat Biotechnol* 27: 465–471
- Elowitz MB, Leibler S (2000) A synthetic oscillatory network of transcriptional regulators. *Nature* 403: 335–338
- Endo K, Stapleton JA, Hayashi K, Saito H, Inoue T (2013) Quantitative and simultaneous translational control of distinct mammalian mRNAs. *Nucleic Acids Res* 41: e135
- Faden F, Ramezani T, Mielke S, Almudi J, Nairz K, Froehlich MS, Höckendorff J, Brandt W, Hoehenwarter W, Dohmen RJ, et al (2016) Phenotypes on demand via switchable target protein degradation in multicellular organisms. *Nat Commun* 7: 12202
- Fan LZ, Lin MZ (2015) Optical control of biological processes by light-switchable proteins. *Wiley Interdiscip Rev Dev Biol* 4: 545–554
- Fernández-Niño M, Giraldo D, Gomez-Porras JL, Dreyer I, González Barrios AF, Arevalo-Ferro C (2017) A synthetic multi-cellular network of coupled self-sustained oscillators. *PLoS ONE* 12: e0180155
- Fire A, Xu S, Montgomery MK, Kostas SA, Driver SE, Mello CC (1998) Potent and specific genetic interference by double-stranded RNA in *Caenorhabditis elegans*. *Nature* 391: 806–811
- Fogelmark K, Troein C (2014) Rethinking transcriptional activation in the Arabidopsis circadian clock. *PLOS Comput Biol* 10: e1003705
- Freeman M (2000) Feedback control of intercellular signalling in development. *Nature* 408: 313–319
- Frey AD, Rimann M, Bailey JE, Kallio PT, Thompson CJ, Fussenegger M (2001) Novel pristinamycin-responsive expression systems for plant cells. *Biotechnol Bioeng* 74: 154–163
- Fung E, Wong WW, Suen JK, Bulter T, Lee SG, Liao JC (2005) A synthetic gene-metabolic oscillator. *Nature* 435: 118–122
- Fuqua WC, Winans SC, Greenberg EP (1994) Quorum sensing in bacteria: The LuxR-LuxI family of cell density-responsive transcriptional regulators. *J Bacteriol* 176: 269–275
- Gaber R, Lebar T, Majerle A, Šter B, Dobnikar A, Benčina M, Jerala R (2014) Designable DNA-binding domains enable construction of logic circuits in mammalian cells. *Nat Chem Biol* 10: 203–208
- Gander MW, Vrana JD, Voje WE, Carothers JM, Klavins E (2017) Digital logic circuits in yeast with CRISPR-dCas9 NOR gates. *Nat Commun* 8: 15459
- Gao Y, Xiong X, Wong S, Charles EJ, Lim WA, Qi LS (2016) Complex transcriptional modulation with orthogonal and inducible dCas9 regulators. *Nat Methods* 13: 1043–1049
- Gardner MJ, Baker AJ, Assie JM, Poethig RS, Haseloff JP, Webb AAR (2009) GAL4 GFP enhancer trap lines for analysis of stomatal guard cell development and gene expression. *J Exp Bot* 60: 213–226
- Gardner TS, Cantor CR, Collins JJ (2000) Construction of a genetic toggle switch in *Escherichia coli*. *Nature* 403: 339–342

Andres et al.

- Gatz C, Froberg C, Wendenburg R (1992) Stringent repression and homogeneous de-repression by tetracycline of a modified CaMV 35S promoter in intact transgenic tobacco plants. *Plant J* 2: 397–404
- Goodwin BC (1963) Temporal Organization in Cells: A Dynamic Theory of Cellular Control Processes. Academic Press, London
- Goodwin BC (1965) Oscillatory behavior in enzymatic control processes. *Adv Enzyme Regul* 3: 425–438
- Gossen M, Bujard H (1992) Tight control of gene expression in mammalian cells by tetracycline-responsive promoters. *Proc Natl Acad Sci USA* 89: 5547–5551
- Gossen M, Freundlieb S, Bender G, Müller G, Hillen W, Bujard H (1995) Transcriptional activation by tetracyclines in mammalian cells. *Science* 268: 1766–1769
- Guido NJ, Wang X, Adalsteinsson D, McMillen D, Hasty J, Cantor CR, Elston TC, Collins JJ (2006) A bottom-up approach to gene regulation. *Nature* 439: 856–860
- Hanson S, Bauer G, Fink B, Suess B (2005) Molecular analysis of a synthetic tetracycline-binding riboswitch. *RNA* 11: 503–511
- Hasty J, Dolnik M, Rottschäfer V, Collins JJ (2002) Synthetic gene network for entraining and amplifying cellular oscillations. *Phys Rev Lett* 88: 148101
- Havko NE, Major IT, Jewell JB, Attaran E, Browne J, Howe GA (2016) Control of carbon assimilation and partitioning by jasmonate: An accounting of growth-defense tradeoffs. *Plants (Basel)* 5: 7
- Hedden P, Thomas SG (2012) Gibberellin biosynthesis and its regulation. *Biochem J* 444: 11–25
- Helander JDM, Vaidya AS, Cutler SR (2016) Chemical manipulation of plant water use. *Bioorg Med Chem* 24: 493–500
- Heng BC, Aubel D, Fussenegger M (2015) Prosthetic gene networks as an alternative to standard pharmacotherapies for metabolic disorders. *Curr Opin Biotechnol* 35: 37–45
- Hörner M, Weber W (2012) Molecular switches in animal cells. *FEBS Lett* 586: 2084–2096
- Jacob F, Monod J (1961) Genetic regulatory mechanisms in the synthesis of proteins. *J Mol Biol* 3: 318–356
- Jaeger KE, Pullen N, Lamzin S, Morris RJ, Wigge PA (2013) Interlocking feedback loops govern the dynamic behavior of the floral transition in Arabidopsis. *Plant Cell* 25: 820–833
- Johnson AAT, Hibberd JM, Gay C, Essah PA, Haseloff J, Tester M, Guiderdoni E (2005) Spatial control of transgene expression in rice (*Oryza sativa* L.) using the GAL4 enhancer trapping system. *Plant J* 41: 779–789
- Kaberniuk AA, Shemetov AA, Verkhusha VV (2016) A bacterial phytochrome-based optogenetic system controllable with near-infrared light. *Nat Methods* 13: 591–597
- Khakhar A, Leydon AR, Lemmex AC, Klavins E, Nemhauser JL (2018) Synthetic hormone-responsive transcription factors can monitor and reprogram plant development. *eLife* 7: e34702
- Kimura M, Kagawa T, Kieber J, Araki T (2006) Phototropin and light-signaling in phototropism. *Curr Opin Plant Biol* 9: 503–508
- Kobayashi H, Kaern M, Araki M, Chung K, Gardner TS, Cantor CR, Collins JJ (2004) Programmable cells: Interfacing natural and engineered gene networks. *Proc Natl Acad Sci USA* 101: 8414–8419
- Kolar K, Weber W (2017) Synthetic biological approaches to optogenetically control cell signaling. *Curr Opin Biotechnol* 47: 112–119
- Kolar K, Wischhusen HM, Müller K, Karlsson M, Weber W, Zurbriggen MD (2015) A synthetic mammalian network to compute population borders based on engineered reciprocal cell-cell communication. *BMC Syst Biol* 9: 97
- Kolar K, Knobloch C, Stork H, Žnidarič M, Weber W (2018) OptoBase: A web platform for molecular optogenetics. *ACS Synth Biol* 7: 1825–1828
- Konermann S, Brigham MD, Trevino A, Hsu PD, Heidenreich M, Cong L, Platt RJ, Scott DA, Church GM, Zhang F (2013) Optical control of mammalian endogenous transcription and epigenetic states. *Nature* 500: 472–476
- Kramer BP, Fischer C, Fussenegger M (2004a) BioLogic gates enable logical transcription control in mammalian cells. *Biotechnol Bioeng* 87: 478–484
- Kramer BP, Viretta AU, Daoud-El-Baba M, Aubel D, Weber W, Fussenegger M (2004b) An engineered epigenetic transgene switch in mammalian cells. *Nat Biotechnol* 22: 867–870
- Lagos-Quintana M (2001) Identification of novel genes coding for small expressed RNAs. *Science* 294: 853–858
- Laplaze L, Parizot B, Baker A, Ricaud L, Martinière A, Auguy F, Franche C, Nussaume L, Bogusz D, Haseloff J (2005) GAL4-GFP enhancer trap lines for genetic manipulation of lateral root development in Arabidopsis thaliana. *J Exp Bot* 56: 2433–2442
- Lavedrine C, Farcot E, Vernoux T (2015) Modeling plant development: From signals to gene networks. *Curr Opin Plant Biol* 27: 148–153
- Lebar T, Bezeljak U, Golob A, Jerala M, Kadunc L, Pirš B, Stražar M, Vučko D, Zupančič U, Benčina M, et al (2014) A bistable genetic switch based on designable DNA-binding domains. *Nat Commun* 5: 5007
- Lienert F, Lohmueller JJ, Garg A, Silver PA (2014) Synthetic biology in mammalian cells: Next generation research tools and therapeutics. *Nat Rev Mol Cell Biol* 15: 95–107
- Lim WA (2010) Designing customized cell signalling circuits. *Nat Rev Mol Cell Biol* 11: 393–403
- Liu W, Stewart CN Jr (2015) Plant synthetic biology. *Trends Plant Sci* 20: 309–317
- Liu W, Yuan JS, Stewart CN Jr (2013) Advanced genetic tools for plant biotechnology. *Nat Rev Genet* 14: 781–793
- Lowder LG, Zhang D, Baltes NJ, Paul JW III, Tang X, Zheng X, Voytas DF, Hsieh TF, Zhang Y, Qi Y (2015) A CRISPR/Cas9 toolbox for multiplexed plant genome editing and transcriptional regulation. *Plant Physiol* 169: 971–985
- Lu TK, Khalil AS, Collins JJ (2009) Next-generation synthetic gene networks. *Nat Biotechnol* 27: 1139–1150
- Lutz R, Bujard H (1997) Independent and tight regulation of transcriptional units in *Escherichia coli* via the LacR/O, the TetR/O and AraC/I1-2 regulatory elements. *Nucleic Acids Res* 25: 1203–1210
- McClung CR (2006) Plant circadian rhythms. *Plant Cell* 18: 792–803
- McKenzie MJ, Mett V, Stewart Reynolds PH, Jameson PE (1998) Controlled cytokinin production in transgenic tobacco using a copper-inducible promoter. *Plant Physiol* 116: 969–977
- Medford JI, Prasad A (2016) Towards programmable plant genetic circuits. *Plant J* 87: 139–148
- Moon TS, Lou C, Tamsir A, Stanton BC, Voigt CA (2012) Genetic programs constructed from layered logic gates in single cells. *Nature* 491: 249–253
- Morffy N, Faure L, Nelson DC (2016) Smoke and hormone mirrors: Action and evolution of karrikin and strigolactone signaling. *Trends Genet* 32: 176–188
- Motta-Mena LB, Reade A, Mallory MJ, Glantz S, Weiner OD, Lynch KW, Gardner KH (2014) An optogenetic gene expression system with rapid activation and deactivation kinetics. *Nat Chem Biol* 10: 196–202
- Müller K, Engesser R, Metzger S, Schulz S, Kämpf MM, Busacker M, Steinberg T, Tomakidi P, Ehrbar M, Nagy F, et al (2013a) A red/far-red light-responsive bi-stable toggle switch to control gene expression in mammalian cells. *Nucleic Acids Res* 41: e77
- Müller K, Engesser R, Schulz S, Steinberg T, Tomakidi P, Weber CC, Ulm R, Timmer J, Zurbriggen MD, Weber W (2013b) Multi-chromatic control of mammalian gene expression and signaling. *Nucleic Acids Res* 41: e124
- Müller K, Siegel D, Rodriguez Jahnke F, Gerrer K, Wend S, Decker EL, Reski R, Weber W, Zurbriggen MD (2014) A red light-controlled synthetic gene expression switch for plant systems. *Mol Biosyst* 10: 1679–1688
- Müller K, Naumann S, Weber W, Zurbriggen MD (2015) Optogenetics for gene expression in mammalian cells. *Biol Chem* 396: 145–152
- Müller S, Hofbauer J, Endler L, Flamm C, Widder S, Schuster P (2006) A generalized model of the repressilator. *J Math Biol* 53: 905–937
- Nash AI, McNulty R, Shillito ME, Swartz TE, Bogomolni RA, Luecke H, Gardner KH (2011) Structural basis of photosensitivity in a bacterial light-oxygen-voltage/helix-turn-helix (LOV-HTH) DNA-binding protein. *Proc Natl Acad Sci USA* 108: 9449–9454
- Nevozhay D, Adams RM, Murphy KF, Josic K, Balázs G (2009) Negative autoregulation linearizes the dose-response and suppresses the heterogeneity of gene expression. *Proc Natl Acad Sci USA* 106: 5123–5128
- Nevozhay D, Zal T, Balázs G (2013) Transferring a synthetic gene circuit from yeast to mammalian cells. *Nat Commun* 4: 1451
- Nielsen AAK, Voigt CA (2014) Multi-input CRISPR/Cas genetic circuits that interface host regulatory networks. *Mol Syst Biol* 10: 763
- Nihongaki Y, Yamamoto S, Kawano F, Suzuki H, Sato M (2015) CRISPR-Cas9-based photoactivatable transcription system. *Chem Biol* 22: 169–174

882

Plant Physiol. Vol. 179, 2019

- Niopek D, Benzinger D, Roensch J, Draebing T, Wehler P, Eils R, Di Ventura B (2014) Engineering light-inducible nuclear localization signals for precise spatiotemporal control of protein dynamics in living cells. *Nat Commun* 5: 4404
- Niopek D, Wehler P, Roensch J, Eils R, Di Ventura B (2016) Optogenetic control of nuclear protein export. *Nat Commun* 7: 10624
- Ochoa-Fernandez R, Samodelov SL, Brandl SM, Wehinger E, Müller K, Weber W, Zurbriggen MD (2016) Optogenetics in plants: Red/far-red light control of gene expression. *Methods Mol Biol* 1408: 125–139
- Okumoto S, Jones A, Frommer WB (2012) Quantitative imaging with fluorescent biosensors. *Annu Rev Plant Biol* 63: 663–706
- Paek KY, Hong KY, Ryu I, Park SM, Keum SJ, Kwon OS, Jang SK (2015) Translation initiation mediated by RNA looping. *Proc Natl Acad Sci USA* 112: 1041–1046
- Park SY, Peterson FC, Mosquna A, Yao J, Volkman BF, Cutler SR (2015) Agrochemical control of plant water use using engineered abscisic acid receptors. *Nature* 520: 545–548
- Parker C (2009) Observations on the current status of *Orobanche* and *Striga* problems worldwide. *Pest Manag Sci* 65: 453–459
- Patron NJ (2014) DNA assembly for plant biology: Techniques and tools. *Curr Opin Plant Biol* 19: 14–19
- Phillips R, Kondev J, Theriot J (2009) *Physical Biology of the Cell*. Garland Science, New York
- Piatek A, Ali Z, Baazim H, Li L, Abulfaraj A, Al-Shareef S, Aouida M, Mahfouz MM (2015) RNA-guided transcriptional regulation in *planta* via synthetic dCas9-based transcription factors. *Plant Biotechnol J* 13: 578–589
- Pillai RS, Artus CG, Filipowicz W (2004) Tethering of human Ago proteins to mRNA mimics the miRNA-mediated repression of protein synthesis. *RNA* 10: 1518–1525
- Pokhilko A, Mas P, Millar AJ (2013) Modelling the widespread effects of TOC1 signalling on the plant circadian clock and its outputs. *BMC Syst Biol* 7: 23
- Polstein LR, Gersbach CA (2015) A light-inducible CRISPR-Cas9 system for control of endogenous gene activation. *Nat Chem Biol* 11: 198–200
- Prindle A, Samayoa P, Razinkov I, Danino T, Tsimring LS, Hasty J (2011) A sensing array of radically coupled genetic 'biopixels.' *Nature* 481: 39–44
- Purcell O, Savery NJ, Grierson CS, di Bernardo M (2010) A comparative analysis of synthetic genetic oscillators. *J R Soc Interface* 7: 1503–1524
- Roberts GR, Garoosi GA, Koroleva O, Ito M, Laufs P, Leader DJ, Caddick MX, Doonan JH, Tomsett AB (2005) The alc-GR system: A modified alc gene switch designed for use in plant tissue culture. *Plant Physiol* 138: 1259–1267
- Rockwell NC, Lagarias JC (2006) The structure of phytochrome: A picture is worth a thousand spectra. *Plant Cell* 18: 4–14
- Roslan HA, Salter MG, Wood CD, White MRH, Croft KP, Robson F, Coupland G, Doonan J, Laufs P, Tomsett AB, et al (2001) Characterization of the ethanol-inducible alc gene-expression system in *Arabidopsis thaliana*. *Plant J* 28: 225–235
- Roybal KT, Lim WA (2017) Synthetic immunology: Hacking immune cells to expand their therapeutic capabilities. *Annu Rev Immunol* 35: 229–253
- Roybal KT, Williams JZ, Morsut L, Rupp LJ, Kolinko I, Choe JH, Walker WJ, McNally KA, Lim WA (2016) Engineering T cells with customized therapeutic response programs using synthetic notch receptors. *Cell* 167: 419–432.e16
- Ryback BM, Odoni DI, van Heck RGA, van Nuland Y, Hesselman MC, Martins Dos Santos VAP, van Passel MWJ, Hugenoltz F (2013) Design and analysis of a tunable synchronized oscillator. *J Biol Eng* 7: 26
- Salinas F, Rojas V, Delgado V, Agosin E, Larrondo LF (2017) Optogenetic switches for light-controlled gene expression in yeast. *Appl Microbiol Biotechnol* 101: 2629–2640
- Samodelov SL, Zurbriggen MD (2017) Quantitatively understanding plant signaling: Novel theoretical-experimental approaches. *Trends Plant Sci* 22: 685–704
- Savageau MA (1974) Comparison of classical and autogenous systems of regulation in inducible operons. *Nature* 252: 546–549
- Schaumberg KA, Antunes MS, Kassaw TK, Xu W, Zalewski CS, Medford JJ, Prasad A (2016) Quantitative characterization of genetic parts and circuits for plant synthetic biology. *Nat Methods* 13: 94–100
- Schena M, Lloyd AM, Davis RW (1991) A steroid-inducible gene expression system for plant cells. *Proc Natl Acad Sci USA* 88: 10421–10425
- Schibler U, Sassone-Corsi P (2002) A web of circadian pacemakers. *Cell* 111: 919–922
- Schwab R, Ossowski S, Rieger M, Warthmann N, Weigel D (2006) Highly specific gene silencing by artificial microRNAs in *Arabidopsis*. *Plant Cell* 18: 1121–1133
- Sheen J (2010) Discover and connect cellular signaling. *Plant Physiol* 154: 562–566
- Smole A, Lainšček D, Bezeljak U, Horvat S, Jerala R (2017) A synthetic mammalian therapeutic gene circuit for sensing and suppressing inflammation. *Mol Ther* 25: 102–119
- South PF, Cavanagh AP, Liu HW, Ort DR (2019) Synthetic glycolate metabolism pathways stimulate crop growth and productivity in the field. *Science* 363: eaat9077
- Stanley SA, Gagner JE, Damanpour S, Yoshida M, Dordick JS, Friedman JM (2012) Radio-wave heating of iron oxide nanoparticles can regulate plasma glucose in mice. *Science* 336: 604–608
- Stein V, Alexandrov K (2015) Synthetic protein switches: Design principles and applications. *Trends Biotechnol* 33: 101–110
- Stricker J, Cookson S, Bennett MR, Mather WH, Tsimring LS, Hasty J (2008) A fast, robust and tunable synthetic gene oscillator. *Nature* 456: 516–519
- Tamsir A, Tabor JJ, Voigt CA (2011) Robust multicellular computing using genetically encoded NOR gates and chemical 'wires.' *Nature* 469: 212–215
- Thieffry D, Huerta AM, Pérez-Rueda E, Collado-Vides J (1998) From specific gene regulation to genomic networks: A global analysis of transcriptional regulation in *Escherichia coli*. *BioEssays* 20: 433–440
- Thurley K, Wu LF, Altschuler SJ (2018) Modeling cell-to-cell communication networks using response-time distributions. *Cell Syst* 6: 355–367.e5
- Tigges M, Marquez-Lago TT, Stelling J, Fussenegger M (2009) A tunable synthetic mammalian oscillator. *Nature* 457: 309–312
- Toda S, Blauch LR, Tang SKY, Morsut L, Lim WA (2018) Programming self-organizing multicellular structures with synthetic cell-cell signaling. *Science* 361: 156–162
- Toettcher JE, Mock C, Batchelor E, Loewer A, Lahav G (2010) A synthetic-natural hybrid oscillator in human cells. *Proc Natl Acad Sci USA* 107: 17047–17052
- Toettcher JE, Weiner OD, Lim WA (2013) Using optogenetics to interrogate the dynamic control of signal transmission by the Ras/Erk module. *Cell* 155: 1422–1434
- Tomazou M, Barahona M, Polizzi KM, Stan GB (2018) Computational redesign of synthetic genetic oscillators for independent amplitude and frequency modulation. *Cell Syst* 6: 508–520.e5
- Trewavas A (2005) Green plants as intelligent organisms. *Trends Plant Sci* 10: 413–419
- Vaidya AS, Peterson FC, Yarmolinsky D, Merilo E, Verstraeten I, Park SY, Elzinga D, Kaundal A, Helander J, Lozano-Juste J, et al (2017) A rationally designed agonist defines subfamily IIIA abscisic acid receptors as critical targets for manipulating transpiration. *ACS Chem Biol* 12: 2842–2848
- van Bergeijk P, Adrian M, Hoogenraad CC, Kapitein LC (2015) Optogenetic control of organelle transport and positioning. *Nature* 518: 111–114
- Van Etten J, Schagat TL, Hrit J, Weidmann CA, Brumbaugh J, Coon JJ, Goldstrohm AC (2012) Human Pumilio proteins recruit multiple deadenylases to efficiently repress messenger RNAs. *J Biol Chem* 287: 36370–36383
- Vazquez-Vilar M, Orzaez D, Patron N (2018) DNA assembly standards: Setting the low-level programming code for plant biotechnology. *Plant Sci* 273: 33–41
- Verhounig A, Karcher D, Bock R (2010) Inducible gene expression from the plastid genome by a synthetic riboswitch. *Proc Natl Acad Sci USA* 107: 6204–6209
- Walia A, Waadt R, Jones AM (2018) Genetically encoded biosensors in plants: Pathways to discovery. *Annu Rev Plant Biol* 69: 497–524
- Warashina M, Takagi Y, Stec WJ, Taira K (2000) Differences among mechanisms of ribozyme-catalyzed reactions. *Curr Opin Biotechnol* 11: 354–362
- Weber W, Fux C, Daoud-el Baba M, Keller B, Weber CC, Kramer BP, Heinzen C, Aubel D, Bailey JE, Fussenegger M (2002) Macrolide-based transgene control in mammalian cells and mice. *Nat Biotechnol* 20: 901–907

Andres et al.

- Weinmann P, Gossen M, Hillen W, Bujard H, Gatz C (1994) A chimeric transactivator allows tetracycline-responsive gene expression in whole plants. *Plant J* 5: 559–569
- Wend S, Dal Bosco C, Kämpf MM, Ren F, Palme K, Weber W, Dovzhenko A, Zurbriggen MD (2013) A quantitative ratiometric sensor for time-resolved analysis of auxin dynamics. *Sci Rep* 3: 2052
- Wilde RJ, Shufflebottom D, Cooke S, Jasinska I, Merryweather A, Beri R, Brammar WJ, Bevan M, Schuch W (1992) Control of gene expression in tobacco cells using a bacterial operator-repressor system. *EMBO J* 11: 1251–1259
- Wollenweber B, Porter JR, Lübberstedt T (2005) Need for multidisciplinary research towards a second green revolution. *Curr Opin Plant Biol* 8: 337–341
- Xiao H, Edwards TE, Ferré-D'Amaré AR (2008) Structural basis for specific, high-affinity tetracycline binding by an in vitro evolved aptamer and artificial riboswitch. *Chem Biol* 15: 1125–1137
- Xie M, Fussenegger M (2018) Designing cell function: Assembly of synthetic gene circuits for cell biology applications. *Nat Rev Mol Cell Biol* 19: 507–525
- Xie Z, Wroblewska L, Prochazka L, Weiss R, Benenson Y (2011) Multi-input RNAi-based logic circuit for identification of specific cancer cells. *Science* 333: 1307–1311
- Ye H, Baba MD, Peng R, Fussenegger M (2011) A synthetic optogenetic transcription device enhances blood-glucose homeostasis in mice. *Science* 332: 1565–1569
- Ye H, Xie M, Xue S, Charpin-El Hamri G, Yin J, Zulewski H, Fussenegger M (2017) Self-adjusting synthetic gene circuit for correcting insulin resistance. *Nat Biomed Eng* 1: 0005
- You L, Cox RS III, Weiss R, Arnold FH (2004) Programmed population control by cell-cell communication and regulated killing. *Nature* 428: 868–871
- You YS, Marella H, Zentella R, Zhou Y, Ulmasov T, Ho THD, Quatrano RS (2006) Use of bacterial quorum-sensing components to regulate gene expression in plants. *Plant Physiol* 140: 1205–1212
- Zhang K, Cui B (2015) Optogenetic control of intracellular signaling pathways. *Trends Biotechnol* 33: 92–100
- Zuo J, Niu QW, Chua NH (2000) Technical advance: An estrogen receptor-based transactivator XVE mediates highly inducible gene expression in transgenic plants. *Plant J* 24: 265–273

7.3 Additional publications

Gratz R, Brumbarova T, Ivanov R, Trofimov K, Tünnermann L, Ochoa-Fernandez R,

Blomeier T, Meiser J, Weidtkamp-Peters S, Zurbriggen MD, et al. Phospho-mutant activity assays provide evidence for alternative phospho-regulation pathways of the transcription factor FER-LIKE IRON DEFICIENCY-INDUCED TRANSCRIPTION FACTOR. *New Phytol* **225**: 250–267, January 2020

Contribution: Performance and analysis of the mammalian cell experiments. Writing of the mammalian cell part of the paper.

Blanco-Touriñán N, Legris M, Minguet EG, Costigliolo-Rojas C, Nohales MA, Iniesto E, García-León M, Pacín M, Heucken N, **Blomeier T**, et al. COP1 destabilizes DELLA proteins in *Arabidopsis*. *Proc Natl Acad Sci U S A* **117**: 13792–13799, June 2020

Contribution: Design and analysis of the experiments in mammalian cells. Writing of the mammalian cell part of the paper.